MAGNETIC INTERACTIONS BETWEEN SOLUTE ATOMS IN ALLOYS

Thesis submitted for the Degree of Doctor of Philosophy in the University of London

by

A. P. MURANI

Physics Department
Imperial College of Science and Technology
London SW7

June 1969

ABSTRACT

Interaction effects between solute atoms in some alloy systems have been studied by magnetisation, susceptibility and resistivity measurements. The design and construction of a vibration magnetometer built for the magnetisation and susceptibility measurements is described in detail. The resistance measurements were made using standard potentiometric techniques.

The systems investigated are the Rh based alloys of Fe and Co and the gold-rare earth alloys.

Measurements on Rh-Fe alloys have been made to study the effect of the formation of the quasi-bound state on the onset of magnetic order in the alloys. This onset is indicated by clearly defined maxima in the susceptibility and anomalies in the resistance near the temperatures of the maxima for alloys with more than 3 at.% Fe. Cooling the alloys in a magnetic field produces displaced magnetisation curves indicating a distribution of internal fields that can be disturbed by an applied external field. The high temperature susceptibility of the alloys is interpreted in terms of a large temperature independent contribution and a temperature dependent term obeying Curie law.

The iso-electronic alloy system Rh-Co has been investigated with Co concentrations up to a maximum of 11 at.%. No sign of magnetic order has been observed down to 1.6°K. There is a large increase in the total susceptibility of the alloys due to the addition of Co. This behaviour is similar to that found in Rh-Fe alloys but the temperature dependence is much weaker.

Measurements on some fairly concentrated gold-rare earth alloys have been made in a search for the effect of interactions between solute atoms on the magnetic properties of the alloys. The measurements reported here show that interaction effects in these alloys with concentrations of rare earths within the solubility limit are rather weak. An interpretation of the susceptibility in terms of the crystal field splitting of energy levels is given. The low temperature resistivity of the alloys has been interpreted in terms of the temperature dependent s-f scattering from the crystal field split energy levels.

ACKNOWLEDGEMENTS

I would like to express my sincere thanks to Prof. B.R. Coles for the supervision of this work and for his interest, encouragement and enthusiasm throughout its course. I would also like to thank Dr. S. Doniach for his interest and for the innumerable discussions from which I have greatly benefited.

During the building of the magnetometer I have had many discussions with Dr. D. Griffiths. I am indebted to him for his help and active interest throughout. I am also grateful to Mr. John Halstead, Ultrasonics Group, Imperial College, for providing the information about the bimorphs which was instrumental in the development of the magnetometer.

It is a pleasure to thank all the members of the solid state group for their help at various stages of this project and for discussions which have been most valuable. I would also like to thank Dr. L.L. Hirst for the use of his crystal field computer programme.

My thanks are due to Joy Dunning for typing the thesis and Dr. B. Woodward for his help in the preparation of the diagrams.

I am grateful to the U.K.A.E.A. for a research bursary and for supporting the research programme. The loan of rhodium from Johnson Matthey and Co. is very much appreciated.

CONTENTS

	Page No.
ABSTRACT	2
ACKNOWLEDGEMENTS	4
CONTENTS	5
INTRODUCTION	11
CHAPTER 1 - LOCALISED MOMENTS OF SOLUTE ATOMS IN DILUTE ALLOYS	14
Introduction	14
Friedel Virtual Bound State	15
Anderson Model	17
Wolff-Clogston Model	20
The Kondo Effect	22
The Equivalence between the Anderson Hamiltonian and the s-d interaction Hamiltonian	25
Doubts on the validity of the Hartree-Fock treatment of Anderson Hamiltonian	27
Magnetic Susceptibility	28
Scalapino	28
Yosida and Okiji	32
Nagaoka	33
Hamann	33
Fullenbaum and Falk	33
Electrical Resistivity	34
Kondo	34
Hamann	35
Suhl & Others	35

		Page No.
CHAPTER 2	- THE EFFECT OF CRYSTALLINE FIELDS ON THE PROPERTIES OF DILUTE ALLOYS	38
	1. 3d Transition Series Atoms	38
	2. The Rare Earth Atoms	41
	The Hamiltonian for Rare Earths	42
	The Treatment of the Crystal-Field Interaction	44
	Half Integral J	48
	Integral J	49
	S State Ions	50
	Magnetic Susceptibility	51
	Electrical Resistance	53
CHAPTER 3	- BASIC MECHANISM FOR INTERACTIONS BETWEEN SOLUTE ATOMS	57
	Introduction	57
	The Exchange Interaction Constant	58
	R.K.K.Y. Spin Polarisation	61
	Overhauser	62
	Watson and Freeman	63
	Overhauser and Stearns	63
	Magnetic Coupling between Virtual Bound State Moments	65
	Blandin and Friedel	66
	Caroli	67
	Treatment of Interaction	69
	Mattis	69
	Fedro and Arai	70
	Marshall	71
	Klein and Brout	72
	Liu	75
	Magnetic Susceptibility	78
	Electrical Resistance	81

		Page No
CHAPTER 4	- A SURVEY OF SOME ALLOY SYSTEMS SHOWING MAGNETIC INTERACTIONS	84
	(1) Real Bound State	86
	(2) Magnetised Virtual Bound State	89
	(3) Nagaoka Spin Condensed State	90
	(4) Unmagnetised Virtual Bound State	90
	A.(1) Real Bound Magnetic State in a Simple Matrix	94
	A.(2) Real Bound State in a Simple Transition Metal Matrix and Binary Alloys	96
	A.(3) Real Bound State in an Exchange Enhanced Host Matrix	98
	B.(1) Magnetised Virtual Bound State in a simple Metal Host	100
	B.(2) Magnetic Virtual Bound State in a simple transition Metal and Binary Alloy Hosts	102
	B.(3) Magnetised Virtual Bound State in an Exchange Enhanced Host Matrix	103
	C.(1) Nagaoka Spin Compensated State in simple Metal Host	104
	C.(2) Nagaoka Spin Compensated State in Simple Transition Metals and Binary Alloys	107
	C.(3) Nagaoka Spin Compensated State in an Exchange Enhanced Matrix	109
	D.(1) Unmagnetised V.B.S. in a Simple Metal Host	110
	D.(2) Unmagnetised V.B.S. in Transition Metal Hosts and Binary Alloy	112
	D.(3) Unmagnetised V.B.S. in an Exchange Enhanced Matrix	113

	Page No.
CHAPTER 5 - EXPERIMENTAL METHOD AND APPARATUS	115
THE VIBRATION MAGNETOMETER	115
Introduction	115
The Basic Principle	117
The Bimorph Element and Its Use	119
Coil Design	122
Description of the Apparatus	125
Setting-up Procedure	127
Operation	129
Screening of the Bimorph	133
Minimizing the Induced Sychronous Noise Voltage in the Pick-up Coils	133
Calibration	138
Sensitivity Limits	140
Measurements as a Function of Temperature	141
Possible Improvements in the Design of Magnetometer	143
THE EXPERIMENTAL DETAILS	146
The Cryostat	146
The Dewar Cap	148
The Pick-up Coil	152
The Coil Housing	152
The Nulling Coil	153
Magnetic Moment of the Nulling Coil	154
Magnetoresistance of the Nulling Coil	159
Heating Effects in the Nulling Coil	162
Electronic Circuits	165
(a) The Amplifier	165
(b) The Phase Sensitive Detector	167

Page No.

CHAPTER 5 - (Continued)

Screening and Earthing Arrangement 169

The Power Supply 171

Thermometry 172
(a) The Carbon Thermometer 173
(b) Calibration of the Carbon Thermometer 176
(c) The Copper Resistance Thermometer 178
(d) Checking the Thermometry 180

Experimental Procedure 181

Data Processing 190

CHAPTER 6 - EXPERIMENTAL RESULTS AND DISCUSSION OF SOME RHODIUM BASED ALLOYS 193

A. The Rh-Fe Alloy System 193

Introduction 193

Sample Preparation 194

Rh 0.9 % Fe 197

Rh 2.86 % Fe 201

Rh 4.95 % Fe 207

Rh 10.87 % Fe 212

Rh 15.35 % Fe 217

Discussion 221

B. The Rh-Co Alloy System 238

Introduction 238

Sample Preparation 239

Rh ½% Co 240

Rh 11% Co 243

		Page No.
CHAPTER 7	EXPERIMENTAL RESULTS AND DISCUSSION OF SOME GOLD-RARE EARTH ALLOYS	246
	Introduction	246
	Sample Preparation	248
	Au 0.3 % Gd	249
	Au 2.3 % Yb	254
	Au 3.9 % Yb	259
	Au 2.0 % Ho	265
	Au 1.5 % Dy	275
	Conclusion	283
REFERENCES		285

INTRODUCTION

The study of magnetism in metals is an important tool for the investigation of the electronic structure of metals, the properties and behaviour of electrons in metals and their interactions with each other. Magnetic order in pure metals, such as the 3d transition series elements, is a complex phenomenon because of the nature of the various types of interactions involved. In fact, the magnetism of some classical ferromagnets, iron for example, is still not well understood (Herring, Magnetism, Rado & Suhl (Editors) vol.2)

Dilute alloys in principle, provide situations which are in some ways simpler. The investigation of systems in which a small concentration of magnetic atoms is dissolved in a non-magnetic host matrix can lead to very useful information about the magnetic properties of the isolated magnetic atom and its interactions with the conduction electrons. Many interesting effects have been observed in dilute alloys which have led to considerable theoretical understanding of their electronic structure. However, some of the observed phenomena in dilute alloys are still not well understood.

Progress towards an understanding of magnetism can be made through the study of systems in which the concentration

of the magnetic solute atoms is systematically varied. For instance, the manner in which magnetic order occurs as a function of concentration not only provides useful information about the possible mechanisms of interactions between the atoms, but is also related to the magnetic state of the atoms in the dilute limit, and the electronic structure of the host metal in which it is dissolved.

A classification of the various alloy systems according to the nature of the host matrix and the magnetic state of the solute atom in the dilute limit has been attempted. The experimental investigation has been made with a view to studying interaction effects between solute atoms in a few alloy systems representing particular members of the above classification.

Chapter 1 reviews some theories of dilute alloys and the expressions derived by various authors for the magnetic susceptibility and the electrical resistivity for these. The effect of the crystal field of the lattice on the properties of dilute alloys is discussed in Chapter 2. The basic mechanisms of interactions between solute atoms and the resulting modification of the susceptibility and the electrical resistivity are examined in Chapter 3. In Chapter 4, a survey of the some of the existing experimental data classified according to the nature of the host matrix and the magnetic state associated with the solute atom is

given. In Chapter 5 the vibration magnetometer built for the magnetisation and susceptibility measurements is described. Experimental details are also included in this chapter. The results of measurements on Rh - Fe and Rh - Co alloys are presented and discussed in Chapter 6, and gold-rare earth alloys are similarly treated in Chapter 7.

CHAPTER 1

LOCALISED MOMENTS OF SOLUTE ATOMS IN DILUTE ALLOYS

Introduction

The state of magnetisation of a given isolated solute atom in an alloy is a function both of the nature of the solvent matrix and the type of magnetic shell of the free atom. In the case where the unfilled shell is well localised and tightly bound, the effect of the matrix on the state of magnetisation of the solute is small. The 3d transition series atoms, however, show large variations in their magnetic properties when in solution in a metallic matrix due to the large interaction between the extended 3d wave function and the conduction electrons. Matthias et al (1) investigated the magnetisation of iron dissolved in various second row transition metals and their alloys. They found large variations in the magnetic moment per dissolved Fe atom as the electrons per atom ratio of the matrix was varied. Iron atoms were in fact found to carry no magnetic moment in certain solvents! This remarkable behaviour led to two different models being proposed to explain the effect. One of these was by Anderson (2), the other

was the treatment of Wolff (3) and a similar one by Clogston (4).

Both these models are based on the earlier ideas of virtual bound state proposed by Friedel (5), who used them to explain the residual resistance of some alloys containing the first-row transition element solutes.

Friedel Virtual Bound State

Friedel considers the scattering of conduction electrons from a potential V(r) presented by the impurity atom having an excess charge Z. The incident free electron wave functions are analysed in spherical harmonics. The effect of the scattering in terms of the phase shifts η_l of the radial parts of the l^{th} harmonics is calculated by solving the Schrödinger equation and applying boundary conditions on the surface of a large sphere of radius R. From the resultant scattered wave function, the screening charge per unit k within the sphere is found to be

$$\int_0^R \frac{d}{dk}(\rho - \rho_o)4\pi r^2 dr = \frac{2}{\pi}\sum_l (2l+1)\left[\frac{d\eta_l}{dk} - \frac{1}{k}\sin \phi_l \times \cos(2kR + \eta_l - l\pi)\right], \quad 1.1$$

where the degeneracy of l^{th} spherical component is taken into consideration.

Integration of this expression for all k vectors up to k_F gives the total screening charge within the sphere, which, from neutrality condition, must be equal to Z, the excess impurity charge. The oscillatory term gives a negligible contribution, hence the result becomes

$$Z = \frac{2}{\pi} \sum' (2l + 1)\eta_l(k_F) \qquad 1.2$$

This can be interpreted in terms of a shift in the density of states of each l^{th} component by an amount proportional to $d\eta_l(E)/dE$. The density of states is non-uniform and has a peak for a certain energy E where

$$\sum_l' (2l + 1)d\eta_l(E)/dE$$

is large. This represents a virtual bound state and is localised about the impurity.

Friedel (5) qualitatively considers the possibility that the virtual bound state will split into two halves of opposite spin directions due to the exchange energy within the state. The splitting can only occur if the energy gain from

the splitting is more than the width W of the state. If p is the number of electrons in the d state and E is the average energy gained when two d electrons are in the same spin state, then the condition for splitting is

$$p\,\Delta E \geqslant W \qquad 1.3$$

This is the same result as that obtained by a detailed calculation by Blandin and Friedel (6).

Anderson Model

Anderson (2) treated the problem by considering a simplified case of a single localised d level of the impurity with an energy somewhere in the conduction band of the host matrix. An interaction V_{kd} between the conduction electrons and the d state causes the latter to broaden in energy and form a virtual bound state. The repulsive energy between the up and down state electrons causes the level to split into two halves. The relative magnitude of the splitting and width W of the level, and the position of the latter relative to the Fermi sea determines whether the state becomes magnetised or not.

The Anderson Hamiltonian H can be written as

$$H = H_k + H_d + H_{kd} \qquad 1.4$$

where

$$H_k = \sum_{k,\sigma}' \varepsilon_k \; a^+_{k\sigma} a_{k\sigma}$$

is the energy of the free electrons of the conduction band

$$H_d = \sum_{\sigma}' \varepsilon_d \; C^+_{d\sigma} C_{d\sigma} + U \; C^+_{d\uparrow} C_{d\uparrow} C^+_{d\downarrow} C_{d\downarrow} \qquad 1.5$$

is the energy associated with the single d orbital, U is the repulsion energy between the up and down spin electron, which keeps them apart and

$$H_{kd} = \sum_{k\sigma}' V_{kd} \; (a^+_{k\sigma} C_{d\sigma} + C^+_{d\sigma} a_{k\sigma}) \qquad 1.6$$

In the above second quantisation notation $a^+_{k\sigma}$, $a_{k\sigma}$ are the creation and annihilation operators for the conduction electrons, $C^+_{d\sigma}$, $C_{d\sigma}$ those for the d level.

H_{kd} represents the energy of interaction between the conduction electrons and the d level. This mixing causes the d level to broaden to form a virtual bound state. The state has a lifetime, τ, which is related to the broadening Δ by $\Delta = \hbar/\tau$

Anderson solved the Hamiltonian in the Hartree Fock self consistent field approximation. Using the single particle

Green's function

$$G(\varepsilon + is) = \frac{1}{(\varepsilon + is - H)} \qquad 1.7$$

solution for the density of the d state gives

$$\rho_{d\sigma}(\varepsilon) = \frac{1}{\pi} \frac{\Delta}{(\varepsilon - E_\sigma)^2 + \Delta^2} \qquad 1.8$$

where the width $\Delta = \pi \langle V^2 \rangle_{av} \rho(\varepsilon)$, $\rho(\varepsilon)$ is the modified density of states of the conduction electrons and E_σ is the energy of the spin state σ. Integration of this up to the Fermi energy gives the average number of electrons per spin state given by the two equations

$$\langle n_{d+} \rangle = \frac{1}{\pi} \cot^{-1} \frac{E - \varepsilon_F + U \langle n_{d-} \rangle}{\Delta}$$

and

$$\langle n_{d-} \rangle = \frac{1}{\pi} \cot^{-1} \frac{E - \varepsilon_F + U \langle n_{d+} \rangle}{\Delta} \qquad 1.9$$

If these two equations are solved simultaneously, it is found that when the parameter $U/\Delta < 1$ there is only one solution possible giving $\langle n_{d+} \rangle = \langle n_{d-} \rangle$ For $U/\Delta > 1$, however, solutions giving $\langle n_{d+} \rangle \neq \langle n_{d-} \rangle$ are also possible. This is, therefore, the condition for the state to be magnetised. The

other condition assumed to exist is that $0 \leqslant \frac{\mathcal{E}_F - E}{U} \leqslant 1$ This means that the energy E of the unperturbed d state must not be more than an amount U below the Fermi level.

Wolff-Clogston Model

Friedel's ideas have been used in another approach to the problem of localised moments in the treatment of Wolff (3) and a similar one by Clogston (4). The problem is treated as a scattering of Bloch waves from a single impurity represented by a potential V. The impurity electrons are assumed to be part of the conduction band.

The treatment of Slater and Koster (7) is followed, where the total wave function is expanded in terms of Wannier functions constructed from a single band.

$$\Psi = \frac{1}{\sqrt{N}} \sum_{R_i} U(R_i)\, a_n\,(R_o - R_i) \qquad 1.10$$

Further, the potential V is assumed to have no matrix elements between Wannier functions from different bands or those centred about any other site except the impurity. That is

$$\left\langle a_n(R_o-R_i) \middle| V \middle| a_{n'}(R_o-R_j) \right\rangle = V_{nn'}\, \delta_{nn'}\, \delta(R_i-R_o)\delta(R_j-R_o) \qquad 1.11$$

The solution for Ψ is given by the equation

$$\Psi = \varphi_{k,m} + \left[\frac{1}{E_m(k) - H_o + is}\right] V\Psi \qquad 1.12$$

This formulation leads to a solution for the amplitude $U(R_o)$, which has a large value for a certain energy E_o. If E_o is outside the band in question, $U(R_o) \longrightarrow \infty$ and one gets a real bound state. If, however, E_o is within the band, $U(R_o)$ has a resonance maximum. This is the origin of the virtual bound state. Wolff proceeds from this idea to include in V, the potential $Un_\uparrow n_\downarrow$ in the same way as Anderson. He considers the same band structure as used by Slater and Koster, namely

$$E(k) = 2\varepsilon(1)\left[\cos(k_x a) + \cos(k_y a) + \cos(k_z a)\right] \qquad 1.13$$

and arrives at two simultaneous equations for the amplitudes $U_\uparrow(R_o)$ and $U_\downarrow(R_o)$. The effect of these, in the Hartree-Fock approximation, on the impurity field is calculated. Expressions for the potentials $\delta V_\uparrow$ and $\delta V_\downarrow$ are obtained, and conditions for solutions with $\delta V_\uparrow \neq \delta V_\downarrow$ are examined. Apart from the initial approach to a virtual bound state, the treatment is similar to Anderson's.

The Kondo Effect

An important development in the theory of dilute alloys was made by J. Kondo (8). He assumed a localised moment to exist, characterised by a spin S. This interacts with the conduction electrons through an exchange interaction of the form

$$H_{ex} = - J\Omega \, \underline{S} \cdot \underline{s}(o) \qquad 1.14$$

where s(o) is the spin density of the conduction electron at the impurity site, J is the strength of the interaction, and Ω is the atomic volume. This Hamiltonian has been used earlier by Zener (9) Kasuya (10) and Yosida (11), in treatment of the indirect interactions between solute atoms.

Kondo calculated the effect of this interaction on the scattering amplitude of conduction electrons in the second Born approximation, taking Pauli principle into account in the intermediate states of the second order terms. The author shows that two types of scattering processes can arise. One is a single electron scattering process and the other is a two electron scattering process. The interference between these two processes leads to a divergent scattering amplitude.

The first process is where a conduction electron with spin up, denoted by k_+, is scattered to an intermediate state q_-. The z-component of the spin of the solute atom is increased by one unit in the process. The electron is then scattered into the final state k'_+ and the solute atom spin flips back to its original state. This process contributes to the scattering amplitude by an amount

$$- \frac{J^2 V_c}{N} \sum_q \frac{(1 - f_q)}{(\varepsilon_k - \varepsilon_q)} \; S^+ \; S^- \qquad 1.15$$

where V_c is the volume of the Wannier cell, J is the interaction constant, S^+ and S^- are the raising and lowering operators for the spin state of the solute atoms, f_q is the Fermi function and ε_k, ε_q are the energies of the initial and the intermediate states of the conduction electron.

In the second type of scattering process a background electron in the state q_- is first scattered to a state k'_+, and lowers the spin state of the solute atom by one unit. A second electron, in the state k_+, now scatters from the solute atom, ends up in the state q_- and the solute atom flips back to its original spin state. This process gives rise to the scattering

amplitude given by

$$- \frac{J^2 V_c}{N} \sum_q' \frac{f_q}{(\varepsilon_k + \varepsilon_q - \varepsilon_k' - \varepsilon_k)} \quad S^- S^+ \qquad 1.16$$

If the scattering is elastic then the initial and the final states k and k' have the same energy, that is $\varepsilon_k = \varepsilon_{k'}$. The sum of the two scattering amplitudes gives:

$$\frac{J^2 V_c}{N} \left\{ \sum_q' \frac{1}{\varepsilon_k - \varepsilon_q} + \sum_q' \frac{f_q [S^- S^+]}{\varepsilon_k - \varepsilon_q} \right\} \qquad 1.17$$

The first term is the usual result for the scattering amplitude in the second Born approximation. The second term gives a non-zero contribution because the spin operators S^- and S^+ do not commute. At T=0, the summation can be easily performed

$$\frac{1}{N} \sum_q' \frac{f_q}{\varepsilon_k - \varepsilon_q} \simeq \nu(\varepsilon_F) \int_0^{\varepsilon_F} \frac{d\varepsilon}{\varepsilon_k - \varepsilon} = -\nu(\varepsilon_F) \ln \frac{\varepsilon_k - \varepsilon_F}{\varepsilon} \qquad 1.18$$

This is the logarithmic divergence found by Kondo. A proper calculation shows that this gives rise to a $N(o)Jc \ln (T)$ term in the resistance.

For negative J, the magnetic contribution to resistance increases with decreasing temperature which, combined with the phonon contribution, gives a minimum in the total resistance at some temperature T_{min}. This result explained the long standing anomaly of the resistance minimum found in many alloys (17).

The s-d interaction Hamiltonian was further investigated by several people (12), (13), (14) who found that this interaction could lead to a bound state between the localised impurity and the conduction electrons below a temperature $T_k = T_F \exp(1/|J|\rho)$ if the coupling of the local spins to the conduction electrons spins is antiparallel. This antiferromagnetic coupling of the conduction electrons leads to a spin compensation of the local moment.

The equivalence between the Anderson Hamiltonian and the s-d interaction Hamiltonian used by Kondo has been demonstrated by Schrieffer and Wolff (15). They have shown that when $U/\Delta \gg 1$ the Anderson Hamiltonian can be transformed into a form similar to s-d interaction Hamiltonian. They consider the Hamiltonian H as made of two parts

$$H = H_o + H_{kd}$$

where H_o consists of $H_k + H_d$, the Hamiltonians for the conduction band and the d states respectively, and H_{kd} is the Hamiltonian representing the mixing between the conduction electrons and the localised d state. H is transformed to $\tilde{H}$ where

$$\tilde{H} = e^{S} H e^{-S}$$
$$= H_o + \left[H_1 + \left[H_o, S\right]\right] + \left\{\left[H_1, S\right] + \tfrac{1}{2}\left[\left[H_o, S\right], S\right]\right\} \quad 1.19$$

and S is chosen such that

$$H_1 + \left[H_o, S\right] = 0$$

which eliminates H_1 to first order from H. The leading interaction term in the resultant Hamiltonian is H_2 where

$$H_2 = \tfrac{1}{2}\left[H_1, S\right]$$

This term is second order in H_1. It can be expressed as a sum of four terms, the important one of these being an exchange term whose interaction constant, for k & k' $\simeq k_F$, is given by

$$J_{k_F k_F} = J_{eff} = -2\left|V_{k-d}\right|^2 \frac{U}{\varepsilon_d(\varepsilon_d + U)} \quad 1.20$$

which is negative, representing an antiferromagnetic exchange between the conduction electrons and the d state spin. This

antiferromagnetic J_{eff} arising from V_{kd} had been pointed out earlier by a number of workers including Kondo, de Gennes, Anderson and Clogston.

Doubts on the validity of the Hartree Fock treatment of Anderson Hamiltonian have been raised by Schrieffer and Mattis (18). They argue that under the condition $U/\Gamma > 1$ it is unreasonable to consider one electron as interacting with an average number of others, and that correlation effects must be taken into account. When the interaction time $\hbar/U$ is smaller than the time $\hbar/\Gamma$ required for electrons to hop on or off the impurity, an electron on the impurity feels the instantaneous potential of the particular ionization state of the impurity at the time. These large fluctuations possible in the Hartree-Fock approximation are physically unreasonable. Correlation effects which keep the charge state of the ion neutral are important. These have the effect of keeping electrons apart in the unpolarised state. The additional energy upon spin polarization is therefore smaller than that calculated in the Hartree-Fock approximation. They find that for a single, partly occupied d state orbital, the correlation energy tends to prevent the appearance of a moment!

However, if there are two or more degenerate localised d orbitals on the impurity with probability of occupation by two or more electrons, (so that Hund's rule is operative) the localised moment formation is easier.

Expressions based on the theoretical models for localised moment have been derived by many authors for macroscopic properties like magnetic susceptibility, electrical resistivity, specific heat, thermo power, etc. Some expressions for magnetic susceptibility and electrical resistivity are reviewed below.

Magnetic Susceptibility

Scalapino (19) has used Anderson's single non-degenerate d orbital model to derive an approximately Curie-Weiss behaviour of the susceptibility. The H_{kd} term in the Hamiltonian is treated as a perturbation in calculating successive order terms in the expansion of the free energy

$$F = - kT \ln Z \qquad 1.21$$

where Z is the partition function. The susceptibility is given by

$$\chi = -(\partial^2 F/\partial H^2)_{H=0} \qquad 1.22$$

The zero order susceptibility is

$$\chi^0 = \chi_p + \mu^2/kT \qquad 1.23$$

where χ_p is the temperature independent conduction band contribution and μ^2/kT is the contribution from a non-interacting impurity. The lowest order correction is from a term second order in V. This gives

$$\chi^{(2)} = (\mu^2/kT)\, N(o)J \qquad 1.24$$

where N(o) is the density of states at the Fermi level and J is the exchange interaction constant given by Eq. 1.20.

The next order correction is a term fourth order in V. This gives a contribution

$$\chi^{(4)} = -(\mu^2/kT)\left[N(o)J\right]^2 \ln (kT/W) \qquad 1.25$$

The terms up to fourth order in V give a total contribution to χ of

$$\chi = \chi_p + \mu^2/kT \left\{1 + N(o)J + \left[N(o)J\right]^2 \ln\left(\frac{kT}{W}\right)\right\} \qquad 1.26$$

Scalapino argues that if higher order terms of the form

$$\mu^2/kT\ N(o)J \left[N(o)J \ln (kT/W)\right]^n$$

are included, the susceptibility can be written as

$$\chi \sim \chi_p + \mu^2/kT \left\{1 + \frac{N(o)J}{1-N(o)J \ln (kT/W)}\right\} \qquad 1.27$$

The solution diverges when

$$kT = W \exp (1/N(o)J) \quad (\text{where } W = kT_F) \qquad 1.28$$

giving an unphysical result.

By substituting Eq. 1.28 in Eq. 1.27 the result can be rewritten as

$$\chi \sim \chi_p + \mu^2/kT \left[1 - 1/\ln (T/T_k)\right] \qquad 1.29$$

The susceptibilities given by Eq. 1.26 and Eq. 1.29 are shown in Fig. 1 for a few parameters $N(o)J$ and T_k. It appears that Eq. 1.26 is qualitatively in better agreement with the type of susceptibility behaviour observed in systems like Cu-Fe (26) and Rh-Fe (25) than Eq. 1.29.

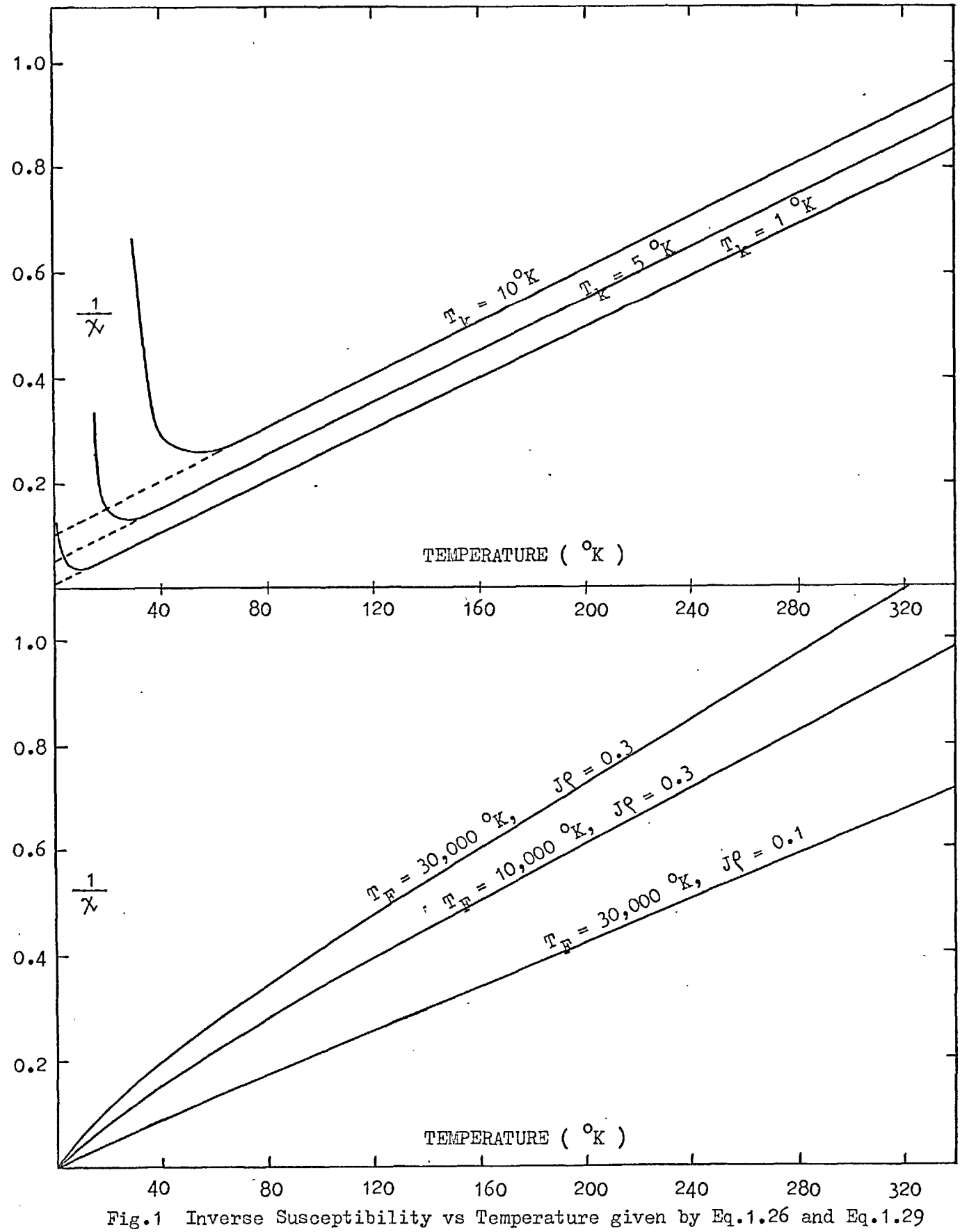

Fig.1 Inverse Susceptibility vs Temperature given by Eq.1.26 and Eq.1.29

Yosida and Okiji (20) have calculated the temperature dependence of a localised moment in the s-d interaction model using Rayleigh-Schroedinger perturbation theory. The moment $\langle S_z \rangle$ is expanded in terms of the s-d perturbation

$$\langle S_z \rangle = S_z + \langle S_z \rangle^{(2)} + \langle S_z \rangle^{(3)} + \langle S_z \rangle^{(4)} \qquad 1.30$$

where zeroth order term is S_z, and first order term vanishes. The second order term is calculated to be

$$\langle S_z \rangle^{(2)} = 2S_z(\rho J/2N)^2 \ln (kT/D) \qquad 1.31$$

where $\rho \equiv N(o)$ the density of states, and $J/2N \equiv J_{eff}$

The first two terms therefore give a total contribution of

$$\langle S_z \rangle = S_z(1 + 2(\rho J/2N)^2 \ln (kT/D)) \qquad 1.32$$

Inclusion of contributions from all the other terms gives

$$\langle S_z \rangle = S_z\left[1 - N(o)J + N(o)J\left(1 + \frac{N(o)J}{2} \ln (kT/D)\right) + \ldots\right]$$

$$= S_z\left[1 - \frac{\rho J}{2N}\left(1 - 1/\left[1 - \frac{\rho J}{N} \ln (kT/D)\right]\right)\right] \qquad 1.33$$

This result shows that the average z component of the moment is reduced. However it is not clear what form of susceptibility behaviour can be obtained from this analysis.

Nagaoka (12) has attempted to analyse the Kondo problem by using an equation of motion method employing a decoupling scheme for double time Green functions. He has derived an expression for χ for the case where the g factors of the local moments and conduction electrons are equal. It is given by

$$\chi = (g^2\mu_B^2/3T)\left[S(S+1)\,(1+\Gamma/2) + \langle S \cdot s_e \rangle\right] \qquad 1.34$$

Hamann (13) has evaluated this expression and finds that for $T \gg T_K$

$$= \chi_o\left[1 - \ell n^{-1}\,(2T/T_K)\right] \qquad 1.35$$

where $\chi_o = C/T$ is the susceptibility of the free spin.

Another calculation of the susceptibility has been made by M. S. Fullenbaum and D. S. Falk (23), using the s-d interaction model. They calculate the free energy F of the system to order J^2. Again the second derivative of F with respect to field H gives

$$\chi(J) - \chi(o) = (J\rho/N)\,\frac{2g\mu_B^2\,S(S+1)}{3kT}\left[1+\frac{J\rho g}{2N}\,\ell n\left(\frac{\pi k T}{2VD}\right)\right] \qquad 1.36$$

This can be rewritten as

$$\chi = \frac{C}{T}\left[1+2(J\rho/N) + (J\rho/N)^2\,\ell n\left(\frac{T}{T_K}\right)\right] \qquad 1.37$$

Apart from the differences in the various expressions for the high temperature magnetic susceptibility there is a divergence of view among many authors about the behaviour of susceptibility at temperatures approaching zero. Some authors (21), (22) have suggested that the moment should be completely compensated so that the initial susceptibility at T=0 is finite. (A value of $\chi = \mu_B^2/3kT_K$ has been suggested (22).) Others (21) argue that as the moment is continuously reduced, the susceptibility increase will still diverge at T = 0. Measurements on Mo-Co (25) and Cu-Fe (26) are shown to support this view, but those on Rh-Fe and Ir-Fe (25) are thought to indicate a finite susceptibility.

Electrical Resistivity

An expression for resistivity having a logarithmic divergence was first derived by J. Kondo (8) as mentioned previously. The total resistivity of a dilute alloy is shown to be

$$\rho = \rho_L + c\rho_A + c\rho_M (1 + (3zJ/\epsilon_F) \ln T) \qquad 1.38$$

where ρ_L is the lattice term, ρ_A is the potential scattering by the impurity. ρ_M is the spin dependent magnetic scattering

c is the concentration of impurities, z the number of conduction electron per atom and $\mathcal{E}_F$ is the Fermi energy.

Subsequently more refined treatments of the Kondo problem have been attempted. Expressions showing an increase of resistance with decreasing temperature are obtained but the divergence at T=0 has been removed. Hamann (12) shows that the expression for magnetic contribution to resistance $\Delta\rho$ is

$$\Delta\rho = \frac{2\pi c}{ne^2 k_F}\left\{1-\ln\,(T/T_K)\left[\ln^2\left(T/T_K\right)+S(S+1)\pi^2\right]\right\} \qquad 1.39$$

where the symbols have the usual meaning.

Recently a series of articles have been published by Suhl (27) and others (29), (30) reporting calculation of resistivity and susceptibility for dilute alloys. They use the standard many body perturbation theory applied to a model of a degenerate electron gas described by a Hamiltonian consisting of kinetic energy, Coulomb interaction and structureless impurity potential V. This is similar in some ways to the Wolff model of local moment formation but the treatment is beyond the Hartree-Fock approximation. The authors have published graphs of the resistivity and susceptibility which have been redrawn in Fig. 2 in familiar co-ordinates. These clearly show that the observed behaviour of dilute alloys can also be explained by a model different from Kondo's s-d interaction.

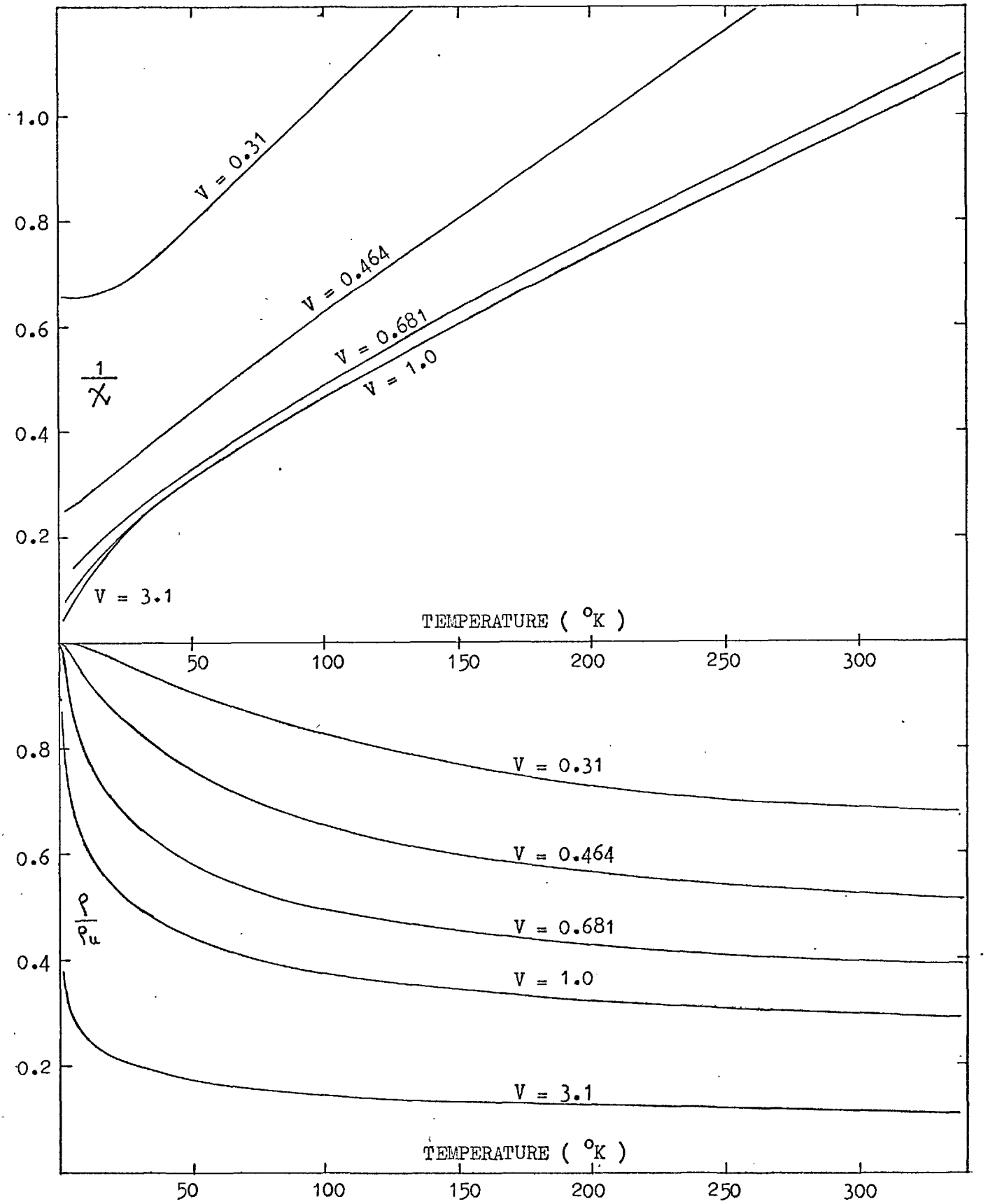

Fig.2 Resistivity and Inverse Susceptibility vs Temperature (After Suhl & Others)

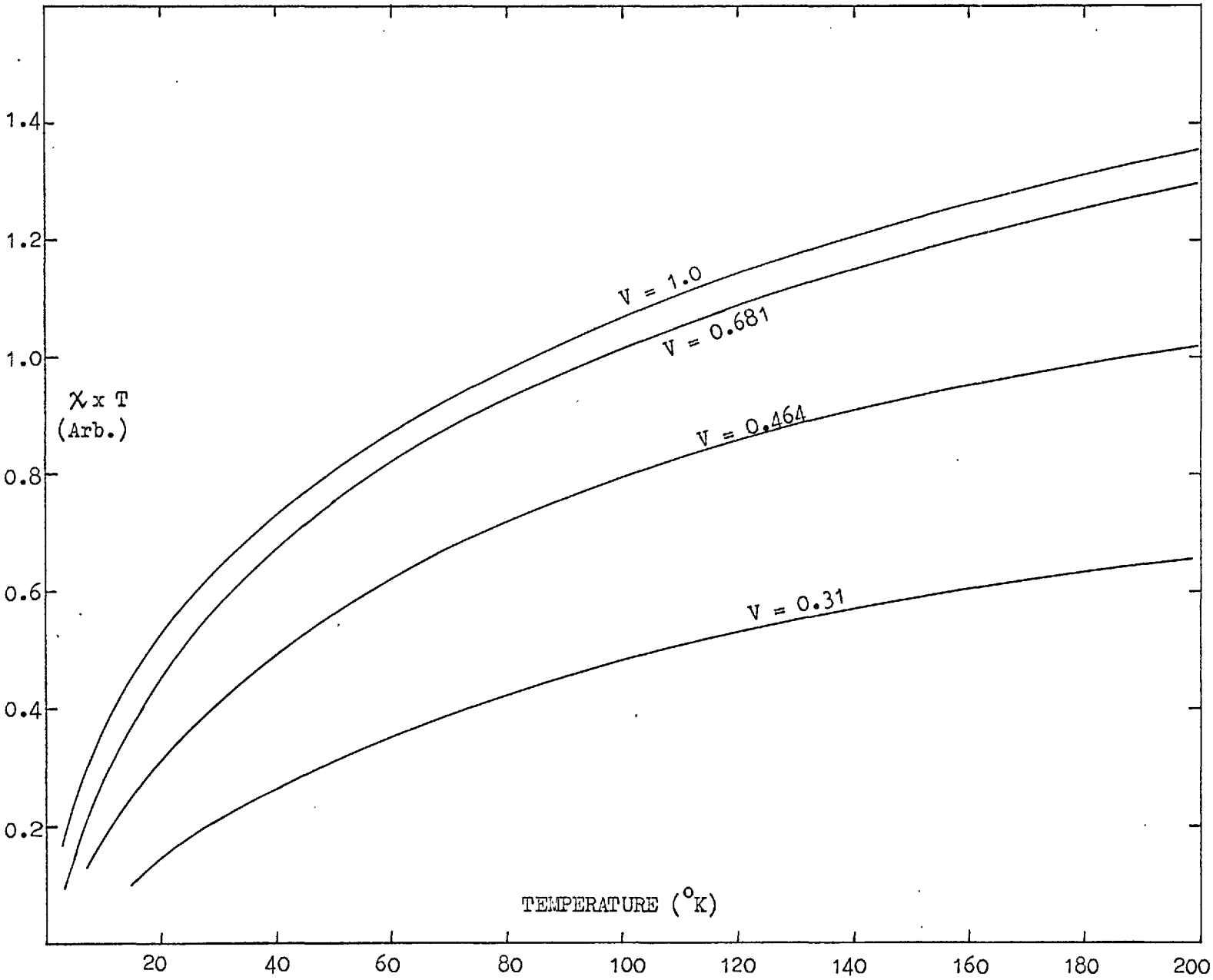

Fig.3 (Susceptibility) x (Temperature) vs Temperature (After Levine & Suhl)

CHAPTER 2

THE EFFECT OF CRYSTALLINE FIELDS ON THE PROPERTIES OF DILUTE ALLOYS

1. 3d Transition Series Atoms

The magnetic moment of a 3d transition series solute atom in a metallic matrix is considered to be due to the difference in the spin angular momentum of the two spin states of the virtual bound level. The orbital angular momentum of the d state is quenched so that only the spin angular momentum contributes to the moment. This assumption is found to be valid to a good approximation in most cases. Anderson (2), in his treatment of the localised magnetic states in metals, has pointed out that this quenching of the orbital angular momentum is the result of the interaction of the d state with the band electrons. In the discussion of the orbitally degenerate localised level, he has derived the condition for the Hartree fields for the two orbitally degenerate states to become different, and has suggested that the quenching of the orbital angular momentum results under certain conditions.

Even in the absence of the s-d interactions as say in insulators, the large crystal fields experienced by the extended d state wave functions can lead to quenching of the orbital angular momentum. In such systems the crystal field energies are about two orders of magnitude larger than the spin-orbit interaction so that the L-S coupling breaks down. The crystal field lifts the degeneracy of the 3d state, often leaving an orbitally non-degenerate ground state with the result that the orbital angular momentum is quenched. This can be understood in terms of the following argument.

The Hamiltonian for the system is real, so that in the absence of a magnetic field the wave function for the non-degenerate groundstate is real. The expectation value for the z component of the angular momentum L_z is

$$\langle L_z \rangle = \langle 0 | L_z | 0 \rangle \qquad 2.1$$

where 0 is the orbitally non-degenerate ground state described by the wave function U_o, and the angular momentum operator is given by

$$\hat{L}_z = \frac{\hbar}{i} \left(x \frac{\partial}{\partial y} - y \frac{\partial}{\partial x} \right) \qquad 2.2$$

Now

$$\langle 0|\hat{L}_z|0\rangle = \frac{\hbar}{i}\int U_o^*\left(x\frac{\partial}{\partial y} - y\frac{\partial}{\partial x}\right) U_o \, d\tau \qquad 2.3$$

All the quantities inside the integral are real so that $\langle L_z\rangle$ is a pure imaginary quantity unless the integral vanishes. But $\langle L_z\rangle$ must be real, the integral must therefore vanish, and $\langle L_z\rangle = 0$. Similarly it can be argued that

$$\langle 0|L_x|0\rangle = \langle 0|L_y|0\rangle = 0$$

Hence the orbital angular momentum is quenched.

The spin-orbit interaction will of course mix in some orbital angular momentum into the state with the result that the magnetic moment cannot be simply described by a quantum number S with a g value of 2. The difference of the g value from 2 is a measure of the orbital angular momentum component in the state. Application of a magnetic field also causes a g shift proportional to the field due to an admixture of the higher states into the ground state, resulting in a small net circulation of charge in the state. In a metal, of course, the applied field produces a g shift due to the polarisation of conduction electrons which interact with the local moment.

2. The Rare Earth Atoms

The 4f shell of a rare earth atom is well localised and tightly bound inside the ion core, hence considerable shielding from interactions with the matrix is provided by the outer closed shells of electrons. The interaction between the 4f shell electrons and the conduction band of the matrix is smaller than the s-d interaction between the 3d state and the conduction electrons. The L-S coupling is, however, stronger in the rare earth atoms than in the 3d transition series atoms because of the greater charge on the nucleus. The effect of the crystal field of the matrix on the magnetic shell of the rare earth is also smaller than on the 3d shell of the first transition series atoms. In a non-metallic matrix, the crystal field is normally regarded as arising from the charge sources on the lattice sites surrounding the ion. These charges are, however, screened by the conduction electrons in a metal so that the origin of the crystal fields in a metal is not very obvious. The magnetic properties such as the magnetic susceptibility (72), (67) and electron spin resonance (134) of gold and silver-rare earth alloys are explained quite well by the crystal field theory. However, the crystal field parameters (see below) required to explain the observed effects are very

much larger than obtained by calculations assuming point charge sources. The signs of the parameters, too, do not agree with the point charge model.

A conjecture on the possible origin of the crystal fields in metals has been made by Orbach (147). He suggests that the d wave functions of the Bloch states carry the symmetry of the lattice. The polarisation resulting from the overlap of the d states with the f shell gives rise to the crystal fields observed. Coles (135) and Doniach (136) have recently suggested that the conduction electrons can couple the symmetry of the matrix to the magnetic shell through a mixing interaction V_{kf}, similar to Anderson's V_{kd} interaction (2). The actual mechanism giving rise to the crystal field in Doniach's work is, however, different from that considered by Anderson in the quenching of the orbital angular momentum of the virtual bound state.

The Hamiltonian for Rare Earths

The Hamiltonian for a rare earth atom in a crystal lattice in the absence of a magnetic field can be written in the non-relativistic approximation as

$$H = \sum_i \left(\frac{Pi^2}{2m} + \frac{Ze^2}{r_i} \right) + \sum_{\substack{i,j \\ i \neq j}} \frac{e^2}{r_{ij}} + \underline{L} \cdot \underline{S} + \left[V \right] \qquad 2.4$$

where the first term is the kinetic energy of the electrons, the second is the coulomb interaction energy of the electrons with the nucleus. The third term is the electrostatic repulsion between the electrons. The fourth term is the spin-orbit interaction. It is assumed that Hund's rules are obeyed in determining the angular momentum quantum numbers L and S. The spin orbit coupling is sufficiently strong so that the quantum state of the atom is defined by the total angular momentum quantum number J. The last term V is the crystal field interaction energy, in the absence of which the eigen-states of the ion are 2J+1 fold degenerate and are denoted by the eigen vectors $|J,J_z\rangle$. The crystal field $[V]$ is treated as a perturbation to the free ionic energy, with spin-orbit as the main first order interaction.

In a metallic matrix the exchange and the mixing interaction between the conduction electrons and the 4f shell are also present and must be formally included in the Hamiltonian. The exchange interaction, however, does not modify the observed crystal field effects. The mixing interaction V_{kf} may be thought of as included in the crystal field potential $\left[V \right]$. It has

also the effect of broadening the energy levels of the ion, but this does not affect the quantitative behaviour of the ion calculated from crystal field theory assuming no such broadening.

The Treatment of the Crystal Field Interaction

The usual treatment of the crystal fields assumes that the electrostatic potential V at the ion site is due to charge sources on lattice sites surrounding the ion. Since the charge sources are external to the ion, the potential satisfies the Laplace equation

$$\nabla^2 V = 0 \qquad 2.5$$

The solutions of this equation are the generalised Legendre polynomials. The potential V can therefore be expanded in terms of the polynomials as

$$V = \sum_{n} \sum_{m=n}^{-n} \sum_{k} A_n^m \, r^n \, Y_n^m (\theta_k, \phi_k) \qquad 2.6$$

The number of terms in the expansion is limited to terms up to n=6, for the rare earth atoms. This is because the wave functions of the 4f orbital are also expressed in terms of the

spherical harmonics as

$$\psi_{\lambda}^{m} = A\, R(r)\, Y_{\lambda}^{m}(\theta,\phi) \qquad 2.7$$

where R(r) is the radial part of the wave function and $Y_{\lambda}^{m}(\theta,\phi)$ is its angular dependence, A is a normalisation constant.

The matrix elements of the interaction are of the form

$$\langle \psi_{\lambda}^{m'} | V_{n}^{m} | \psi_{\lambda}^{m''} \rangle$$

which are zero for all V_{n}^{m} with $n>2\lambda$.

The symmetry of the crystal field reduces further the number of terms in the expansion. The requirement of invariance of the matrix elements under inversion ($x\to -x$, $y\to -y$, $z\to -z$) eliminates all terms with odd n. This is because the product $\psi_{\lambda}^{m*}\psi_{\lambda}^{m}$ remains unchanged through inversion, whereas the potential $V = \sum_{n,m} V_{n}^{m}$ changes sign. Similarly, other cubic symmetry operations remove some of the terms with other n values. Neglecting the term with n=0, which is constant and shifts all the levels of a given configuration by the same amount, the cubic crystal field potential can be written as (137)

$$V = -D_4\left[\frac{14}{9}Y_4^0 + \frac{1}{9}(70)^{\frac{1}{2}}(Y_4^4 + Y_4^{-4})\right] + D_6\left[\frac{8}{9}Y_6^0 + \frac{4}{9}(14)^{\frac{1}{2}}(Y_6^4 + Y_6^{-4})\right] \qquad 2.8$$

where $$D_4 = \frac{Ze^2 r^4}{a^5 (4\pi/9)^{\frac{1}{2}}}$$

and $$D_6 = \frac{Ze^2 r^6}{a^7 (4\pi/13)^{\frac{1}{2}}} \qquad 2.9$$

where Z is the effective nuclear charge and a is the Bohr radius.

An analysis of the crystal field interaction was first attempted by Bethe (138), who showed that group theoretical arguments can be used to predict the multiplicities of the various crystal field split levels. A basis for the quantitative calculations has been laid down by Stevens (139) who developed an operator equivalent technique in which the terms in the expansion of the electrostatic potential are replaced by suitable angular momentum operators which transform in the same manner. Lea, Leask and Wolff (140) have published the results of their computer calculations of the crystal field levels for the whole series of rare earth atoms. They have calculated the eigen states and eigen values of the crystal field split levels as a function of two parameters which define the magnitude of the crystal field energy. They write the electrostatic potential as

$$H = B_4(O_4^0 + 5O_4^4) + B_6(O_6^0 - 21O_6^4) \qquad 2.10$$

where the terms in the Hamiltonian are given by their operator equivalents as

$$O_4^0 = 35J_z^4 - [30J(J+1)-25]J_z^2 - 6J(J+1)+3J^2(J+1)^2$$

$$O_4^4 = \tfrac{1}{2}(J_+^4 + J_-^4)$$

$$O_6^0 = 231J_z^6 - 105[3J(J+1)-7]J_z^4 + [105J^2(J+1)^2 - 525J(J+1)+294]J_z^2$$
$$- 5J^3(J+1)^3+40J^2(J+1)^2-60J(J+1)$$

$$O_6^4 = \tfrac{1}{4}[11J_z^2 - J(J+1)-38](J_+^4 + J_-^4)+\tfrac{1}{4}(J_+^4+J_-^4)\,[11J_z^2 - J(J+1)-38]$$

2.11

The coefficients B_4 and B_6 are linear functions of $\langle r^4 \rangle$ and $\langle r^6 \rangle$, the mean fourth and sixth powers of the radii of the magnetic electrons. These quantities are difficult to calculate exactly, hence they are used as parameters in the calculation. The magnitudes and signs of B_4 and B_6 control the overall splittings of the levels.

The calculation of the crystal field levels is fairly straightforward. Using as the basis functions the set of degenerate eigen-states $|J,J_z\rangle$ of the free ion, the (2J+1)x(2J+1)

matrix is written down. The matrix elements have been tabulated by Stevens (139), and Elliot and Stevens (141). The form of the Hamiltonian suggests that only the states with J_z values different by 4 are coupled by the interaction. The matrix is diagonalised on a computer to obtain the eigen states and the eigen values. (An I.B.M. share program subroutine 'Mitres' is used for the diagonalisation). The splittings and degeneracies of the various levels and especially of the ground state is found to follow two distinct patterns depending on whether the angular momentum J is integral or half integral. The effect of the crystal field on an S state ion (orbital angular momentum L=0) is very small.

Half Integral J

The crystal field splitting of energy levels of an ion with an odd number of electrons obeys Kramer's theorem (142) which states that, 'there will always be at least a two-fold degenerate state in the presence of electric fields of any symmetry, provided the ion has an odd number of electrons'. Wigner (143) has shown that this is the direct result of the invariance of the Hamiltonian under time reversal (in the absence of magnetic fields). If K is a time reversal operator such that,

$$KH(\underline{r},\underline{p},\underline{s})K^{-1} = H(\underline{r},-\underline{p}-\underline{s}) \qquad 2.12$$

and ψ and $\psi' = K\psi$ are the wave functions corresponding to $H(\underline{r},\underline{p},s)$ and $H(\underline{r},-\underline{p},-s)$. Then it can be shown that ψ and ψ' are necessarily independent when n, the number of electrons in the shell, is odd. Hence the energy states corresponding to ψ and ψ' are always degenerate.

The eigen-vectors describing the sub-levels transform in the same way as the irreducible representation Γ_i of the cubic group, where i can take the values 6, 7, 8 as in Bethe's notation. These representations have the degeneracies 2,2 and 4 respectively.

Integral J

When an ion has an even number of electrons, the cubic field gives rise to a series of sub levels which have the symmetry of the irreducible representations Γ_i, i=1, 2, 3, 4 and 5 of the cubic group. In crystal fields of such high symmetry, the ground state may often be degenerate. However, there is a restriction on the degeneracy of the ground state as given by the Jahn-Teller theorem (144). This states that 'with the exception of linear molecules and systems which have Kramer's degeneracy, a degenerate ground state is not stable and the

degeneracy is removed by the displacement of the neighbouring nuclei' (which lowers the symmetry of the field). The physical reason for this effect is simple. If a perturbation removes the degeneracy by splitting the levels, one of the levels will have a lower energy than the unsplit level (since the centre of gravity of the levels must be unchanged). Hence, there will be a tendency for the ion to assume the lowest energy state by distortion of its environment.

S State Ions

For ions such as Gd^{3+} and Eu^{2+} which have an exactly half-filled f shell, the ground state is an orbital singlet (L=0). The degeneracy of the energy levels of such ions can not be removed by the crystal field or the spin orbit interaction alone. Van Vleck and Penney (148) have suggested that higher order perturbation involving simultaneously the crystal field and the spin-orbit coupling are necessary to split the S state. An overall splitting of about $0.1^{\circ}K$ has been suggested for Gd (137).

The effect of the crystal field splitting of energy levels of rare earth ions will manifest itself in the modification of the 'normal' behaviour of many macroscopic properties including the magnetic susceptibility and the electrical resistivity of alloys containing them. The magnetic susceptibility shows departures from a Curie law which is observed in dilute alloys such as Au-Gd containing the S state ion. Also there is an extra contribution to the electrical resistance due to the inelastic scattering between the crystal field split levels. These two properties of the alloys are discussed below.

Magnetic Susceptibility

The contribution to the magnetic susceptibility of an ion is from two sources, the permanent magnetic moment μ_i of the various states of the ion and the induced moments due to the applied magnetic field.

Application of a magnetic field causes the polarisation of a level. The polarisability α_i is given by

$$\alpha_i = 2\mu_B^2 g_J^2 \sum_j \frac{|\langle i|J_z|j\rangle|^2}{(\varepsilon_i - \varepsilon_j)} \qquad 2.13$$

The magnetic moment μ_i of a state is

$$\mu_i = g_J \mu_B \langle i | J_z | i \rangle \qquad 2.14$$

If the energies of the various states are ε_i, then the partition function Z is

$$Z = \sum_i \exp(\varepsilon_i / kT) \qquad 2.15$$

The susceptibility is then (145)

$$\chi = \frac{N}{Z} g_J^2 \sum_i \left\{ \mu_B^2 \frac{|\langle i | J_z | i \rangle|^2}{kT} \exp(-\varepsilon_i / kT) + \sum_j 2\mu_B^2 \frac{|\langle i | J_z | j \rangle|^2}{(\varepsilon_i - \varepsilon_j)} \exp(-\varepsilon_i / kT) \right\} \qquad 2.16$$

The second term is often referred to as the Van Vleck susceptibility.

Having obtained all the eigen-states and eigen-values by the diagonalisation of the crystal field Hamiltonian, this expression is used in the computation of the susceptibility. For high temperatures the expression can be simplified further. The departures of the susceptibility from a Curie law can be expressed as

$$\chi = \frac{C}{T + \Delta} \qquad 2.17$$

where Δ is a pseudo Curie-Weiss constant which is in fact a

function of temperature. It will be zero at temperatures very high compared to the overall splitting of the energy levels of the ion. At temperatures of the order of the crystal field splitting, Δ can be finite. At very low temperatures, when only the ground state has a finite Boltzmann probability of occupation, Δ again becomes very small.

If the ground state of an ion is a well isolated non-magnetic singlet, the contribution to the susceptibility from the first term in Eq. 2.15 is small. The second term called the Van Vleck term, gives the major contribution and the temperature dependence of χ is fairly small.

Electrical Resistance

A recent calculation of the resistivity due to s-f interaction in dilute rare earth alloys has been given by Hirst (146). The Hamiltonian for the interaction is written as

$$H_{s-f} = V_c - 2(g_J-1)\, J_{ex}\, \underline{J}\cdot\underline{s} \qquad 2.18$$

where V_c is the spin independent coulomb scattering term, J_{ex}

is the exchange interaction constant, g_J is the Lande g-factor for the free ion, $\underline{J}$ is the total angular momentum of the ion and $\underline{s}$ is the spin of the conduction electron.

The resistivity is calculated using the Boltzmann equation. Suppose f(k,m) describes the distribution function for the electron of wave-vector k and z-component of angular momentum $m(=\pm\frac{1}{2})$, the rate of change of f(k,m) with time due to interaction of the electrons with the rare earth ions is given by

$$\left.\frac{\partial f(k,m)}{\partial t}\right|_{\text{coll.}} = \sum_{m'} \int \frac{d^3k'}{(2\pi)^3} \Big\{ W(k;m' \; ; \; k,m) f(k',m') \Big[1-f(k,m)\Big] - W(k,m \; ; \; k;m) f(k,m) \Big[1-f(k;m')\Big] \Big\} \qquad 2.19$$

where the transition rate W(k,m ; k;m') is given by the time dependent perturbation theory

$$W(k,m;k;m') = c\,\frac{2\pi}{\hbar} \sum_{ii'} \left|\langle k,m,i \left| H_{s-f} \right| k;m;i' \rangle\right|^2 \exp(-\varepsilon_i/kT) \times \delta(E_{k,m} - E_{k;m'} + \Delta_{i,i'}) \qquad 2.20$$

where $\Delta_{i,i'}$ is the energy difference between the core states due to the crystal field splitting. Many of the core states are degenerate so that the $\Delta_{i,i'}$ are zero for these. In the

presence of an external magnetic field, the $\Delta_{i,i'}$ also include the splitting due to the field. The energy of the conduction electrons $E_{k,m}$ is given by

$$E_{k,m} = E_k + 2\mu_B mH \qquad 2.21$$

The current relaxation rate for the collisions is

$$\frac{1}{\tau} = \frac{1}{j}\left(-\frac{\partial j}{\partial t}\right)_{coll.} \qquad 2.22$$

The calculation yields

$$\frac{1}{\tau} = c\,\frac{2\pi}{\hbar}\,N_E^{(1)} \int \frac{d\Omega'}{4\pi} \int \frac{d\Omega'}{4\pi}\; 3\,(\eta-\eta') \sum_{i,i} \exp(\varepsilon_i/kT)\,\frac{\Delta_{i,i'}}{kT} \times$$

$$\left[e^{\Delta_{i,i'}/kT} - 1\right] \times \tfrac{1}{2} \sum_{m,m'} \left|\langle k',m',i\left|H_{s-f}\right|k,m,i\rangle\right|^2 \qquad 2.23$$

where $\eta = \cos(\underline{k},\underline{\varepsilon})$, and $\underline{\varepsilon}$ is the applied electric field. $N_E^{(1)}$ is the density of states for one spin direction. The author considers the interference between the exchange and the potential scattering to be negligible and obtains the expression for the resistivity

$$\rho_{mag} = cR(g_J-1)^2 \sum_{ii} \exp(\varepsilon_i/kT)\,\frac{\Delta_{i,i'}/kT}{e^{\Delta_{i,i'}/kT}-1} \times \tfrac{1}{2}\sum_{mm'}\left|\langle m',i'\left|\underline{J}\cdot\underline{S}\right|m,i\rangle\right|^2 \qquad 2.24$$

where

$$R = \frac{m^*}{zN_v e^2} \frac{2\pi}{\hbar} N_E^{(1)} (2J_{ex})^2 \qquad 2.25$$

and m* is the effective mass of the conduction electrons N_v is the atomic density of the lattice in cm^{-3}. If kT is very much greater than the overall crystal field splitting then

$$\rho_{mag} = cR(g_J-1)^2 J(J+1)/4 \qquad 2.26$$

In the case where the ground state of the ion is a well isolated non-magnetic singlet, the inelastic spin scattering will be small. It will be small even for a magnetic ground state provided it is well isolated from other energy levels. In this case, the probability of scattering into the other states will be small.

CHAPTER 3

BASIC MECHANISMS FOR INTERACTIONS BETWEEN SOLUTE ATOMS

Introduction

The scattering of conduction electrons from the potential presented by a solute atom produces charge density oscillations of decreasing amplitude but fairly long range, as was shown by Friedel (5). The magnetic moment on the atom also introduces further scattering of conduction electrons through spin-spin or exchange interaction resulting in a spin polarisation of the band electrons. A second solute atom situated within the range of the spin polarisation set up will be influenced by the quantum state of the first atom. There is thus a resultant correlation between the spins of the two atoms, and is the main mechanism for interactions between solute atoms in dilute alloys.

Ferromagnetic coupling between atomic moments through a uniform polarisation of conduction electrons induced by exchange interaction with the atomic moment was suggested by Zener (9). A similar uniform polarisation of conduction electrons through interaction with nuclear spins was treated much earlier by Frohlich and Nabarro (32).

Kasuya (10) investigated the interaction between localised d electron spins on a solute atom and conduction electrons to second order perturbation, which gave a coupling between the atomic moments. This result was similar to that of Ruderman and Kittel (33) who had investigated the nuclear moment-conduction electron interaction to second order and explained the anomalous broadening of nuclear magnetic resonance linesin metals due to the indirect coupling of nuclear spins.

The s-d exchange interaction with the resultant oscillatory spin polarisation of conduction electrons was treated in detail by Yosida (11). He considered the first order perturbation to the free electron wave function which is written as

$$\phi_k = \phi_k^o + \sum_{k'} \frac{H_{kk'}}{E_k - E'_k} \phi_{k'}^o \qquad 3.1$$

where ϕ_k^o is plane wave $(1/V)^{\frac{1}{2}} e^{i\underline{k}\cdot\underline{r}}$ and $H_{kk'}$ is the s-d interaction Hamiltonian given by

$$H_{kk'} = - J(k,k') \underline{S}\cdot\underline{\sigma} \qquad 3.2$$

where $J(\underline{k},\underline{k}')$ is the exchange interaction constant which is a function of the wave vectors k and k'.

$$J(\underline{k},\underline{k}') = \langle \psi_d(\underline{r}_1)\phi^o_{\underline{k}}(\underline{r}_2) | V(\underline{r}_1,\underline{r}_2) | \psi_d(\underline{r}_2)\phi^o_{\underline{k}'}(\underline{r}_1) \rangle \qquad 3.3$$

where ψ_d is the localised wave function on the solute atomic site. $V(r_1,r_2)$ is the interaction potential which is usually the coulomb potential e^2/r_{12}. If $V(r_1,r_2)$ is approximated by a delta function, then $J(\underline{k},\underline{k}')$ becomes

$$J(\underline{k},\underline{k}') = \int dr_1 dr_2 \psi^*_d(\underline{r}_1)\, e^{i\underline{k}\cdot\underline{r}_2}\, \delta(\underline{r}_1-\underline{r}_2)\, \psi_d(\underline{r}_2)\, e^{-i\underline{k}'\cdot\underline{r}_1} \qquad 3.4$$

$$= \int dr\, \psi^*_d(\underline{r})\, \psi_d(\underline{r})\, e^{i(\underline{k}-\underline{k}')\cdot\underline{r}}$$

Thus $J(\underline{k},\underline{k}')$ depends only on the magnitude of $(\underline{k}-\underline{k}')$ and is written as $J(\underline{k}-\underline{k}')$ or $J(\underline{q})$. If, however, $V(\underline{r}_1,\underline{r}_2)$ is the coulomb potential e^2/r_{12}, it is not accurate to consider $J(\underline{k},\underline{k}')$ as a function of the magnitude of $(\underline{k}-\underline{k}')$.

In a real situation, of course, the range of the potential $V(r_1,r_2)$ is much shorter than that of the coulomb potential, e^2/r_{12}, because of the screening of the latter by other electrons. The approximation $J(\underline{k},\underline{k}') = J(\underline{k}-\underline{k}')$ is therefore not so bad and is generally assumed.

The polarisation of the conduction electrons spins is easily obtained from the first order perturbed wave function.

It can be written as

$$\rho_{\pm}(r) = \rho_o\left\{1 \mp \frac{3}{8E_F N} \int_o^{\infty} dq\ J(q)f(q)S^z\left[\exp(iq\cdot r)+\exp(-iq\cdot r)\right]\right\} \qquad 3.5$$

where ρ_o is the mean conduction electron density, N the number of lattice points, E_F the Fermi energy and f(q) is the susceptibility function, also known as the dielectric function or Lindhard function and is given by

$$f(q) = 1 + \frac{4k_F^2 - q^2}{4k_F q} \ln\left[\frac{2k_F+q}{2k_F-q}\right] \qquad 3.6$$

The first derivative of the function has a pole at $q=2k_F$ which is the result of the sharpness of the Fermi surface.

The exact form of the final expression after integration over q, depends on the assumed variation of J(q) with q. If J(q) is taken constant, equal to J(o), the result for the spin density becomes,

$$\rho_{\pm}(r) = \rho_o\left\{1 \mp \frac{18\pi}{E_F}\left(\frac{n}{N}\right) J(o)S^z F(2k_F r)\right\} \qquad 3.7$$

where the function F(x) is defined as

$$F(x) = \frac{x\cos x - \sin x}{x^4} \qquad 3.8$$

The same function has been obtained by Friedel in his potential scattering calculation. It was also obtained by Ruderman and Kittel (33).

The result 3.7 is known as the R.K.K.Y. spin polarisation. The spin density $\rho_{\pm}(r) \longrightarrow \infty$ as $r \longrightarrow 0$ which is the direct result of assuming $J(q)=J(o)$ for all values of q. However, J(q) must decrease with increasing q. Yosida therefore considers the approximation

$$J(q)f(q) = 2J(o) \quad \text{for} \quad q < 2k_F$$

$$= 0 \quad \text{for} \quad q > 2k_F$$

and obtains for spin polarisation

$$\rho_{\pm}(r) = \rho_o \left[1 \mp \frac{36}{E_F} \frac{n}{N} J(o) S^z F(2k_F r) 2k_F r\right] \qquad 3.9$$

which has a finite value at $r=R_n$

The interaction energy between two solute atoms coupled through R.K.K.Y. interaction is given by

$$E(R) = 18\left(\frac{n}{N}\right)^2 \frac{J^2}{E_F} \underline{S}_1 \cdot \underline{S}_2 \; F(2k_F R)$$

In the derivation of the R.K.K.Y. spin polarisation, the conduction electron states are considered as plane waves. The conduction electrons therefore have an infinite mean free

path. In a real case, however, this will not be so because of the normal scattering of conduction electrons by impurities, defects, phonons and similar causes. In an equivalent sense, the result of the scattering is to smear out the Fermi surface which is assumed to be sharp in the above derivation. De Gennes (31) has considered the magnetic order in the rare earth metals through R.K.K.Y. interaction and points out that as the temperature is increased from a very low value the interaction between the atoms will be modified by the scattering of conduction electrons from the spin-waves, with the result that the wavelength of the spiral ordered structure will change. In general, the R.K.K.Y. interaction will be modified by all scattering processes which reduce the mean free path of the electrons.

Overhauser (35) in his spin density wave treatment of the local moment-conduction electron interaction has considered the form factor approximation for $J(q)$. From Eq. 3.4 it follows that $J(q)$ can be written as $J(o)f(q)$, where $f(q)$ is the atomic form factor which is the Fourier transform of the finite spatial distribution of the localised spin. If this form factor approximation is used in the evaluation of Eq. 3.5, a spin polarisation of a different form from the two results quoted above is obtained.

Watson and Freeman (36) have evaluated J(q) by treating the exchange integral between a 4f wave function of a Gd atom and orthogonalised plane waves localised on the Gd site representing the conduction electrons. They restricted the range of q to small values by considering scattering in the region around the Fermi surface (small q values determine the spin density at a distanee from the atom). The form of the spin polarisation they obtain is quite different from R.K.K.Y. or that obtained using the form factor approximation. The maximum in the spin density is at about 2Å units from the solute atom and not at the centre of the atomic site as in the R.K.K.Y. and the form factor approximations.

All the above calculations assume a simple form for the susceptibility function f(q) for the non-interacting electron gas, (Eq. 3.6). This approximation is in general not valid. The form of f(q) for most real metals is very much different from that for a free electron gas so that the actual spin polarisation will also be different.

Overhauser and Stearns (55) examined the possible forms of the susceptibility function which would explain the hyperfine fields at the non-magnetic solute atom sites in a matrix of Fe, as observed in the experiments of Stearns and Wilson (56). The form of the susceptibility function $\chi(q)$ which gave the best agreement with experimental results was

$$\chi(q) = \chi_o(q) + \alpha\chi_p \exp\left[\beta^4\left(\frac{q}{2k_f} - 1\right)^4\right] \qquad 3\cdot10$$

where $\chi_o(q)$ is the susceptibility function for the free electron gas (related through constants to $f(q)$). χ_p is the Pauli paramagnetic susceptibility, α and β are constants having the values, $\alpha = 1.7$ and $\beta = 3.25$.

Strong exchange interactions in the conduction band of the matrix gives rise to a large enhancement of the susceptibility. This has been calculated in the random phase approximation (57) to be

$$\chi(q) = \frac{\chi_o(q)}{1-I\chi_o(q)} \qquad 3.11$$

where I is the exchange interaction constant of the matrix band. Giovannini et al (37) considered the effect of the enhanced susceptibility on the range of the conduction electron spin polarisation. They obtain a large amplitude and a greatly increased range of polarisation which are functions of the exchange enhancement factor of the matrix. For no enhancement in the band, the usual R.K.K.Y. result is obtained.

Kim and Schwartz (38) have calculated the spin polarisation as a function of the magnetisation $(n_+ - n_-)/2n$ of the matrix. They find a very long range of polarisation and a large amplitude, both increasing with the magnetisation - a result somewhat similar to that of Giovannini et al (37).

Magnetic Coupling Between Virtual Bound State Moments

In the preceeding discussion J(k,k') is assumed to be the simple exchange integral between a localised moment and the plane wave electron states. While this approximation is valid for the case of the rare earth ions with a well localised real bound magnetic state, it does not seem a reasonable approximation for the case of a magnetised virtual bound state. The exchange integral as expressed by Eq. 2 is a positive quantity. In many situations the sign of the interaction is often found to be negative. Schrieffer and Wolff (15) have shown that the Anderson Hamiltonian is equivalent to the s-d interaction Hamiltonian, where the interaction constant J(k,k') is of the form: (c.f. Eq. 1.20)

$$J(k,k') = 2\left|V_{kd}\right|^2 \frac{U}{E_d(E_d + U)}$$

This expression is valid for scattering in the region around the Fermi sphere (k & $k' \simeq k_F$). The energy E_d is negative (measured with respect to the Fermi level) so that when $U > E_d$ the exchange parameter is negative. It has also a large magnitude because of the large mixing term V_{kd}. Two different treatments of the magnetic interactions between solute atoms possessing virtual bound state moments have been put forward.

One of them is by Blandin and Friedel (6) and the other is the treatment of Caroli (40).

Blandin and Friedel (6) consider that when a virtual bound state is magnetic, the phase shifts for the spin up and spin down scattered conduction electrons will be different. This gives rise to a spin density which oscillates in sign at large distances, and provides a mechanism for interactions between the solute atoms.

If one of the virtual states, say the spin down state is well above the Fermi surface, so that only the spin up state is occupied, then the phase shift $\eta_{-}=0$. Now if only the $l=2$ phase shift for the spin up electrons is assumed to be non-zero, then the polarisation is given by

$$\Delta\rho_{+} = \frac{5}{2\pi^2 r^2}\int_0^{k_F} \sin\eta_2 \sin(2kr+\eta_2)dk \qquad 3.12$$

where η_2 is a function of k, and varies rapidly from o to π within a short range of k. The form of $\Delta\rho_{+}$ obtained depends on the assumed variation of η_2 with k. If η_2 varies from o to π linearly within a range k_1 about k_o, the centre of the state, and if k_F lies above the top of the state of spin up then

$$\Delta\rho_+ = \frac{5}{4\pi r^3} \frac{\sin k_1 r \cos 2k_o r}{k_1 r + \pi} \qquad 3.13$$

This polarisation is much larger than the R.K.K.Y. result, but it decreases as $1/r4$ at large distances, so that it falls to zero more rapidly than the R.K.K.Y. polarisation. The energy of interaction between two solute atoms on this model is

$$E = 2V_A \Delta\rho(R) \Delta F \qquad 3.14$$

where V_A is the atomic volume and ΔF is the s-d exchange energy which is of the order of the interaction constant J.

A mechanism of interaction between solute atoms within the Friedel-Anderson model of localised moments has been suggested by Caroli (40). He considers two solute atoms at a distance R from each other which couple through a double resonance scattering of conduction electrons from the two sites. The wave function, at a large distance r, of an electron of spin σ and wave vector $\underline{k}$ after scattering from one solute atom is given by

$$\psi^o_k(r) \simeq e^{i\underline{k}\cdot\underline{r}} + \frac{e^{ikr}}{kr} e^{i\phi^o_o} \sin \phi^o_o \qquad 3.15$$

where ϕ^o_o is the phase shift produced.

The electron is then scattered from a second solute atom. This interaction is treated exactly by the Anderson model, but the matrix element V_{kd_2} at the second site $\langle k|V|d_2^\sigma\rangle$ is replaced by $\langle \psi_k^\sigma|V|d_2^\sigma\rangle$ which therefore becomes

$$V_{kd_2}\ (e^{i\underline{k}\cdot\underline{R}} + \frac{e^{ikR}}{kR}\ e^{i\phi_o^o}\sin\phi_o^o) \qquad 3.16$$

The calculation yields an interaction energy $E_{int}(R)$ between the two solute atoms given by

$$E_{int}(R) = \frac{E_F}{\pi}\sum_\sigma \sin\phi_1^\sigma \sin\phi_2^\sigma \frac{\cos(2k_FR+\phi_1^\sigma+\phi_2^\sigma)}{(k_FR)^3} \qquad 3.17$$

This has been simplified further to give

$$E_{int}(R) = \frac{25}{2\pi} E_F \sin^2\phi \frac{\cos(2k_FR + 2\phi)}{(k_FR)^3}\ \underline{u}_1\cdot\underline{u}_2 \qquad 3.18$$

where $\underline{u}_1$ & $\underline{u}_2$ are the unit spin vectors.

For Cu-Mn alloys, if the typical values $E_F \simeq 7$eV and $\phi = \pi/5$ are assumed, the result becomes

$$E_{int}(R) = 9.6 \frac{\cos(2k_FR + 2\pi/5)}{(k_FR)^3}\ \underline{u}_1\cdot\underline{u}_2\ (eV) \qquad 3.19$$

This may be compared with the energy obtained from the R.K.K.Y. interaction where, for Cu-Mn alloys J=0.2 eV and $\frac{n}{N}=1$ have been assumed.

$$E_{int}(R) = 7.7\times10^{-2} \frac{\cos(2k_F R)}{(k_F R)^3} \underline{u}_1 \cdot \underline{u}_2 \text{ (eV)} \qquad 3.20$$

This is roughly two orders of magnitude smaller than Caroli's.

Treatment of Interaction

It is clear from the above discussion that the actual magnitude of the interaction between two solute atoms through the medium of the conduction electrons depends very much on the type of the magnetic state of the solute atoms. However, all interactions considered above fluctuate in sign as a function of the distance between the solute atoms. The oscillatory nature of such interactions can lead either to ferromagnetism or antiferromagnetism in the alloys. The type of magnetic order produced depends on the type of interaction between the solute atom and conduction electrons, and on the number of conduction electrons per magnetic atom. Mattis (58) has calculated the stability condition for ferromagnetism and

antiferromagnetism assuming R.K.K.Y. interaction (J(q)=J(o), a constant). He finds that ferromagnetism and antiferromagnetism appear alternately as the number of conduction electrons per atom increases.

Fedro and Arai (39) have considered various forms of J(q) and determined stability conditions for various types of magnetic order as a function of $k_F a$, which is related to the number of electrons per magnetic atom. They find that the magnetic ordering patterns are very similar for the cases where J(q) is constant (R.K.K.Y.) and where J(q) has the atomic form-factor dependence (Overhauser). A marked difference is found for the case where J(q) calculated by Watson and Freeman (36) is assumed. In this case the authors find that only ferromagnetism appears for all values of $k_F a$.

The type of magnetic order produced and its onset as a function of temperature are in general difficult properties to explain. In most random solid solution alloys the onset of magnetic order is not sharp, as evidenced by a broad maximum in the susceptibility of the alloys. This fact is corroborated by the high temperature persistence of the excess specific heat suggesting that spin-spin correlation persists well above the broad ordering region. Any anomaly in the electrical

resistance associated with magnetic order is also broadened out over a finite temperature range.

Many attempts have been made to derive useful theories to explain the observed effects quantitatively, but none of them have proved completely satisfactory. Perhaps the most useful theory for such alloy systems is the distribution of effective field theory due to Marshall (41).

In order to explain the low temperature specific heat behaviour of alloys of Mn dissolved in Cu (59) and Ag (60), ($\frac{\Delta c}{T}$ = constant, independent of concentration as $T \to 0$), Marshall proposed the existence of a distribution of internal fields P(H,T) acting on the solute atoms. He argued that the R.K.K.Y. type of coupling between solute atoms in a random alloy will lead to a distribution of internal fields of varying magnitude and sign. He suggested that the distribution P(H,T) would be Lorentzian in shape with suitable cut-off limits and having a width proportional to concentration. This was thought to be so in analogy with the line shape of nuclear magnetic resonance in a dilute sample of randomly distributed nuclear spins coupled to each other via magnetic dipole-dipole interactions. He argued that a Gaussian distribution was not possible as it predicts a width proportional to the square root of the concentration.

Klein and Brout (42) and Klein (43) have adopted Marshall's ideas to develop a statistical theory of interactions in Cu-Mn type of alloy systems. They have used the Ising model for the solute atom moment, and interaction through R.K.K.Y. spin polarisation is assumed. The authors (42) first demonstrate that by considering the partition function for a single spin and neglecting all correlations between the spins, the field P(H) seen by the impurity at the origin due to all other impurities distributed randomly through the alloy is a Lorentzian with a width proportional to concentration, in agreement with Marshall's arguments. The authors further show that by excluding the possibility of any two spins coming closer than the nearest neighbour distance, the distribution function becomes a Gaussian with a width also proportional to the concentration.

In their statistical calculation of P(H) the authors consider the two particle correlation functions $\langle \mu_i \mu_j \rangle$. They expand the partition function diagrammatically in a power series in solute concentration, and perform averages over the spin as well as the spatial configurations. This is the well known linked cluster expansion method due to Brout (45). The main result of the analysis is that the field H_o at a given solute atom is made up of two parts $H_o = H_1 + H_2$ where H_1 is

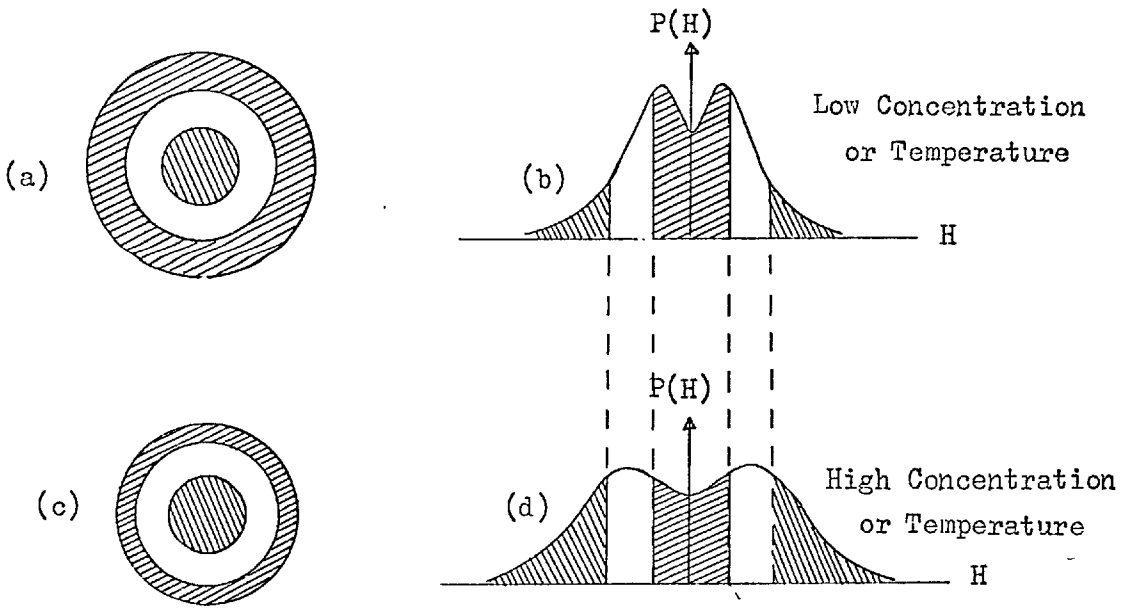

Fig.4 Correlation Volumes and P(H) Distributions (After M.W.Klein)

the field from the spins within a volume of radius R_c around the solute atom, which are strongly correlated to it and H_2 is the field due to spins outside this region. The total field distribution $P(H_o)$ is the convolution of the probability distributions $P(H_1)$ and $P(H_2)$. The form of the probability distribution $P(H_o)$ and the correlated region of spins contributing to it are shown in Fig. 4. The correlated volume is divided into three regions. The outside region contributes the lower fields around $H_o=0$, whereas the inside region gives rise to the higher field tail of the P(H) distribution. As concentration is increased the correlation volume becomes smaller, Fig. 4 (c). The average number of spins within the correlated volume remains constant independent of the concentration. The corresponding P(H) is shown in Fig. 4 (d). The effect of increasing the temperature is the same as that of increasing the concentration, the P(H) function again changing from that in Fig. 4 (b) to Fig. 4 (d).

The actual forms of the P(H) distribution for various alloys were calculated on a computer by Klein (43). These were used in the calculations of the low temperature specific heats of Cu-Mn, Cu-Fe and Cu-Co alloys, which were all shown to be in good agreement with the measured values.

S. H. Liu (46) has criticised the Klein and Brout treatment of the effective field theory of dilute magnetic alloys. The author believes that their theory is only applicable to solute concentrations of less than 1 at. % because of the treatment of the partition function in terms of the two spin correlation function. In order to treat larger concentrations and carry out the analysis at finite temperatures and external magnetic fields, the author suggests that Marshall's phenomenological theory is the most suitable. He assumes a symmetric distribution of effective fields about the origin of the form

$$P(H) = \frac{a}{(H-b)^2 + c^2} + \frac{a}{(H+b)^2 + c^2} \quad \text{for } H<H_c$$

$$= 0 \qquad \text{for } H > H_c \qquad 3.21$$

where H_c is some cut off limit of the Lorentzian which is necessary to keep the moments of the distribution finite, a is a normalisation constant, b is the value of the field about which the distribution is peaked and c is the width of the peak, representing the fluctuation of the effective field about the most probable value b. c is assumed to be temperature independent for a given alloy. It is thought to increase with increasing

concentration when the latter is large enough to sustain long range order. The variation of b with temperature is assumed to be of the form

$$b = b_o \eta \qquad 3.22$$

where b_o is proportional to the concentration and

$$\eta = \int_o^\infty P(H)\ B_S(\beta H) dH \qquad 3.23$$

Here $B_S(\beta H)$ is the Brillouin function for spin S. This is the major point of difference of this theory from that of Klein and Brout (42). The latter theory predicts that the most probable field shifts to higher values as the temperature is raised, whereas the above dependence of b is exactly the opposite. Early Mossbauer measurements on Cu-Fe (47) were thought to support Klein and Brout's ideas, but the later work of Gonser et al (48) shows the opposite behaviour in agreement with Liu's assumption.

Despite this main difference between the two treatments of the effective field theories, it seems to be the most promising one for random solid solution alloys. The theory has so far mainly been used to explain the specific heat results

and the line shape of the Mossbauer spectrum of some alloys. Recently, however, Harrison and Klein (49) have examined the effect of internal fields on the resistivity of dilute concentrations of magnetic impurities in non magnetic metal hosts. They find that the effective field distribution obtained from the low temperature specific heat measurements gives the slope of the low temperature resistivity against temperature in good agreement with experiment. They also find a maximum in the resistivity at higher temperatures arising from the suppression of the Kondo lnT term by the presence of internal fields. S. D. Silverstein (50) has also investigated the effect of internal field distribution P(H) on the resistivity of dilute alloys. He obtained an expression for the maximum in the resistivity which is in good agreement with experiment if a Gaussian field distribution with a width proportional to concentration is assumed. A cut off Lorentzian with a width proportional to concentration gives the wrong concentration dependence of the maximum.

The effect of interactions on the magnetic susceptibility and electrical resistivity, expressed in analytic forms by various authors, is considered below.

Magnetic Susceptibility

The susceptibility behaviour for interacting solute atoms in random solid solution alloys cannot be interpreted by a simple Curie-Weiss law. The Curie temperature Θ obtained from such an interpretation is usually unrelated to the temperature where the magnetic order appears. For instance, in the alloys of Mn in Cu the higher temperature paramagnetic susceptibility gives positive Θ values (51) despite the fact that antiferromagnetic order appears at low temperatures.

De Gennes (31) has shown that for the case of rare earth solutes the R.K.K.Y. coupling leads to a Curie temperature given by

$$k\Theta = \frac{3\pi Z^2}{4} J_{ex}^2 (g_J-1)^2 J(J+1) \sum_{i\neq j}' F(2k_F R_{ij}) \qquad 3.24$$

where Z is the number of valence electrons per atom, J is the total angular momentum, g_J is the Landé g factor. The sum $\sum_{i\neq j}' F(2k_F R_{ij})$ is difficult to perform except in the case of ordered structures.

Blandin and Friedel (6) have derived a high temperature series expansion for susceptibility in powers of $\frac{1}{T}$ using a statistical method due to Opechowski (52) the coefficient of $\frac{1}{T^2}$ term is taken as the Curie temperature Θ which becomes

$$\Theta = \frac{S(S+1)}{3k} \sum_{n \neq m} J_{nm}$$

where J_{nm} is the interaction energy between two spins at n and m in the R.K.K.Y. model.

If ensemble average over the possible impurity positions R_n is performed, one gets (53)

$$\sum_{n \neq m} J_{nm} = c \sum_{\substack{\text{all sites} \\ n \neq m}} J_{nm} = c\, J_{q=o} \qquad 3.26$$

where c is the concentration of the solute atoms and $J_{q=o}$ is the q=o component of the Fourier transform of J_{nm}. Hence the Curie temperature is given by

$$\Theta = \frac{cS(S+1)}{3k} J_{q=o} \qquad 3.27$$

An expression for susceptibility within the P(H) field distribution model has been derived by Liu (46). He considers

the following situation. If the internal field at a given site is $\underline{H}$ and an external field $\underline{H}_e$ is applied then the total field $\underline{H}_1$ is given by

$$\underline{H}_1 = \underline{H} + \underline{H}_e \qquad 3.28$$

$$|H_1| = \left[H^2+H_e^2+2HH_e \cos\theta\right]^{\frac{1}{2}} \qquad 3.29$$

θ is the angle between $\underline{H}$ and $\underline{H}_e$. If α is the angle between $\underline{H}_1$ and $\underline{H}_e$, then the magnetisation σ in the direction of $\underline{H}_e$ is given by

$$\sigma = cNS \int P^1(\Omega)d \int_0^\infty P(H)B_S(\beta H_1)\cos\alpha\, dH \qquad 3.30$$

where $P^1(\Omega)$ is the angular distribution function for the internal field c is the concentration, N is the number of atoms per gm (per cc), S is the spin angular momentum, and $B_S(\beta H)$ is the Brillouin function which can be approximated by $\tanh(\frac{1}{2}\beta H)$.

The susceptibility χ is given by

$$\chi = \left.\frac{\partial\sigma}{\partial H_e}\right|_{H_e\to 0} \qquad 3.31$$

After differentiation of σ and a little calculation χ is found to be

$$= cNS\int_0^\infty P(H)\ \tfrac{1}{2}\beta\,\mathrm{sech}^2(\tfrac{1}{2}\beta H)\ \cos^2\theta + \tfrac{1}{2}H^{-1}\tanh(\tfrac{1}{2}\beta H)(1-\langle\cos^2\theta\rangle)\,dH \qquad 3.32$$

where

$$\langle\cos^n\theta\rangle = \int P^1(\Omega)\cos^n\theta\,d\theta$$

and $\langle\cos\theta\rangle = 0$ is assumed for antiferromagnetic distribution of internal field $\underline{H}$. Furthermore, for dilute alloys a random distribution of $\underline{H}$ may also be assumed which gives $\langle\cos^2\theta\rangle = \frac{1}{3}$. $\langle\cos\theta\rangle$ may in fact have a finite value and $\langle\cos^2\theta\rangle$ will then also be different from $\frac{1}{3}$.

Electrical Resistance

The s-d interaction between the conduction electrons and the localised moment leads to an increase in the resistance because of the increased scattering as was shown by Kasuya (9). Yosida (54) included interaction behaviour solute atoms in the molecular-field approximation and obtained a temperature dependent resistivity which was in agreement with that observed in Cu-Mn alloys with more than 1 at % Mn. For the lower concentration alloys a minimum in the resistance occurs at a temperature above the maximum. Yosida could, however, only explain the monotonic decrease in the resistance below the maximum. The minimum in the alloys was of course explained later by Kondo (16).

Harrison and Klein (49) considered in detail the effect of internal field distribution and the Kondo scattering on the resistance of the alloys and obtained satisfactory agreement with experiment. Silverstein (50) has also considered the same problem. Using the method of Yosida (54) the author writes down the total collision integral given by the sum of elastic and inelastic contributions as

$$\left(\frac{\partial f_k^0}{\partial t}\right)_{coll.} = cS(S+1)A(\varepsilon_k)E\left[1 - \frac{1}{S(S+1)}\left\langle\!\left\langle S_z \tanh \frac{\mu_B g H}{2kT}\right\rangle\!\right\rangle\right] \quad 3.33$$

where

$$\left\langle\!\left\langle S_z \tanh \frac{\mu_B g H}{2kT}\right\rangle\!\right\rangle = \int_{-\infty}^{\infty} P(H) \tanh \frac{\mu_B g H}{2kT} \; B_S\left(\frac{g h_B H}{kT}\right) dH$$

and

$$A(\varepsilon_k) = \frac{1}{2\pi\hbar^4} \frac{V}{N} (2m)^{3/2} k_x \frac{\partial f k^0}{\partial \varepsilon_k} \varepsilon_k^{\frac{1}{2}} \Phi(\varepsilon_k) J^2 \left[1 - \frac{2|J|}{N} \sum_{k_1}' \frac{(1-2f_{k_1}^0}{k_1 \; k}\right]$$

also, c is the concentration, S the spin angular momentum. The other quantities have the usual meanings.

Using the above collision integral in the Boltzmann equation and solving for $\phi(\varepsilon_k)$ the spin contribution to the resistivity is calculated to be

$$\rho_S = c\rho_m(T)\left[1 + \frac{3z|J|}{\varepsilon_F}\ (\text{const} + \ln T)\right]^{-1} \qquad 3.34$$

where z=no. of conduction electrons per atom.

$$\rho_m(T) = \rho_m(\infty)\left[1 - \langle\langle S_z \tanh(\mu_B gH/2kT)\rangle\rangle / S(S+1)\right]$$

and

$$\rho_{m(\infty)} = 3\pi m J^2\, S(S+1)V/2Ne^2\hbar\varepsilon_F$$

Silverstein has used this result to explain the concentration dependence of the resistivity maxima in Cu-Mn alloys.

CHAPTER 4

A SURVEY OF SOME ALLOY SYSTEMS SHOWING MAGNETIC INTERACTIONS

The various types of interactions between solute atoms in an alloy can be divided into four general classes according to the nature of the magnetic state of the solute atoms. Magnetic states which are commonly encountered in dilute alloys are:-

(1) Real local bound state with a well defined free ionic magnetic moment.

(2) Magnetised virtual bound state where the magnetic moment is well defined, but is usually different from the free ionic value.

(3) Nagaoka spin compensated state where the magnetic moment is reduced through anti-parallel coupling with the conduction electrons.

(4) Unmagnetised virtual bound state which has no effective magnetic moment (in Friedel-Anderson sense).

It is perhaps important to point out that the groups (2), (3) and (4) may be regarded as members of one general class

where the difference is only of degree of spin compensation. For example, an unmagnetised virtual bound state may be regarded as a spin compensated state with a very high Kondo temperature T_K, whereas the magnetised virtual bound state with well defined moment can be thought of as a system with very low Kondo temperature. It may also be remarked that since no examples of a spin compensated state are known for a real bound state, the phenomenon of a spin compensated state should be regarded as a property of the virtual bound state. It may be argued, however, that s-f interaction between a real bound state and the conduction electrons is usually ferromagnetic (positive J) so that no spin compensation will occur. In any case, the s-f interaction is rather weak so that even for antiferromagnetic coupling (-veJ), the Kondo temperature will be very small.

Although the classes (2), (3) and (4) are a little artificial in the above sense, it is instructive to consider them separately, at least for the present purpose of distinguishing between various types of solute-solute interactions and the resulting magnetic order. We first consider a few general properties of each system.

(1) Real Bound State

The magnetic moment for a real bound state is well defined and essentially the same as the free atomic one. The examples of such impurity states occur for the atoms of the rare earth series which have their partially filled magnetic 4f shell well localised and tightly bound. Because of this, the mixing with the conduction band of the general matrix is small. The main perturbation to the moment of the ion is from the crystalline field of the matrix in which it is situated. In the rare earth atoms $\underline{L}$-$\underline{S}$ coupling is strong, so that Hund's rule is obeyed and J is a good quantum number. The effect of the crystalline field is partially to lift the degeneracy of the J multiplet and give rise to a series of sub-multiplets of lower degeneracies, occupying a spectrum of discrete energies. The eigen states of each multiplet can be expressed as a linear combination of some of the eigen states $|J,J_z\rangle$ of the free ion, the coefficients depending on the crystal field parameters, which also determine the total amount of splitting of the levels. Crystalline field splitting may affect the onset of magnetic order in two ways.

If the rare earth atom has an even number of electrons

(Integral J), the crystal field split ground state may be a non-magnetic singlet separated from the next level by an energy Δ. Trammel (61) and recently Cooper (62) have shown that for such a system there is a threshold value of the ratio of exchange to crystal field energy for magnetic order to occur even at $T = 0^{\circ}K$. They demonstrate this by considering a situation where the second excited level is also a singlet. Cooper's argument is as follows:-

If $|0\rangle$ and $|1\rangle$ are the two singlet levels such that

$$\langle 0|J_z|0\rangle = \langle 1|J_z|1\rangle = 0$$

and

$$\langle 0|J_z|1\rangle = \alpha$$

Then the susceptibility χ of the system is given by

$$\chi = \frac{2g^2\beta^2\alpha^2}{\Delta} \tanh \frac{\Delta}{2T}$$

where

$$\beta = \frac{1}{kT}$$

If exchange interaction between the atoms is included using the molecular field approximation, the expression for χ can be written as

$$\frac{1}{\chi} = \frac{\Delta}{2g^2\beta^2\alpha^2} \qquad \frac{1}{\tanh\ \Delta/2T} - A$$

where $A = 4J(0)\frac{\alpha^2}{\Delta}$ and $J(0)$ is the exchange coupling for $q=0$.

At $T = 0^{o}K$ the susceptibility first diverges when $A = 1$, which defines the threshold value of $J(0)/\Delta$ for magnetic order to occur.

Even if the ground state of the solute atom is not a singlet, but a magnetic doublet, triplet or even a quartet, as is the case when the f shell has an odd number of electrons, the crystalline field has the effect of reducing the magnitude of the s-f coupling, and hence the effective exchange interaction between the atoms. This can be seen by considering the R.K.K.Y. expression for spin polarisation due to s-f exchange interaction which is according to Eq. 3.9

$$\rho_{\pm}(r) = \frac{n}{v} \mp \frac{1}{v}\ \frac{4(3n)^2}{E_f}\ J(0)\ N^{-1}\ \ 2k_m|r - R_n|F(2k_m r)S^z$$

The magnitude of this spin density depends on the z component of the spin S. If the ground state of the solute atom is well isolated and has an average value of the J_z component $\langle 0|J_z|0\rangle$, , then the z component of the spin is

given by

$$S^z_{av} = (g_J - 1) \langle 0 | J_z | 0 \rangle$$

This is usually smaller than the magnitude of S^z for the free ion.

(2) Magnetised Virtual Bound State

The occurrence of a virtual bound state is most common with the solutes of the 3d transition series. The formation of the v.b.s. is a result of large mixing with the conduction electrons. This gives rise to a large effective exchange interaction constant J when the virtual bound state is magnetised. The R.K.K.Y. exchange interaction is not strictly applicable to this case, although the interaction with the conduction electrons causes large amplitude of spin polarisation of the latter of the form qualitatively similar to R.K.K.Y.. The strong interaction with the conduction electrons leads to strong coupling between solute atoms, so that effects of magnetic interactions can be observed in some alloys down to the lowest practicable concentrations.

(3) Nagaoka Spin Condensed State

The Nagaoka spin condensed state is characterised by properties similar to those of a normal magnetic state at temperatures above a characteristic temperature T_k, whereas below this temperature, the magnetic moment appears to be reduced due to the formation of a spin compensated state through a negative exchange coupling of conduction electrons to the local moment. A conduction electron spin cloud with a coherence length which is inversely proportional to the Kondo temperature and typically of the order of a few hundred angstrom units (for a Kondo temperature of a few degrees Kelvin) is thought to exist around the local moment (16),(44). Whether a spin cloud with such a wide range would enhance interactions between the atoms is not certain. The argument breaks down when carried further to a normal magnetic state which has a very small Kondo temperature and hence a very large coherence length. What seems probable, however, is that the reduced moment will lower the tendency for any onset of magnetic order. Some evidence to support this is reviewed later.

(4) Unmagnetised Virtual Bound State

The interaction properties of an unmagnetised virtual

bound state are very much different from all the others. Such systems would normally be expected to show no interaction effects at all. However, as the concentration of the solute is increased a stage is often reached when the system develops magnetic order. The reason for this behaviour is that although conditions for the virtual bound state to magnetise are not satisfied, there is local exchange enhancement of this susceptibility at the impurity site (63). The coupling between the localised enhancement and the band electrons leads to a modification of the susceptibily of the alloy which becomes (64).

$$\chi_{\text{alloy}}(q,\omega) = \frac{\chi_{\text{matrix}}(q,\omega)}{1 - c\,\Delta I_{\text{eff}}(\omega)\chi_{\text{matrix}}}(q,\omega)$$

This leads to a critical concentration c_{crit} for the static susceptibility to diverge given by

$$c_{crit} = (\Delta I_{\text{eff}}\chi_{\text{matrix}})^{-1}$$

This condition is very similar to the Stoner criterion for ferromagnetism in an itinerant electron system. χ_{matrix} in the above formula may itself be an exchange enhanced susceptibility for the pure matrix.

Another, perhaps less likely, cause of the above

behaviour is the following. When the solute atoms are alloyed in a metallic matrix, the band structure and the Fermi level of the latter are changed. This may give rise to favourable conditions for the virtual bound state to magnetise. A local moment therefore appears at the impurity site, and magnetic order develops as a result of interactions between these moments.

Another explanation, based on the formation of clusters of solute atoms has been advanced for this type of behaviour. As the concentration increases the random probability for the number of clusters with a few solute atoms as near neighbours becomes significant. Interactions within these groups of atoms will induce them to magnetise .. Magnetic order is then a result of interactions between these clusters. This effect may be enhanced by actual chemical clustering giving rise to the phenomenon of superparamagnetism.

In the above analysis, effect of the host matrix on the nature of interactions has not been explicitly considered. The solvent matrix not only plays a role in the type of magnetic state acquired by the isolated impurity but is also

(often because of this) significant in determining the nature of interactions between the solute atoms. The solvent hosts considered below are pure metals as well as ordered binary alloys. They can be divided into three general classes according to the nature and properties of their band electrons. Each class of hosts when combined with the various impurities may give rise to some or all of the systems described above. The three classes of hosts considered here are.

A. A simple metal like Cu, Ag, Au in which the electrons at the Fermi surface are mainly from the s band, the d band being full and below the Fermi surface. The effect of the p band on magnetic properties is usually small. The total susceptibilityof such a metal is small and diamagnetic.

B. Transition metals such as Nb, Mo, V which have an unfilled d band at the Fermi surface but with little exchange enhancement of the band susceptibility. The total matrix susceptibility is paramagnetic due to the large density of states in the d band. Included in this group are binary alloys such as $LaAl_2$, La_3In and other pure metals such as La, Sc, and Y. Rh and Ir may also be considered members of this class but there

is a small exchange enhancement of susceptibility in both these metals.

C. Transition metal hosts with large exchange enhancement of susceptibility of the d band. Well known examples of these are Pd and Pt. The binary alloy $LaRu_2$ has also been suggested to have a highly exchange enhanced susceptibility (65). The exchange enhancement in such a matrix is below the critical value required for ferromagnetism in the itinerant electron model of Stoner (66).

In order to illustrate the above analysis a few examples of the various classes are reviewed below from the existing experimental results. The survey is only partial and only a few typical systems are discussed.

A.(1) Real Bound Magnetic State in a Simple Matrix

Most rare earth solutes retain their free ionic magnetic moment when dissolved in Ag and Au. The effect of crystalline field on magnetic susceptibility of dilute rare earth alloys

has been investigated by Williams (67). Resistance measurements by Bijovet et al (68) and G. de Vries and Bijovet (69) on some silver-rare earth alloys show a decreasing resistance with decreasing temperature below $4.2^{\circ}K$, in the case of Gd, Tb, Ho and Dy as solutes. Recent measurement by Edwards and Legvold (70) on Au-Gd, Au-Tb, and Au-Ho alloys show a similar decrease of resistance at low temperatures. However, there appears no logical concentration dependence of the slope of this resistance against temperature for any given solute. Also for a Au-2 at. % Ho specimen the authors (70) find a sharp kink in the resistance at about $6^{\circ}K$, which they tentatively suggest may be due to a magnetic transition. The same authors have estimated the magnitude of the s-f exchange constant from their data and from this calculate the Curie temperature in molecular field approximation to be $\sim 10^{-3}\ ^{\circ}K$. Susceptibility measurements on an Au-2 at. % Ho sample reported in this thesis show no indication of any interaction effects, down to $1.6^{\circ}K$.

Evidence of some interaction effects in relatively dilute silver-rare earth alloys has been suggested by Williams (67) and Williams and Hirst (71) and Hirst et al (72). A paramagnetic Curie temperature of $2^{\circ}K$ has been reported (71)

in the case of a Ag 0.5 at. % Gd alloy. Measurements on an Au-0.5 at. % Gd specimen reported here, however, show that the susceptibility obeys a Curie law nearly exactly down to 1.6°K, the Curie-Weiss θ is perhaps smaller than .05°K. Susceptibility measurements by Gainon et al (73) on 0.50 at. % Eu in Au and Ag show a ferromagnetic Curie point (determined by plotting H/σ against σ^2) of $6.5 \pm .5$°K. The solubility of the lighter rare earth atoms is rather small in the noble metals. Data of Rider et al (74) show a solubility of Eu to be only about 1/4 at. %. The observed effect on susceptibility of Eu in Ag and Au may therefore be due to chemical clustering or formation of second phase intermetallic compound.

Measurements on some gold-rare earth alloys presented here seem to indicate that interaction effects are rather weak in these systems.

A.(2) Real Bound State in a Simple Transition Metal Matrix and Binary Alloys

Sugawara (75) has measured the electrical resistivity of various Y-rare earth alloys, and finds evidence of magnetic transitions in the case of Y-Gd and Y-Tb alloys. The lowest concentration alloys measured for which magnetic order was

found were around one per cent for both systems. No magnetic transition was observed for the 3.2 at. % Pr or 2 at. % of Dy, Ho and Er in yttrium. Magnetic susceptibility measurements were made by the same author, but no details are given in the paper.

Child et al (76) have made a detailed neutron diffraction study of heavy rare earths Tb, Dy, Ho, Er and Tm dissolved in yttrium. They deduced the transition temperatures T_n from the temperature dependence of the intensity of one or more satellite lines. They found that the alloys ordered into an oscillatory anti-ferromagnetic structure similar in type to that of the parent rare earth. The transition temperatures T_n for the whole set of alloys were found to follow a universal curve as a function of $\xi = c(g-1)^2 J(J+1)$ where c is the concentration of the rare earth, g is the Landè g-factor and J is the angular momentun quantum number. The functional dependence of T_n on ξ was found to be $\xi^{2/3}$. Nagasawa and Sugawara (77) have measured magnetic susceptibilities of a series of Y-Tb alloys with up to 3.7 at. % Tb. They plotted the temperatures T_n of the maximum in the susceptibilities as a function of the parameter and find a deviation from the $\xi^{2/3}$ dependence. The curve makes a finite intercept on the ξ axis indicating that a finite concentration of the

rare earth is required for magnetic ordering to occur. The authors have also plotted the values of T_n derived from neutron diffraction on Y-Tb alloys by Child et al (76), and an ordering temperature derived from the susceptibility measurements on Y-Dy alloys by Nelson et al (78), and show these lie on their curve, as distinct from the $\xi^{\frac{2}{3}}$ curve.

Sugawara and Eguchi (79) have measured the low temperature resistivity, magnetic susceptibility and superconducting transition temperature of alloys of Lanthanum with a few rare earth solutes. There is no indication of interaction effects in either the susceptibility or the resistivity measurements of any of these alloys.

A.(3) Real Bound State in an Exchange Enhanced Host Matrix

Susceptibilities of some alloys of rare earth solutes dissolved in palladium have been measured by Shaltiel et.al. (80). They determined Θ values from Curie-Weiss plot of $1/(\chi - \chi_0)$ against T where χ_0 was matrix susceptibility with Lu replacing the rare earths. The values of Θ obtained are as follows

Rare Earth	Conc.	$P_{eff.}$	$\theta^{o}K$
Ce	4.0	1.1	4
Pr	2.0	3.3	-4
Nd	3.2	3.07	-2
Gd	3.0	6.28	+3
Tb	1.0	8.4	0
Ho	0.23	10.8	0
Yb	4.0	4.54	-2

The authors have not reported whether actual magnetic order was observed at low temperatures. Since the crystal field splitting can give a pseudo Curie-Weiss θ, it is difficult to be certain whether the above values of θ represent a measure of interaction effects, except say in the case of Gd and perhaps Ce.

Crangle (81) has reported the occurence of ferromagnetism in Pd-Gd alloys containing up to 9.7 at. % Gd. He finds that normal ferromagnetism persists in the alloys down to less than 1 at. % Gd. The observed moment per Gd atom is also found to be less than the expected value of 7 Bohr magnetons, which is attributed to a negative spin polarisation of conduction electrons in the matrix.

Williams (67) has measured Pd-$\frac{1}{2}$ at. % Gd and Pd-$\frac{1}{2}$ at. % Er. The M-H plots at the lowest temperature of 1.7^{o}K show no sign of interaction effects.

H. Cottet et al (65) have measured the susceptibility of $(La_{.94}\ Gd_{.06})Ru_2$ and find a ferromagnetic Curie point of 10 ± 1^{o}K (from H/σ vs σ^2 plot) and a paramagnetic Curie temperature of 16 ± 2^{o}K.

B.(1) Magnetised Virtual Bound State in a Simple Metal Host

Alloys of Cr, Mn and Fe dissolved in the simple metals Au, Ag and Cu have been the subject of wide theoretical and experimental investigation since the discovery by Gerritsen and Linde (82) of resistance minimum followed at lower temperatures by a maximum in an alloy of 0.1 at. % Mn in Ag. The maximum is now understood to be due to the combination of Kondo's logarithmic increase in resistance (with decreasing temeperature) and the quenching of spin disorder scattering due to the onset of magnetic order which gives a decreasing contribution to the resistance. The maximum has a well defined concentration dependence and is typically 25^{o}K per atomic percent for Cr, Mn and Fe in the noble metals. The susceptibility of the alloys also go through a maximum at a temperature lower

than the resistance maximum, but there is some disagreement in the literature about the concentration dependence of this. In fact Van Itterbeek et al (83) find no maximum in susceptibility down to 1.2°K for a concentration as high as 1.6 at. % Mn in Cu and Ag. This is in disagreement with the results of Owen et al (51) who find susceptibility maxima for alloys of similar concentration.

Lutes and Schmit (84) have measured the susceptibility of various concentrations of Cr, Mn and Fe dissolved in Au and find well defined maxima even for alloys with 0.5 at. % Cr and Fe and 1 at. % Mn.

The magnetic order in the alloys can be disturbed by cooling in an applied magnetic field. J. S. Kouvel (85) observed large thermal remanant moments when Cu-Mn and Ag-Mn alloys were cooled in a magnetic field to a temperature below the susceptibility maximum, and D. Griffiths (86) observed marked effects in EPR of Cu 5 at. % Mn and Cu 15 at % Mn alloys showing the onset of magnetic order of some sort which was modified by cooling in a magnetic field.

Evidence of magnetic order is also seen in the specific heat measurements of these alloys where a broad maximum is found in the excess specific heat at low temperatures. Cu-Mn

alloys of various concentrations were measured by Zimmerman and Hoare (59) and Ag-Mn alloys by de Nobel and du Chatenier (60). Magnetic entropy was calculated by integrating $\frac{\Delta c}{T}$ over the temperature range, from which the spin degeneracy was found to be between 2 and 5/2.

B.(2) Magnetised Virtual Bound State in a Simple Transition Metal and Binary Alloy Hosts

Matthias et al (1) have measured the magnetisation at 1 at. % Fe dissolved in Mo and Mo-Nb alloys. They find that the addition of Nb to Mo progressively reduces the magnetic moment on the Fe, until the virtual bound state is completely unmagnetised for more than 40% Nb. Coles (87) has measured the resistivity of Mo-0.65 at.. % Fe and finds a maximum around $4^{\circ}K$ and a broad minimum around $22^{\circ}K$. This is similar to the behaviour of the resistance in Cu-Mn type of alloys. Waszink (88) has measured the magnetic susceptibility of the same alloy down to $3^{\circ}K$ and finds no evidence of magnetic order. Further investigation of this system will prove very interesting in its comparison with Cu-Mn alloys.

B.(3) Magnetised Virtual Bound State in an Exchange Enhanced Host Matrix

The observation of "giant moment of Fe" dissolved in palladium was first made by Crangle (89) since then considerable interest has been shown in both the experimental and theoretical study of such systems. Co too, shows a similar behaviour when dissolved in palladium and platinum. The phenomenon is due to the polarisation of matrix atoms around the impurity within an average radius of around 10 Å. This has been experimentally varified by Low (90). Clogston et al (4) studied this behaviour as a function of the electrons per atom ratio of the matrix and found the largest moment per iron atom in an alloy of Pd with about 10 at. % Rh.

The Pd-Fe alloys show ferromagnetism for very low concentrations of Fe. The transition temperature is about $40^{\circ}K$ per atomic per cent Fe. Coles et al (92) have reported resistance measurements which show a rapid decrease below a well defined temperature T_c. Recently Williams and Loram (93) have made resistance measurements of very dilute Pd-Fe alloys in the He^3 temperature range, and find a similar behaviour.

The excess specific heat of Pd-Fe alloys measured by Veal and Rayne (91) shows the characteristic maximum indicative

of magnetic order. The entropy calculation gives spin value $S = 1.1 \pm 0.3$ which differs very much from $S = 3.7 \pm 0.4$ deduced by Crangle (89) from magnetisation measurements.

A similar discrepancy is observed in the Mossbauer experiments on Pd-Fe (94). The hyperfine field at an iron nucleus shows the best fit to a Brillouin function with angular momentum quantum number $J = 6$. Using a model due to Takahashi and Shimizu (95), Doniach and Murani (97) have attempted to reconcile the two results. They show that besides the matrix polarisation, interaction effects play an important role in producing the observed magnetisation curves.

C.(1) Nagaoka Spin Compensated State in a Simple Metal Host

Cu-Fe, Au-V, Cu-Co, Au-Co are some of the systems which belong to this class. Daybell and Steyert (26) have measured the electrical resistivity and magnetic susceptibility of dilute Cu-Fe alloys. They show that if a Kondo temperature of $16^{\circ}K$ is assumed for this system, the resistivity could be fitted to an expression derived by Nagaoka (12) and would also agree with his low temperature limit for the excess specific heat, although the total entropy change calculated from

specific heat is smaller than predicted by the theory. Susceptibility behaviour, however, does not agree with that predicted by the theory. The solubility of Fe in Cu is rather low so that this is not a good system for the study of interaction effects.

Susceptibility measurements of dilute Cu-Co and Au-Co by Hildebrand (99) show that the results cannot be interpreted in terms of a meaningful Curie-Weiss law as the values of θ obtained were a few hundred degrees Kelvin. Susceptibility measurements down to $2^{\circ}K$ on a 2 at. % Co in Cu alloy by Schmit and Jacobs (100) showed no remanance, nor did the Au 1 at. % Co alloy measured by Lutes and Schmit (84) down to $0.5^{\circ}K$. Domenicali and Christenson (102) have measured the resistivity of Au-Co alloys which show a logarithmic variation above room temperature, but flattening off at lower temperatures in a manner characteristic of a spin compensated state. They have suggested a Kondo temperature of about $300^{\circ}K$ for this system. Ford et al (103) have further investigated the resistivity of Au-Co alloys down to $0.4^{\circ}K$ and find a further levelling off of the resistivity below $2^{\circ}K$ for 3 at. % Co alloy indicating interaction effects.

Kume (104) made resistance and susceptibility measurements on the Au-V system, from which he obtains a Kondo temperature of around 290°K. No sign of interaction effects are observed even for the 2 at. % V alloy down to 1.4°K.. Lutes and Schmit (101) have measured susceptibility of Au 1 at. % V alloy which they find nearly temperature independent. No remanence was observed down to 0.5°K.

Narath et. al. (105) have made N.M.R. measurements on Au-V alloys with up to 10 at. % V. They find that the Knight shift at the V^{51} nucleus is independent of concentration for more than 2 at. % V and that the N.M.R. line width is proportional to the external magnetic field strength. From the hyperfine field of 18 kOe/μ_B they deduce a moment per vanadium atom of 0.08μ_B. The line width expected from ordered moments of this magnitude is greater than the observed value. The authors therefore conclude that there is no long range anti-ferromagnetic order in these alloys. Cravelling et al (106) find that the susceptibility of the alloys is made up of a temperature independent term proportional to concentration of vanadium atoms and a Curie-Weiss term with a concentration independent Curie constant. This behaviour is explained by assuming that pairs or clusters of nearest neighbour

vanadium atoms in the random alloy become unmagnetised as they do in vanadium metal. Since increasing the concentration produces an increasing number of such clusters, the effective number of isolated vanadium atoms showing the Curie-Weiss behaviour does not change very much with concentration.

C.(2) Nagaoka Spin Compensated State in Simple Transition Metals and Binary Alloys

Mo-Co is perhaps one example of this system. Susceptibility measurements by Knapp (25) on alloys with up to 1 at. % Co showed a marked deviation from Curie-Weiss behaviour at low temperatures. Below $1^{\circ}K$ the susceptibility also became slightly field dependent. A Curie-Weiss fit to the data above $4.2^{\circ}K$ gave an intercept of $24^{\circ}K$. Booth et al (108) have also measured the susceptibility of Mo-Co alloys between $27^{\circ}K$ and $300^{\circ}K$ and obtained results similar to Knapp's. Brog et al (109) have measured resistivity of these alloys with up to 1 at. % Co.and find a minimum at low temperatures. The resistance increase at low temperatures flattens off for higher concentrations. S. Mozunder (110) has measured the resistivity of 0.5 at. % Mo-Co alloys down to $0.4^{\circ}K$, but finds no maximum even for the 5 at. % Co alloy.

Resistance measurements on Y-Ce alloys by Sugawara (79) show a Kondo like minimum. Recently Sugawara et al (111) have extended the measurements down to He^3 temperature range, and also made susceptibility measurements on these alloys with up to 2 at. % Ce. The resistance could not be fitted to any existing theory of the s-d interaction. The susceptibility shows a Curie-Weiss behaviour with a pseudo θ value of -40 ± 5 for all concentrations up to 2 at. % Ce. There is no indication of interactions between Ce atoms in these measurements.

The electrical resistance of dilute Rh-Fe alloys (112) is very different from the usual resistance minimum behaviour of the Kondo systems, but the susceptibility is similar to the Mo-Co system, and other generally recognised spin compensated systems like Cu-Fe. If we regard Rh as a simple transition metal, the Rh-Fe system can be considered a member of this group. A study of interaction effects in Rh-Fe alloys is reported in this thesis.

M. B. Maple and Z. Fisk (113) have investigated the effect on the depression of superconducting transition temperature

T_c of $LaAl_2$ due to additions of various rare earth solutes. They find an abnormally large depression due to the addition of cerium, which they ascribe to the large s-f interaction between the conduction electrons and the 4f shell of cerium. There is also an additional contribution from the Kondo effect, as shown by the resistance minimum, which enhances the depression of T_c. Study of interaction effects in this system will throw further light on to the nature of the magnetic state of cerium in such alloys.

C.(3) Nagaoka Spin Compensated State in an Exchange Enhanced Matrix

Resistivity measurements on dilute Pd-Cr alloys show a Kondo type anomaly (114). The Kondo temperature being of the order of $10^{\circ}K$. W. M. Star et al (115) have also investigated the resistivity, susceptibility and specific heat of these alloys with up to 4 at. % Cr. The resistance behaviour is peculiar in that for the 4 at. % Cr alloy the rate of increase of resistance at low temperatures is sharper than for the 2 at. % Cr alloy. The resistance continues increasing down to $1^{\circ}K$, the lowest temperature of measurement. Specific heat results do notagree with any theoretical calculation of the spin condensed state. The authors find the susceptibility

behaviour difficult to interpret in terms of a Curie-Weiss law, as is possible for other spin condensed systems. It is difficult to be certain whether this represents a true Nagaoka spin condensed system or whether the observed effects are due to some other mechanism.

No other examples of a spin compensated system in an exchange enhanced matrix have so far been suggested.

D.(1) Unmagnetised V.B.S. in a Simple Metal Host

Two well known examples of this system are Cu-Ni alloys. Measurements by Pugh et al (116) on Cu-Ni alloys up to 2.5 at. % Ni in the range 2.5° to 300° showed an almost temperature independent susceptibility. A small increase at low temperatures was thought to be due to the presence of small quantities of iron in the samples. Later measurements by Ryan et al (117) show that Cu-Ni system becomes Ferromagnetic around a critical concentration of about 40 at % Ni. The Curie-Weiss constant C for some alloys around this critical concentration was higher than expected by assuming a moment of $0.6\mu_B$ per Ni atom. The authors have ascribed this behaviour to formation of superparamagnetic clusters in the alloys. Measurements of Ni rich Cu-Ni alloys by Aheren et al (118) show a decreasing

magnetic moment per atom of the alloy in the manner described by the rigid band model.

Van Elst et al (119) have made magnetisation measurements on some Cu-Ni alloys around the critical concentration. The behaviour for alloys with more that 50 at. % Ni is similar to that found by Aheren et al (118). However, alloys with less than 40 at. % Ni show departures similar to that found by Ryan et al (117).

Recent neutron scattering experiments by Hicks et al on Cu-Ni alloys around the critical composition show the existence of large spin polarisation clouds, distributed randomly through the alloy. The concentration of the clouds varies linearly with the deviation of alloy composition from a critical value which the authors quote as 44 at. % Ni. They also find in these alloys a clustering effect which they believe is too short ranged to be responsible for the superparamagnetic behaviour suggested for these alloys (121). From their saturation magnetisation measurements at $4.2^{o}K$, on alloys with more than 46 at. % Ni the authors obtain magnetic moment μ_o per atom which is in agreement with previous results (122).

The differences in the observed behaviour for alloys around the critical concentration is probably a result of different

methods of alloy preparation. The recent minimum polarity theory (123) suggests the existance of nearly independent d sub-bands for Ni and Cu, in contrast to the rigid band model which is, infact, qualitatively incorrect. Existence of an independent d-band for nickel in copper rich Cu-Ni alloys has been suggested previously by Coles (124).

Kaufmann et al (121) have also made magnetisation measurements on Au-Ni alloys and find a behaviour very similar to that in Cu-Ni alloys. The critical concentration for ferromagnetism in Au-Ni alloys is also around 40 at. % Ni.

D.(2) Unmagnetised V.B.S. in Transition Metal Hosts and Binary Alloys

Magnetisation measurements of Clogston et al (4) show that Fe does not carry a moment in Nb, V or Ru, in the dilute limit. (Fe is, however, magnetic in V-Ru alloys over a considerable range of composition). D. J. Lam et al (127) have investigated magnetic susceptibilities and nuclear magnetic resonance in V-Fe alloys as a function of increasing iron concentration. The susceptibilities were measured between $4.2^{\circ}K$ and room temperature. For low concentrations of Fe in V the susceptibilities were essentially temperature

independent. At around 20 at. % Fe there was an increase in paramagnetic susceptibility at low temperatures which became more pronounced at higher concentrations. The critical concentration of Fe is around 28 at. % when the alloy becomes ferromagnetic and the high temperature susceptibility obeys a Curie-Weiss law.

Bucher et al (128) have measured magnetic susceptibilities at 1.4°K and specific heats of some Rh-Ni alloys, and find the maximum susceptibility for Rh 63 at. % Ni alloy which became ferromagnetic at 40°K. The investigation was made with a view to observing the exchange enhancement effects so that the exact critical concentration for magnetic order has not been determined.

N.M.R. measurements on dilute Rh-Co alloys have been made by Walstedt et al (129) and resistance measurements have been made by Mozumder (110) on the dilute alloys. A susceptibility measurement on Rh 1.1 at. % Co alloy is reported in this thesis but no magnetic order has been observed down to 1.6°K.

D.(3) Unmagnetised V.B.S. in an Exchange Enhanced Matrix

Pd-Ni is the best known example of this system.

Susceptibility measurements by Shaltiel et al (80) show that in the dilute limit Ni is nonmagnetic in Pd. Susceptibility of the alloy is slightly larger than that of pure palladium. The authors find that for Ni concentrations larger than 2 at. % the susceptibility shows a Curie-Weiss behaviour, indicating a threshold concentration around this value. The system also becomes ferromagnetic at low temperatures. Schindler and Rice (132) reported resistance measurements of some dilute Pd-Ni alloys which they interpreted in terms of a concentration dependent uniform exchange enhancement model (133). The coefficient A of the T^2 term in the resistance was found to be roughly linear in susceptibility χ which could not be explained by the theory. Lederer and Mills (63) proposed a model of localised exchange enhancement which not only gives a critical concentration for magnetic order (133) but explains the resistivity behaviour and gives the correct dependence of the coefficient A on χ .

CHAPTER 5

EXPERIMENTAL METHOD AND APPARATUS

THE VIBRATION MAGNETOMETER

Introduction

Among the direct methods available for the measurement of static magnetisation and susceptibility, force methods have proved the most sensitive. Methods based on the principle of electromagnetic induction can also, in theory, be extremely sensitive. The development of a high sensitivity vibrating sample magnetometer has been reported by Foner (149). The principle of the method is the detection of the voltage induced in a suitable set of pick-up coils by a sample vibrating in their vicinity. D. O. Smith (150) has developed a vibrating coil magnetometer. This method, it has been pointed out (149), is not equivalent to a vibrating sample method, and its performance can be very seriously affected by any non-uniformity of the magnetic field.

Vibration magnetometers and other electro-magnetic induction techniques have the advantage of being adaptable for

most types of measurements on a large range of magnetic materials. The force methods are limited to measurements within a certain range of forces, and measurements in zero fields and uniform fields cannot be made. Vibration magnetometers are also in general much easier to use. The signals to be detected are audio frequency voltages, hence suitably designed narrow band amplifiers and detectors can be used to give extremely high sensitivity. Very often, however, the limiting factor to the accuracy of measurement is not the Johnson noise in the pick-up coils and the noise figure of the amplifiers, but the synchronous voltages induced in the pick-up coils through vibrations transmitted to them. A small coupling between the vibrating specimen and the pick-up coils, often indirectly through other parts of the apparatus, is difficult to avoid and can lead to large induced synchronous background signals.

An important feature of Foner's magnetometer is that the sample vibration is perpendicular to the magnetic field. This eliminates the need for an extensive modification of the laboratory electromagnet required in some arrangements for vibrating a specimen or a pick-up coil in the direction of the applied field.

We describe here a simple, compact vibrating sample magnetometer, originally designed for the measurement of specimen magnetisations rather larger than those requiring the ultimate sensitivity of the best force methods, but having the advantage over them of allowing measurements in the zero field. The use of a piezo-electric transducer, the bimorph, in a tuning fork arrangement permits sample motion in the direction of the field and with respect to a pick-up coil symmetrically distributed around it. The tuning fork arrangement of the bimorphs reduces the transmission of the vibrations to other parts of the apparatus so that the unwanted synchronous background is minimized. Null measurements of the magnetic moment (151) are made by passing a current through a coil wound around the specimen. The current at null is directly proportional to the magnetic moment and gives a measure of the moment in absolute units.

The Basic Principle

The principle of the apparatus is represented schematically in Fig. 5. B_1 and B_2 are the two bimorph elements driven by an a.c. voltage from an oscillator. The specimen S vibrating in a magnetic field induces a signal in the pick-up coil C. This is amplified and detected in a suitable manner

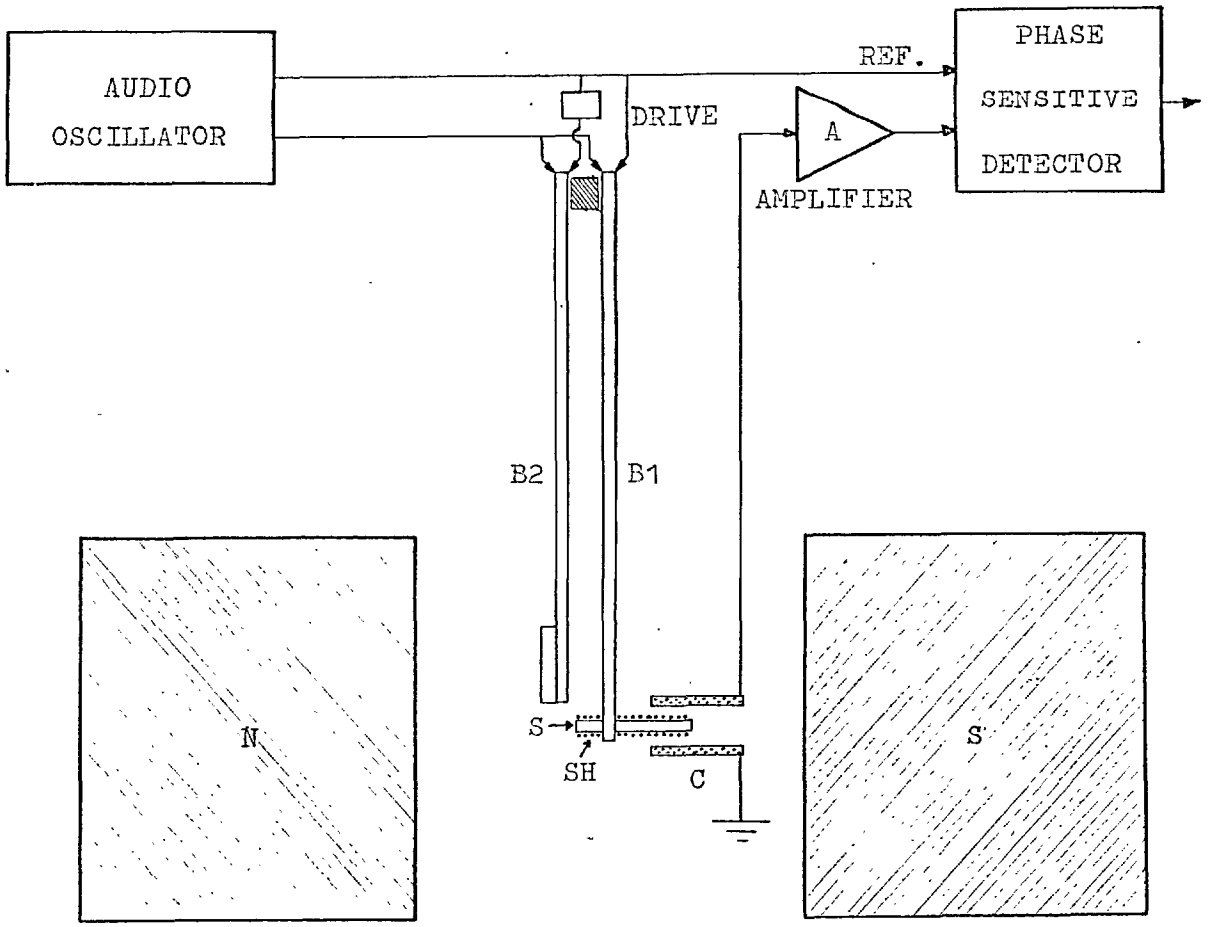

Fig.5 THE BASIC PRINCIPLE OF THE VIBRATION MAGNETOMETER

or the coil SH wound around the specimen is used for the nulling current method of measurement.

The Bimorph Element and its Use

The bimorph elements used in this application are in plate form. They are made from piezo-electric ceramics, in the present case lead zirconate titanate, two layers of which sandwich a thin brass plate Fig. 6.. The two outer surfaces are covered with thin silver films or other conducting material. The bimorphs are obtainable as square or rectangular plates from which strips of the required size can be cut. If one end of a bimorph strip is clamped and an alternating voltage is applied between the two silver electrodes the free end will vibrate at the applied frequency. The cantilever thus formed has a certain resonant frequency at which large amplitudes of vibration ($\sim$ 2 mm) can be obtained. There are other modes of vibrations of the bimorph, but this one is the most suitable for the present application. A specimen attached to the free end of a bimorph strip can be made to vibrate, the amplitude depending on the frequency and the driving voltage. Strips of size 5 cm x 3.5 mm x 0.175 mm were chosen for a specimen of typical weight $\frac{1}{4}$ gm. An audio frequency oscillator with an output impedence of 1000 Ω

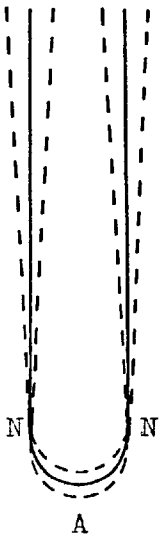

Fig.7 THE TUNNING FORK

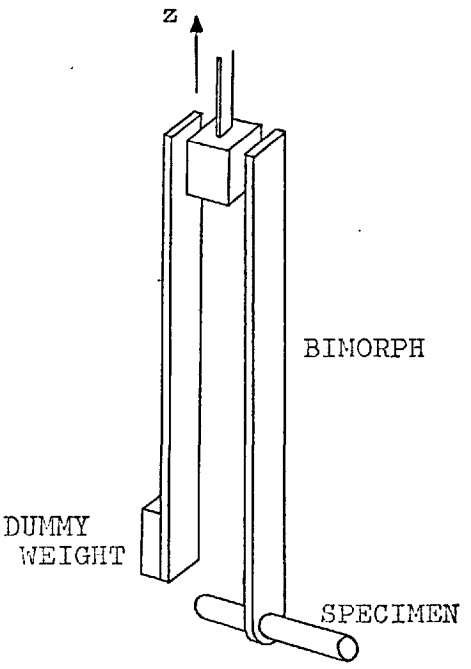

Fig.8 THE SPECIMEN VIBRATOR

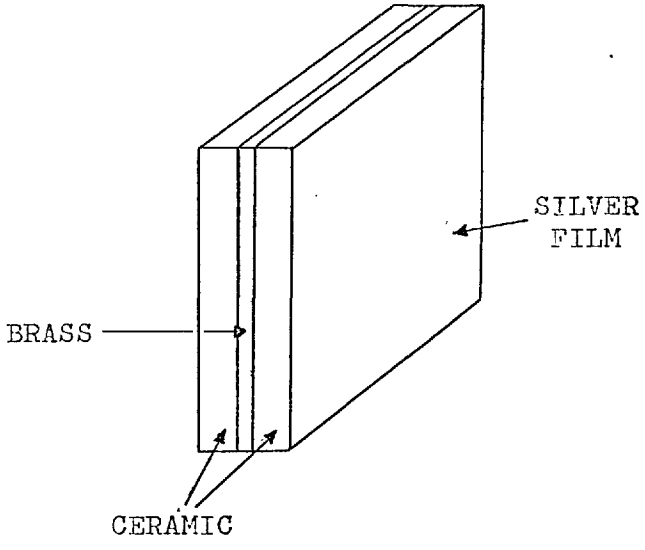

Fig.6 THE BIMORPH ELEMENT

providing an output of up to 10 V (rms) gave adequate drive. Amplitudes of specimen movement of around one millimeter were obtained.

The reaction to vibration of a single cantilever must be provided at the support to which it is clamped. Vibrations would therefore be transmitted to other parts of the apparatus and communicated to the pick-up coils however much care is taken in practice in isolating them from the vibrating parts of the apparatus.

If, however, two bimorphs are clamped together, both loaded equally so as to have the same resonant frequency, and made to vibrate in antiphase to each other then the reaction at the support is negligible. In fact the two bimorphs can vibrate even if suspended from a piece of cotton thread ! The bimorphs form a tuning fork arrangement. The latter is described as a long bar bent through 180° about the middle. It has two nodes N, Fig. 7., and an antinode A. The amplitude of vibration at the antinode is very small, especially if the two nodes are close together. The point of suspension of the bimorphs is at the antinode, hence small amplitude of vibrations in the z direction, Fig. 8., will be coupled to the coil assembly through the suspension. This mode of vibration transmitted to the pick-up coil

will produce only a small amount of synchronous noise if the magnetic field is reasonably uniform in the vertical plane.

The main contribution to the synchronous noise voltage is from a twisting mode about the suspension. This is produced if the mass on the two bimorphs is unsymmetrically distributed about the axis of the suspension. It is very difficult to align the bimorphs so that the mass distribution on the two is a mirror reflection of each other. The noise voltage induced through this mode is proportional to the total field strength, and hence it can be quite large.

Coil Design

A long cylindrical specimen shape was considered to be the most suitable for a nulling current method of measurement. A pick-up coil of circular cross section distributed symmetrically about the axis of the specimen has been used in this arrangement and the considerations given below are limited to this geometry.

The synchronous background voltage induced in a pick-up coil is proportional to the total turn area of the coil, but the contribution to the induced signal from a given turn in the coil decreases rapidly as the diameter of the turn increases. The induced signal in a given turn of the coil also varies with its

position relative to the specimen. In order to simplify the analysis the specimen is approximated by a thin dipole of length 2ℓ. The flux change $d\phi$ produced in a single turn of radius y placed at a distance x along the axis of the dipole from its midpoint due to a displacement dx of the latter is easily calculated to be

$$d\phi = 2\pi M\left[\frac{y^2}{\left[(x-\ell)^2+y^2\right]3/2} - \frac{y^2}{\left[(x+\ell)^2+y^2\right]3/2}\right]$$

where M is the magnetic moment of the dipole. The synchronous background voltage produced in the circular turn is proportional to the square of the radius. Hence the ratio of the signal to background voltage is proportional to the quantity

$$\left[\frac{1}{\left[(x-\ell)^2+y^2\right]3/2} - \frac{1}{\left[(x+\ell)^2+y^2\right]3/2}\right]$$

This quantity is plotted as a function of x/ℓ for a few values of y/ℓ in Fig. 9. Since the thickness of the specimen is finite, this analysis only gives an order of magnitude estimate for the real situation. However, it seems clear that a short cylindrical coil situated at one end of the specimen will give the best signal to synchronous noise ratio.

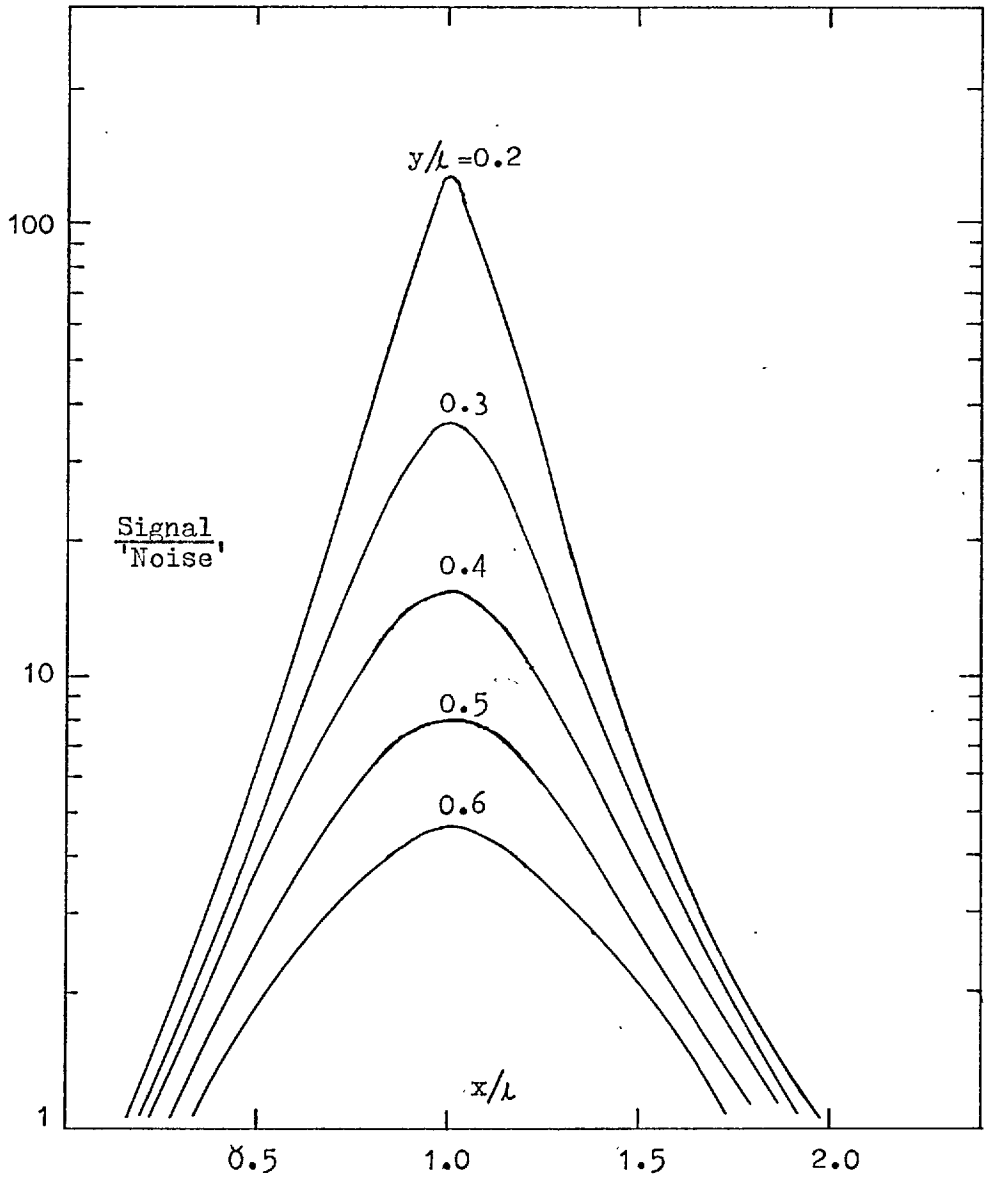

Fig.9 Graph of $\frac{\text{Signal}}{\text{'Noise'}}$ vs x/λ for Various Values of y/λ

The actual size of the coil used in the present arrangement is fairly long (0.6"). This has the advantage of making the induced signal insensitive to fairly large (few millimeters) variations in the specimen position relative to the coil. Although this is not necessary for a nulling current method of measurement, it is quite useful for the measurements on highly magnetic materials where the nulling current method cannot be used and direct measurement of induced signals have to be made. For materials of very low susceptibility, however, where high sensitivity is required, an optimum coil design is essential.

Description of the Apparatus

The basic arrangement is quite simple (Fig. 10), C1 is the main pick-up coil. C2 and C3 are dummy coils of identical geometry and the same turn area as C1. B1 and B2 are the two bimorph strips clamped together at C which has provision for electrical contacts to the silver electrodes of the bimorphs to be made . S is the suspension made of thin phosphor-bronze strip a few millimeters wide. SH is a specimen holder which is a solenoidal coil wound evenly on a thin walled glass tube. DW is a dummy weight for matching the resonance frequencies of

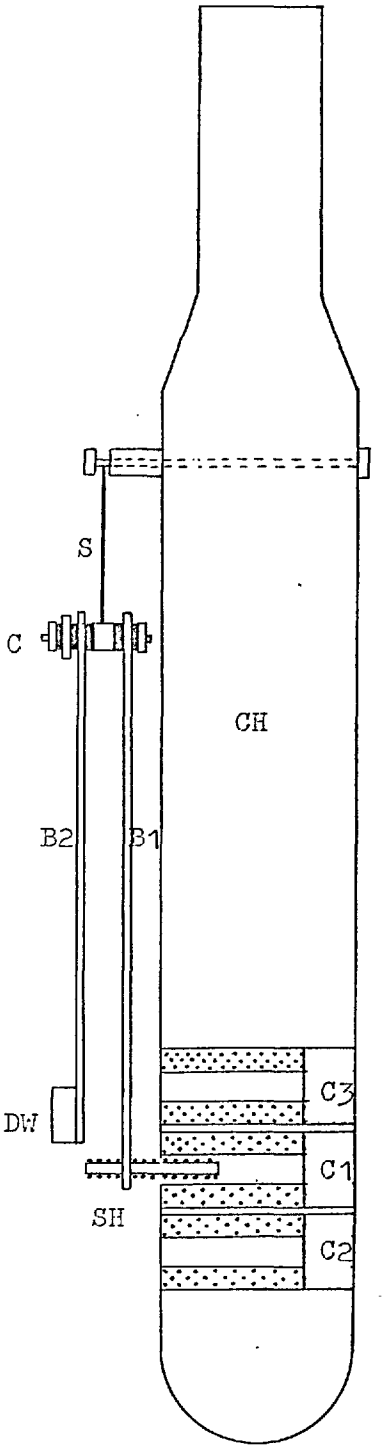

Fig. 10 The Basic Arrangement of the Vibrator and Pick-up Coils

the two bimorphs. CH is the coil housing made out of a Tufnol rod.

Setting up Procedure

A specimen of cylindrical shape machined to the correct dimensions fits inside the specimen holder. A lip formed by heating one end of the glass former in a gas flame helps to locate the specimen to its exact position inside the coil and prevents it from slipping out from that end. The open end can be plugged by a soft cork or small rubber bung; alternatively, easily removable glue or GE varnish is used. It is important that the specimen is fixed firmly inside the coil, as any relative motion between the two will cause damping of the vibration and produce other complex effects.

The pick-up coil is long and cylindrical with a hole through the middle. The specimen is mounted so that half its length is inside the pick-up coil; some clearance around the specimen is necessary for its free movement. The slightest contact between the vibrating specimen and the inside of the pick-up coil gives a large increase in the unwanted synchronous background voltage. The specimen must be located parallel to the coil axis and the bimorphs must not be free to twist about

the suspension. The latter is therefore made of a thin phosphor-bronze strip about 3 mm wide. Since the bimorphs are suspended from the top of the coil housing, some of the vibrations are transmitted to the pick-up coils. Fortunately the effect is small and can be further minimized as explained later. In locating the specimen inside the pick-up coil, the small differential thermal expansion between the material of the coil housing and the bimorphs must be allowed for. As the bimorph itself is made of two different materials, brass in the middle and ceramic on the outside, it bends a small amount when cooled to low temperatures. This bending is generally small unless the surface of the bimorph is cracked or if one side of the bimorph is weaker than the other. A good bimorph, however, performs satisfactorily down to the lowest temperature of 1.5°K used here.

The resonant frequencies of the two bimorphs must be matched and this can be achieved by selecting a suitable dummy weight DW. This is best done when the two bimorphs are clamped together in their final positions. To do this, the common clamp C, Fig. 10, is first fixed rigidly to the body of the coil housing by putting a spacer between the clamp and the coil housing, and tying the two with a piece of wire or thread. The resonant frequency of the bimorph B1 is observed while B2 is held fixed.

The bimorph B2 is loaded until it has the same resonant frequency as B1. The dummy weight can be any weakly diamagnetic alloy or non-metallic substance. Use of a pure metal is not recommended as any eddy currents induced in it can give a large contribution to the signal at the pick-up coils.

Operation

Fig. 11 is a block diagram of the vibrating specimen magnetometer. The two bimorphs are driven by the output from the same oscillator divided into two channels. One output goes via a phase shifter and an attenuator, while the other is connected directly to one of the bimorphs. The relative phase and amplitude of the driving voltages to the two bimorphs can be adjusted to give the maximum amplitude of vibration and hence the minimum reaction of the common clamp C. If the bimorphs are well matched, however, it is only necessary to drive one of them and the second will follow in antiphase.

The voltage induced in the pick-up coil is amplified with a low noise narrow band audio amplifier. The output is fed to a phase sensitive detector, the reference of which is derived directly from the oscillator. The output from the phase sensitive detector is observed on a centre zero ammeter, a

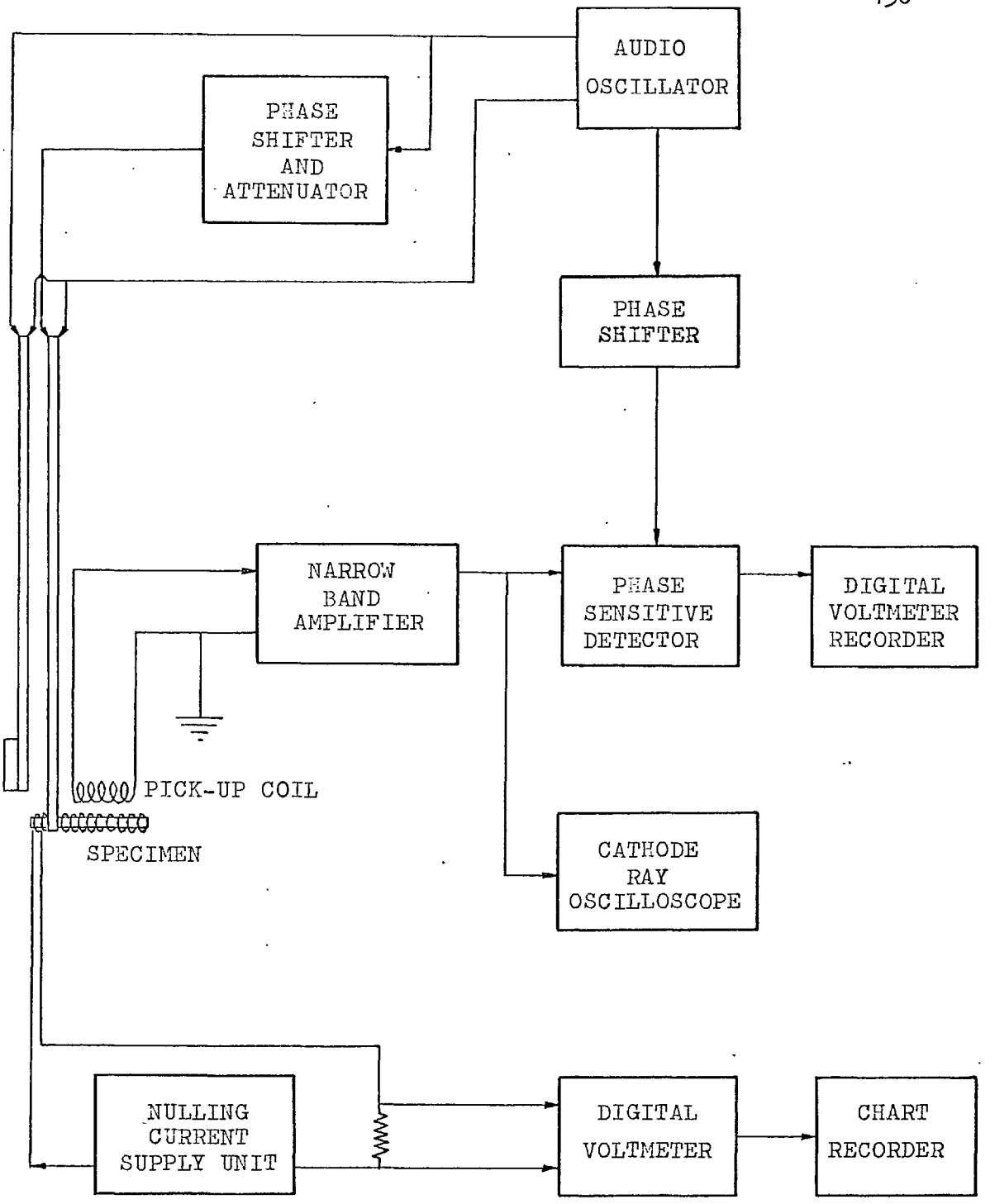

Fig.11 The Block Diagram of the Vibration Magnetometer

digital voltmeter, or a chart recorder. The amplified signal can be observed directly on an oscilloscope connected in parallel with the phase sensitive detector input.

For materials of moderate susceptibility ($\sim 10^{-5}$ emu/gm) the nulling current method is ideal. Besides making unnecessary any allowance for the demagnetisation factor of the specimen, this method makes the measurements independent of any drift in gain of the amplifier and other electronic circuits used. A servo mechanism working off the output of the P.S.D. could be used to vary the current automatically. The use of a digital voltmeter and other accessories to produce digitised output on a paper tape will facilitate automatic recording and quick data processing.

The nulling current method of measurement is impracticable for strongly magnetic materials because the large nulling currents required produce an excessive amount of heating in the coil. A direct measurement of the induced signal is therefore made. This is done in the following manner. A calibration signal produced by a known current of convenient magnitude through the nulling coil is measured on the phase sensitive detector, when the applied magnetic field is zero. Large signals can now be measured in terms of the equivalent nulling currents by using

a calibrated voltage divider at the input to the amplifier. Correction due to the demagnetisation factor of the specimen must be made. This is quite small for the long thin specimen used. For strongly magnetic materials the image effects must also be considered. The image of the specimen produced in the high permeability material of the pole faces will give a contribution to the induced signal in the coil. In the present arrangement, both the specimen and the pick-up coil are in the middle of the pole faces and are sufficiently far away from them for the image effects to be negligible.

The susceptibilities of materials of high electrical conductivity are difficult to measure accurately because of eddy currents induced in them due to the non-uniformity of the field over the volume they displace during vibration. Very large diamagnetic contribution due to eddy currents was observed at $4.2^{\circ}K$ for a specimen of pure gold, despite the fact that a magnetic field having a uniformity in the central volume of 1 cc of better than 1 part in 10^5 was used. Materials of such high conductivity must be laminated or powdered for measurements at low temperatures.

Screening of the Bimorph

A bimorph element is equivalent to a parallel plate capacitor. An alternating voltage applied to the two silver electrodes will give rise to a magnetic field in the region around the bimorph.

This will induce a voltage in the pick-up coils unless the bimorph is screened. A simple way to do this is to use the same principle as employed in a co-axial cable. The bimorph is covered in a piece of masking tape which is painted on the outside with 'aquadag' silver paint. One of the two silver electrodes of the bimorph is connected to this paint and this forms the earthed electrode. The magnetic field is now contained within the volume of the masking tape.

Minimizing the Induced Synchronous Noise Voltage in the Pick-Up Coils

In the present arrangement, the bimorphs are suspended from the top of the pick-up coil housing about 7 centimeters from the main pick-up coil. The suspension is made of a thin phosphor-bronze strip which can transmit various modes of oscillations to the coil housing. The main one is a twisting mode

about the vertical axis giving the largest contribution to the synchronous noise. An independent suspension for the bimorphs would greatly reduce the amount of vibrations coupled to the coils, but the present method has the advantage of making the location of the specimen relative to the pick-up coil much easier.

The total turn-area of the pick-up coil can be represented by an area vector $\underline{A}$ in the horizontal plane. This will be at an angle θ to the magnetic field vector $\underline{H}$ also in the same plane, Fig. 12. The flux linked by the coil is proportional to $\underline{A}\cdot\underline{H}$. Hence the signal induced in the coil due to the rotational mode of vibration about the vertical axis will be proportional to

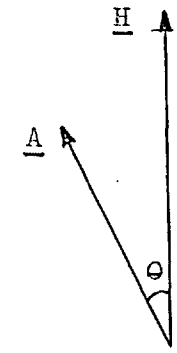

Fig. 12.

$$\frac{\partial}{\partial\theta}(\underline{A}\cdot\underline{H}) = -AH\sin\theta$$

This is obviously zero when $\theta=0$. To set the coil in this position in the presence of a specimen, it is necessary to separate the signal

from the pick-up coil into two components; the true signal due to the magnetisation of the specimen and the inphase component of the synchronous background due to the vibration of the pick-up coil.

It is observed experimentally that the total signal (true signal + synchronous background) is proportional to the amplitude of vibration of the specimen for a given driving frequency. Hence, the ratio of the true signal to the synchronous background signal is independent of the amplitude of vibration, at a given frequency. As a function of the frequency, however, the relative magnitudes of the synchronous background signal and the true signal change in some complicated manner. It is found that the component of the total signal inphase with the specimen signal is given by the equation

Total Signal = True signal from the specimen + $A(\omega)$ sin θ

where $A(\omega)$ is some function of the driving frequency ω, and θ is the angle between the magnetic field and the area vector of the coil. For small θ

$$\sin \theta \simeq \theta$$

If the total inphase signal is plotted as a function of the angle θ for a few frequencies ω around the resonant frequency of the bimorphs, a family of straight lines is obtained, all crossing at one point, Fig. 13. This point represents the true signal due to the specimen only. Actually the point of intersection of the lines has a small spread ($\sim 0.2^{\circ}$ maximum). The corresponding uncertainty in the signal sets the lower limit to the accuracy of the measurements. That this situation is real may be checked by repeating the measurements with either of the two dummy coils as detector. While doing this the magnetic moment of the specimen is bucked out with the nulling current found above (to avoid direct flux linkage from the specimen). The optimum angle for these coils will of course be different (in practice the area vectors of the various coils could be as much as two degrees out of line with each other) but the corresponding signal will be zero or a very small value.

At the optimum angle there is still a small synchronous component in quadrature to the specimen signal. This makes it necessary to detect only the inphase component both while setting up as above and making the actual measurements. The phase of the reference signal to the P.S.D. is easily set to measure the

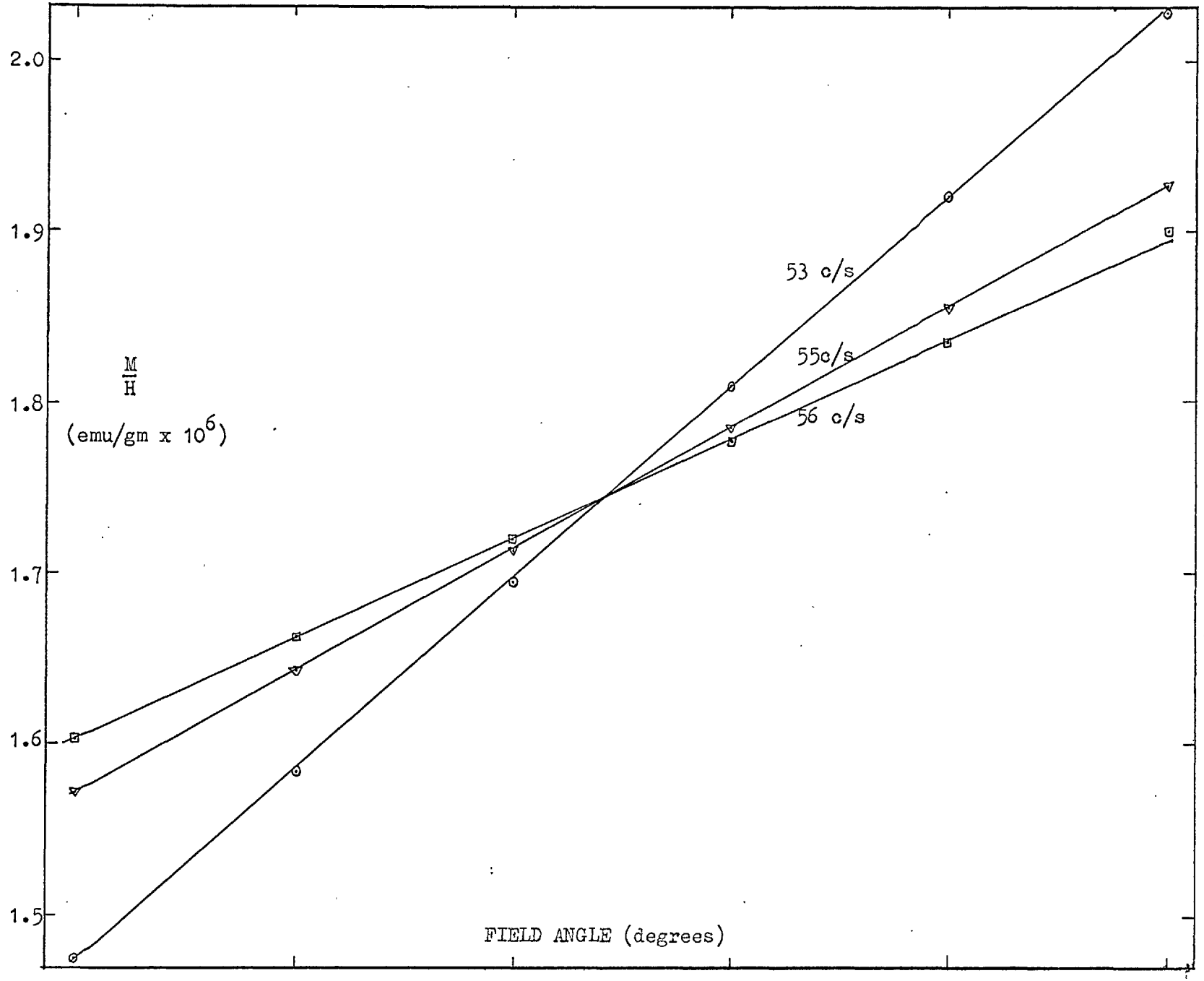

Fig.13 Graph of Signal vs Field Angle for Various Frequencies

inphase component by maximising the observed signal from a magnetic moment produced by a D.C. current through the nulling coil when the applied magnetic field is zero.

The more widely used method of minimizing the synchronous background voltage is to connect a dummy coil having the same turn area and geometry in opposite sense to the main pick-up coil, so that there is no resultant flux linkage with the applied magnetic field. This method reduces the synchronous noise pick-up but does not give the best results in the present instance. This is because it is difficult to get the two area vectors of the coils exactly parallel. As mentioned above, they can be as much as 2 degrees out of line with each other. Also the angle between them will further change in an unknown manner due to distortions produced by temperature changes. As it is possible to get one pick-up coil aligned to the field to an accuracy of a small fraction of one degree, this method will give the least synchronous noise.

Calibration

The magnetic moment of the coil per unit current can be calculated in absolute units from the dimensions and the

number of turns in the coil. However, the accuracy of this procedure is not very good because of the uncertainty in measured dimensions of small coils.

A more accurate method is the calibration of the nulling coil by means of a specimen of known susceptibility. A specimen of pure palladium whose susceptibility was previously measured in a Faraday balance was used to calibrate the nulling coil. The absolute accuracy of calibration was estimated to be better than $\pm 1\%$.

Sensitivity Limits

The residual synchronous noise at the optimum alignment of the coil to the field vector sets the limit to the accuracy of measurement. This is found to represent an uncertainty in the magnetic moment of about 10^{-5} emu in a field of 4 kOe., the specimen mass being 0.25 gm. This corresponds to an error of about 10^{-8} emu/gm in the measurement of the susceptibility. As the synchronous noise is proportional to the field, measurements at higher fields cannot improve the accuracy. The induced signal in the pick-up coil from a specimen of magnetic moment 10^{-5}emu is 2×10^{-7} V (p/p). The Johnson noise in the pick-up coil at room temperature ($R_{coil} \simeq 3k\Omega$) is 7×10^{-9}V(rms), in a bandwidth of 1 cycle. This is further reduced by a factor of 5 at nitrogen temperature ($R_{coil} \sim 500\,\Omega$). Changes in the susceptibility χ of 10^{-9} emu/gm are therefore easily detected at the output of the phase sensitive detector using a suitable time constant ($\sim$1 sec).

The reproducibility for a given specimen (after removal and replacement of the specimen) is better than 0.5 %, but it is important to ensure that the specimen is located exactly in the

same position inside the permanent nulling coil and that the two are of equal length.

Measurement as a Function of Temperature

The elastic constants of the bimorph change with temperature. As the stiffness of the bimorphs increase on cooling so also does the resonant frequency. Between room and liquid helium temperatures the resonant frequency changes by as much as 20%. When making measurements as a function of temperature, the frequency of the driving signal to the bimorphs must be altered to keep in step with the resonant frequency.

The reference signal to the phase sensitive detector is obtained directly from the oscillator. Small but finite changes in temperature will produce corresponding changes in the resonant frequency. As the latter drifts a small amount, the phase angle between the driving signal and specimen vibration, will also change. This means that the phase angle between the reference and the detected signal changes. When the temperature is varying continuously, it is very inconvenient to have to adjust the phase of the reference signal or the driving frequency by small amounts in order to detect the inphase signal.

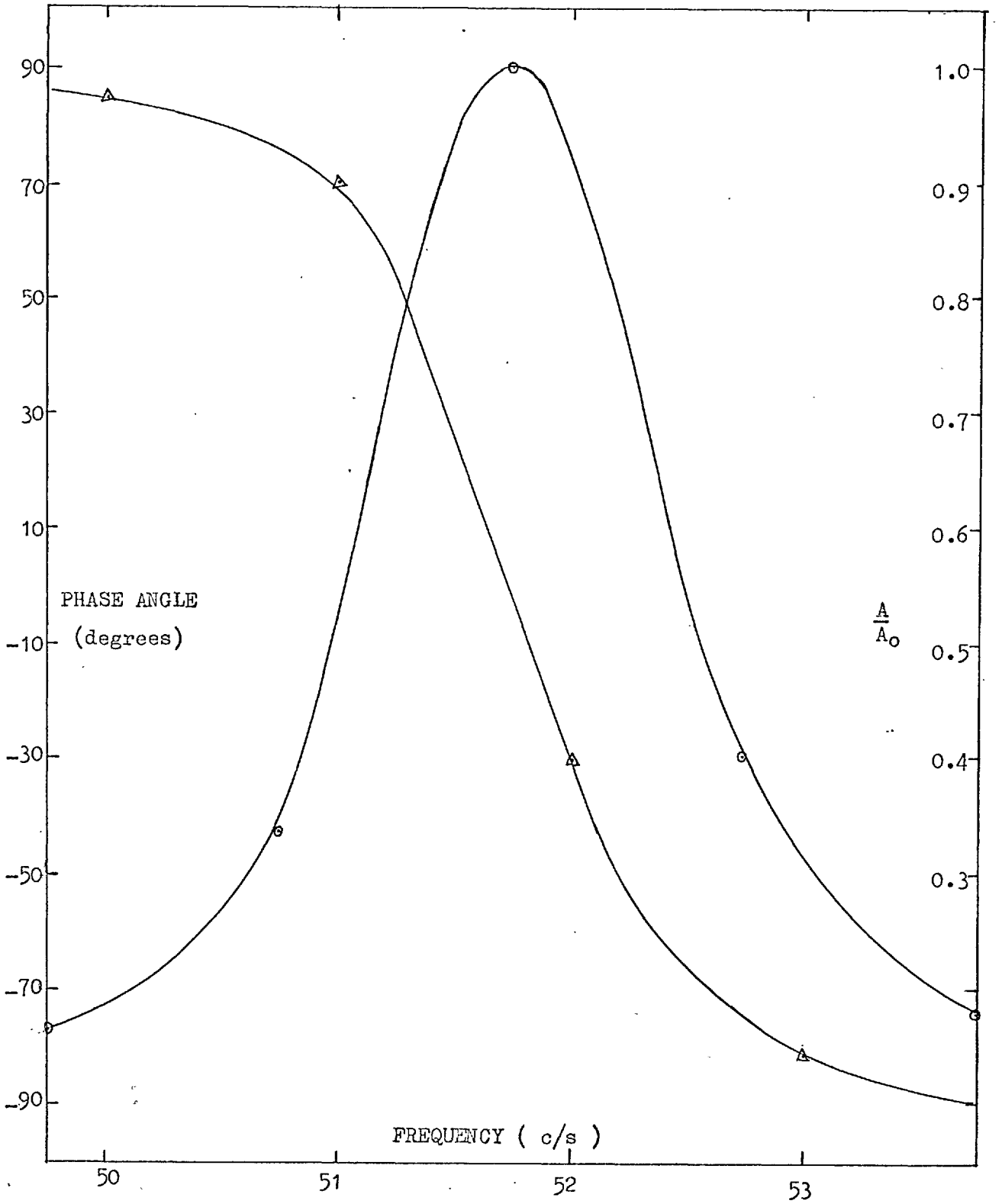

Fig.14 Graph of the Frequency Response of the Bimorphs

The variation of amplitude of vibration of the specimen and the phase angle ϕ between it and the driving signal is shown in Fig. 14. The resonance has a Q-factor of around 30. At one cycle off resonance the amplitude is reduced by about half but the phase angle is in a region where it is changing only slowly with frequency. The bimorphs are therefore driven one cycle off resonance, on the side away from the direction of the drift in the resonant frequency. The amplitude of vibration is, of course, set to the required amount by adjusting the driving voltage. A change in the temperature and hence the resonant frequency only produces a significant change in the amplitude; the effect on the phase angle is fairly small. It is now easy to correct for the frequency change, and measure only the inphase component by adjusting the driving frequency every few degrees change in temperature so as to keep approximately one cycle off resonance.

Possible Improvements in the Design of the Magnetometer

While discussing the coil design, it was pointed out that the optimum coil length for high sensitivity is much shorter than actually used here. When a nulling current method of magnetisation measurement is used, any change in the position of the specimen relative to the coil is unimportant. Hence the use of a coil of optimum size is possible.

The mass of the specimen used is rather small. It is feasible, with the help of slightly larger bimorphs, to use specimens four or five times the mass of the present one. The use of larger specimens will increase the 'filling factor' inside the pick-up coil, and improve the 'pick-up efficiency' of the coil. Let us define the filling factor as the square of the ratio of the diameter of the specimen to the internal diameter of the pick-up coil. A certain amount of clearance between the inside of the pick-up coil and the nulling coil is necessary for free movement. The nulling coil and the glass former on which it is wound also occupy a certain finite volume. Both these can be kept to a minimum. If the two together occupy a wall thickness α then the filling factor is the quantity

$$\left(\frac{d}{d+2\alpha}\right)^2$$

where d is the diameter of the specimen. Clearly an improved filling factor results for a larger specimen.

An independent suspension of the bimorphs from the pick-up coil assembly, taking care to isolate the latter as much as possible from any parts which may communicate the vibrations of the bimorphs will infact lead to the greatest

improvement in the signal to synchronous background signal ratio. The use of any coil geometry which makes the specimen location relative to the coil easy or unimportant (for a nulling current method of measurement) will facilitate the independent suspension of the bimorphs.

THE EXPERIMENTAL DETAILS

The Cryostat

The cryogenic design for a system for operation between room temperature and pumped helium temperature range ($300^{\circ}K$ to $1.5^{\circ}K$) is fairly simple. Liquid nitrogen is used to obtain temperatures down to $77^{\circ}K$ after which liquid helium is transferred into the dewar. By pumping on the helium bath with a rotary pump temperatures down to $1.6^{\circ}K$ are obtained. Temperatures above $4.2^{\circ}K$ are obtained by the normal warm up due to the heat leak into the system which can be augmented by electrical heating.

Two pyrex glass dewars with silvered walls are used, one of which is for liquid helium and the other for liquid nitrogen. The helium dewar has a pumping line connected to the interspace so that it can be flushed out with pure nitrogen and re-evacuated before every run. This is necessary because helium gas in the dewar diffuses through the walls and softens the vacuum over a period of time. Flushing out the interspace with pure nitrogen permits a very high vacuum to be obtained at helium temperatures as any residual nitrogen in the dewar freezes out at these temperatures leaving a very hard vacuum in the interspace. The nitrogen dewar interspace is permanently evacuated and sealed off.

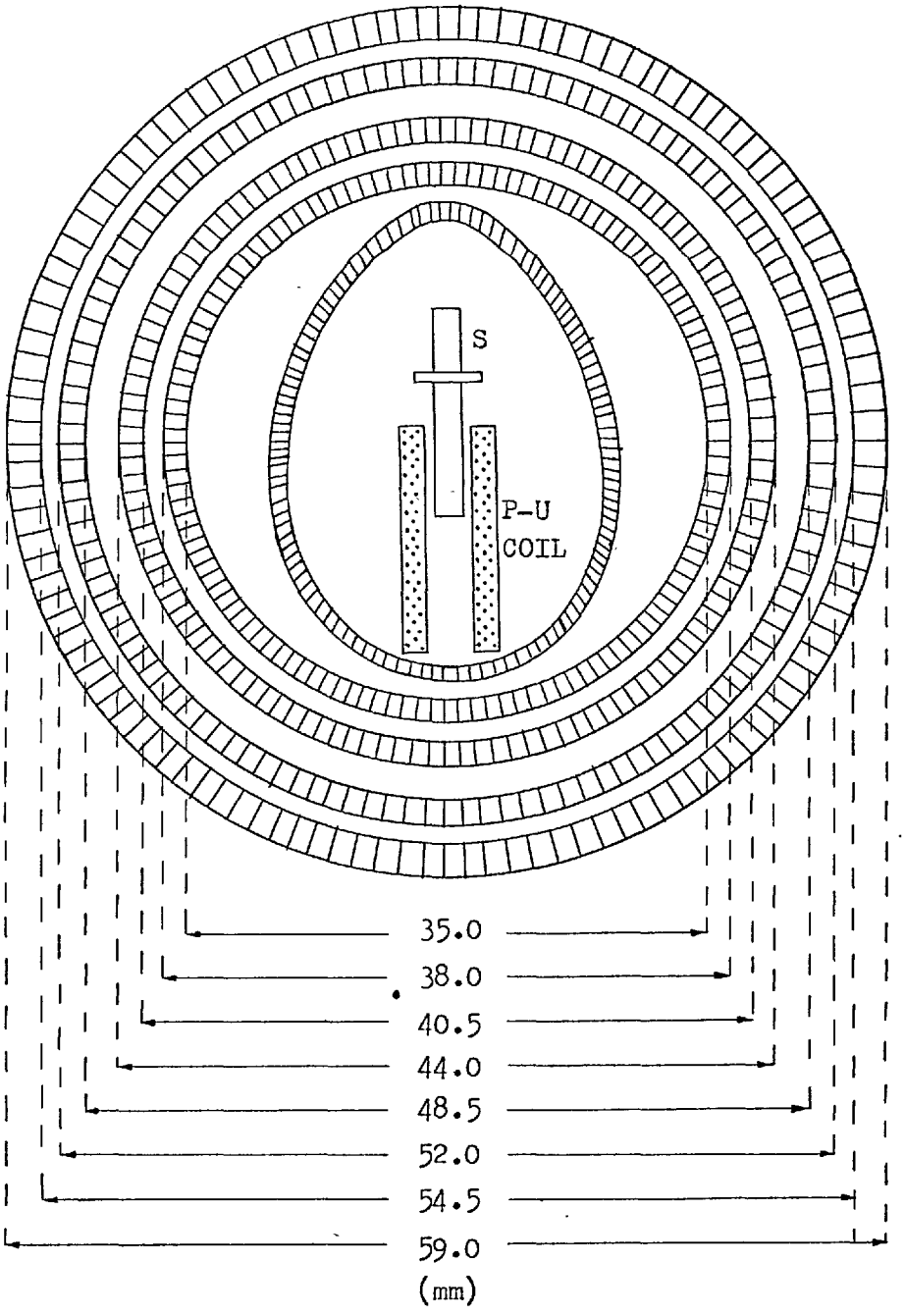

Fig.15 Diagram of the Cross Section of the Tail of the Dewars

The dewars were designed for use with the Newport type D magnet with 6 cm pole gap. The cross section of the tail-half of the dewar is therefore made narrow enough to fit between the pole faces. In order to obtain the maximum possible space inside the helium dewar for the magnetometer and the glass tube enclosing it, the dewars were made from carefully selected high tolerence medium wall (2.5 mm to 3.5 mm) glass tubes. An internal diameter of 35 mm for the tail section of the helium dewar was obtained. The glass tube jacket covering the magnetometer was specially drawn into an approximately oval shape in order for it to enclose the magnetometer and leave enough space inside the dewar for the liquid helium. A diagram of the cross section of the tail of the dewars is shown in Fig.15

The Dewar Cap

A cross section of the dewar cap is shown diagrammatically in Fig. 16 . It is made out of brass and consists of three separate pieces which facilitates dismantling and reassembling. The central brass tube B1 is joined to a glass tube extension G1 which carries the coil assembly at its end.

Aquadag silver paint on the tube helps to screen the pick-up coil leads which pass through its centre and emerge at the top T. A glass to metal seal GM joins the concentric glass tube G2 to a brass connector BC. The latter screws on to the dewar cap and is sealed to it by an O-ring seal shown. The tube G2 is made in two halves which join together by means of a ground glass joint. The purpose of the tube is to hold the coils centrally in position and to provide a cover over the specimen to prevent any air condensing over it during helium transfer. A hole in the bottom of the tube and two small ones half way up allow the helium to enter inside and the gas to escape out of it. This permits measurements below $4.2^{\circ}K$ to be made while the specimen is immersed in a bath of helium. This is useful when the nulling current method is used for the measurements on highly magnetic materials. A completely sealed tube can also be used if required, to isolate the magnetometer completely from the helium dewar. The tube can be evacuated by pumping through the connector C1. There are three more connectors on the side of the dewar cap which have access to the space inside the helium dewar. One of these is used for pumping on the helium with a rotary pump, the other provides a connection for the mercury and oil manometers for vapour pressure measurement

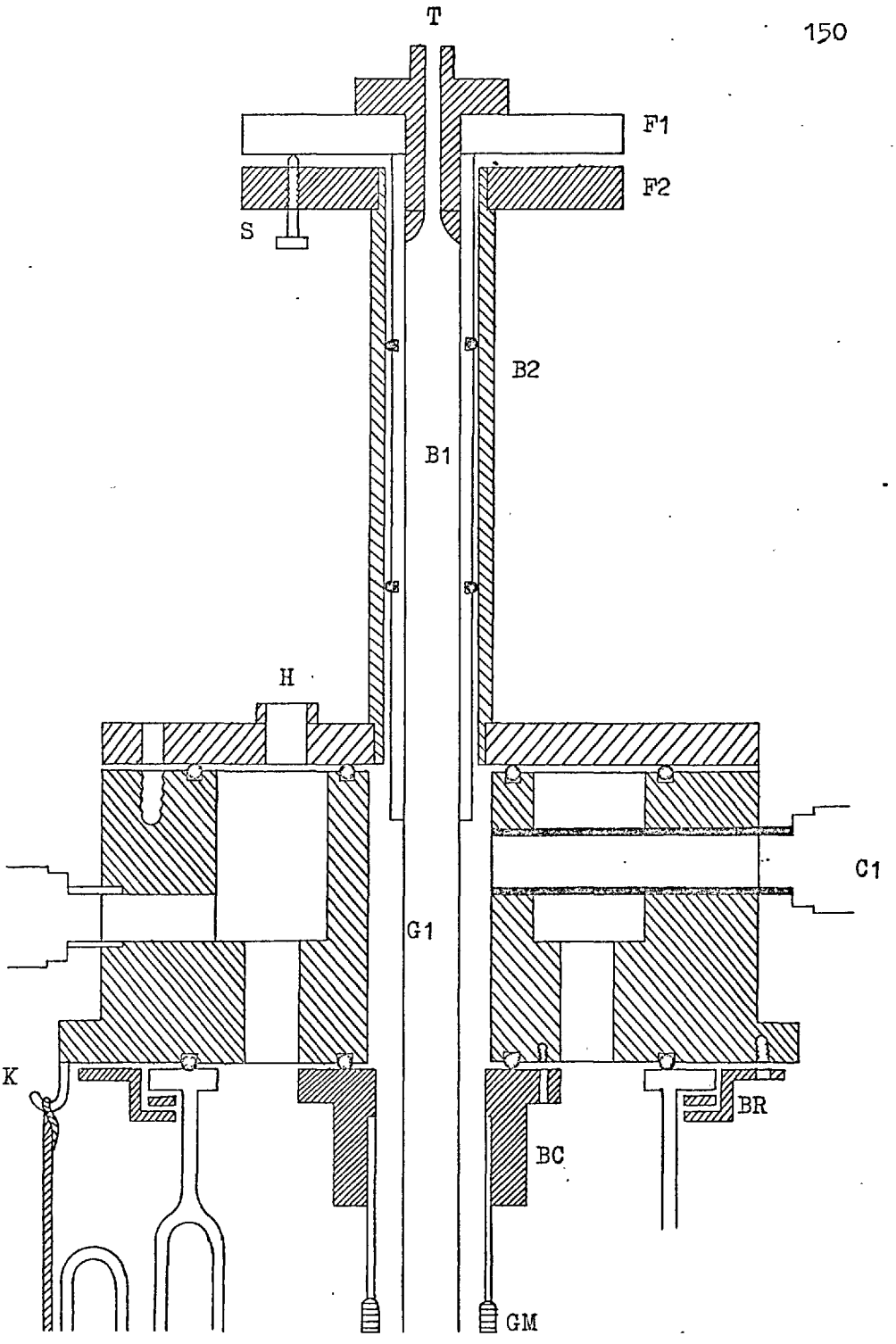

Fig.16 Diagram of the Cross Section of the Dewar Cap

and the third is connected to the helium return line.

The helium dewar is held against the dewar cap by a circular brass ring BR around the dewar flange. There is an O-ring seal between the flange and the dewar cap. The nitrogen dewar fits on the outside of the helium dewar and is held in position by strings hooked to the dewar cap at K. This provides a very flexible mounting and reduces the risk, due to any slight misalignment, of stressing the dewar when wheeling the electromagnet in and out of position.

There is a circular flange F, on top of the inner brass tube B1 and a corresponding one F2 on the concentric outer tube B2. The height of the inner tube relative to the dewar cap can be adjusted by means of the screws S. Two O-rings between the brass tubes B1 and B2 which help to hold them concentric, provide a vacuum tight seal and also permit vertical movement and rotation about the vertical axis of the tube B1 and hence of the coil assembly.

Helium is transferred into the dewar from a storage vessel by means of a helium transfer syphon which is introduced through the hole H. A section from the flanges F1 and F2 is cut out to enable the syphon to be introduced through H.

The Pick-up Coil

The pick-up coil former is machined from a $\frac{1}{4}$" diameter Tufnol rod. The length of the former is 0.6" and the diameter of the hole along the axis is 0.12". About ten thousand turns of 49 s.w.g. enamel coated copper wire are wound on each coil. Short lengths of thicker wires (46 s.w.g.) are soldered to the two ends of the coil as the thin wire used for winding the coil is easily broken while handling it. A coat of G.E. varnish is applied to the top layer of the coil for its protection from scatches.

The Coil Housing

This is machined to a shape similar to that shown in Fig.10, from a Tufnol rod of $\frac{3}{4}$" diameter. Three circular holes drilled near one end of the rod carry the three pick-ups coils. A length of about 2" of the Tufnol rod is turned down to a diameter of $\frac{1}{2}$". This fits inside the central glass tube G1 in the cryostat. The leads from the coil are soldered to a set of terminals formed by fixing short lenghts of 26 s.w.g. copper wires near the coils. Thicker leads, 36 s.w.g. wires, from these terminals pass through a hole along the axis of the Tufnol rod and are joined to a second set of terminals at the top of the thinner end of the Tufnol rod.

The exposed terminals near the coils are covered with Q-compound and the whole of the coil holder is painted with 'aquadag' silver paint for electrical screening. A small D shaped piece of phosphor-bronze strip fixed to the end of the coil.holder helps to fix the latter inside the glass jacket.

The Nulling Coil

The coil former is a commercially obtained thin walled (0.004") pyrex glass tube of internal diameter 0.055" and length about 0.6". One end of the former is heated gently in a gas flame to form a lip which is useful for locating the specimen at a fixed position inside the nulling coil. A two layer nulling coil, for the convenience of having both leads at one end, is wound on the former in the following manner.

The former is gently slipped onto a piece of straight thin rod wrapped with a few turns of soft tissue paper. This is held in a chuck of a hand drill which is clamped in a vice. A reel of 49 s.w.g. enamel coated copper wire is mounted on a straight rod clamped to a retort stand so that the wire can be easily unreeled. The coil winding is begun from one end. The thumb and the index finger of the left hand are used to feed the wire. By adjusting the angle of the feed slightly

away from the normal a very uniform and tightly wound layer can be obtained. When the first layer is wound (about 350 turns) a very thin coat of G.E. varnish (one drop of G.E. varnish diluted with 10 cc of solvent) is applied to it. When this dries the second layer is wound on top of the first in the same manner. A thicker coat of G.E. varnish is then applied, and when this has dried two pieces of 46 s.w.g. wires are soldered to the leads. The soldered ends are insulated by painting with G.E. varnish and the leads are then wrapped around the coil a couple of times in a non-inductive manner. Another coat of G.E. varnish is then applied over the whole coil and allowed to dry. The coil is then fixed in the hole in the piece of thin copper strip extension on one of the bimorphs and glued into position by means of G.E. varnish.

Magnetic Moment of the Nulling Coil

The magnetic susceptibility of the nulling coil, which is made of a glass former and a copper coil both of which are diamagnetic materials would normally be expected to be small, negative and roughly temperature independent.

The susceptibility of the coil is, however, found to be paramagnetic and also field dependent. The major contribution

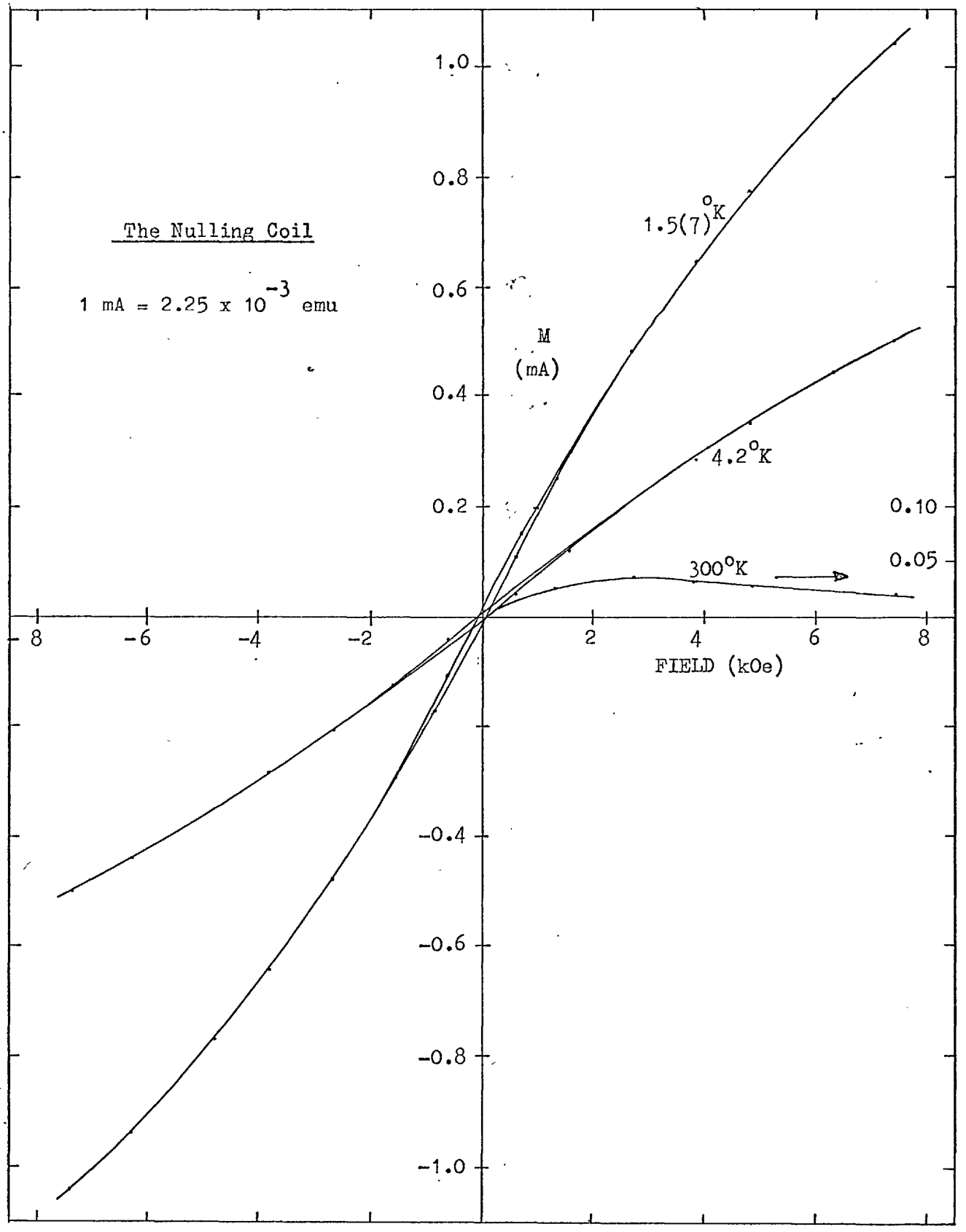

Fig.17 Graphs of Magnetisation vs Field for the Nulling Coil

to the paramagnetism is thought to be due to the impurities in the copper wire, because the susceptibility contribution from a smaller piece of glass tube, similarly manufactured, placed inside the coil, was found to be quite small and temperature independent.

The form of the magnetisation against field for the nulling coil at room and nitrogen temperatures is roughly similar. At room temperature the magnetic moment increases approximately linearly with field for very low fields, begins to curve strongly above 1 kOe and reaches a maximum at 2.5 kOe. For higher fields, it tends to decrease slightly, Fig. 17. This behaviour may be attributed to the presence of a small amount of ferromagnetic impurities in the coil. A small hysteresis loop can be seen in the M-H plot at 77°K, Fig.17. This becomes larger at 4.2°K and 1.6°K, Fig. 17, indicating an increase in the amount of ferromagnetic phase with decreasing temperature.

The magnetisation of the coil as a function of temperature has been measured in a field of 3.83 kOe, Fig. 18, which is close to the fields at which magnetisation versus temperature measurements on most alloys have been made. This is done in order that corrections for the magnetic moment of

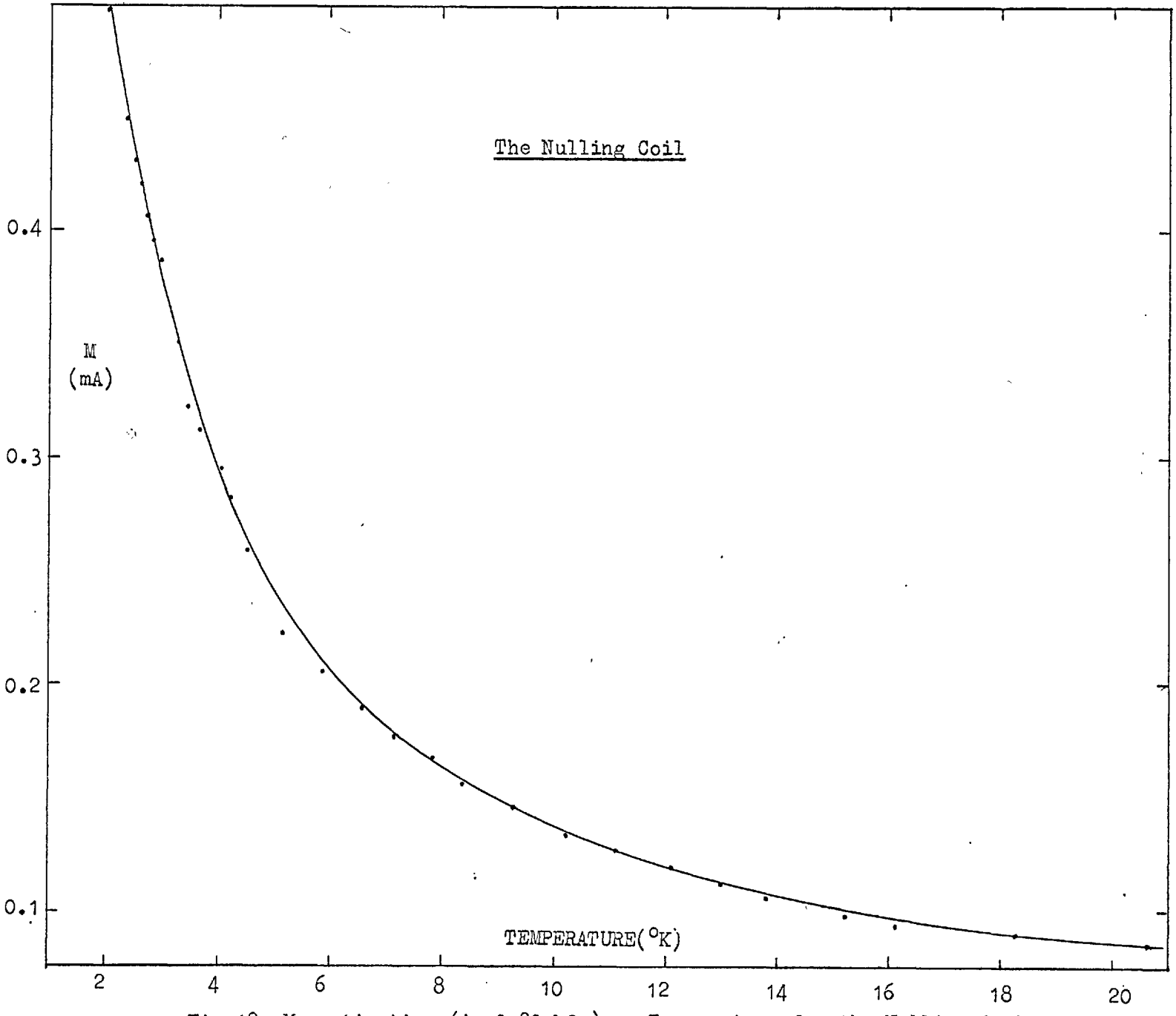

Fig.18 Magnetisation (in 3.83 kOe) vs Temperature for the Nulling Coil

the nulling coil can be made with accuracy. (The allowance for the actual field used is, of course, made).

The corrections for the moment of the coil at other fields (above 1 kOe) have been made by assuming a saturated ferromagnetic component equivalent to a nulling current of .035 mA (which is observed at room and nitrogen temperatures) and a paramagnetic component obtained by linear interpolation from the measured magnetisation in 3.83 kOe (minus 0.035 mA). This is found to provide a correction which has a maximum error of $\pm$ 10% at low temperatures. No attempt was made to obtain a better method of correction (say by measuring M vs T dependence of the coil at other fields) because fields very much different from 3.8 kOe were only used for magnetisation against temperature measurements on highly magnetic materials due mainly to the necessity of keeping the nulling currents low. For these, the correction due to the moment of the coil was usually less than 1% of the specimen moment, so that the error due to the above approximation was negligible. M vs H measurements on the nulling coil at 300, 77, 4.2 and 1.6°K were used to obtain the corrections for the M-H curves of the specimen measured at these temperatures.

Magnetoresistance of the Nulling Coil

The resistivity of a conductor in a magnetic field is a function of both the strength and the direction of the field with respect to the current flow. According to the Kohler's law, the transverse magnetoresistance of a pure metal in low fields is proportional to the square of the applied magnetic field. The increase in the resistance can be expressed as

$$\frac{\Delta\rho}{\rho} = A\left(\frac{H}{\rho}\right)^2$$

or

$$\Delta\rho \times \rho = AH^2$$

where A is a constant having dimensions of (resistivity/field)^2

There will in general be departures from this rule due to many causes, the important one being the presence of magnetic impurities, which give a negative contribution to the magnetoresistance. The whole length of the copper wire in the nulling coil is transverse to the magnetic field. The magnetoresistance observed at 4.2^{o}K is shown in Fig. 19, from which it is clear that Kohler's law is not obeyed.

The magnetoresistance of the coil must be corrected

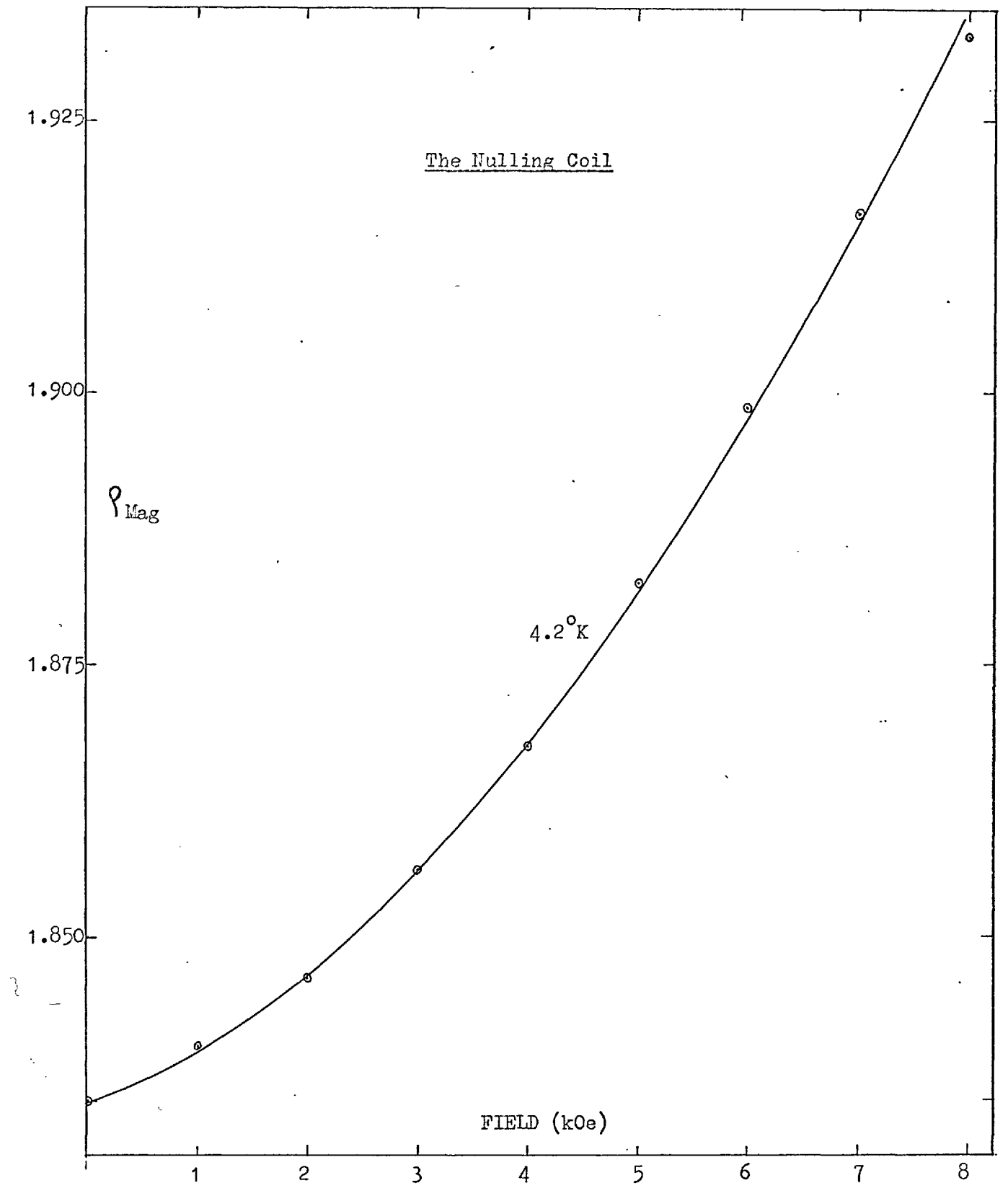

Fig.19 Magnetoresistance of the Nulling Coil

for when determining the temperature from the measured resistance in a finite field. Since Eq. 5 is not followed, an approximate form of variation given by

$$\Delta R \times R = f(H)$$

is assumed where f(H) is the observed functional dependence at $4.2^{\circ}K$.

The same functional dependence was also observed at $20^{\circ}K$ and was assumed to be valid at all temperatures. The correction ΔR to the resistance for any finite field H, and any temperature T is determined by interpolation using the curve of Fig. 19. If R_H is the measured resistance in a field H then

$$(R_H - \Delta R)\,\Delta R = f(H)$$

$$\Delta R = \frac{f(H)}{R_H\left(1-\frac{\Delta R}{R_H}\right)} \simeq \frac{f(H)}{R_H}\left(1+\frac{f(H)}{R_H^{\,2}}\right)$$

The formula gives a correction ΔR which is inversely proportional to the actual resistance R, hence the percentage correction becomes quite small at high temperatures. The errors in the temperature obtained using this approximation are found

to be well within the accuracy of temperature measurement ($\pm 0.1^{\circ}K$ between 20 and $40^{\circ}K$). This fact was confirmed by the susceptibility measurements on an Au-Ho sample in various fields between 1 and 6 kOe, while the specimen was warming up steadily at the rate of $10^{\circ}K$ per hour. The temperatures were obtained from the simultaneous measurement of the resistance of the coil. The scatter in the $\frac{1}{\chi}$ vs T points was no larger than when the susceptibility was measured using a constant field. The correction ΔR to the resistance above $50^{\circ}K$ is negligible for all fields up to 8 kOe.

Heating Effects in the Nulling Coil

The upper limit to the magnetisations which can be measured by the nulling current method is set by the amount of heating produced in the coil and the maximum tolerable error in the temperature of the specimen due to this. The heating effects in the coil were observed in the measurement of the magnetisation as a function of field of some gold-rare earth alloys at low temperatures. If the specimen (and the nulling coil) is immersed in a large bath of liquid helium, the maximum nulling currents which can be used are found to be an order of magnitude larger than if the specimen is above the helium in the gas.

Fig. 20 shows the magnetisation (in mA) as a function of field (kOe) of a Au-Yb specimen at $4.2^{\circ}K$ as measured in liquid helium (curve a) and as measured in the helium gas (curve b). It is seen that the departures in the two curves begin to become apparent around 10 mA. This corresponds to a magnetic moment of $\sim 10^{-2}$ emu. The heat dissipation in the coil ($R=1.6\,\Omega$) is about 10^{-4} Watt and the temperature rise is approximately $0.15^{\circ}K$. The limit to the nulling current when the specimen is immersed in liquid helium was studied by comparing the magnetisation curves of a Au-Ho sample obtained by the direct measurement of the output signal from the pick-up coil Fig. 20(curve a) and by measuring the corresponding nulling current (curve b). The two curves begin to deviate around 120 mA of nulling current, which is equal to a heat dissipation of about 10^{-2} Watt. The corresponding magnetic moment is $\sim 10^{-1}$ emu.

Since the susceptibility measurements above $4.2^{\circ}K$ are made in helium gas, care is taken to use low enough magnetic fields so that the nulling currents required to buck out the moment do not exceed 10 mA. As the temperature increases, of course, the heating effects become relatively less and less important (the fractional rise in temperature due to a given amount of heat dissipation becomes smaller). If it is required

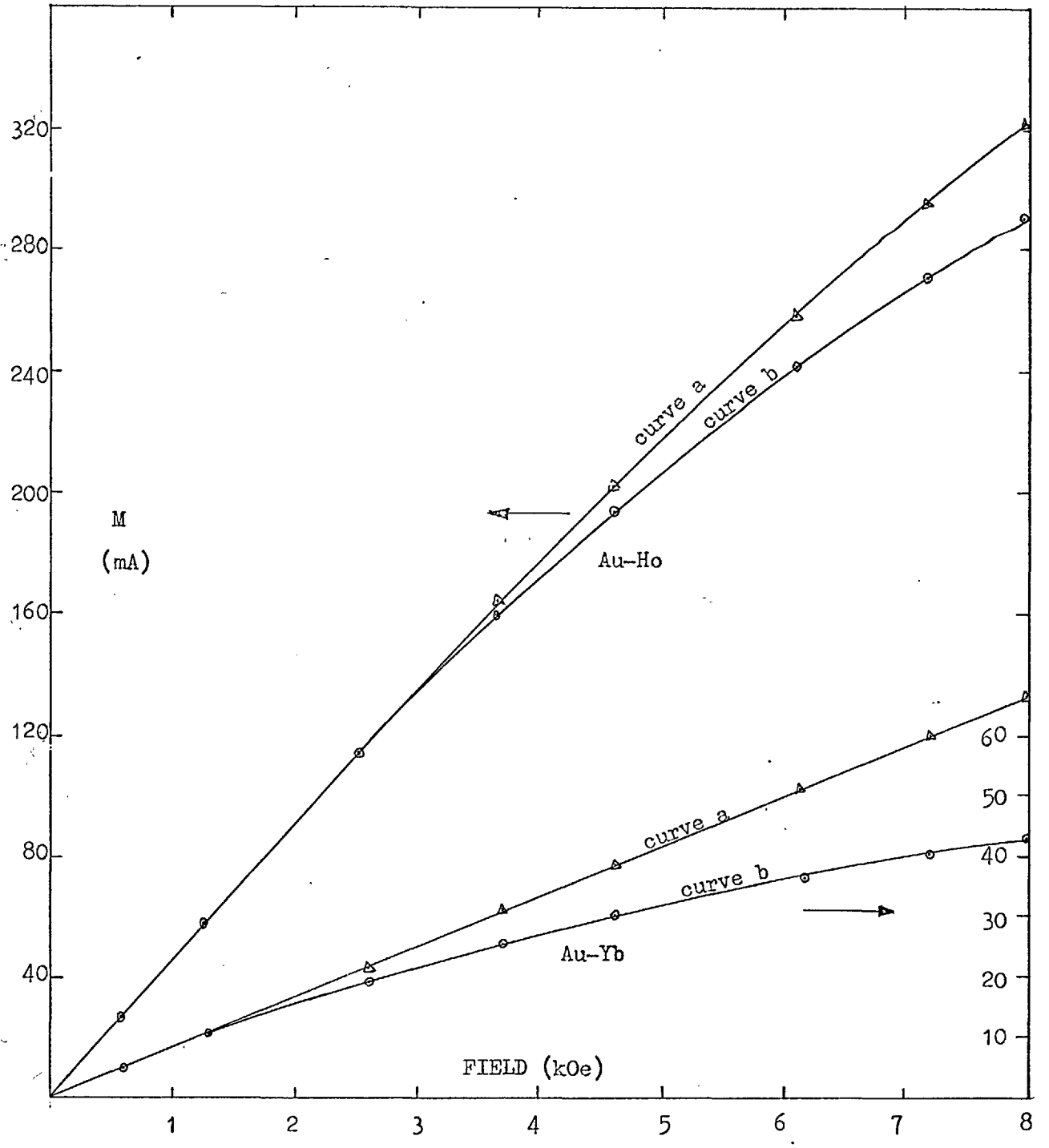

Fig.20 Heating Effects in the Nulling Coil

to measure large magnetic moments the method of direct measurement of the signals is always used.

Electronic Circuits

a) The Amplifier

An audio frequency transistor amplifier was built for the amplification of the induced signals in the pick-up coil. A common emitter configuration of the transistor was used in the amplifying stages. Three such stages were connected in cascade separated by emitter follower stages. The last amplifying stage was partially decoupled from the common battery by means of a series load R' and a capacitor C to prevent the circuit from oscillating due to feed back through the battery. The gain of the amplifier is controlled by a potential divider R at the input to the second stage. A maximum gain of 10^5 can be obtained from the amplifier.

The input impedance of the amplifier is about 10 kΩ. The noise in the amplifier expressed as the equivalent input voltage is 1 V(p/p) in a bandwidth of 1000 Hz (3db points: 20 Hz and 1 kHz) when the source resistance is 500 Ω, which is the resistance of the pick-up coils at nitrogen temperature.

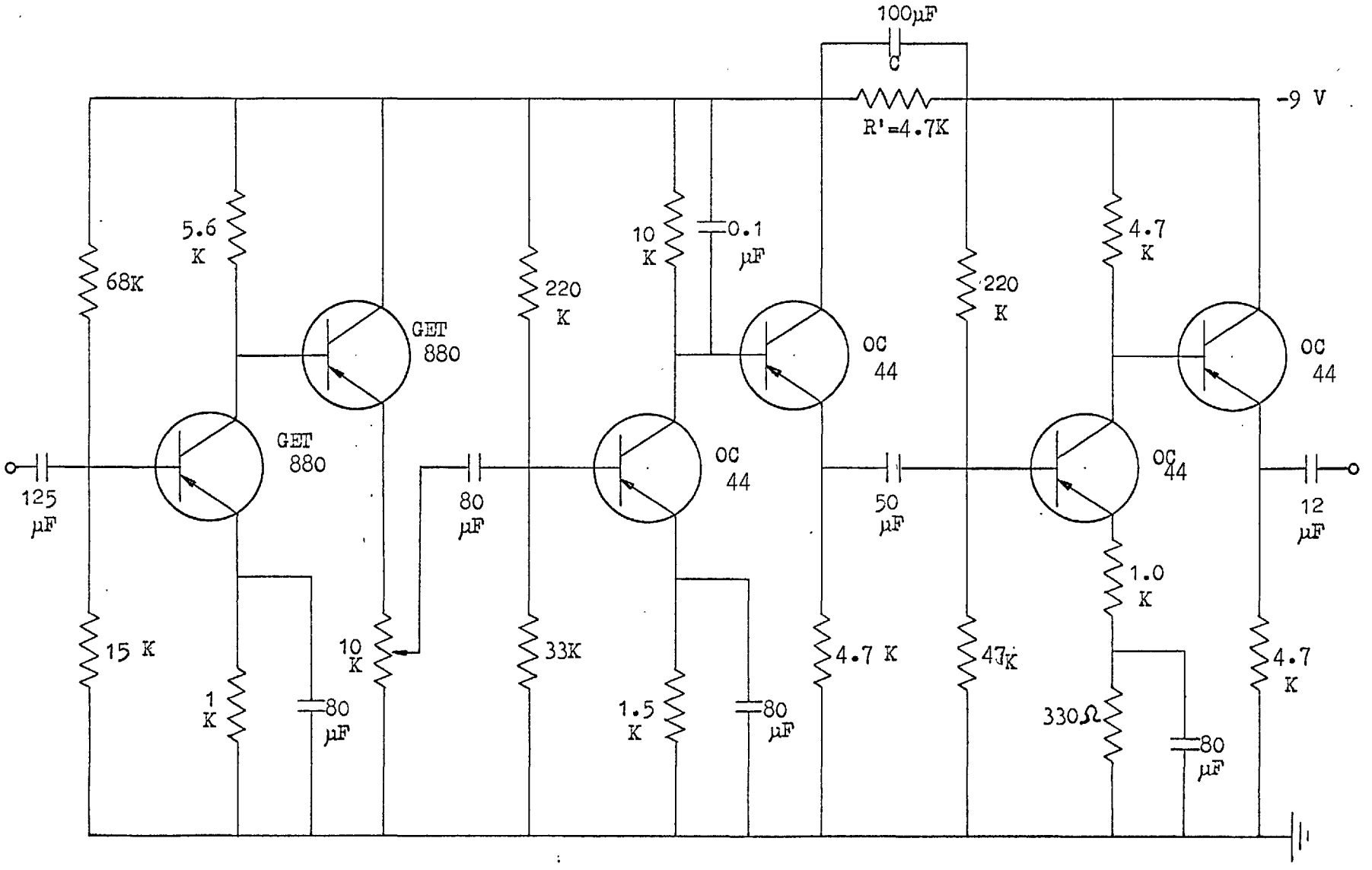

Fig.21 Circuit Diagram for the Amplifier

The noise becomes rapidly worse with increasing source resistances. The equivalent noise voltage at the input increases to 2 V(p/p) at room temperature where the coil resistance is 3 kΩ. A circuit diagram of the amplifier is given in Fig.21 .

The noise figure for the amplifier is poor (~ 10 db) but this does not limit the accuracy of the measurements as the sensitivity of signal detection is an order of magnitude higher than the level of synchronous background due to the vibrations transmitted to the pick-up coil

b) The Phase Sensitive Detector

A transistor phase sensitive detector circuit due to Faulkner and Harding (153) has been used. The circuit diagram is shown in Fig.22a. The circuit uses no transformers or chokes and the switching action is performed without saturating the transistors. The signal is fed to the point S, and a sinusoidal reference of about 1 V (p/p) is applied in antiphase at the points G and H. This is derived from a phase shifter circuit shown in Fig.22b. The gain of the detector can be varied by decoupling part of the resistance R1 with a capacitor C1. This is done in a continuous fashion by using a wire-wound potentiometer R1. Capacitors C2' and C2" are connected across

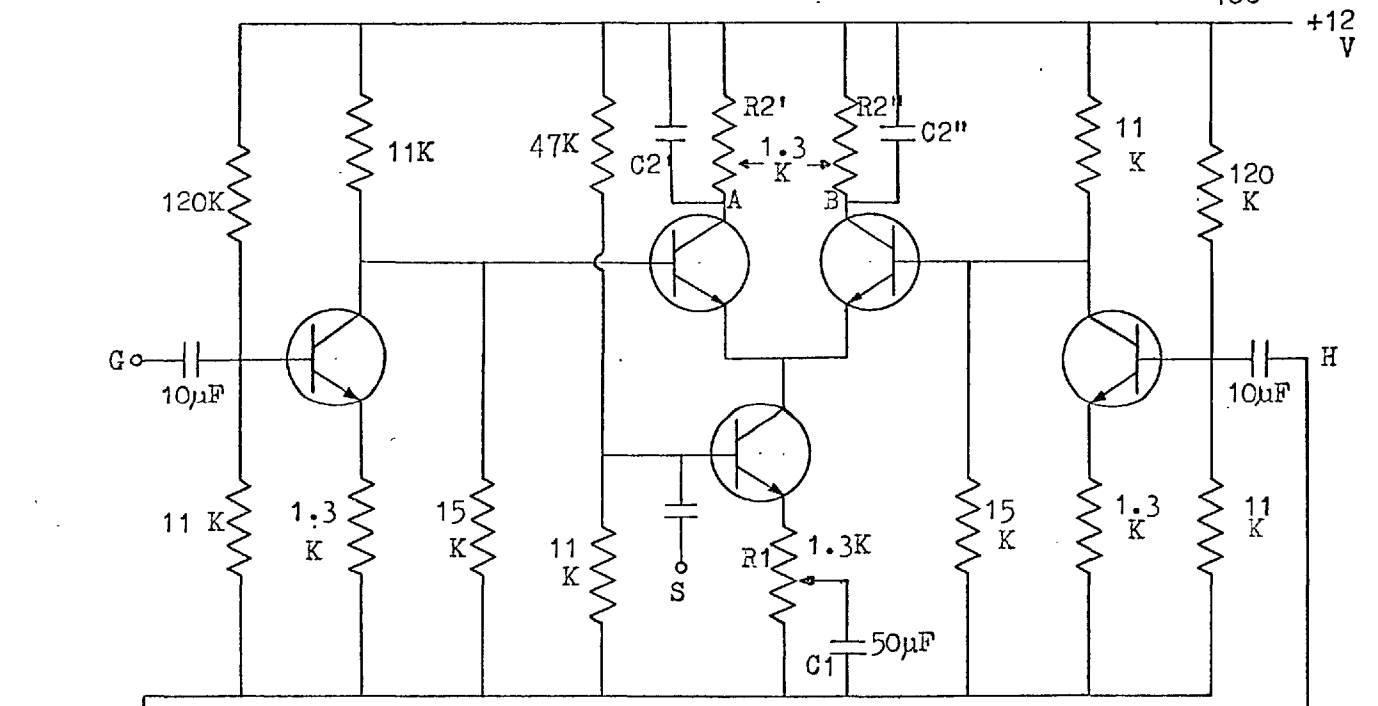

Fig.22a

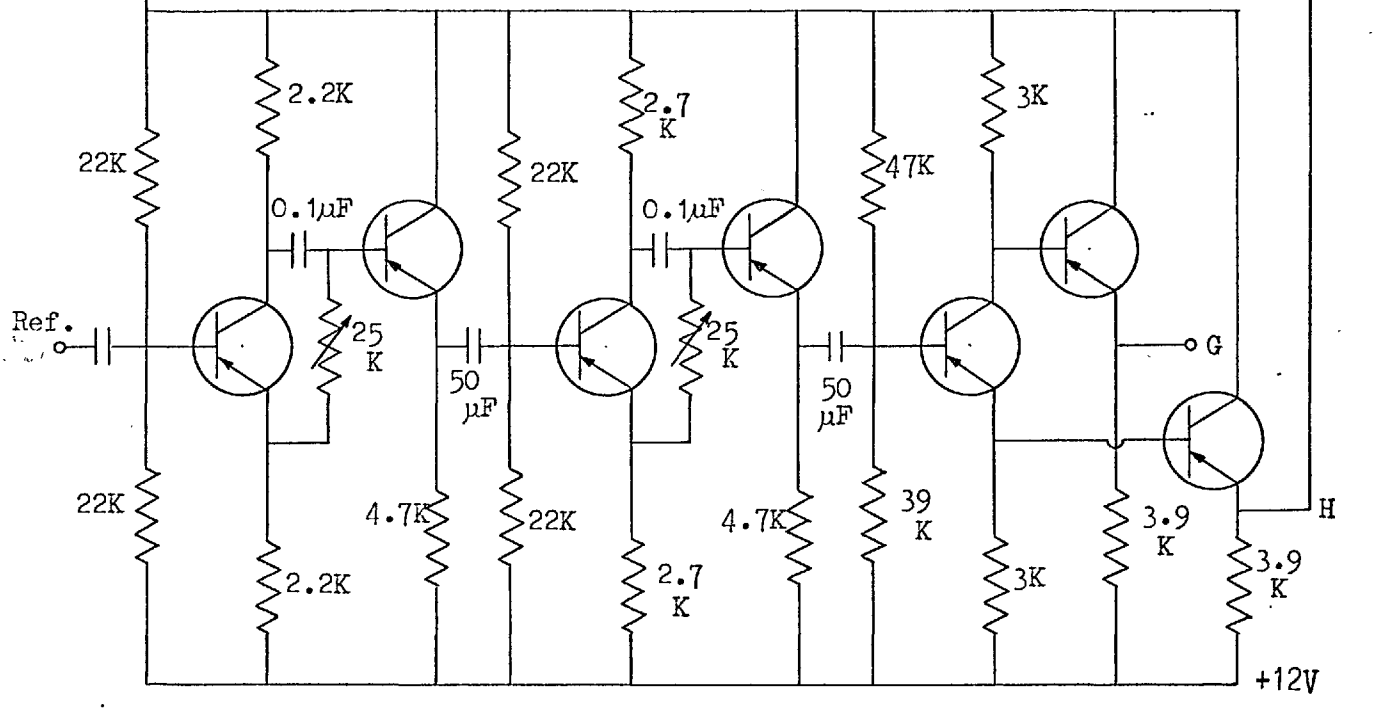

Fig.22b

Fig.22 Circuit Diagrams for the P.S.D. and the Phase Shifter

the resistance R2' and R2" and the output is observed across the points A and B. The magnitude of the capacity used and the collector resistor value determines the time constant of the detector. This can be varied by switching in different values of capacitors C2' and C2". A centre zero ammeter is used to observe the output because of its convenience in the null method of measurement. The output can also be observed as a potential difference across a resistance R connected between the points A and B. This is done when the direct measurements of the induced signals in the pick-up coil are made. The output could also be observed on a chart recorder if required.

Screening and Earthing Arrangement

Fairly large voltages (10 V rms) are used for driving the bimorphs. In order to keep the heat leak into the cryostat to a minimum, the leads carrying the voltage to the bimorphs are made out of 42 s.w.g. copper wires twisted together. Special care is therefore taken to screen the pick-up coil and its leads to avoid pick-up from the driving signal.

The coil housing is painted with aquadag silver paint. A lead painted to the body of the housing emerges from the top T

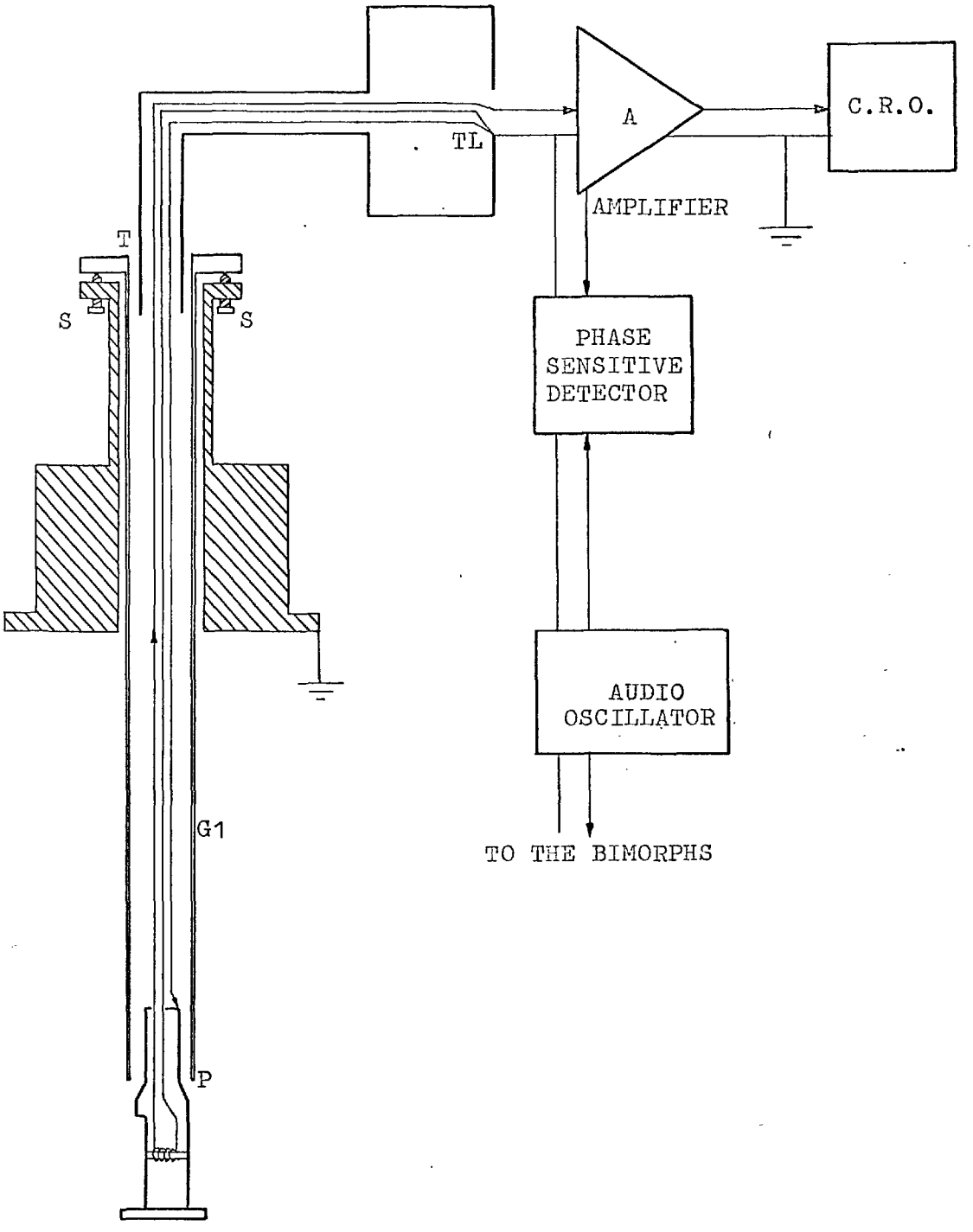

Fig.23 Diagram for the Screening and Earthing Arrangement

of the cryostat along with the leads of the pick-up coil and is there connected to one of the two leads of the coil at the terminal TL. This forms the common line to the electronic circuits which is finally connected to earth at the scope Fig.23. The glass tube G1 which is also painted with aquadag silver paint screens the length of the coil leads inside the cryostat It is separately earthed through the dewar cap by making contact through the screws S on the top flange. Care is taken to ensure that the silvered glass tube G1 and the body of the coil housing do not make an electrical contact at the point P, otherwise an earth loop results; similarly an electrical contact is avoided at the point T. It is difficult to justify the separate earthing for the glass tube G1, but in practice it is found to give the least pick-up.

The Power Supply

A stabilised d.c. power supply with a maximum current output of 15 Amps. was specially made for the magnet by Wareham (Measuring systems) Limited. This permits magnetic fields up to 8 kOe to be obtained with the Newport type D electromagnet with a 6 cm pole gap. The current can be set to a desired value by a ten turn helical potentiometer with the smallest graduated

interval of 15 mA, and having a reset accuracy of 2 parts in 10^4 (specification). It is found that the field can be reset to an accuracy of better than $\pm$ 1 Oe over the whole range. The stability of the power supply over a long period of time is excellent (specification: 0.1% over 1 hour). The best feature of the power supply is the extremely low mains ripple (specification: rms ripple less than 0.01% of output power) which permits the use of a single pick-up coil essential in the present method of minimizing the synchronous background signal. If the ripple and noise from the power supply were large, two pick-up coils connected in series opposition (to balance out the flux linkage of the coils to the field) would be necessary in order not to overload the detector circuits.

Thermometry

For accurate measurement of the temperature of a specimen, the temperature sensor must be in good thermal contact with it. The nulling coil wound around the specimen provides an excellent resistance thermometer satisfying this requirement. Above 25°K the resistance of the copper wire is a strong function of temperature and hence it is a very sensitive

temperature sensor. Below 25°K a carbon resistance thermometer has been used which is also very sensitive below this temperature. It is, however, very difficult to attach it directly to the specimen, hence it is mounted very close to it on the face of the pick up coil. It was checked, using a specimen obeying Curie Law as its own thermometer, that in the range 4-25°K where the equilibrium is provided by the helium gas the temperature indicated by the carbon thermometer was that of the specimen, within the accuracy of measurement (see below). These two thermometers are adequate to cover the whole temperature range (1.6 - 300°K).

a) The Carbon Thermometer

An Allen Bradley Carbon resistor of nominal resistance 47 Ω at room temperature was used as the thermometer. These resistors are very sensitive temperature sensors below 25°K where they exhibit a very rapidly varying resistance with temperature. Clement and Quinnell (152) have observed that the resistance of these carbon resistors can be expressed to within ±0.5 per cent accuracy by a semi-emperical expression

$$\ln R + \frac{K}{\ln R} = A + \frac{B}{T}$$

where K, A and B are constants for a given resistor and must be

determined by calibration. At low temperatures ($<4^{\circ}K$) where the resistance is high, the second term on the left hand side of the equation is small compared to the first term, and the resistance can be expressed to a good approximation as

$$\ln R \simeq A + \frac{B}{T}$$

Hence in order to determine a good value of K, for an accurate calibration sufficient importance must be given to the fixed points at higher temperatures. The resistance-temperature characteristic of the thermometer is found to be reproducible (within the accuracy of measurements) over many temperature cycles between room and nitrogen temperatures. There is, however, a definite tendency towards a long term change in the R-T characteristic, so that for accuracy, the calibration is checked after every dozen or more temperature cycles.

A two terminal method of resistance measurement is used. This is quite satisfactory because up to $25^{\circ}K$ the resistance of the thermometer is high compared with the lead resistance ($\sim 1\%$). The circuit diagram for the method used is shown in Fig. 24. A small potential difference set up across the $3.3\,\Omega$ resistor drives a current through the carbon circuit which is measured on a galvanometer of sensitivity 37 mm/μA and an

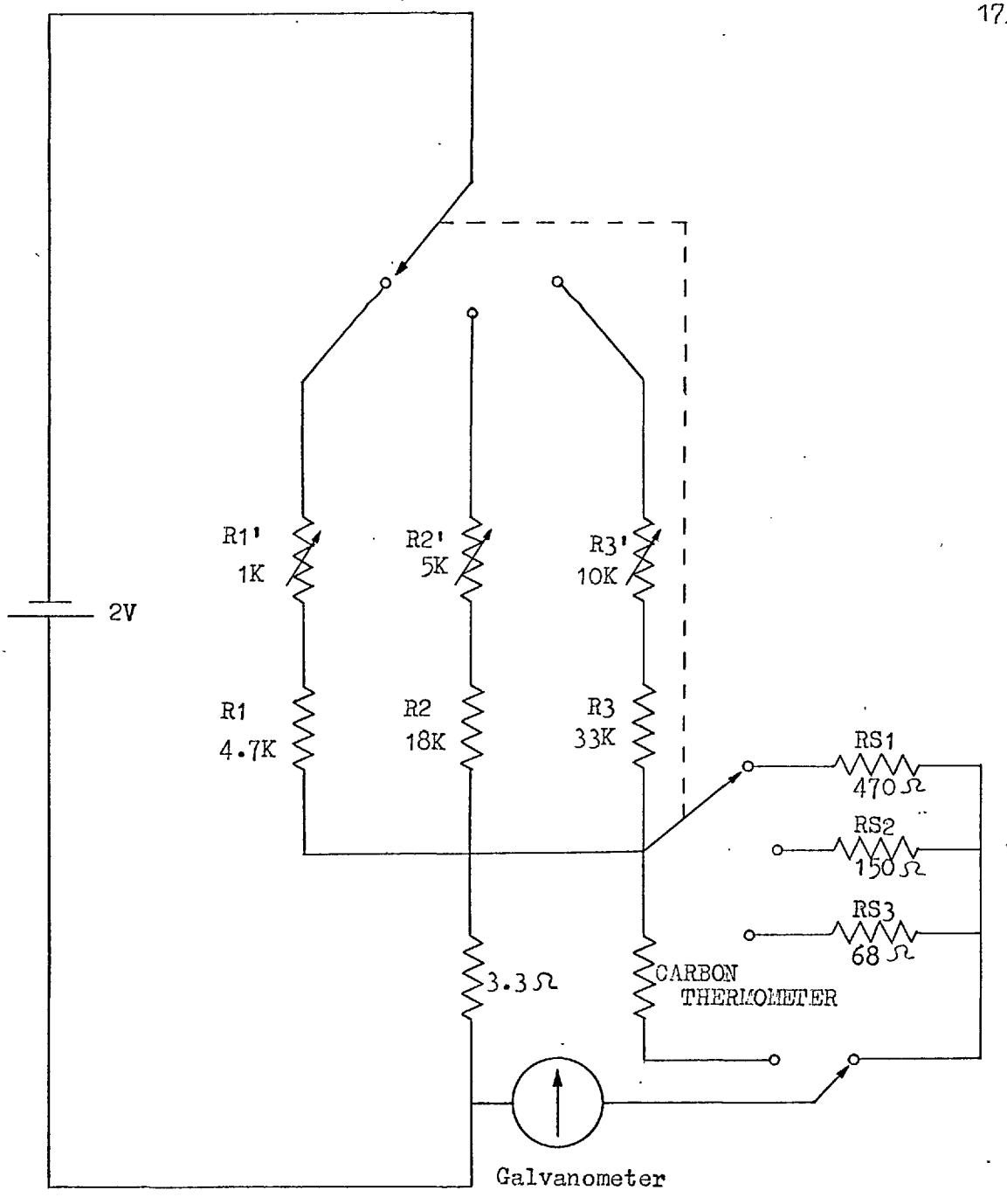

Fig.24 Diagram of the Carbon Thermometer Circuit

internal resistance of 4.9 Ω. The temperature range of measurement is split into three, so as to obtain sufficient sensitivity at higher temperatures. The first range is between 1.5 and 4.2°K where the resistance varies from about 6 kΩ to 530 Ω. The source voltage (across the 3.3 Ω resistance) is set to the required value by adjusting the resistance R1' until a full scale deflection on the galvanometer is obtained when a standard resistance RS1 (=47 Ω) is switched into the circuit in place of the carbon thermometer. The other two ranges are for measurements between 4.2 and 12°K and 12 to 25°K and the corresponding source voltages are set by obtaining full scale deflection with standard resistances RS2 = 150 Ω and RS3 = 68 Ω. The galvanometer deflection is calibrated in terms of the resistance by replacing the carbon thermometer with a resistance box and measuring the deflection as a function of the resistance. This is then translated into galvanometer deflection against temperature by means of the resistance-temperature calibration of the carbon thermometer.

b) Calibration of the Carbon Thermometer

The carbon thermometer was calibrated in the following manner. The resistance was measured for several temperatures between

1.6 and 4.2°K in the pumped liquid helium temperature range. The temperature was determined from the vapour pressure of helium using the published tables of vapour pressure against temperature (154). The resistance was also determined accurately at two other temperatures. These were the fixed points for oxygen (90.18°K) and for ice (274°K).

For a graphical determination of the constants the quantity $In^{R}+K/InR$ was calculated for the various temperatures assuming a value of K which is usually around 2. This quantity was plotted on graph paper as a function of 1/T. The points for temperatures between 1.5 and 4.2°K are always found to lie on a straight line for a large range of values of K (between 1 and 4), but this straight line generally does not pass through the points corresponding the oxygen point and the ice point. The best value of K is the one for which the extrapolated straight line drawn through the points in the liquid helium temperature range also passes through the two higher temperature points.

For accuracy, the calibration was also checked on a computer. A programme was written to determine the best straight line through the points between 1.5 and 4.2°K, using an initial guess

value of K=1. The sum of the squares of the deviation of the two high temperature points (oxygen point and ice point) from the extrapolated straight line was calculated. The value of K was varied until this square-deviation was a minimum. The corresponding values of the parameters A and B for the best fit are also obtained. These parameters (K, A and B) completely define the R-T calibration of the thermometer which is printed out in tabular form by the programme.

c) The Copper Resistance Thermometer

The use of commercial enamel coated copper wire as a thermometer was first reported by Dauphinee and Preston-Thomas (155). They found a high degree of reproducibility for a given thermometer and the differences between a number of different thermometers made from the same wire in terms of the quantity $Z=(R_T-R_{4.2})/(R_{273}-R_{4.2})$ represented an error in the temperatures of less than $0.1^{\circ}K$.

White (156) has published the tabulated values of the function Z for copper from the above authors' data, which, he has suggested, gives a calibration accurate to $0.1^{\circ}K$ for other thermometers of unstrained commercial copper wire having resistance ratios $R_{4.2}/R_{273}$ comparable with 0.01.

The nulling coil used is made from 49 s.w.g. enamel coated copper wire. The coil has a resistance of 1.61 Ω at 4.2°K and 106.23 Ω at 273°K, giving a resistance ratio of ~ 0.015.

Using the published Z values, the temperatures obtained in the range 20-25°K were found to be in execellent agreement (error 0.1°K) with those obtained from the carbon resistance thermomenter. As a further check, the resistance at the oxygen point was also measured. The temperature obtained using the published calibration was 0.4°K higher than the fixed value of 90.19°K. Since the coil is wound on a glass former it is likely that the differential thermal contraction between the two will produce some strain in the wire. The reproducibility of the temperatures was, however, better than 0.1°K over the whole range of temperature (25-300°K) despite the discrepancy of 0.4°K at the oxygen point.

Since there is the observed agreement with the carbon thermometer in the range 20 to 25°K and the forced agreement at 273°K from the use of the fixed value of Z=1.0 for this temperature, it is obvious that the R-T characteristic of the present thermometer deviates a small amount in the intermediate temperature range from the published data. This deviation, is however, likely to be the largest at oxygen point (90.19°K) since it is geometrically between 25°K and 300°K and represents a systematic

error of less than 0.5% which is considered to be not too serious.

The resistance of the coil has been measured using the four terminal method of measurement. The potential difference across the coil for a given nulling current is measured using a digital voltmeter which has an input impedance of over 10 MΩ. The nulling current is measured as a potential difference across a standard resistance (using the same digital voltmeter).

d) Checking the Thermometery

Having calibrated the thermometers, it is important to check whether the temperature they indicate is the same as that of the specimen. Since the nulling coil is wound around the specimen over its whole length, it is likely to be in good thermal contact with the specimen. The carbon thermometer, however, is not mounted on the specimen and although the warm-up rate from 4.2°K is very slow (less than 10 degrees per hour) it is possible for it to be at a slightly different temperature from the specimen.

The susceptibility of a dilute Au-Gd specimen was found to obey Curie law accurately in the temperature region of 1.6 to 4.2°K. (An outside limit to a Curie-Weiss θ is $\pm .05$°K). In this range, the temperature of the specimen is known accurately

since it is immersed in a large bath of liquid helium whose vapour pressure gives an accurate determination of the temperature. The graph of $1/\chi$ against T in the range 1.6 to $4.2^{\circ}K$ is extrapolated to higher temperatures and from this, the temperatures of the specimen were obtained using the measured values of the susceptibility. These were found to agree with those obtained from the two thermometers within the experimental accuracy of $\pm 0.05^{\circ}K$ for $T < 20^{\circ}K$, and $\pm 0.1^{\circ}K$ for $20^{\circ}K < T < 40^{\circ}K$. At higher temperatures the accuracy of the susceptibility measurement is smaller so that the temperatures obtained from it also have a larger error. The accuracy around nitrogen temperature and above was not good enough to correct for the systematic difference in the resistance-temperature characteristic of the nulling coil mentioned above.

Experimental Procedure

The specimen, machined to the correct dimensions for a good sliding fit inside the nulling coil, is given a final etch in concentrated hydrochloric acid, washed thoroughly in distilled water and dried. Just over half its length is then inserted into the nulling coil. A thin coat of G.E. varnish

is applied to the exposed end by means of a clean paint brush. When this has dried a little, but not completely, the specimen is gently pushed inside the coil (using a clean needle) right up to the end where it is stopped at the lip of the coil former. The lip helps to locate the specimen reproducibly to a given position inside the nulling coil. The varnish dries, fixing the specimen firmly inside the coil. When the specimen is to be removed from the coil a small amount of G.E. varnish solvent (which is a mixture of toluene and absolute alcohol in 1:1 ratio by volume) is introduced inside the coil former. This softens the varnish and the specimen can be released with a needle pushed from the opposite end.

Before inserting the glass tube jacket to cover the magnetometer, the clearance between the nulling coil and the inside of the pick-up coils is checked. This is necessary because the suspension of the bimorphs can be easily distrubed while inserting the specimen, so that the latter lies off centre inside the pick-up coil or even makes contact with the walls of the pick-up coil. The glass tube joins to its counterpart at the ground glass joint which is smeared with a little silicon grease to provide a vacuum tight seal.

The helium dewar is then fixed into position by screwing the brass ring around the flange to the dewar cap. The clearance between the glass jacket and the tail of the helium dewar is small so that care is taken no to knock the glass jacket or bend it to one side while inserting the dewar. (The whole tube bends a little at the O-ring seal to the dewar cap). The specimen may get knocked out of alignment if this happens. It is therefore useful, after the dewar has been firmly screwed into position, to check for the free movement of the specimen. This is done by observing the waveform of the signal from the pick-up coil when the field is turned on. Presence of higher harmonics and non-sinusoidal waveform indicate that the specimen is making a slight contact with the walls of the pick-up coil. If the specimen is seriously out of alignment, however, the resonance curve of the bimorphs will be very broad (very low Q) or the specimen may even stop vibrating completely.

Using a rotary pump, the helium dewar interspace is pumped and flushed out with pure nitrogen about three to four times. It is finally pumped out with the rotary pump for half an hour and then the tap is shut off. The helium dewar is next pumped and flushed out with helium a few times. It is finally

left connected to a supply of pure helium, such as the liquid helium in the storage vessel, which maintains an atmospheric pressure of helium gas in the dewar when the latter is cooling to nitrogen temperature.

The nitrogen dewar is eased into position around the helium dewar. It is suspended from the hooks on the dewar cap by strings attached to it around the neck of its tail. The height of the dewar is adjusted by means of screws which move the hooks vertically. The magnet is then wheeled into position. The magnet provides some screening against mains pick-up. It is important to check that the screening of the coils and the leads is good. If this is poor, not only is there a small amount of mains pick-up, but a part of the driving signal to the bimorphs is also observed at the output. The best way to check for the latter effect is to use the full output of the driving signal at a frequency of a few hundred Hz and observe the output signal on a scope. Since the amount of pick-up is proportional to the frequency, use of a higher frequency enhances the observed effect. If the screening is good, any pick-up from the driving voltage is smaller than the amplifier noise (1 V p/p at the input). The usual source of this trouble is from accidental earth loops and bad contacts in the

earth line. These must be corrected before any measurements are made.

The cooling begins when the nitrogen dewar is filled with liquid nitrogen. The cooling rate is slow because of the vacuum in the helium dewar interspace. It normally takes about two and a half hours for the specimen to cool to around the nitrogen temperature, such a slow rate of cooling is essential in order not to produce stresses in the pick-up coils which are made of fine wire (44 s.w.g.) which is liable to break very easily.

When the specimen has reached nitrogen temperatures the frequency of the driving signal is set close to the bimorph resonance. The phase sensitive detector is then set to measure the inphase signal, by adjusting the phase of the reference signal to maximise the output due to a d.c. current in the nulling coil. The magnetic field is then turned on to a convenient value, usually around 4 kOe. The signal from the specimen, in terms of the nulling current, is measured as a function of the magnetic field orientations θ with respect to the pick-up coil for a range of θ of ± 5 degrees around the estimated optimum position. The field is then reduced to zero, another driving frequency close to the resonance is selected and the phase of

the reference signal is adjusted for the inphase signal. The same field is turned on again and another measurement of the nulling current as a function of the magnet angle θ is made. This is repeated for two more driving frequencies. A graph of nulling current against θ for the various frequencies is plotted, A family of straight lines intersecting at a 'common point' is obtained. See Fig. 13. The angle θ corresponding to this is the optimum setting for the minimum synchronous noise.

Magnetisation vs field measurements are made at nitrogen temperature for several values of the field H, both positive and negative. Helium is then transferred into the dewar from the storage vessel. The transfer syphon is introduced through the hole in the dewar cap and is lowered inside the dewar down to the neck of the tail. The dewar is filled with helium to a point about two inches above the neck. (This represents about 1.2 litres of helium used in the transfer). There are several carbon resistor depth gauges for helium at various heights in the cryostat but the helium can also be clearly seen through the slit in the silvering of the dewar. The magnetic field is normally turned off while helium is transferred, unless a field cooling experiment is being done.

The procedure for minimizing the synchronous pick-up is repeated at $4.2^{o}K$. This is necessary because the pick-up can distort a small amount in the relatively fast cooling produced during the transfer. The difference in the optimum angle Θ obtained at helium and nitrogen temperatures is usually smaller than half a degree.

Measurements of magnetisation against field for various field values at $4.2^{o}K$ are obtained. The helium return line to the bags is then shut off and the mercury and oil manometers are connected for pressure measurement. The temperature is lowered by pumping on the helium with a rotary pump. A manostat is used which controls the pumping rate such that a given reference vapour pressure is maintained in the dewar. Measurements of magnetisation in a constant field as a function of decreasing temperature are made. The lowest temperature reached by pumping is about $1.6^{o}K$. Another M vs H plot is obtained at this lowest temperature. The pumping is then stopped and the helium is allowed to warm up. It takes about half an hour for the pressure in the dewar to return to one atmosphere. This rate can be increased and the helium warmed up a little faster by dissipating a small amount of electrical power in the heater suspended below the coil assembly. Usually when the pumping

is over and all the measurements below 4.2°K have been made, the helium level in the dewar is still a few inches above the specimen. This is boiled off to a level below the specimen before the warm up begins. The warm up rate is slow because the evaporating helium in the bottom of the tail of the dewar helps to cool the specimen. The normal warm up rate is about 10°K per hour and can be increased by using the heater, which warms the rising helium gas.

Magnetisation measurements are made in a constant field as a function of increasing temperature. The frequency of the driving signal to the bimorphs is set above the resonant value so that as the temperature increases and the resonant frequency decreases only the amplitude of the specimen vibration decreases by a significant amount: the phase angle between the driving voltage and vibration signal does not alter very much. The driving frequency is corrected by a small amount every few degrees rise in temperature so that it lies roughtly one cycle above the resonant value. This is easily done by observing directly the specimen signal on the oscilloscope (when no nulling current is passed through the coil) and adjusting the frequency so that the ratio of the amplitude of ths signal observed on the scope to the magnetisation of the specimen in terms of the nulling current) is

roughly the same as at 4.2°K where the frequency was set one cycle off resonance by observing the frequency response. Temperatures below 25°K are measured on the carbon thermometer. Measurements of the galvanometer deflection are made simultaneously with those of the nulling currents. (Any drift in the battery voltage in the carbon circuit is corrected for by adjusting the variable resistance R1', etc. (see Fig. 24) to obtain a full scale calibrating galvanometer deflection before making the measurements).

A galvanometer deflection of 6 cm on the 'third range' correspons to a temperature of around 20°K. When this is reached, measurements of the potential difference across the nulling coil are also made using the same digital voltmeter as used to measure the nulling current (in terms of the potential difference across a standard resistance).

A selector switch is used to change over between the two resistances. The ratio of the p.d. across the coil to the nulling current obtained gives directly the resistance of the coil, which begins to show a strong temperature dependence above 20°K. Measurements on the carbon circuit are continued until a deflection of 8 cm on the galvanometer is obtained (corresponding to a temperature of around 25°K), after which only

the measurements of the potential difference across the coil are made. The five degree overlap between the two thermometers gives a check on the behaviour of the thermometers.

The susceptibility obtained at nitrogen temperatures on the warm up run should agree with the previous value obtained before the helium transfer. This is nearly always so, except when excessive power is dissipated in the heater to speed up the warm up rate. This may produce some distortions in the pick-up coil and change the effective area vector of the coil from the optimum alignment. It is generally difficult to check for the synchronous noise at intermediate temperatures because of the small but finite warm up rate. It is therefore best to use a slow warm up rate whenever possible.

The measurements between room and nitrogen temperatures are also made as a function of increasing temperature. When the nitrogen temperature is reached, the nitrogen dewar is emptied of all the nitrogen and replaced into position. This helps to give a reasonably fast warm up rate which is too slow otherwise.

Data Processing

In the measurement of the susceptibility of a specimen

the raw data obtained are the strength of the magnetic field, the nulling current (measured as a p.d. across a standard resistance), the carbon thermometer circuit galvanometer deflection, and the potential difference across the nulling coil.

From these data the temperature is obtained first. Then the nulling current representing the magnetic moment of the nulling coil at that temperature is determined and substracted from the measured total value. Using the calibration of the nulling coil in terms of emu/mA the nulling current is converted into magnetic moment in emu. For a paramagnetic specimen, the susceptibility is obtained directly in emu/gm by dividing the moment by the magnetic field and the mass of the specimen.

The temperature in the range up to 25°K is determined from the galvanometer deflection in the carbon thermometer circuit. The temperature is obtained from a graph giving the calibration of deflection against temperature. In the range above 25°K, the copper resistance thermometer is used. The ratio of the p.d. across the nulling coil to the nulling current gives the resistance of the coil. The correction due to the magnetoresistance is then determined and from the corrected value of the resistance the temperature is obtained.

A computer programme has been written to facilitate data processing. The subroutines in the programme determine the various quantities by interpolation from a set of regularly spaced calibration values. Lagrange's three point interpolation formula has been used. This is given by

$$F(x+p) = \frac{p(p+1)}{2} F(x-\Delta)+(1+p^2)F(x)+ \frac{p(p+1)}{2} F(x+\Delta)$$

where Δ is the interval in x of the tabulated calibration values. The data are punched out on cards. In the first column the number 1, 2 or 3 is punched to indicate the temperature range of the carbon circuit. If it is a blank, the temperature is determined from the coil resistance. In the next four blocks of Format F 10.3 are punched the magnetic field, the nulling current, the galvanometer deflection and the p.d. across the coil, in that order. A table giving the raw data, the various corrections made, and the final susceptibilities and temperatures is finally printed out. A rough graph in the grid 120x55 of susceptibility against temperature is also printed.

CHAPTER 6

EXPERIMENTAL RESULTS AND DISCUSSION OF SOME RHODIUM BASED ALLOY SYSTEMS

A. The Rh-Fe Alloy System

Introduction

The magnetic susceptibility behaviour of dilute Rh-Fe alloys (25),(88) is very similar to that found in many systems such as Cu-Fe (26), showing the Kondo effect. This behaviour in the Rh-Fe alloys has been interpreted in terms of spin compensation of the moment on the iron atoms resulting from their interaction with the conduction electrons of the matrix (25). The anomaly in the specific heat (92) is also similar to that found in systems undergoing spin compensation and is thought to be further proof of the formation of the quasi-bound state. One major difference from the 'simple' Kondo systems, however, is in the electrical resistivity behaviour of dilute Rh-Fe alloys (87), where instead of the usual resistance minimum characteristic of the Kondo systems, an almost opposite behaviour of rapidly falling resistance with decreasing temperature is found.

The present investigation of the Rh-Fe alloys was

carried out with a view to studying the effect of the mechanism causing the continuous reduction of the moment, as interpreted from the susceptibility behaviour, on the onset of magnetic order in the alloys as the concentration of iron atoms was increased. It has been frequently suggested that the effect of the internal field on the solute atoms due to interactions between them would tend to break down the spin condensed state. It was hoped that the present study would confirm such an effect, and shed further light on the nature of the magnetic state associated with the iron atom dissolved in rhodium. Unfortunately no clear conclusion to this effect can be reached from the results presented below. There is, however, a possible interpretation of the susceptibility results in terms of the recent computer calculations of Levine and Suhl (29).

Sample Preparation

Five different alloys with concentrations of iron between 1 and 15% have been studied. The solubility of Fe in Rh extends to beyond 25% Fe, so that the alloy preparation is fairly simple.

The alloys were prepared by arc melting the required amounts of Rh sponge of purity 99.99% (obtained from Johnson Matthey

& Company) and Fe rod of purity 99.998 % (obtained from NPL, Teddington) on a water cooled copper hearth in a $\frac{2}{3}$ atmospheric pressure of argon. The mass of the alloys was usually between 6 and 7 gm. The sponge was compressed using a pressure of 10 tons per square inch in order to avoid particles being blown away by the arc. The alloys were melted and remelted about 6 times in a circular cavity in the copper hearth and then moved into a long narrow groove 3/8" wide and melted once more.

The ingots which were 0.7" long were first slit lengthwise using a carborundum wheel in a fast slitting machine to obtain pieces with square cross-section of side 0.07". The alloys were extremely hard and impossible to machine into the required cylindrical shape by the usual methods. They were instead gently filed down while rotating them in a lathe. A collet and a counter support were used to hold the specimen in the lathe. Care was taken not to apply uneven pressure on the specimen while filing as the alloys were fairly brittle and broke easily. Between 8 and 10 hours of continuous filing was required to reduce each specimen to cylinders .055" in diameter. It was possible to obtain specimen of fairly uniform cross section ($\pm$ .001") over their whole length of $\frac{1}{2}$". The side cuts from the main ingot were analysed on an electron microprobe analyser for the determination of homogeneity and

concentration. The latter were usually well within 10% of the required values. The same specimens were used both for the magnetisation and the resistance measurements. No annealing heat treatments were given to the specimen after arc melting.

Rh 0.9% Fe

The magnetisation of the alloy as a function of field upto 8 kOe has been measured at 77 and 4.2°K, Fig. 25. The magnetisation in a constant field of 3.65 kOe has also been measured as a function of increasing temperature from 1.6°K upwards. The susceptibility (ratio of magnetisation to field) shown in Fig. 26. is in agreement with results obtained by Knapp (25) and Waszink (88). A plot of $\frac{1}{\chi - \chi_{Rh}}$ against T is shown in Fig. 27. It is clear that a Curie Weiss law is not obeyed over the whole temperature range. A straight line through the higher temperature points give an intercept of -49 ± 5°K. Waszink has found a similar result ($\theta = -41$°K) and has shown that by taking off a temperature independent matrix susceptibility contribution of 1.08×10^{-6} emu/gm from the measured values, the Curie-Weiss fit can be extended to lower temperatures and a Curie-Weiss intercept of -15°K obtained. The present results are in reasonable agreement with this observation ($\theta = -15.46$ for $\chi_{matrix} = 1.10 \times 10^{-6}$ emu/gm). Results of least squares fits to the Curie-Weiss law and other susceptibiltiy formulae are discussed later.

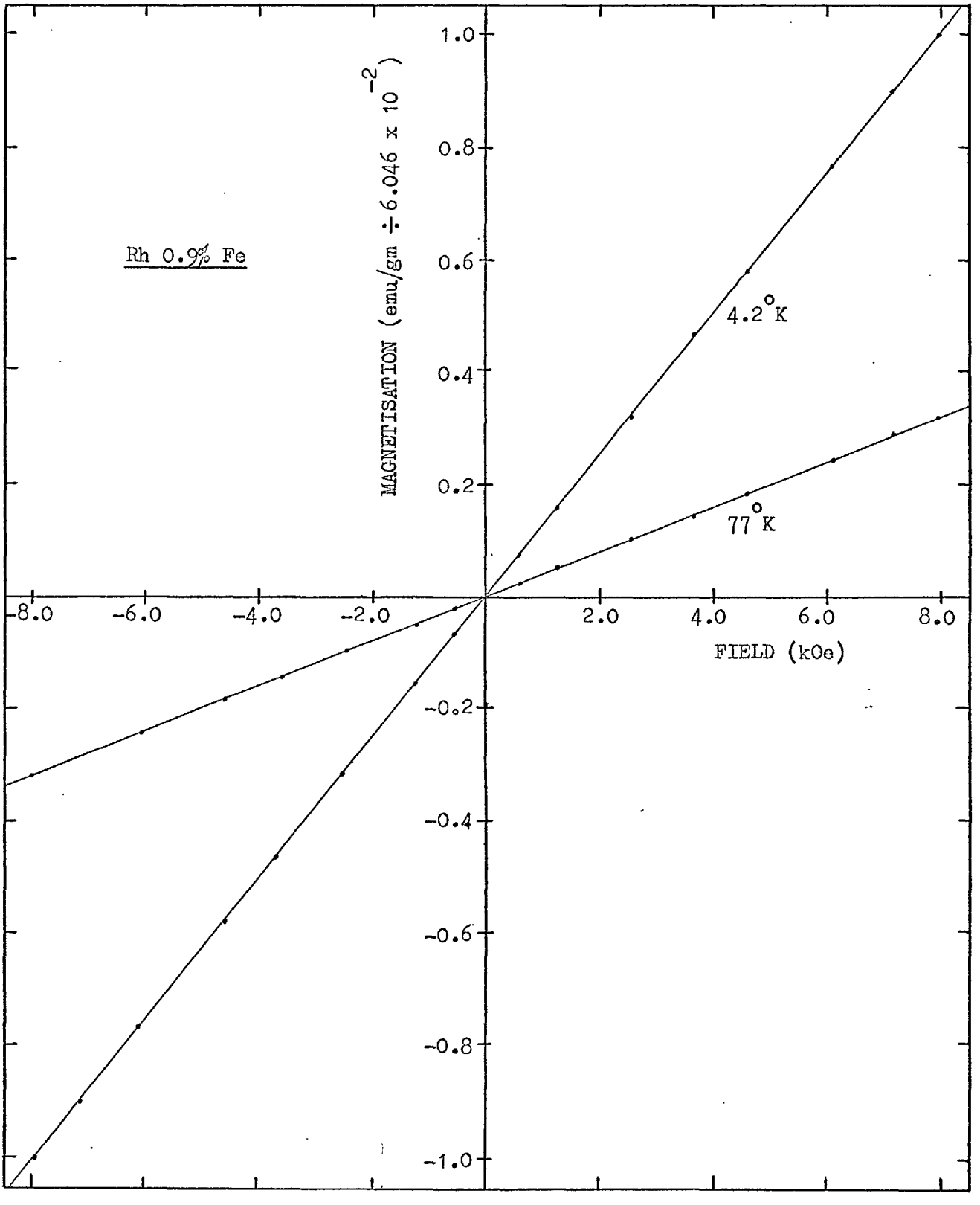

Fig.25 Magnetisation vs Field for Rh 0.9% Fe Alloy

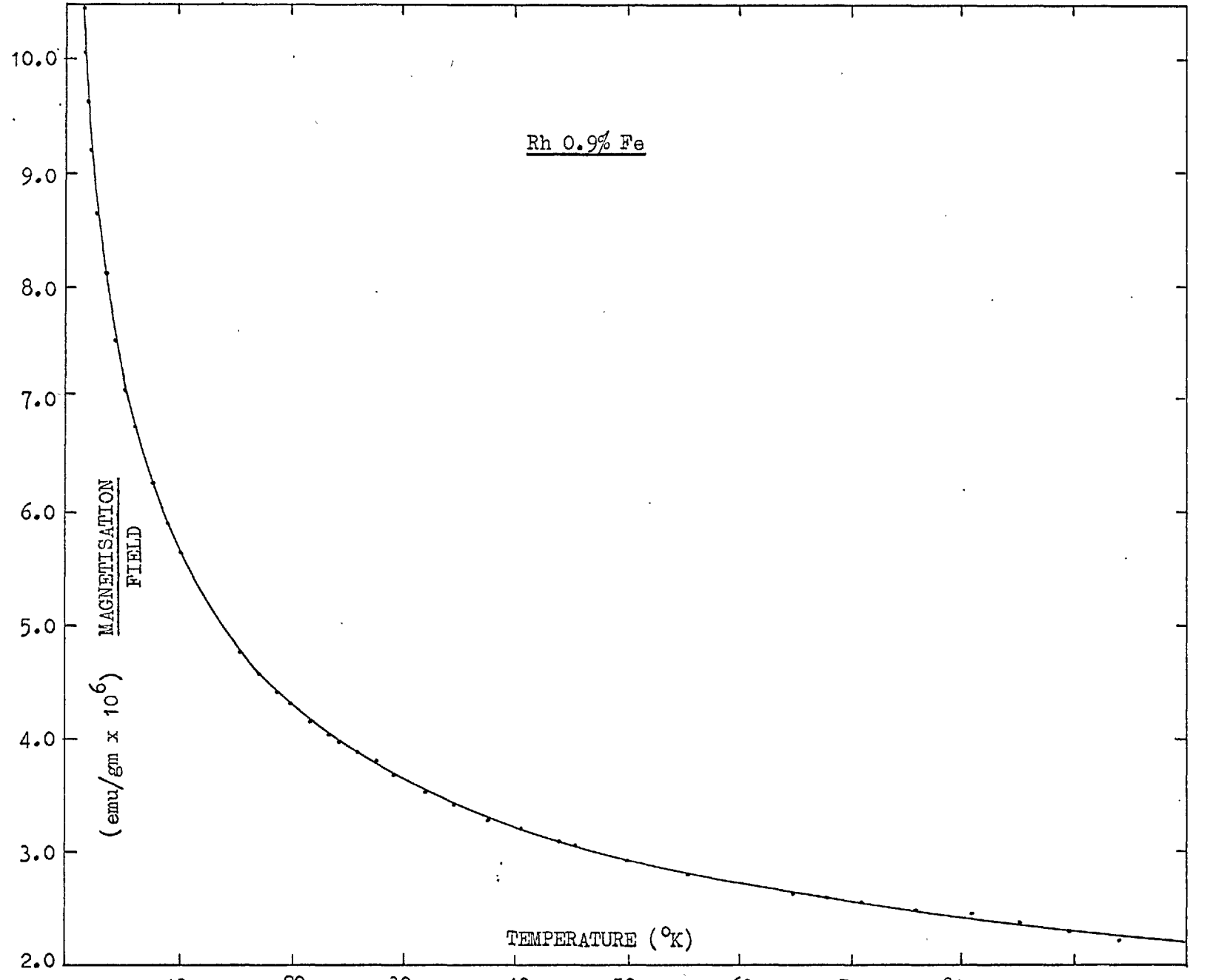

Fig.26 'Susceptibility' vs Temperature of Rh 0.9% Fe Alloy

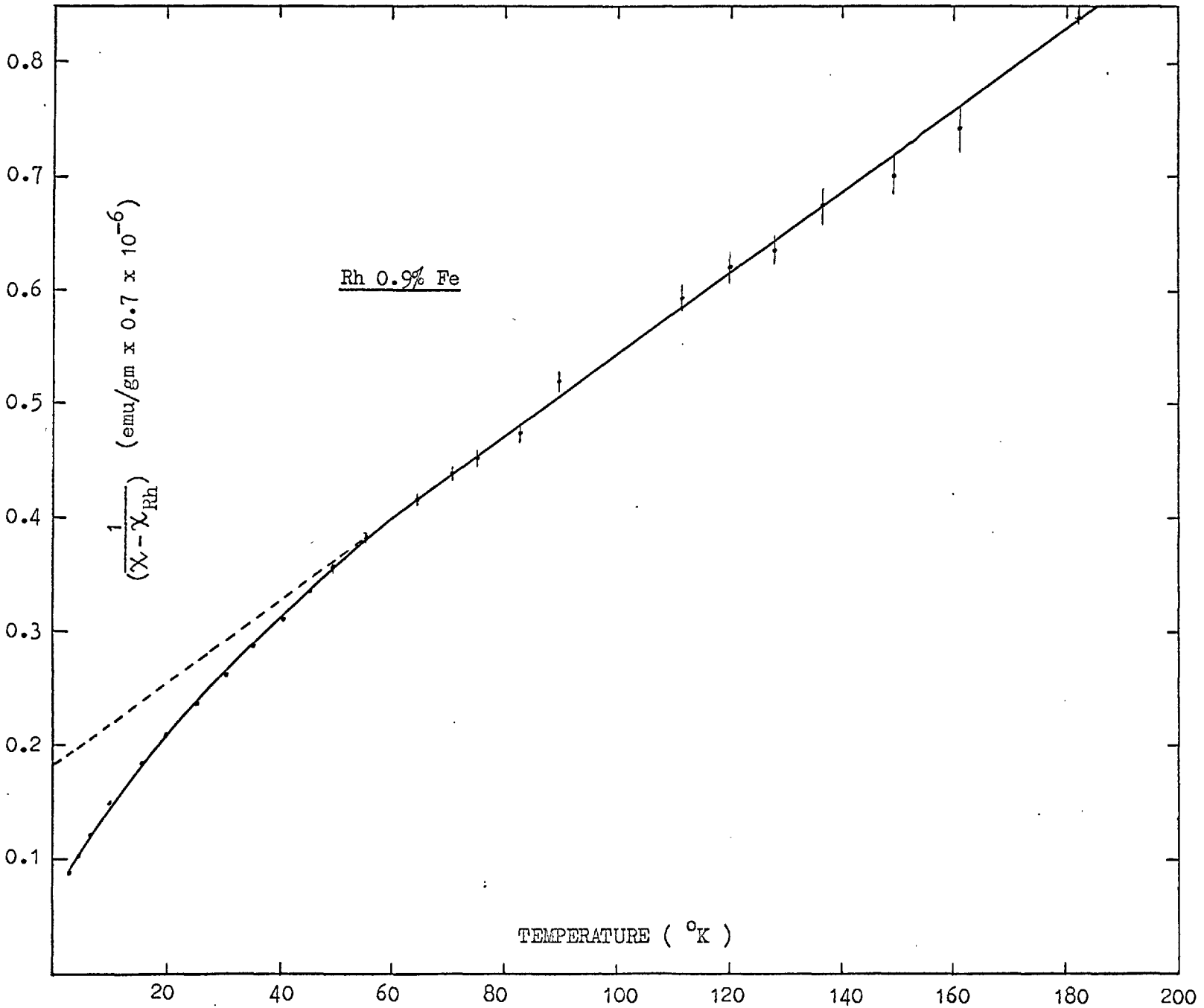

Fig.27 Curie-Weiss Plot for Rh 0.9% Fe Alloy

Rh 2.86% Fe

A linear relation between magnetisation and field is found at 77°K, but there is a slight curvature in the M-H plot at 4.2°K, Fig. 28. The magnetisation measured in a constant field of 3.65 kOe is plotted in Fig. 29. in which a clearly defined maximum with a peak at 2.8°K can be seen. The resistivity of the alloy as a function of temperature is shown in Fig. 30. A closer examination of the resistivity in the region between 1.6 and 4.2°K has been made, Fig. 31. It is possible to draw a small kink through the data points around 2.8°K. There is, in any case, a definite change of slope around 3°K which can be taken as due to the onset of magnetic order, in agreement with the magnetisation results.

A plot of $\frac{1}{\chi - \chi_{Rh}}$ against T is shown in Fig. 32. A straight line through the high temperature points gives an intercept of -85±7°K. By subtracting off a larger temperature independent susceptibility contribution the Curie-Weiss law can be extended to lower temperatures, but as found in the case of Rh 1% Fe alloy, no matrix correction term can give a Curie-Weiss fit over the whole temperature range.

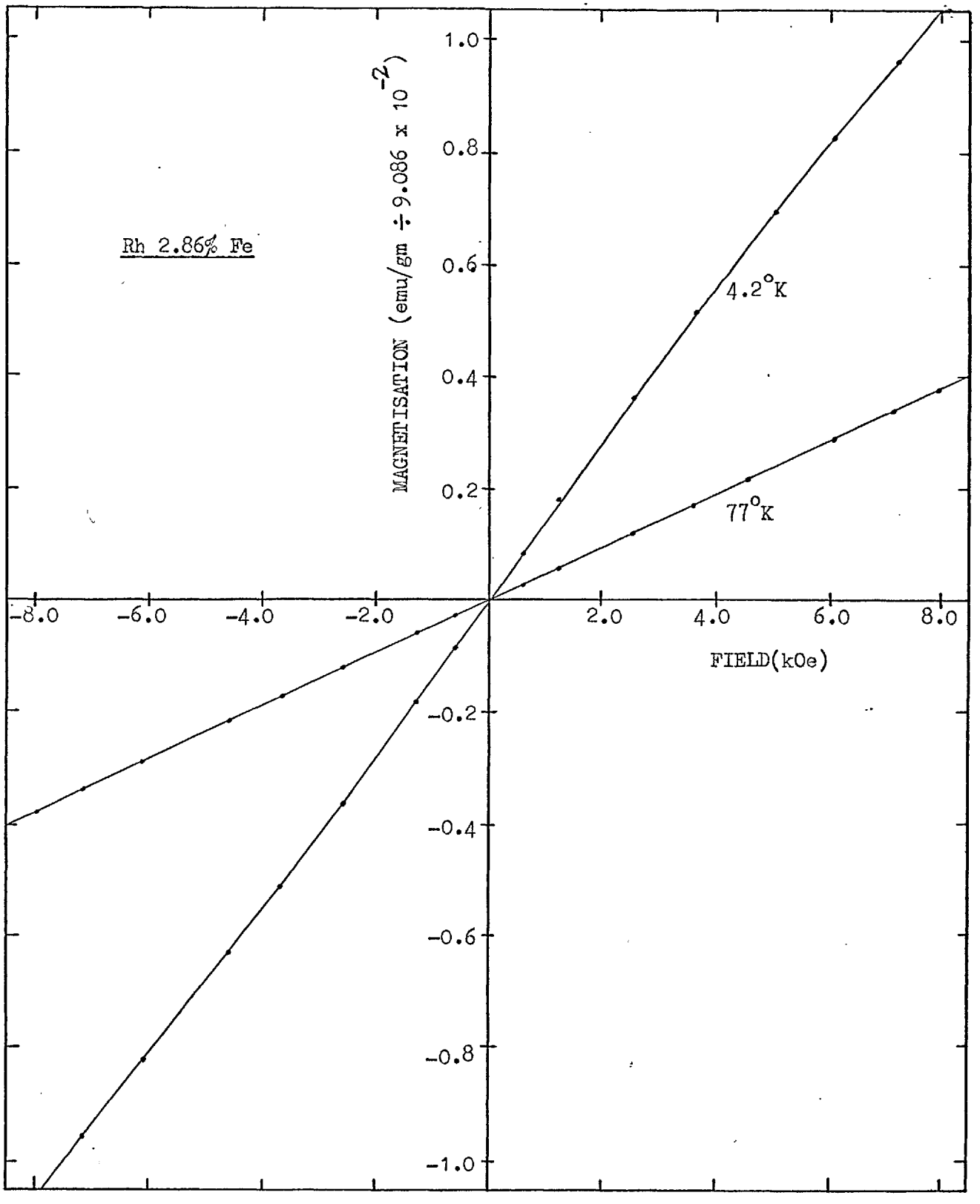

Fig.28 Magnetisation vs Field for Rh 2.86% Fe Alloy

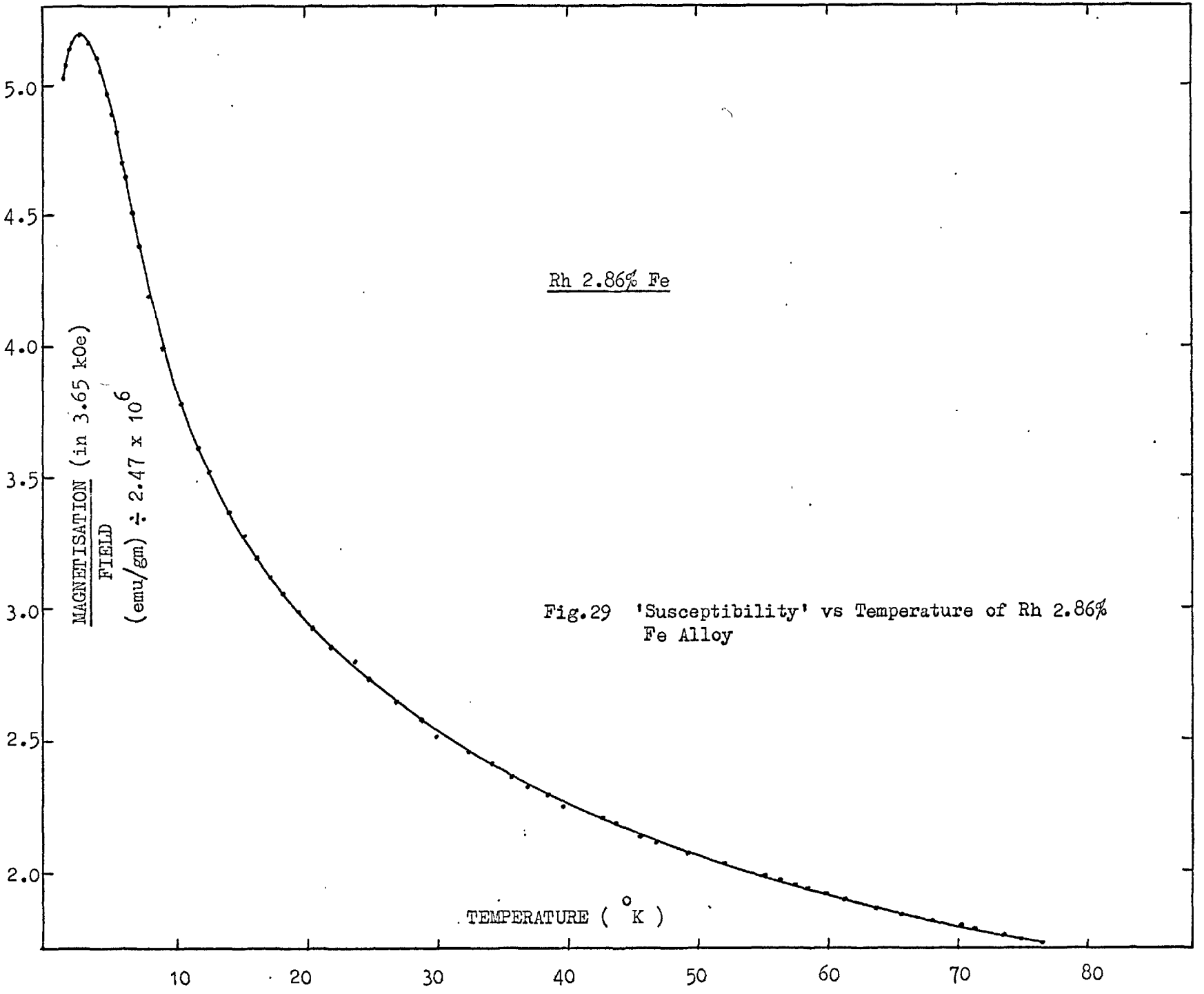

Fig.29 'Susceptibility' vs Temperature of Rh 2.86% Fe Alloy

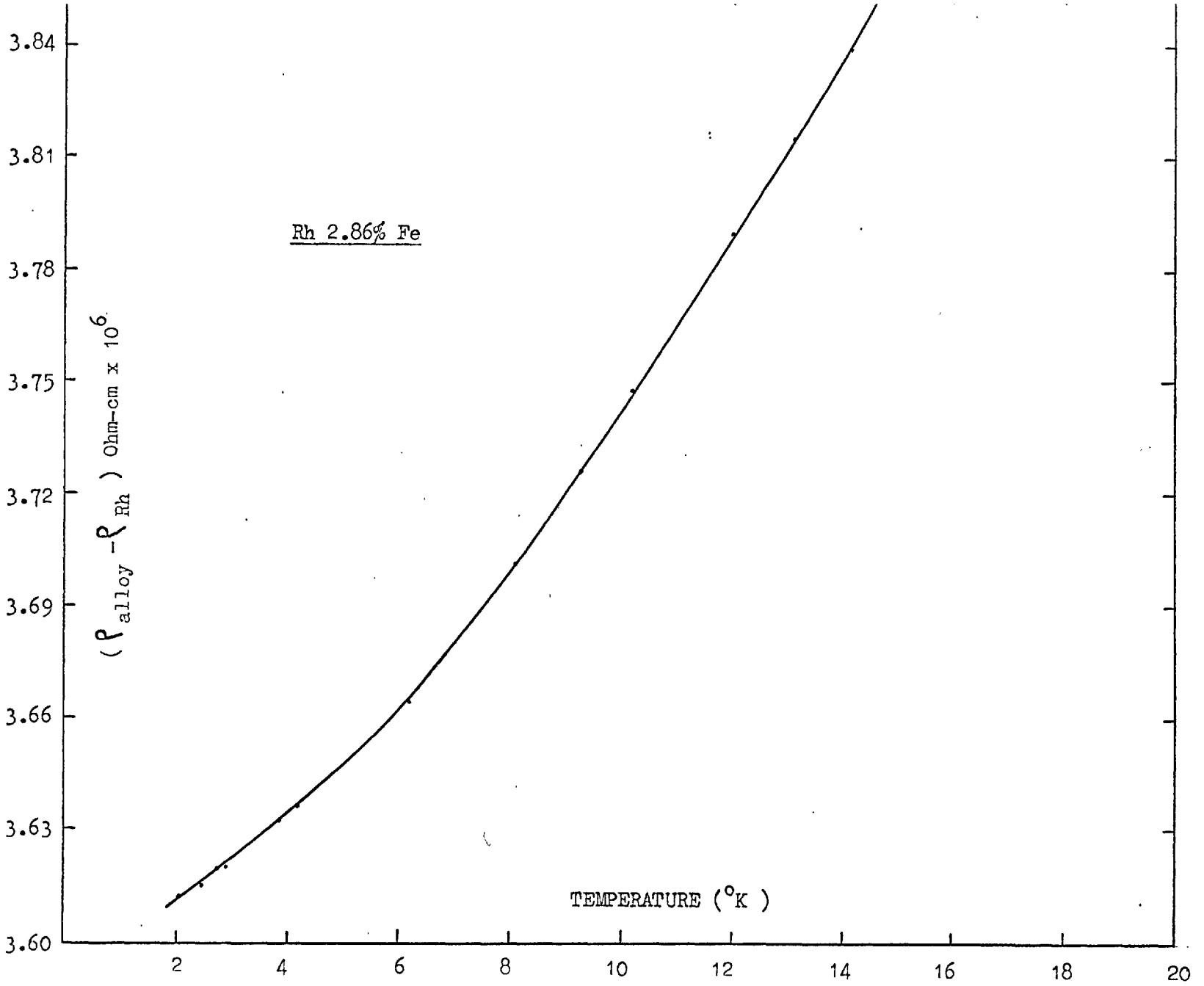

Fig.30 Excess Resistivity vs Temperature for Rh 2.86% Fe Alloy

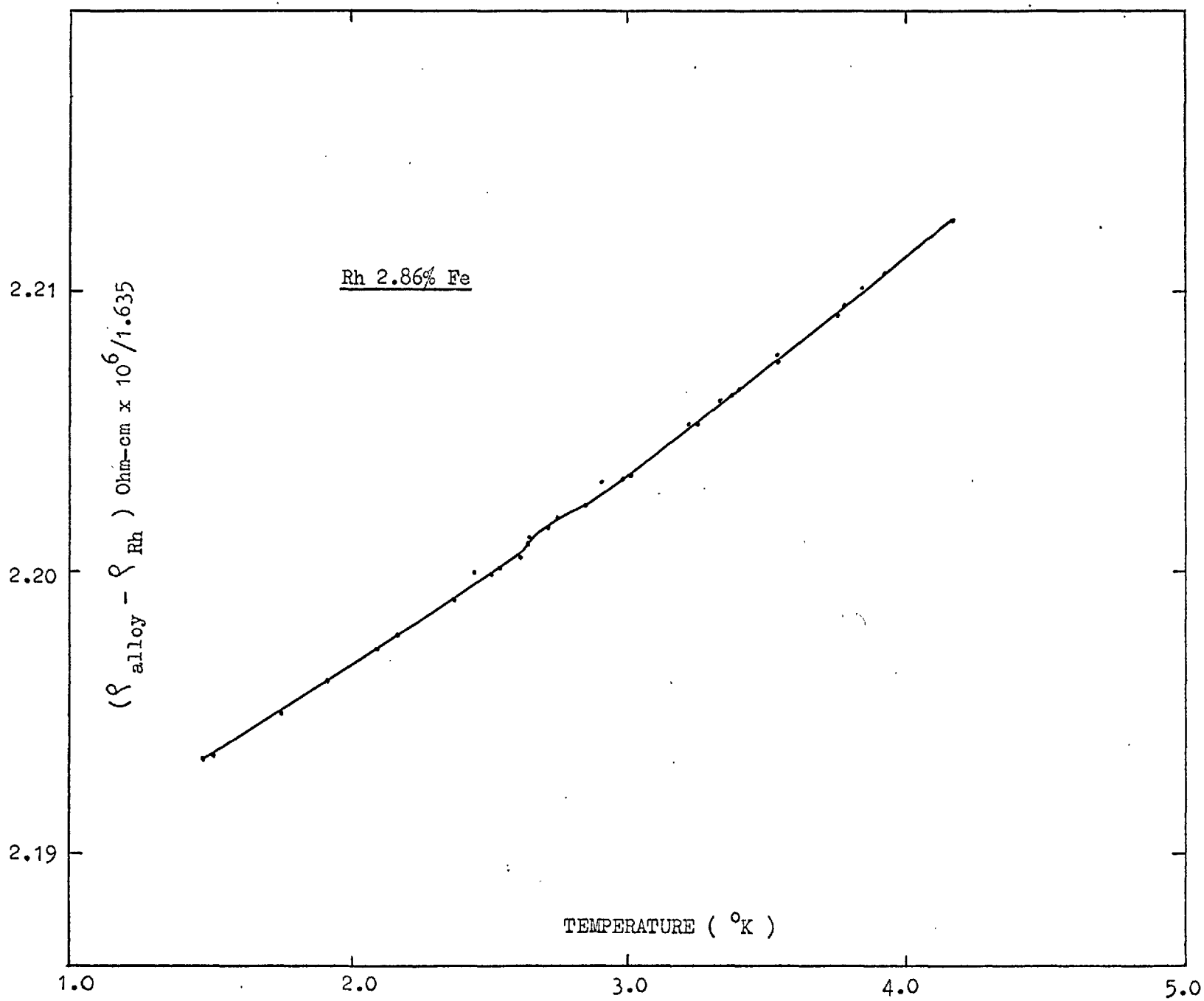

Fig.31 Excess Resistivity vs Temperature for Rh 2.86% Fe Alloy

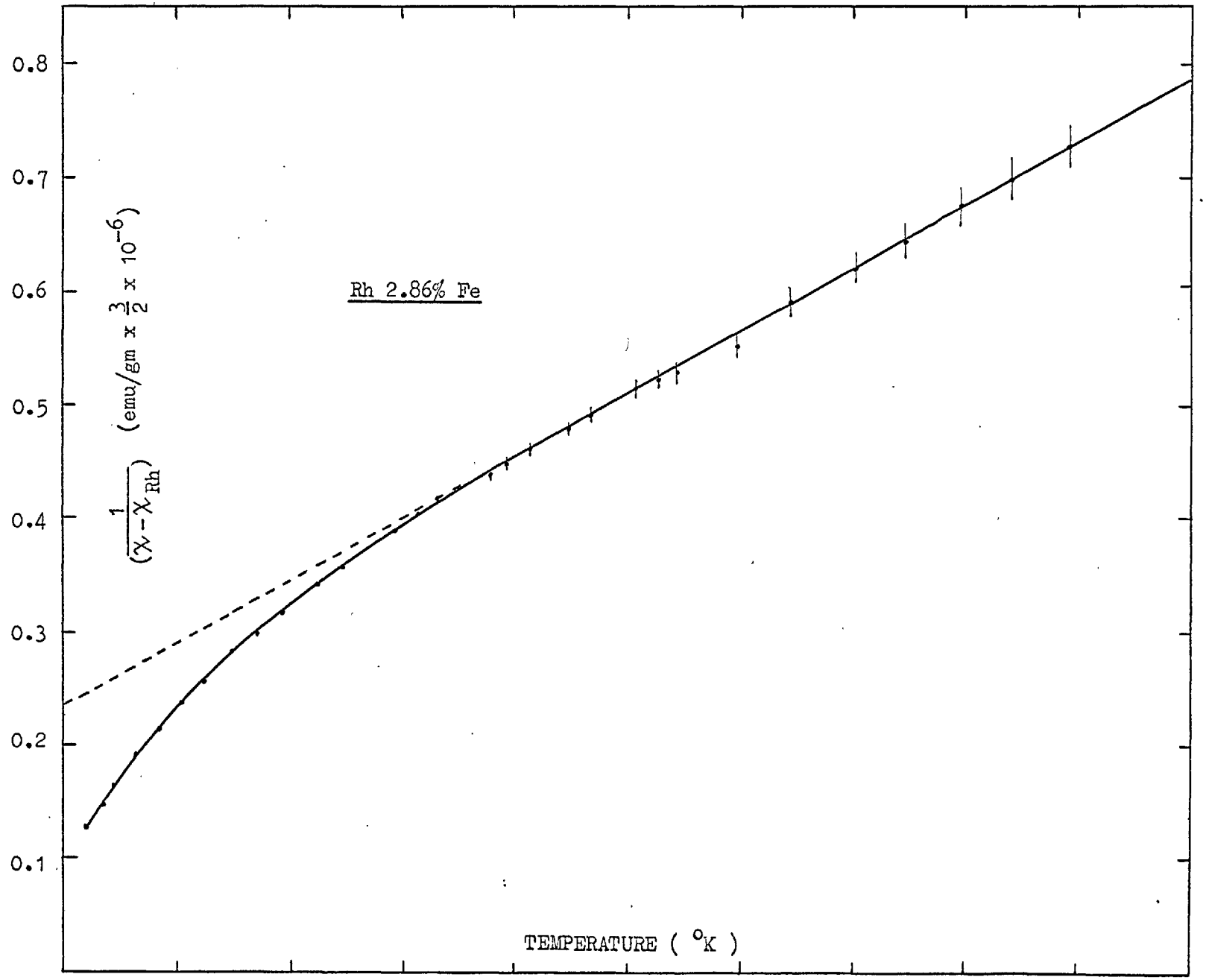

Fig.32 Curie-Weiss Plot for 2.86% Fe Alloy

Rh 4.95% Fe

The field dependence of the magnetisation of the alloy at 4.2°K is non-linear and has a small amount of hysteresis Fig. 33. The magnetisation measured in a field of 3.65 kOe from 1.6°K upwards shows a well defined maximum with a peak at 6.8°K. A thermoremanent moment is induced in the specimen if it is cooled in a magnetic field to a temperature below the maximum in the 'susceptibility'. Fig. 34. also shows the magnetisation measured in a field of 3.65 kOe after cooling the specimen to 1.6°K in a field of 8 kOe. The result of field cooling can also be seen in the displaced M-H curve, Fig. 33, which is measured at 1.6°K. The thermoremanent moment decreases with increasing temperature going to zero at the temperature of the maximum.

There is a marked change of slope in the electrical resistivity against temperature curve at around 7°K which provides further evidence for the onset of magnetic order Fig. 35. A plot of $\frac{1}{\chi - \chi_{Rh}}$ is shown in Fig.36 in which a straight line through the higher temperature points gives a Curie-Weiss intercept of 123 ± 10°K.

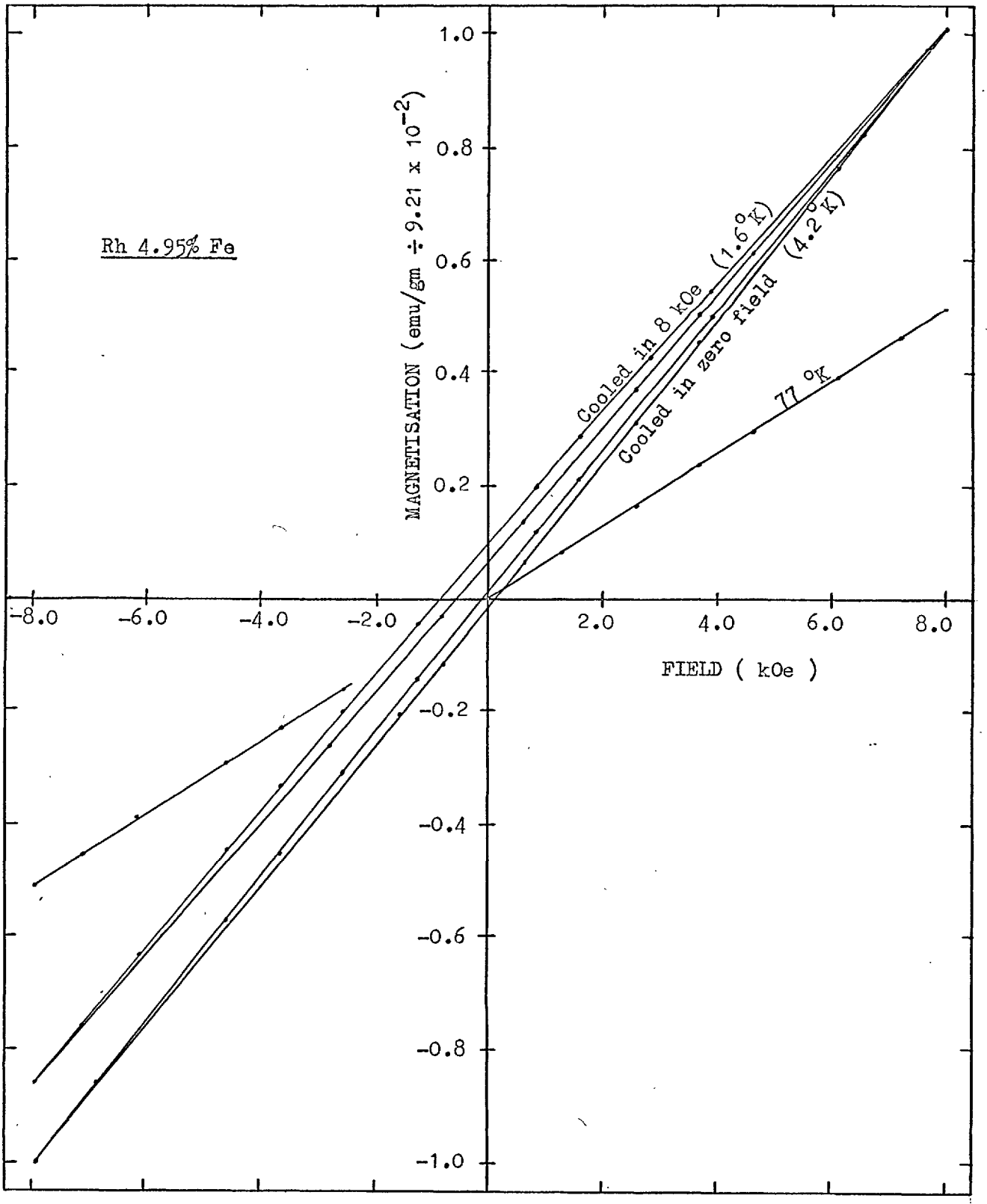

Fig.33 Magnetisation vs Field for Rh 4.95% Fe Alloy

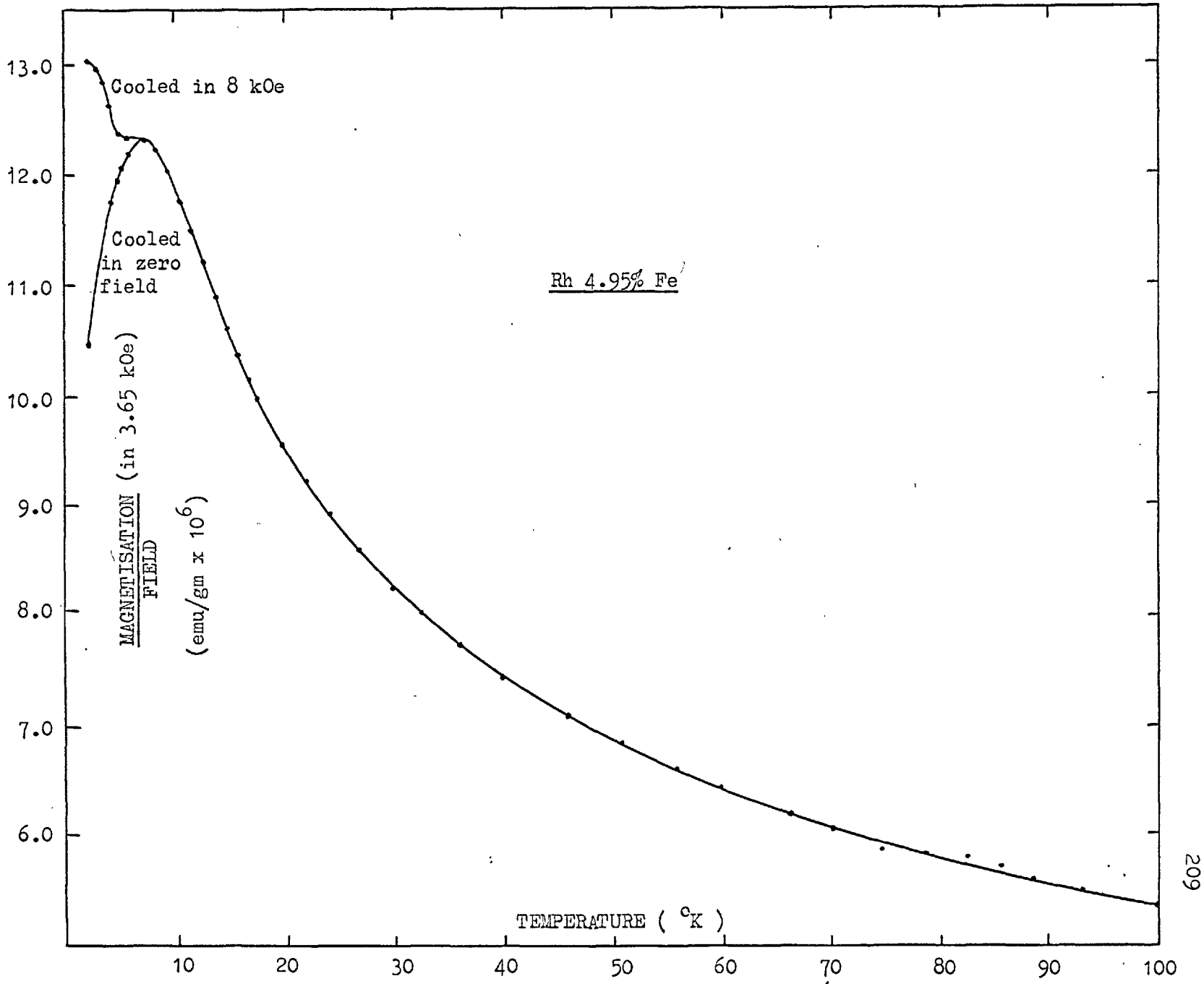

Fig.34 'Susceptibility vs Temperature of 4.95% Fe Alloy

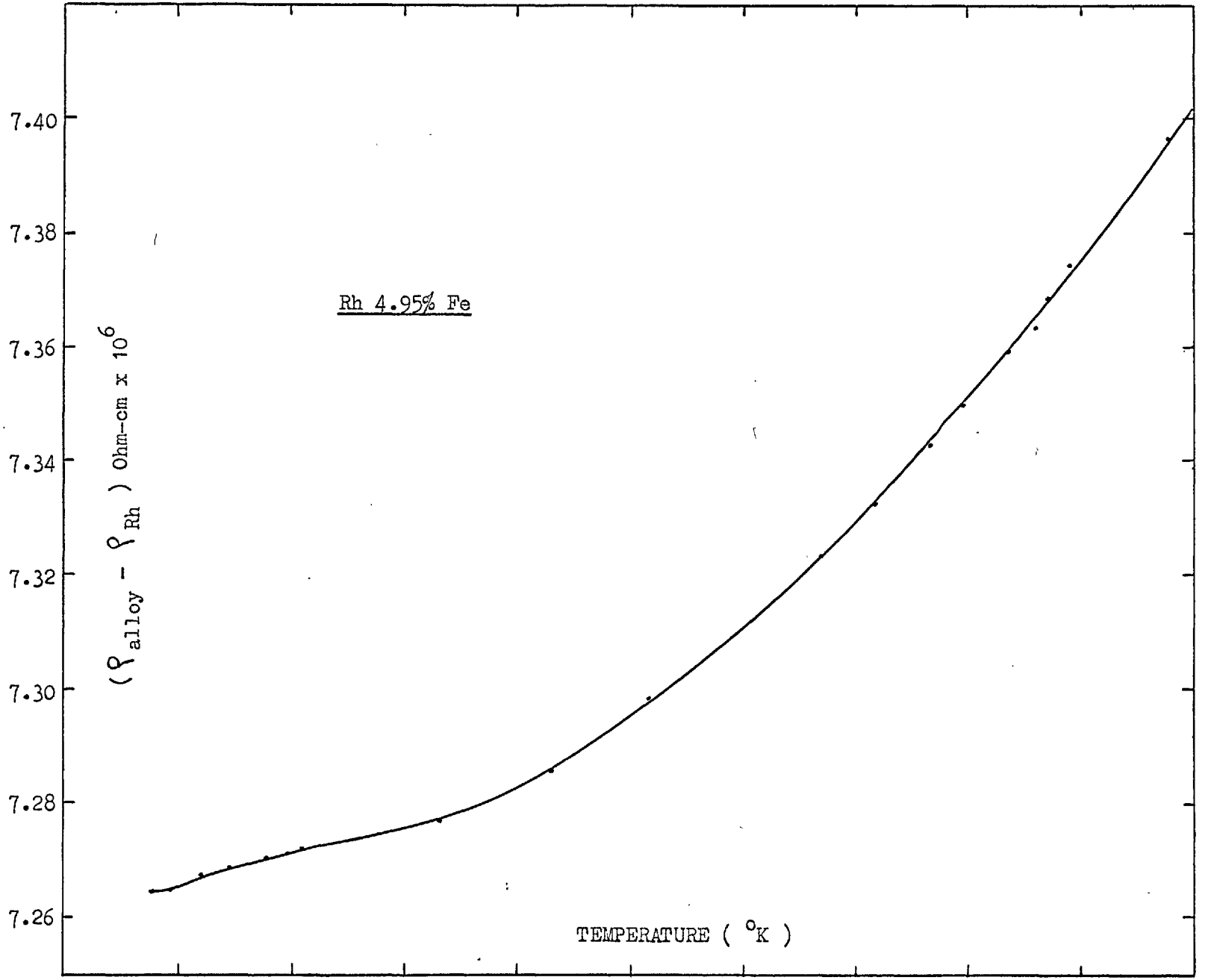

Fig.35 Excess Resistivity vs Temperature for Rh 4.95% Fe Alloy

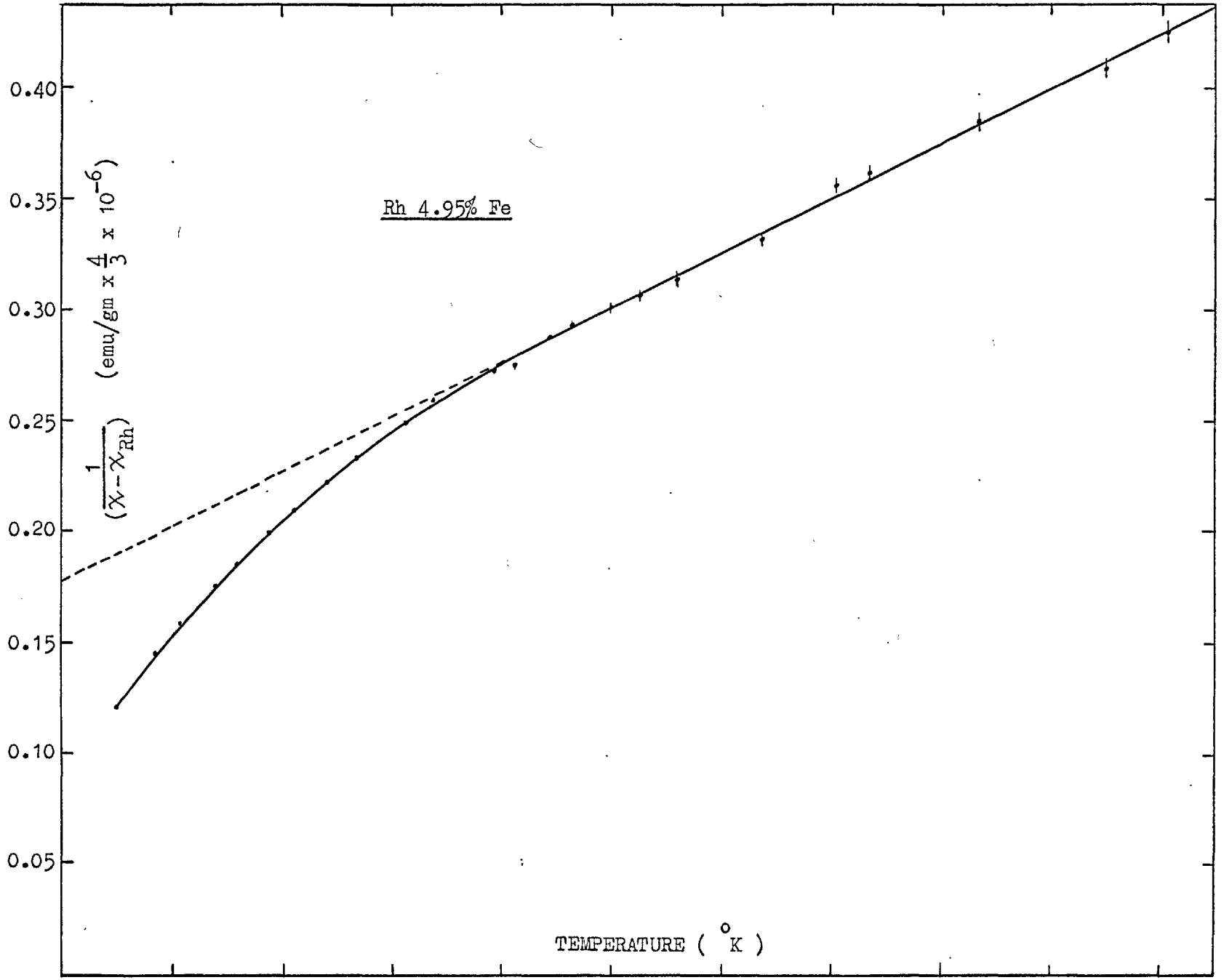

Fig.36 Curie-Weiss Plot for Rh 4.95% Fe Alloy

Rh 10.87% Fe

Fig. 37 shows the magnetisation of the alloy against applied field at 4.2°K. Cooling the specimen in a magnetic field of 8 kOe down to 4.2°K produces a displaced magnetisation curve which is also linear and parallel to the non-field cooled one. There is a marked absence of any hysteresis in either curves. The reason for this is that the magnetisation vs. field measurements are made well below the ordering temperature of 24°K (Fig. 38) where most of the spins are well locked into the ordered state. Fig. 38 also shows magnetisation of the alloy measured in a field of 3.65 kOe as a function of increasing temperature after cooling the alloy to 4.2°K in fields of 4 and 8 kOe. The thermal remanent moment decreases steadily and goes to zero at the temperature of the maximum in the susceptibility. The resistance of the alloy goes through a minimum at about the same temperature Fig. 39. A plot of $\frac{1}{\chi - \chi_{Rh}}$ against T is shown in Fig. 40. The Curie-Weiss intercept for this alloy is 270±20°K.

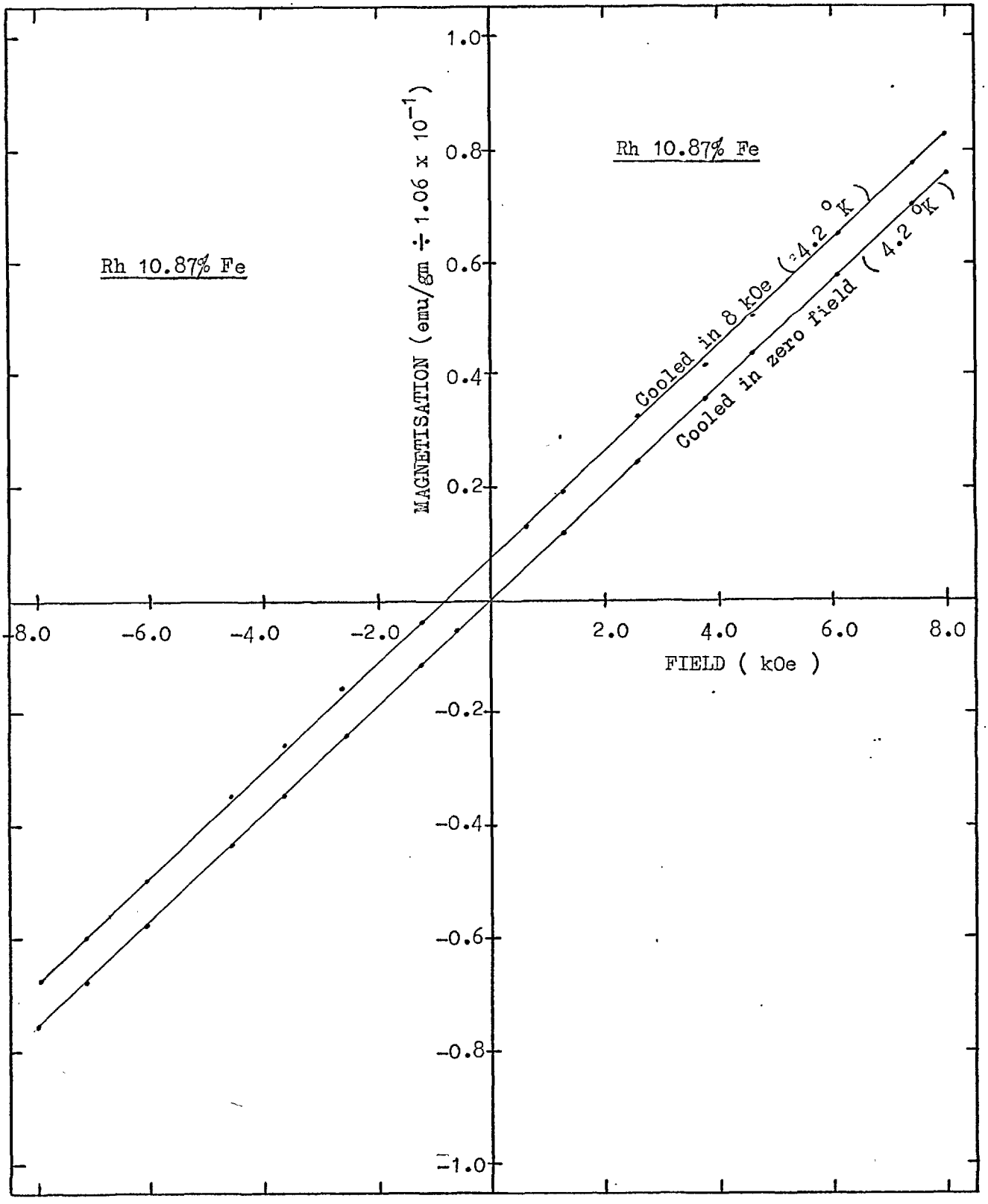

Fig.37 Magnetisation vs Field for Rh 10.87% Fe Alloy

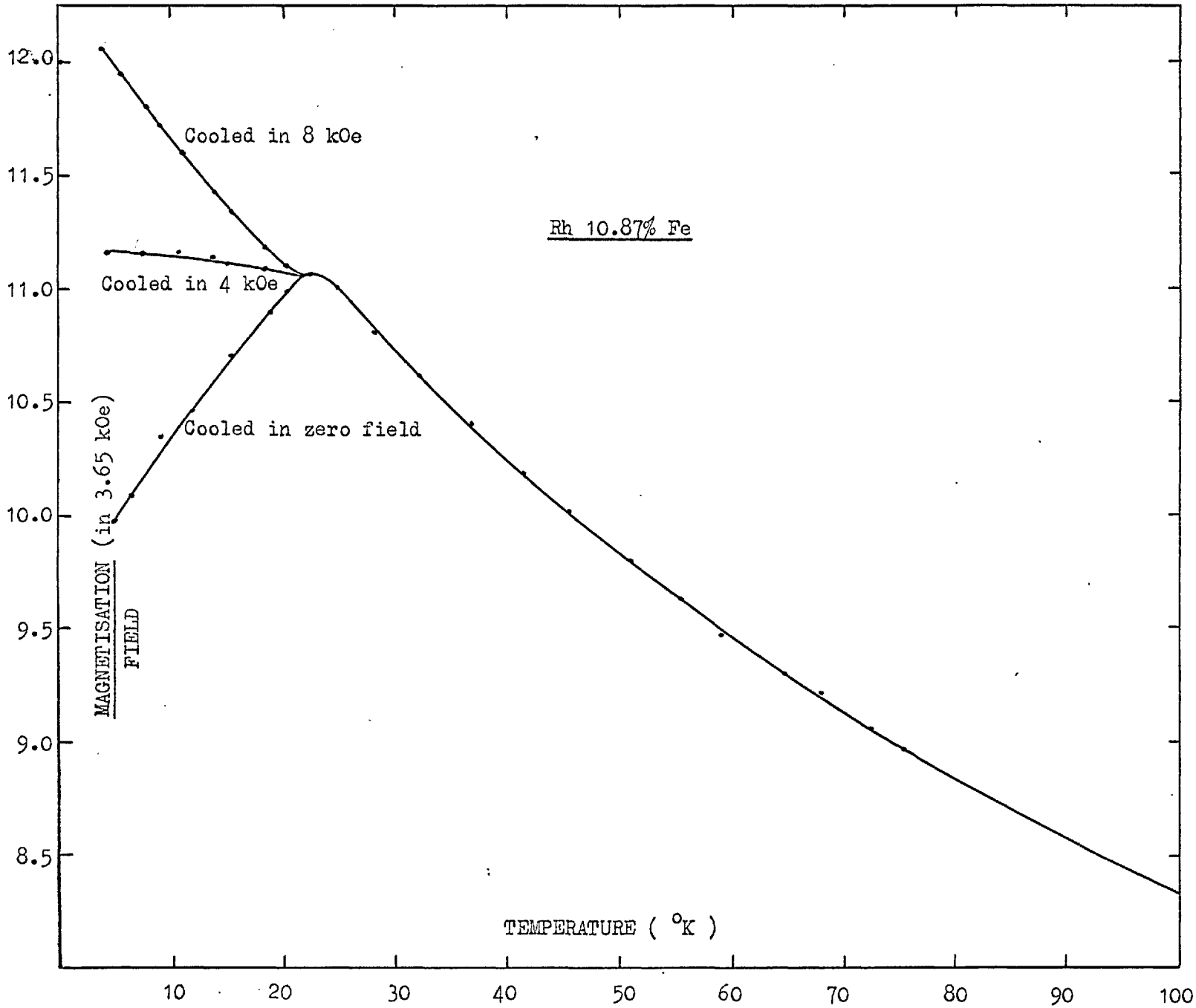

Fig.38 'Susceptibility' vs Temperature of Rh 10.87% Fe Alloy

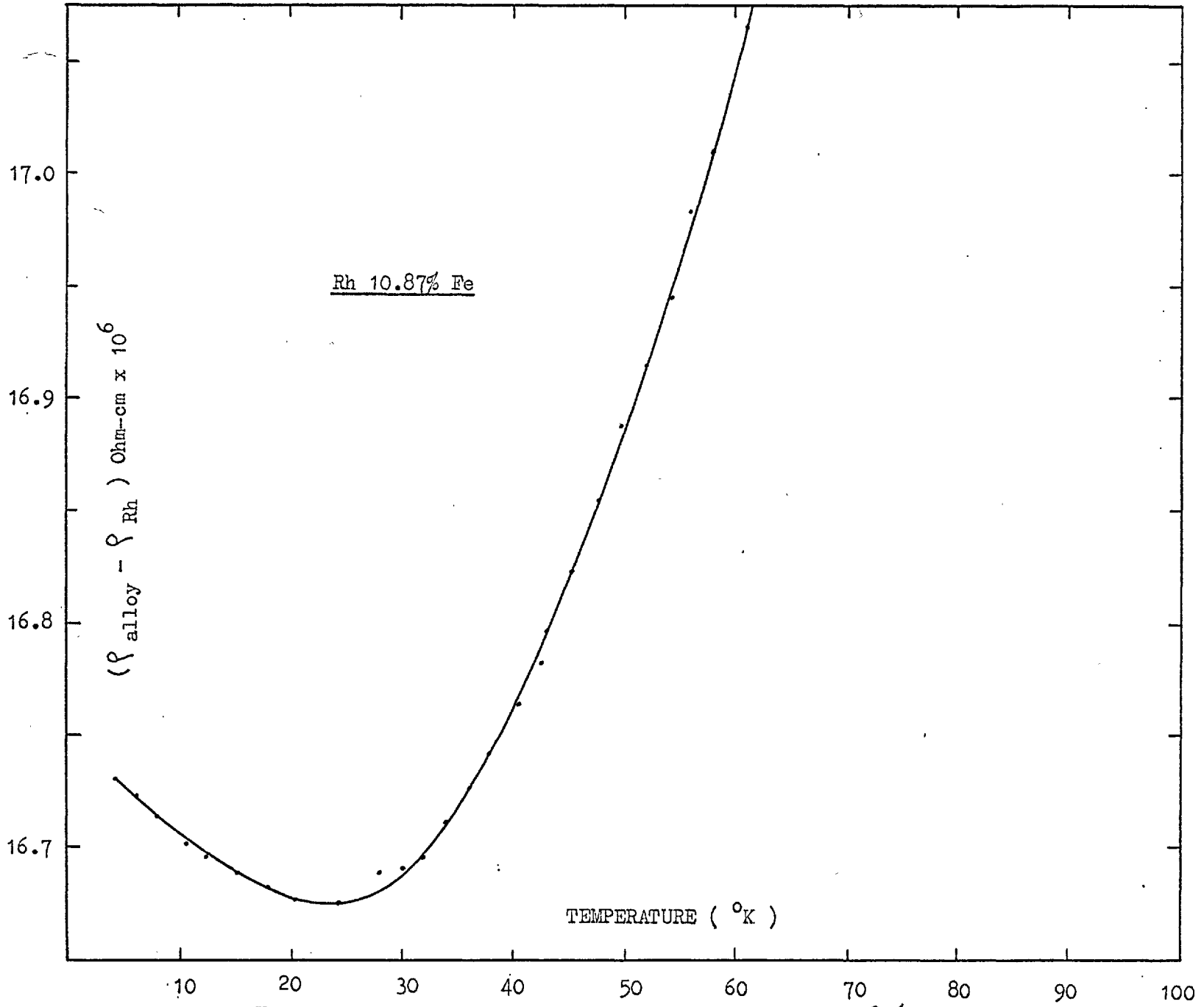

Fig.39 Excess Resistivity vs Temperature for Rh 10.87% Fe Alloy

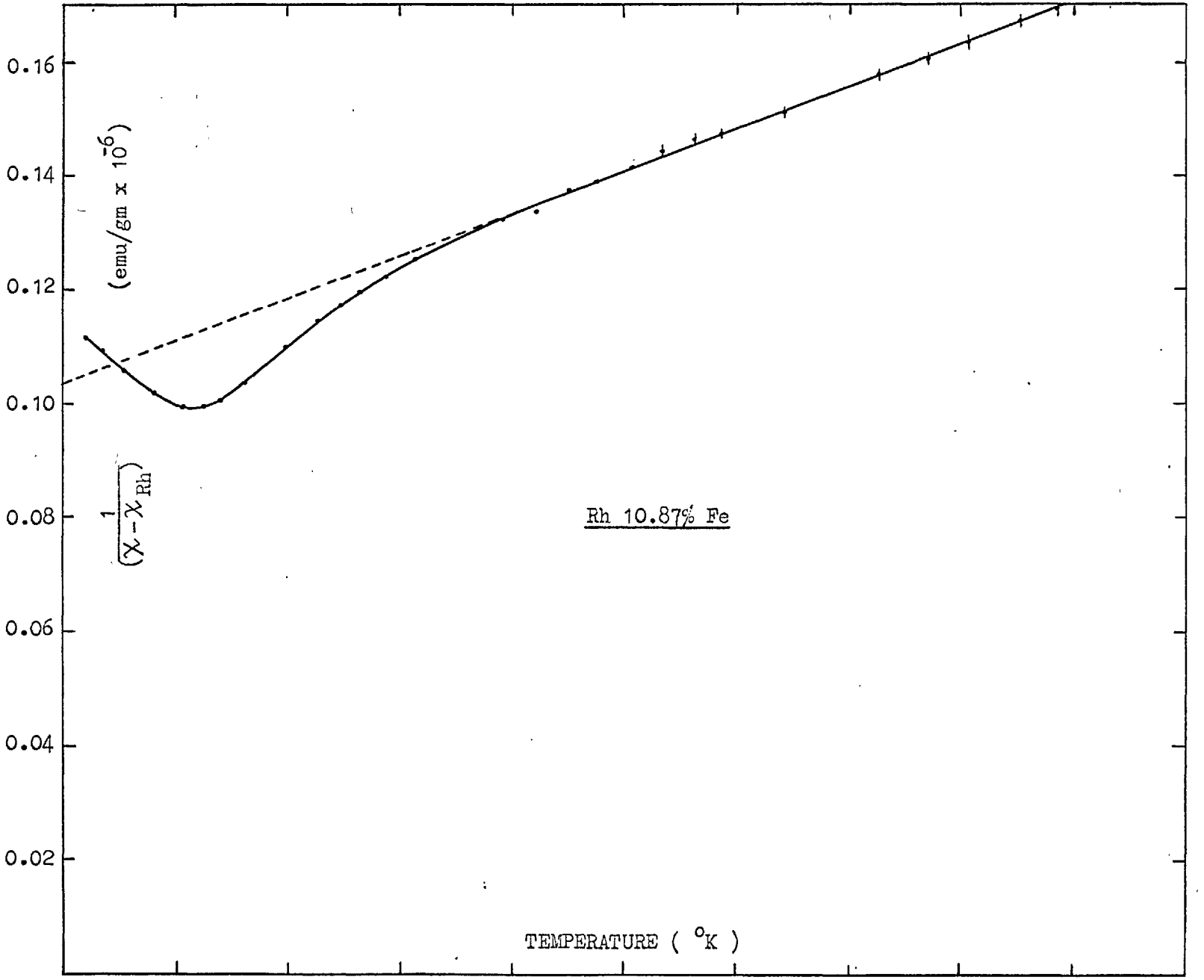

Fig.40 Curie-Weiss Plot for Rh 10.87% Fe Alloy

Rh 15.35% Fe

The field dependence of the magnetisation of the alloy at 4.20°K is very similar to that found in the Rh 10.87% Fe alloy. Fig. 41. The effect of field cooling is again to produce a displaced magnetisation curve parallel to the "non-field cooled" one. A broad maximum in the 'susceptibility' with a peak at about 48°K is observed when measured without field cooling, Fig. 42. The approximately linear decrease in the thermoremanent moments induced by field cooling the alloy in 4 and 8 kOe extrapolate to meet the non-field cooled curve at a temperature approximately 10°K below the temperature of the maximum in the 'susceptibility'. In fact, the magnetisation curve obtained after field cooling the alloy in 8 kOe appears to go through a shallow minimum. It is interesting to note that the resistivity of the alloy also goes through a minimum at about the same temperature and not at the temperature of the maximum as found in the case of the Rh 10.87% Fe alloy.

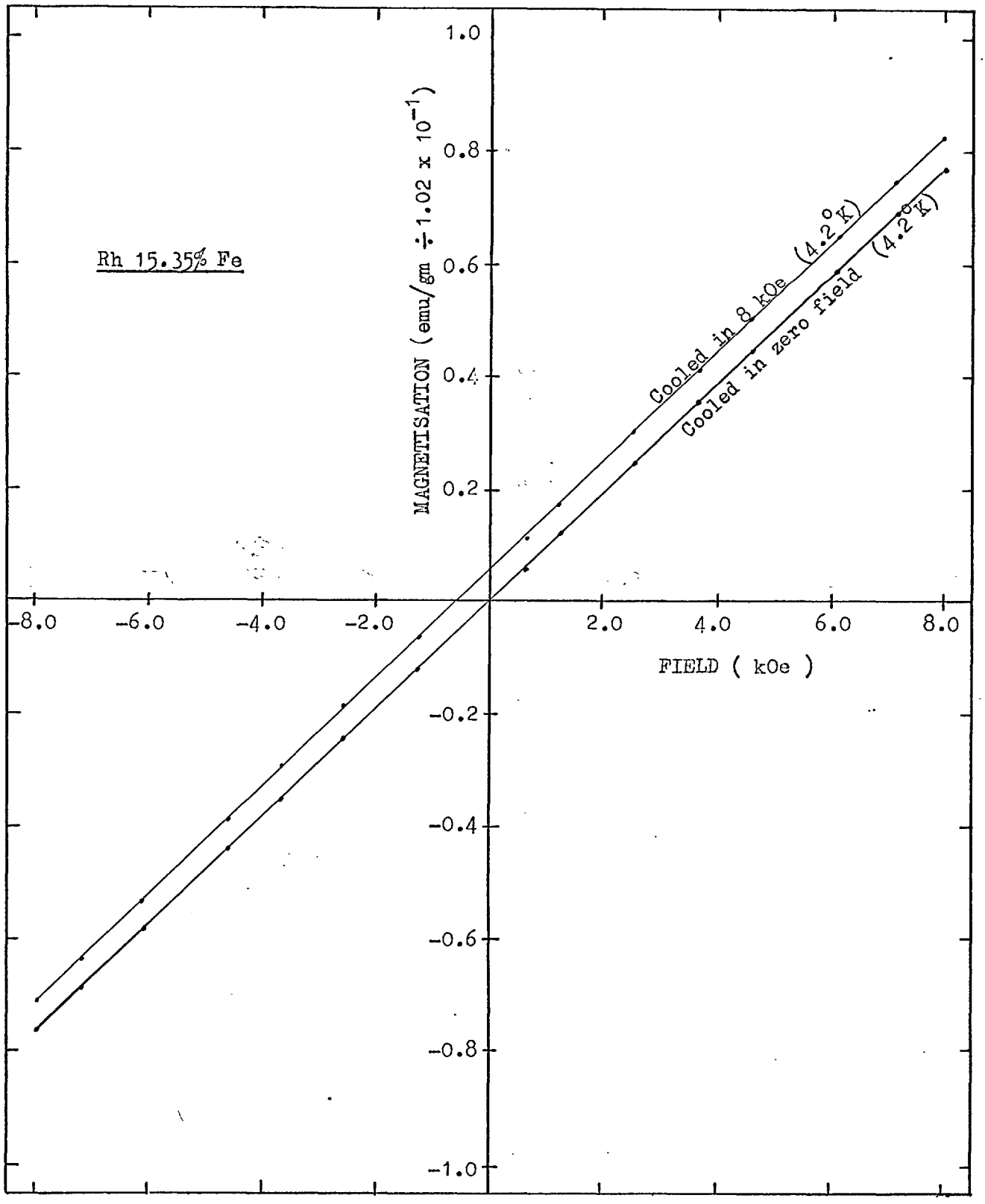

Fig.41 Magnetisation vs Field for Rh 15.35% Fe Alloy

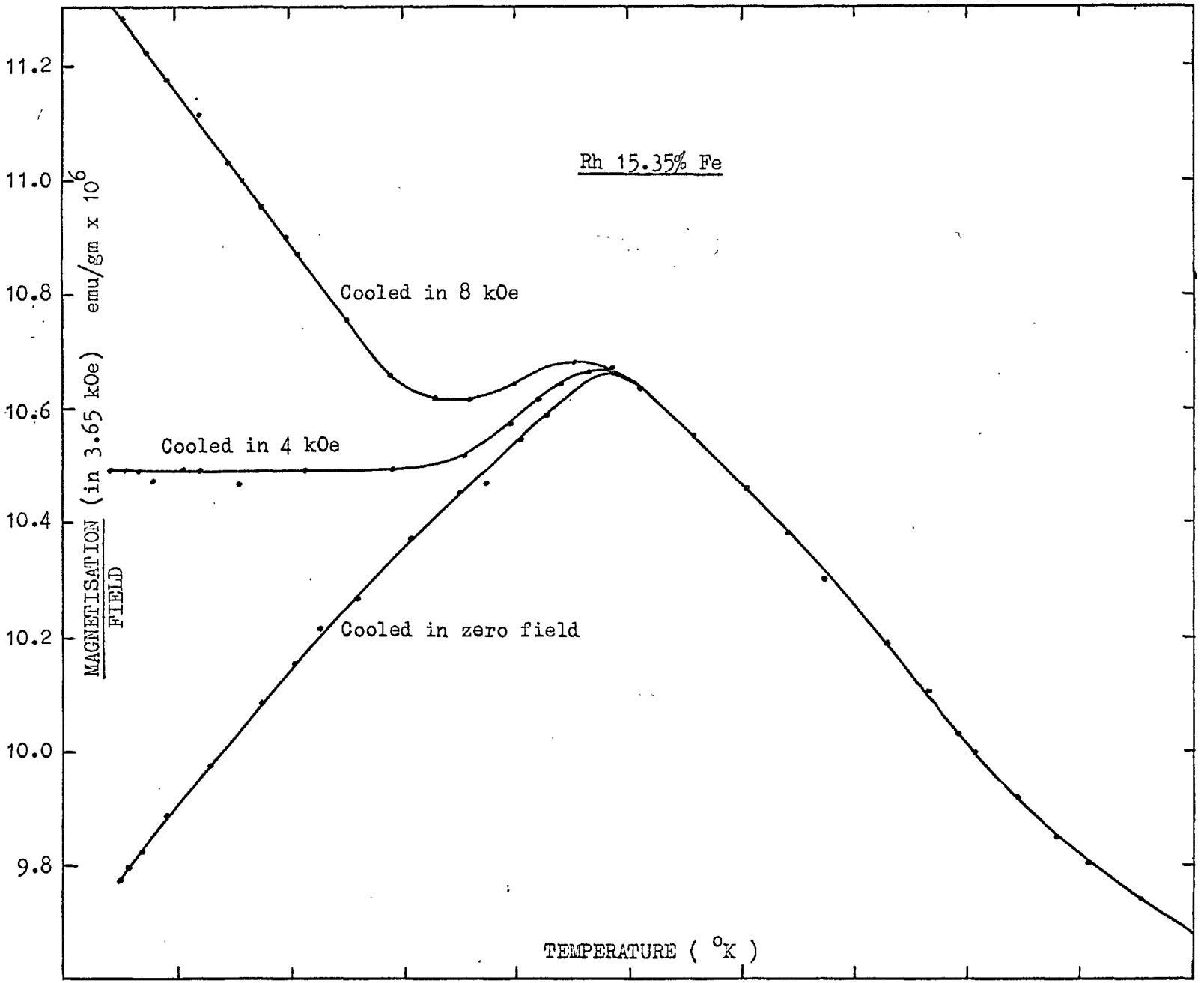

Fig. 42 'Susceptibility' vs Temperature of 15.35% Fe Alloy

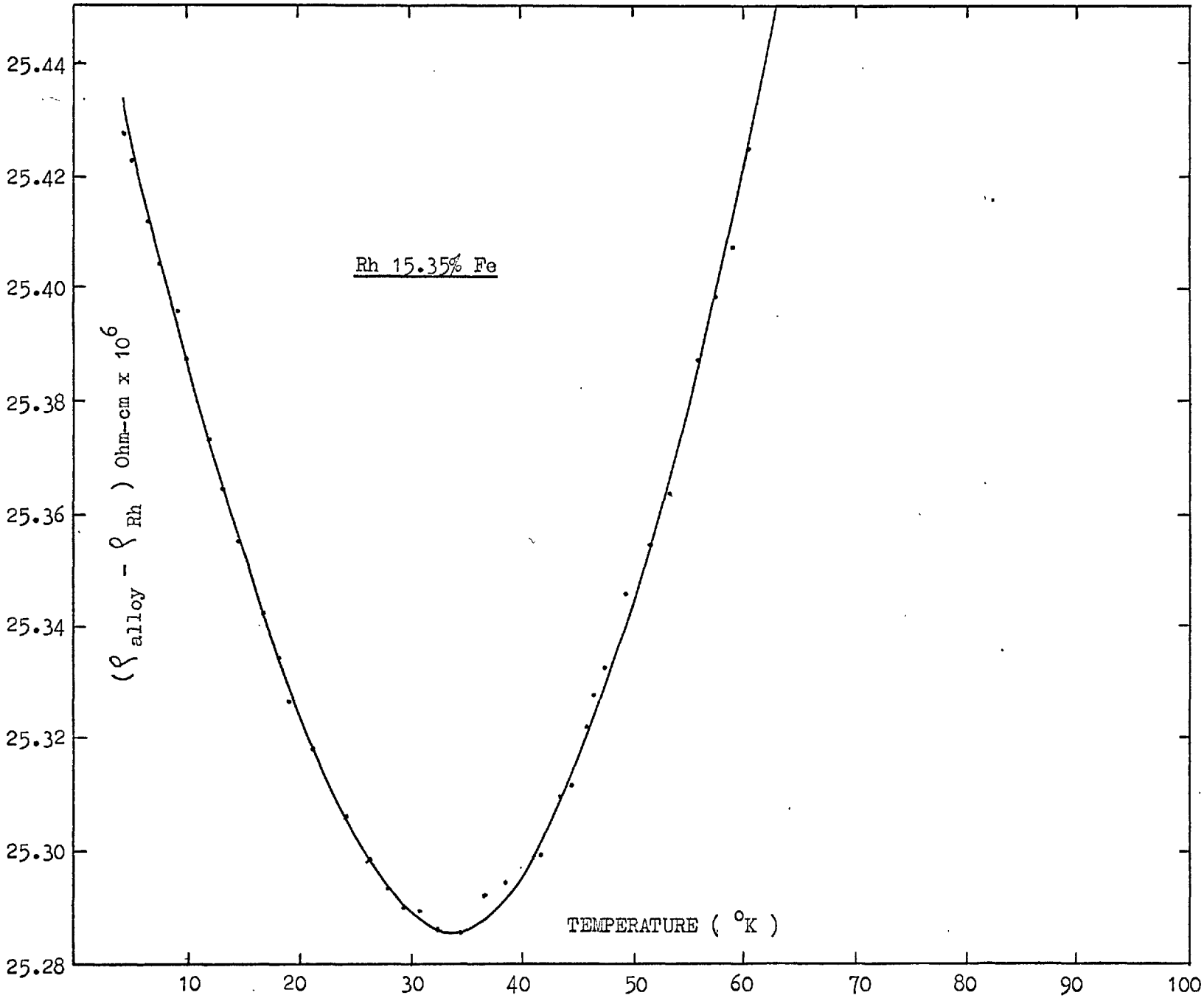

Fig.39 Excess Resistivity vs Temperature for Rh 15.35% Fe Alloy

DISCUSSION

If the temperature of the maximum in the susceptibility is taken as a measure of the interaction energy between the solute atoms, then the variation of this temperature gives an indication of the concentration dependence of interaction energy between solute atoms in the alloys.

In the dilute limit, with concentrations upto 1% Fe, Knapp (25) has reported that the susceptibility contribution from each iron atom is independent of their total concentration down to 0.4 ^{o}K. If this is so, it follows that there is no tendency towards the onset of magnetic order in the 1% Fe alloy down to 0.4^{o}K. A graph of T_{max} against concentration is shown in Fig. 44 in which a bar showing the upper limit of 0.4^{o}K for the 1% Fe alloy is also included. It is clear that the onset of magnetic order is inhibited at the lower concentrations. This behaviour may be considered to be intermediate between those found in Cu-Mn alloys on the one hand and in systems such as Cu-Ni on the other. In the former type where the moment on the solute atoms is well defined, magnetic order is observed down to the lowest concentrations. In Cu-Ni type of alloys, however, where the solute atoms carry no magnetic moment in the dilute limit, large concentrations are required before any magnetic order is observed.

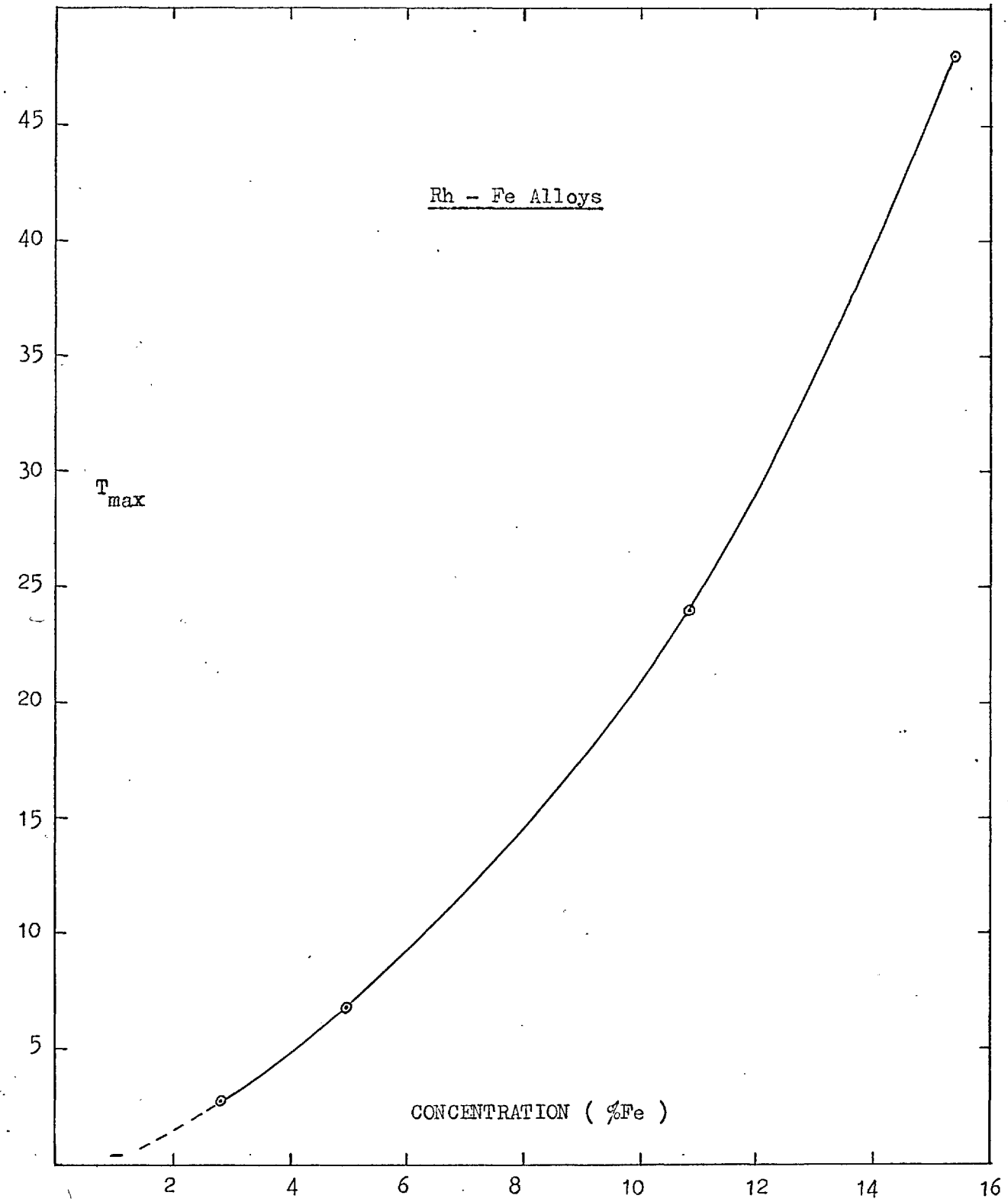

Fig.44 Graph of T_{max} vs Concentration of Iron

In Rh-Fe alloys T_{max} varies as a much higher power of the concentration than in Cu-Mn or La-Gd alloys where approximately linear dependence is found. Whether this behaviour may be considered to be an indication of the breakdown of the quasi bound state is not clear, as the high temperature susceptibility of the alloys when fitted to a Curie-Weiss law give progressively larger negative Curie-Weiss intercepts θ. If one followed the practice of regarding the θ values as a measure of the Kondo temperature (44) ($T_K \simeq 1/5\ \theta$) one would reach the rather unlikely conclusion that there is an increase in the s-d interaction energy and consequently a stronger spin compensation of the moment !

As mentioned before, a Curie-Weiss fit to the data is not possible over the whole temperature range. Waszink (88) has shown that by subtracting from the observed susceptibilities, a temperature independent matrix contribution which is larger than the pure Rh value, the Curie-Weiss fit can be extended to lower temperatures and smaller Curie-Weiss intercepts θ obtained. It is interesting that the value of 15^{o} that he obtains in this way for the 1% alloy is close to that found by Knapp using $\chi_0 = \chi_{Rh}$ for very dilute alloys. We have tried least squares fits of the data to a Curie-Weiss law of the form

$$\chi - \chi_o = \frac{C}{T-\theta}$$

where χ_o, C and θ are taken as independent variables. Since no value of χ_o gives a Curie-Weiss fit over the whole temperature range, the effect of varying both the lower and the upper limit of the data points over which fitting is done was studied. The best parameters obtained varied with the temperature range considered, but the variation caused by increasing the lower limit to above 20°K and keeping the upper limit constant at 200°K was small. The results obtained are:

Conc. % Fe	Curie-Weiss θ°K	χ_o emu/gmx10^6	P_{eff} μ_B
0.9%	-10 ± 2	1.44 ± .02	2.8 ± .1
2.86%	-26 ± 3	1.92 ± .03	2.65 ± .1
4.95%	-40 ± 10	2.5 ± 0.3	2.5 ± .2

A least squares fit to the susceptibiltiy formula (Eq. 1.29)

$$\chi - \chi_o = \frac{C}{T}\left(1 - \frac{1}{\log(\frac{T}{T_K})}\right)$$

has also been tried. In the high temperature limit this expression is similar in form to a Curie-Weiss relation (Fig. 1). The

corresponding parameters obtained are:

Conc. % Fe	T_K °K	χ_o emu/gmx10^6	P_{eff} μ_B
0.9	2.3 ± .1	1.44 ± .02	3.1 ± .04
2.86	5.3 ± .3	1.95 ± .03	2.85 ± .05
4.95	7.2 ± .5	2.65 ± .1	2.65 ± .1

If the susceptibility is calculated in the Anderson model to include only the terms upto the second order in the free energy, a formula of the type

$$\chi - \chi_o = \frac{C}{T}\left(1 + (J\rho)^2 \log \frac{T}{T_F}\right)$$

is obtained (Eq. 1.26). This formula has also been fitted to the data assuming values of T_F of 10,000, 20,000 and 30,000°K. (corresponding to a Fermi energy E_F of ~ 1 to 3 eV). It is found that the effect of varying T_F on the parameters obtained is small. The results obtained assuming a T_F of 10,000°K are:

Conc. % Fe	$\lvert J\rho \rvert$	χ_o emu/gmx10^6	P_{eff} μ_B
0.9	0.33 ± .01	1.25 ± .05	4.2 ± .2
2.86	0.36 ± .02	1.5 ± .1	4.1 ± .1
4.95	0.36 ± .02	2.5 ± .3	3.7 ± .3

The mean square deviation of the data points for the best fit to this formula is over an order of magnitude larger than obtained in the previous two formulae, suggesting that the fit is not as good in this case. It is also interesting to note that using the relation

$$T_K = T_F \exp(-1/|J\rho|)$$

a Kondo temperature of $\sim 200^{\circ}K$ is obtained. This is unreasonably high, and since the formula is only valid above T_K, it is inconsistent with the temperature range over which the fitting has been done.

Recently Levine and Suhl (29) have made computer calculations of the susceptibility using Wolff's model beyond the Hartree-Fock approximation. The results for the susceptibility are very similar (Figs.2&3) to those found for the Rh-Fe alloys, although the calculated resistivity (30) still increases with decreasing temperature in a manner similar to that given by the s-d interaction models. Hamann (34) has recently derived an analytic expression for the susceptibiltiy starting from the Anderson model and obtained results very similar to Levine and Suhl's.

A graph of $\frac{(\chi - \chi_{Rh}) \times T}{\text{Conc.}}$ against T is shown in Fig. 45. At high temperatures all the curves are nearly parallel straight lines, indicating that there is a temperature independent contribution to the susceptibility of the alloys which is proportional to the concentration of the solute atoms. Addition of solute atoms to a matrix usually produces changes in the band structure so that the matrix susceptibility may become modified. The total temperature independent part of the susceptibility of the alloy may therefore be written as

$$\chi_o = \chi_{Rh} + \Delta\chi \times C$$

where χ_{Rh} is the susceptibility of pure Rh, C is the concentration in % of Fe and $\Delta\chi$ is the extra contribution per per-cent of iron.

If $\Delta\chi = 0.42 \times 10^{-6}$ emu/gm/%Fe is assumed and the resulting χ_o subtracted off from the measured susceptibilities, the graphs of $\frac{(\chi - \chi_o) \times T}{\text{Conc.}}$ against T reduce to the form shown in Fig. 46. At high temperatures, the susceptibilities of all the alloys obey Curie-Law but the moment begins to decrease with decreasing temperature below about 90°K for all the alloys. The departure from the Curie law can also be seen in the plots of $\frac{1}{\chi - \chi_o}$ against T Figs. 47, 48, 49, and 50 . The effective

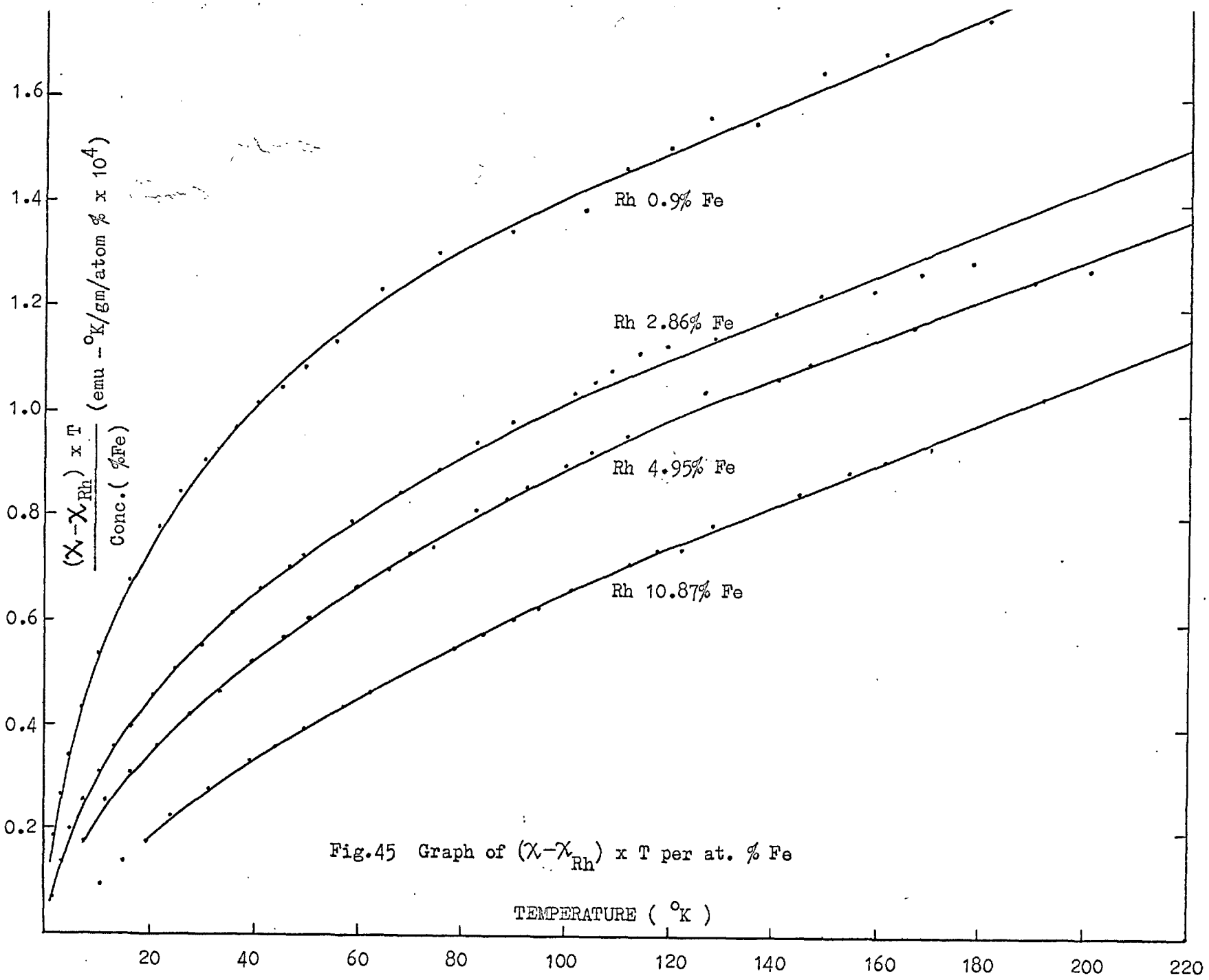

Fig.45 Graph of $(\chi-\chi_{Rh})$ x T per at. % Fe

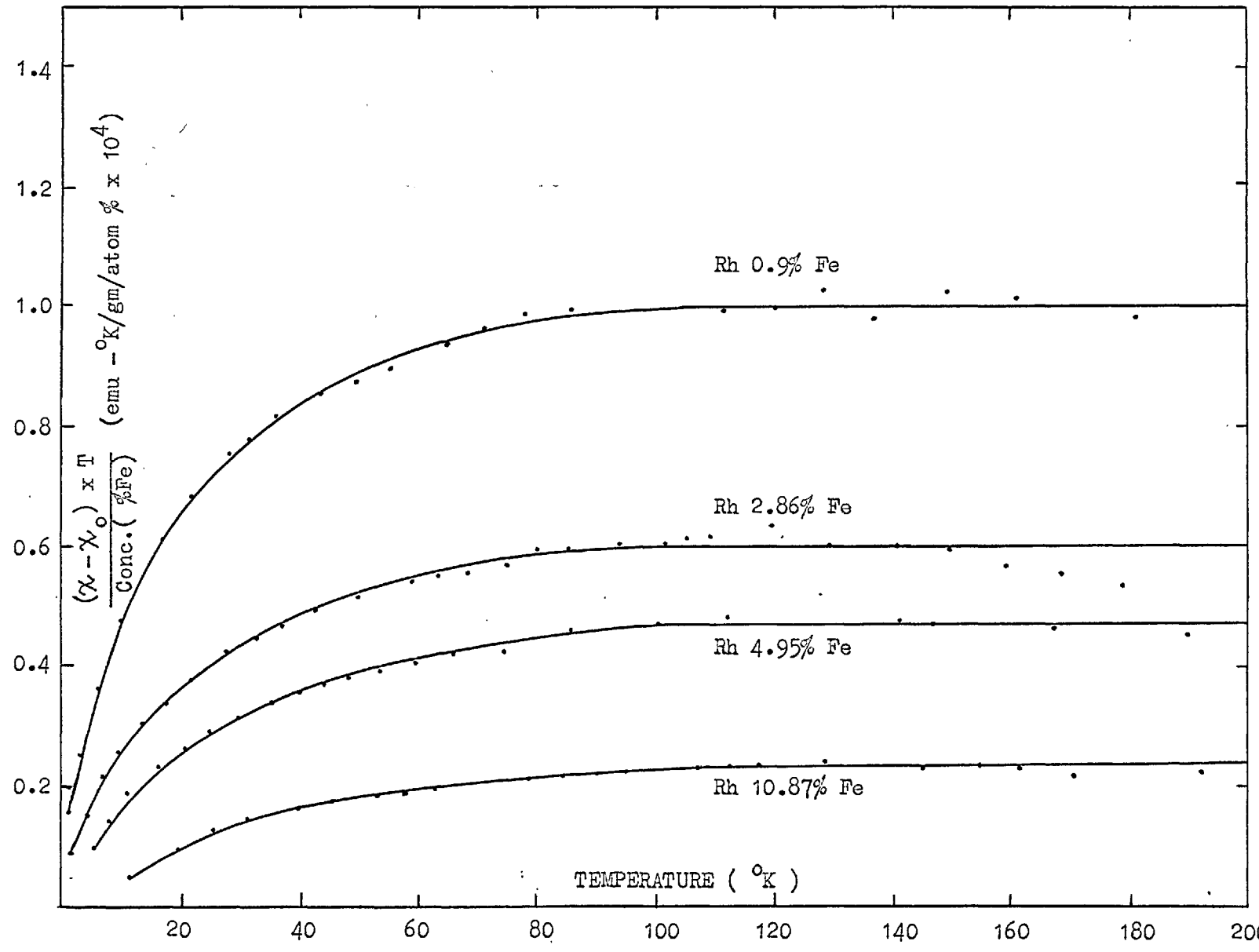

Fig.46 Graph of $(\chi-\chi_o)$ x T per at. % Fe

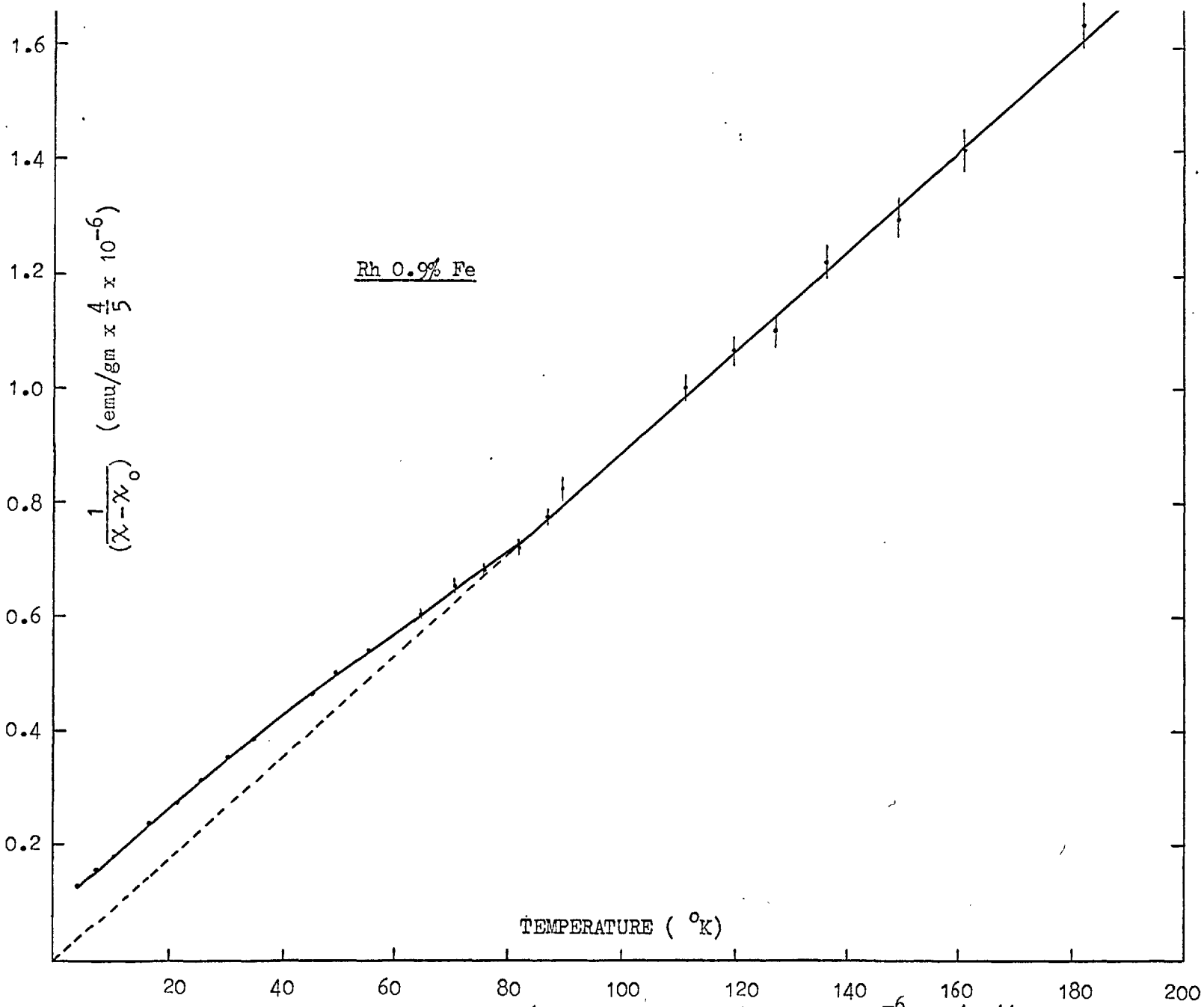

Fig.47 Curie-Weiss Plot for Rh 0.9% Fe Alloy using χ_o=0.42 x 10^{-6} emu/gm/%Fe

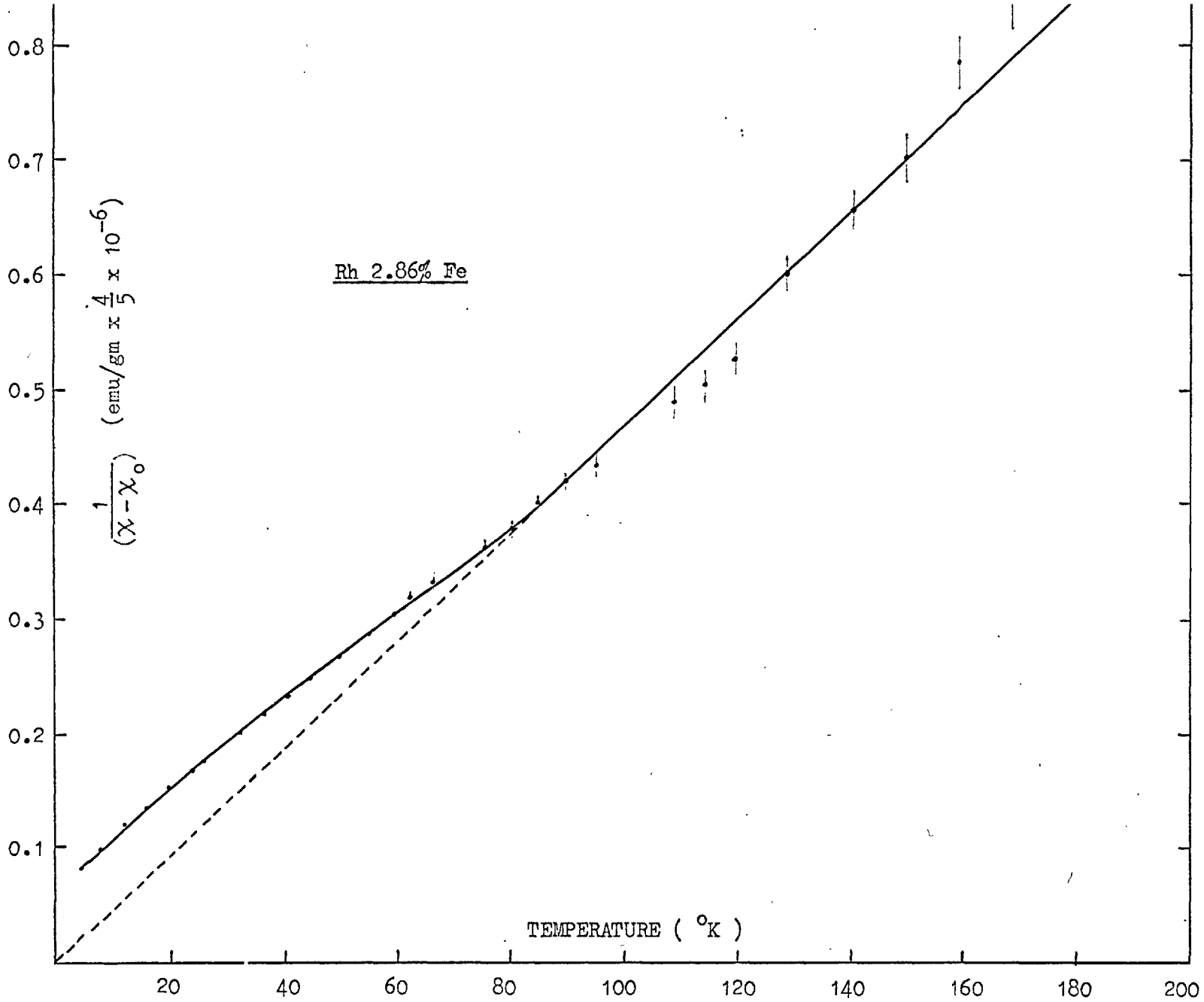

Fig.48 Curie-Weiss Plot for Rh 2.86% Fe Alloy using χ_o=0.42 x 10^{-6} emu/gm/%Fe

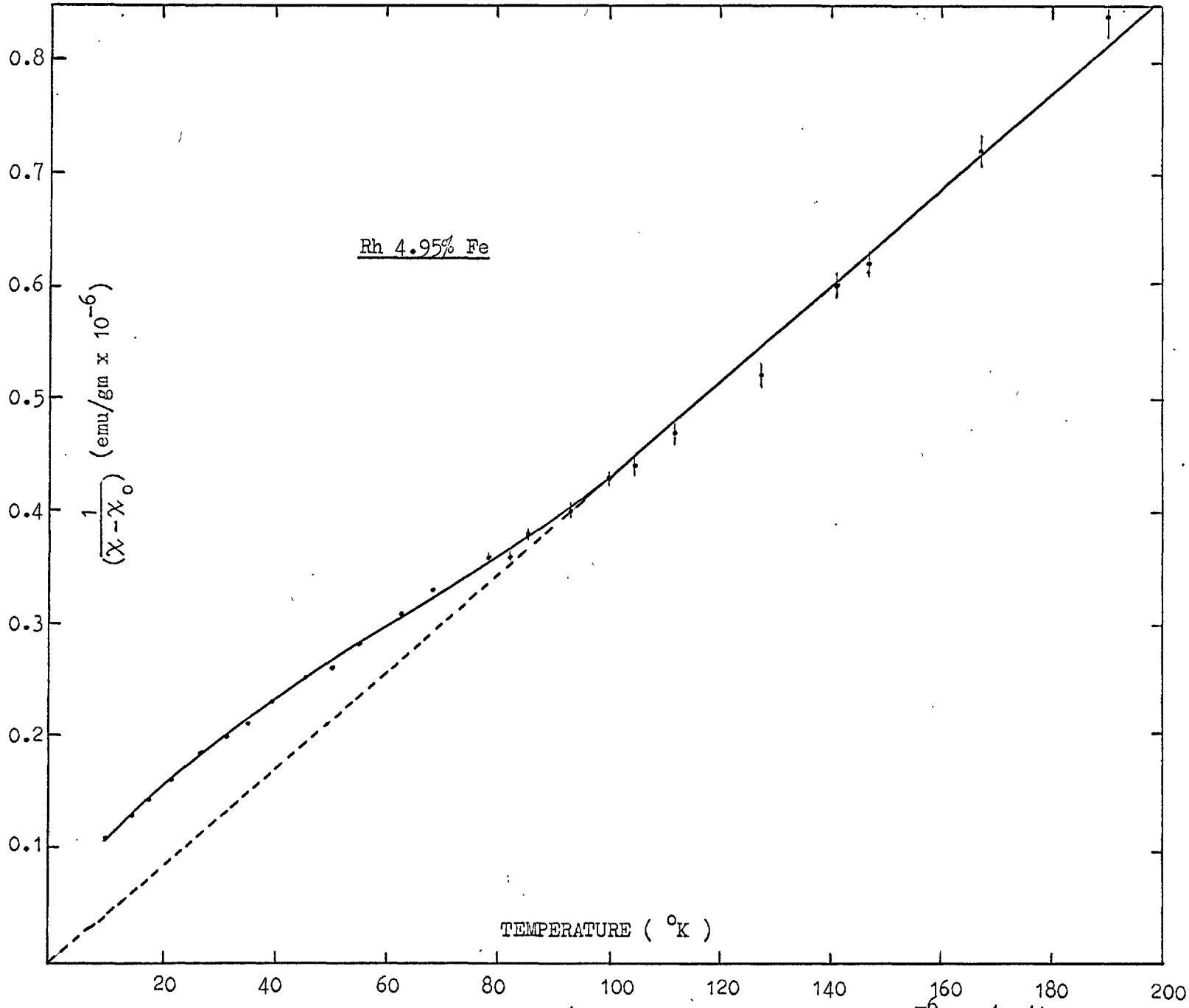

Fig.49 Curie-Weiss Plot for Rh 4.9% Fe Alloy using χ_o = 0.42 x 10^{-6} emu/gm/%Fe

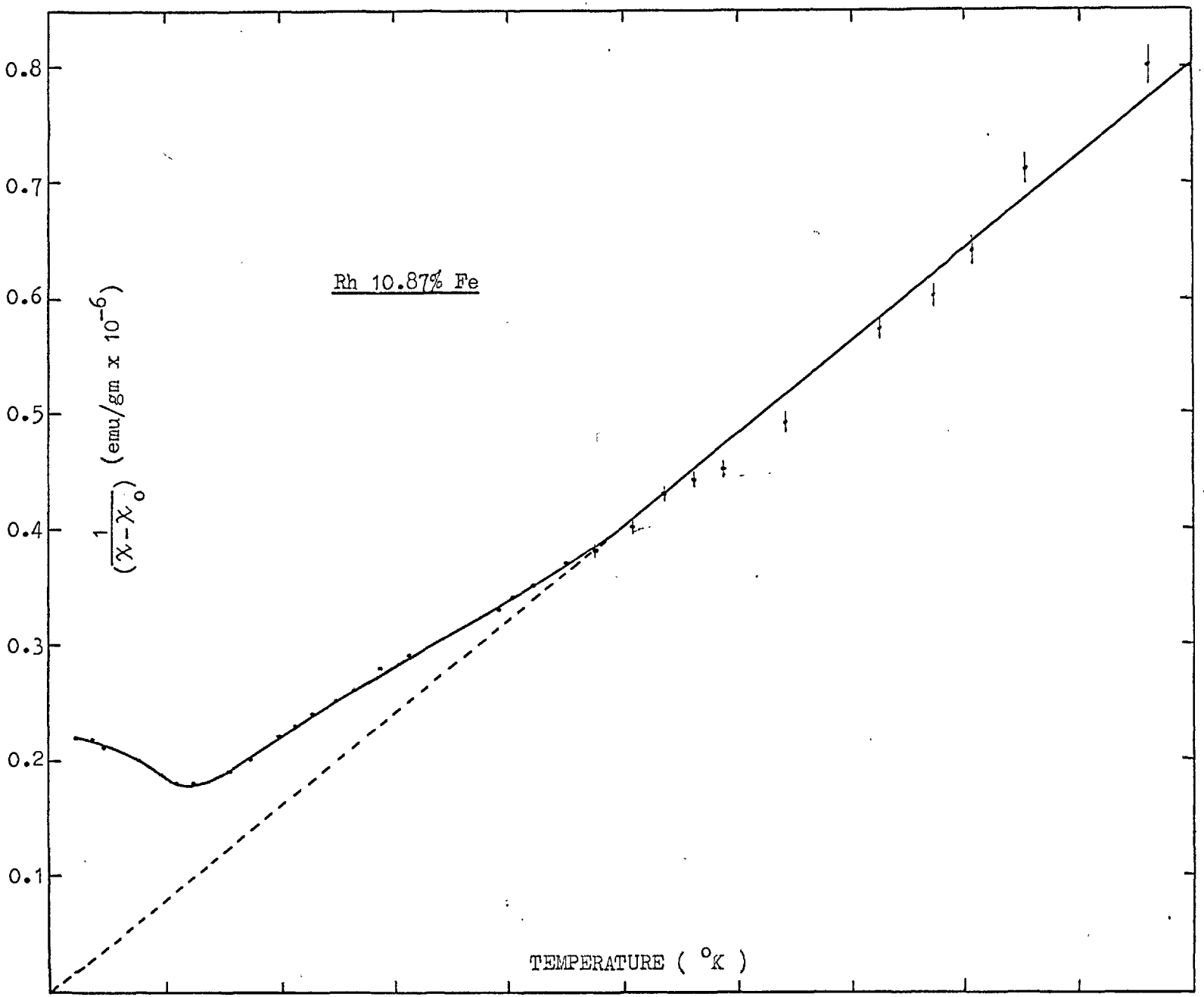

Fig. 50 Curie-Weiss Plot for Rh 10.86% Fe Alloy using χ_o=0.42 x 10^{-6} emu/gm/%Fe

high temperature moment per iron atom is also reduced as the concentration increases.

The magnitude of the temperature independent susceptibility contribution $\Delta\chi$ of 0.42×10^{-6} emu/gm/%Fe is very much larger than expected from any modification of the band structure of the host and the resulting change in the density of states. It is also unlikely to be due to an increase in the exchange enhancement in the band, as the enhancement per iron atom is required to be an order of magnitude larger than the value for palladium atoms in the pure metal. There is, however, the possibility that it is due to a localised enhancement at the iron site. Measurements on Rh-Co alloys reported here show that such a large localised enhancement of the susceptibility is possible. The temperature dependence of the susceptibility of Rh-Co is small but the temperature independent susceptibility corresponds to $\Delta\chi = 0.28\times10^{-6}$ emu/gm/% Co.

The high temperature susceptibiltiy at the iron site may be regarded as due to two contributions. One is a temperature dependent part and obeys Curie law and the other is a temperature independent contribution discussed above. The high temperature susceptibility contribution from each iron atom may be written as

$$\chi = \frac{cC}{T} + c\Delta\chi$$

If the high temperature susceptibility calculated by Suhl is separated as above into two parts, the ratio of the coefficients C and $\Delta\chi$ is found to be about $3.1\times10^{-3}(^{\circ}K)$. In the Rh-Fe alloys, the ratio varies from $4.2\times10^{-3}(^{\circ}K)$ for the 1% Fe alloy to $17.5\times10^{-3}(^{\circ}K)$ the 10% Fe alloy. The quantity $\frac{\Delta\chi}{C}/p^2_{eff}$ is of course constant for the Rh-Fe alloys (since $\Delta\chi$ is constant) and is equal to $5.4\times10^{-4}(^{\circ}K)$. Since Levine & Suhl have made calculations using $S = \frac{1}{2}$, this quantity for their case is $\simeq 1\times10^{-3}(^{\circ}K)$ which is about twice the value for Rh-Fe alloys.

Knapp (25) has used a two band model in a phenomenological theory of the resistance anomaly in the Rh-Fe alloys. He considers that mainly the d band electrons are involved in the spin condensation of the moment. Since most of the current is carried by the s band, a decrease in the effective moment on the iron atoms due to spin compensation results in a smaller scattering cross section and hence the fall in the resistance

with decreasing temperature. Doniach (130), however, believes that the resistance anomaly in Rh-Fe alloys should be interpretable in terms of the spin fluctuation model, although no calculations have yet been made by the author to support this.

A significant result of the present resistivity measurements is that as the concentration of Fe is increased, the resistance contribution per iron atom no longer shows the concentration independence found in the dilute limit. Furthermore, the striking dilute limit temperature dependence disappears as the Fe concentration increases and is replaced by smaller effects associated with magnetic ordering. The contrast between the resistivity behaviour of the more concentrated alloys and the dilute ones is clearly visible in Fig. 51 where the results of the measurements by Coles (87) of dilute Rh-Fe alloys are also included.

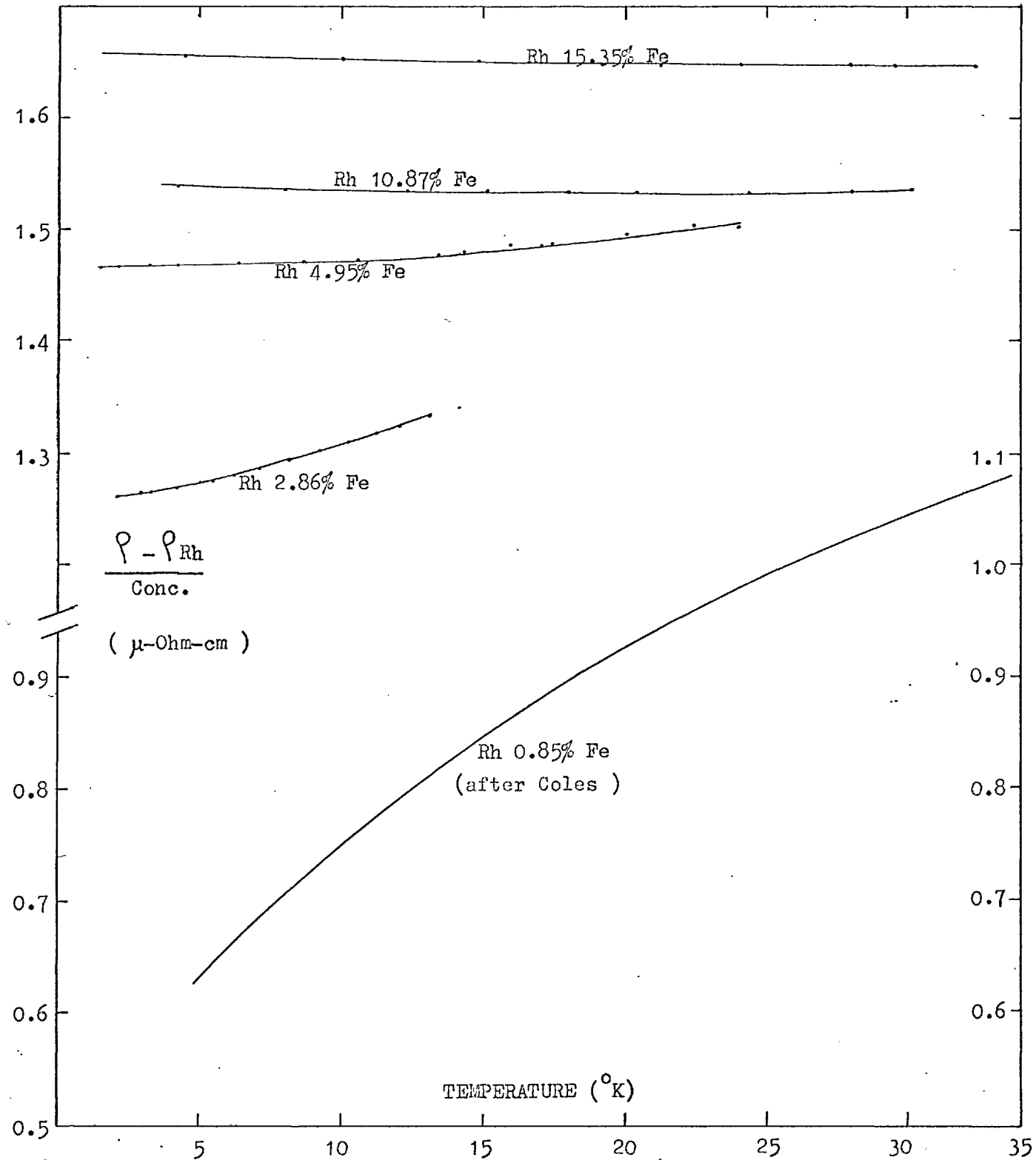

Fig.51 Graphs of Excess Resistivity per at. % Fe for Rh-Fe Alloys

B. The Rh-Co Alloy System

Introduction

The localised exchange enhancement on the Ni atom in Pd-Ni alloys (63) gives rise to many interesting effects in the macroscopic properties such as the magnetic susceptibility (80), the electrical resistivity (132) and the specific heat of the alloys (131). Shaltiel et al (80) have reported that in the dilute limit Ni atoms are non magnetic in Pd. As the concentration of Ni was increased, however, a threshold was reached ($\sim$2 at.% Ni) when the alloy became ferromagnetic. Schindler and Rice (132) reported the observation of a T^2 term in the electrical resistance of dilute Pd-Ni alloys, and Schindler and Mackliet (131) have reported specific heat measurements which have an enhanced value for γ which is also a sensitive function of the concentration of Ni.

Rh-Co is an iso-electronic alloy system similar to Pd-Ni where the localised exchange enhancement on the Co atoms would be expected to manifest itself in some properties similar to those found in Pd-Ni alloys. The uniform band enhancement in Rh metal is much smaller than in Pd so that the effect of the

intra atomic exchange on the Co atom on the properties of the Rh-Co alloys is expected to be smaller.

Measurements of the susceptibility of dilute Rh-Co alloys have been made by Walstedt et al (129). The authors report a weakly temperature dependent susceptibility increase $\Delta\chi(Co) \sim 20 \times 10^{-4}$ emu/mole, as compared to a $\chi_{Rh} \sim 1 \times 10^{-4}$ emu/mole. Measurements on a dilute Rh-Co alloy by Mozumder (110) shows essentially temperature independent resistivity at low temperatures.

Magnetisation measurements on two Rh-Co alloys are reported below. The temperature dependence of the excess susceptibility is found to be roughly similar. There is no indication of magnetic order down to 1.6°K even in the high concentration (Rh 11 at.% Co) alloy suggesting that a threshold value if any, is at a much higher concentration.

Sample Preparation

The Rh ½% Co alloy was obtained from the Mond Nickel Co. Ltd. and the Rh 11% Co alloy was prepared in the laboratory using Rh sponge of purity 99.99% and Co wire of purity 99.99%. The same technique of sample preparation as used for Rh-Fe alloys was employed in this case also.

Rh ½% Co

Fig. 52 shows the magnetisation of the alloy measured at 77 and 4.2°K as a function of the magnetic field. A small temperature dependence is observed in the magnetisation measured in a constant field of 3.83 kOe (Fig. 52). Since the susceptibility of pure Rh is temperature dependent (0.92×10^{-6} emu/gm at 20°K and 0.99×10^{-6} emu/gm at 300°K) it is difficult to make an accurate allowance for the matrix susceptibility. The increase in χ due to Co is calculated assuming constant values for the matrix term of $\chi_o = 0.99 \times 10^{-6}$ emu/gm and $\chi_o = 0.95 \times 10^{-6}$ emu/gm. The results are tabulated below for a few temperatures where the units for χ are in emu/gm x 10^{-6}.

T °K	χ_{Tot} ±.005	$\Delta\chi$ (χ_o=0.99)	$\Delta\chi$ (χ_o=0.95)
77	1.25	0.26	0.30
20	1.28	0.29	0.33
10	1.315	0.325	0.365
5	1.345	0.355	0.395
2	1.365	0.377	0.417

The susceptibility increase $\Delta\chi$ at 77°K is about 0.26×10^{-6} emu/gm. Analysis of the concentration of Co in

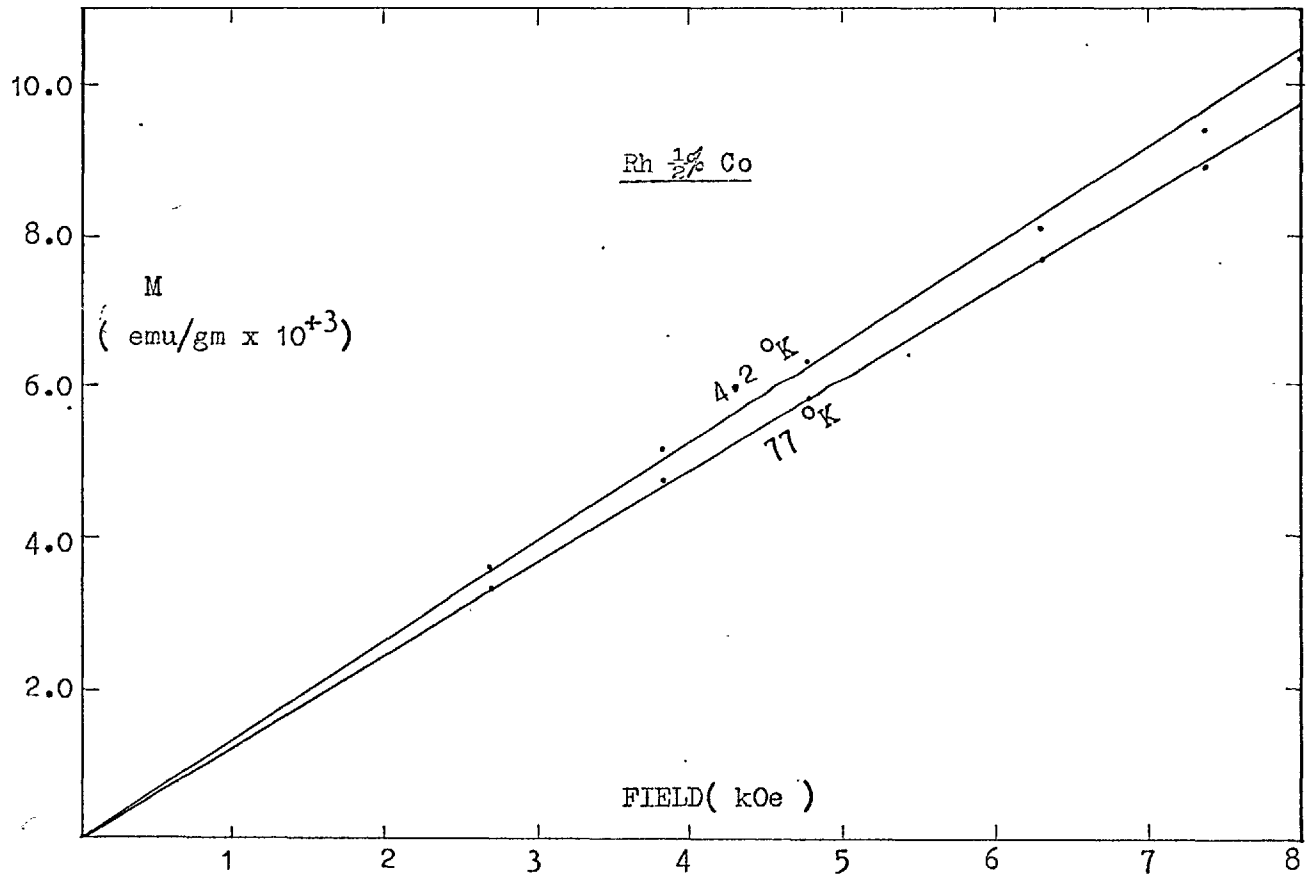

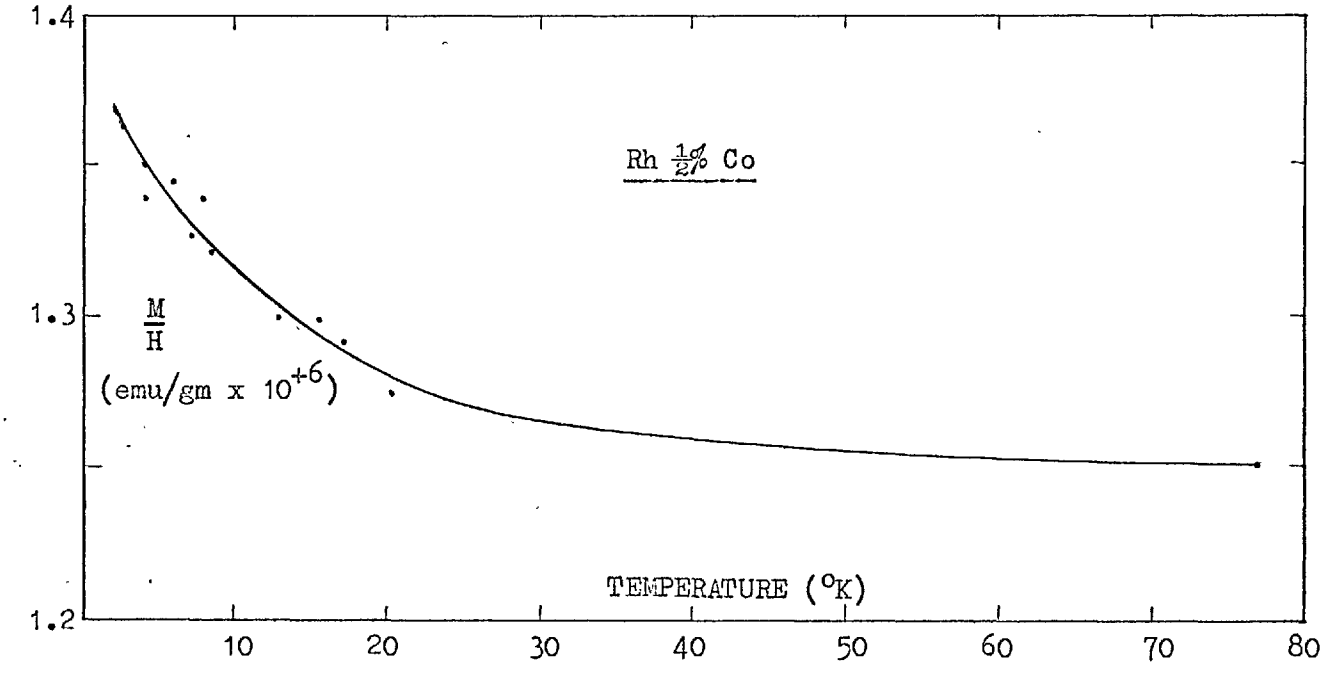

Fig.52 Graphs of Magnetisation vs Field and Temperature for Rh½% Co Alloys

the alloy is not available at present but it is thought to contain $\frac{1}{2}$ wt.% Co (i.e. $\sim$0.9 at.% Co). Hence the susceptibility contribution of Co in Rh is $\sim 29 \times 10^{-6}$ emu/gm. Walstedt et al (129) have reported that the susceptibility of dilute Rh-Co alloy is weakly temperature dependent and the increase $\Delta\chi$ due to Co is 20×10^{-4} emu/mole which is equal to 34×10^{-6} emu/gm. Since $\Delta\chi$ is temperature dependent and also sensitive to the magnitude of the matrix term subtracted off, the small difference with the present result is not surprising.

Rh 11% Co

The magnetisation of the alloy as a function of the field has been measured at 77 and 4.2°K, Fig.53 . The magnetisation has also been measured as a function of the temperature in a constant field of 3.65 kOe from 1.6°K upwards. The temperature dependence of the susceptibility is similar to that found for the lower concentration alloy and scales with it to 10% over the temperature range, as can be seen by comparing the following table with that for the ½% alloy.

T	χ_{Tot}	$\Delta\chi$	$\Delta\chi$
°K	±.005	(χ_o = 0.99)	(χ_o = 0.95)
77	3.87	2.88	2.92
20	4.15	3.16	3.20
10	4.245	3.255	3.295
5	4.36	3.37	3.41
2	4.68	3.69	3.73

The weak temperature dependence of χ is thought to be a real effect due to Co, and not due to the presence of impurities such as iron, as both Rh and Co used were fairly pure. The iron content in the alloy required to explain the observed increase between 2 and 10°K is estimated to be 0.11 at.%.

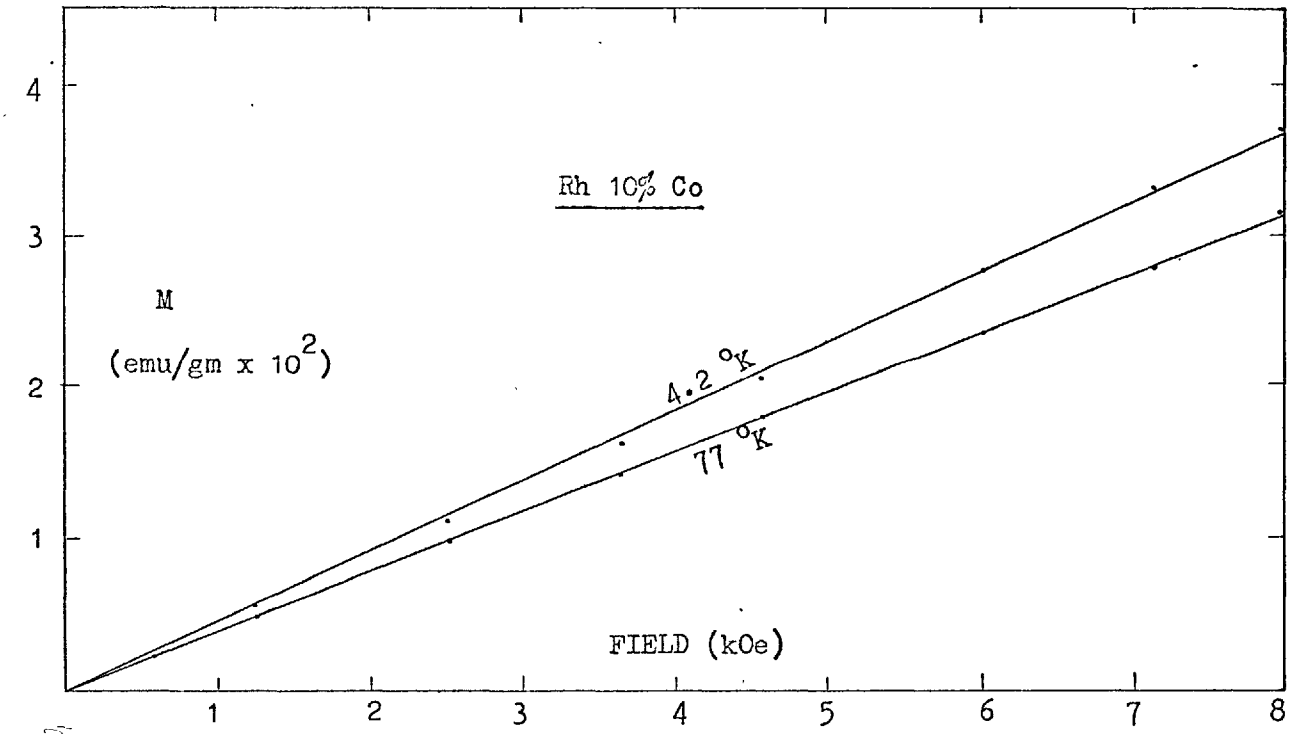

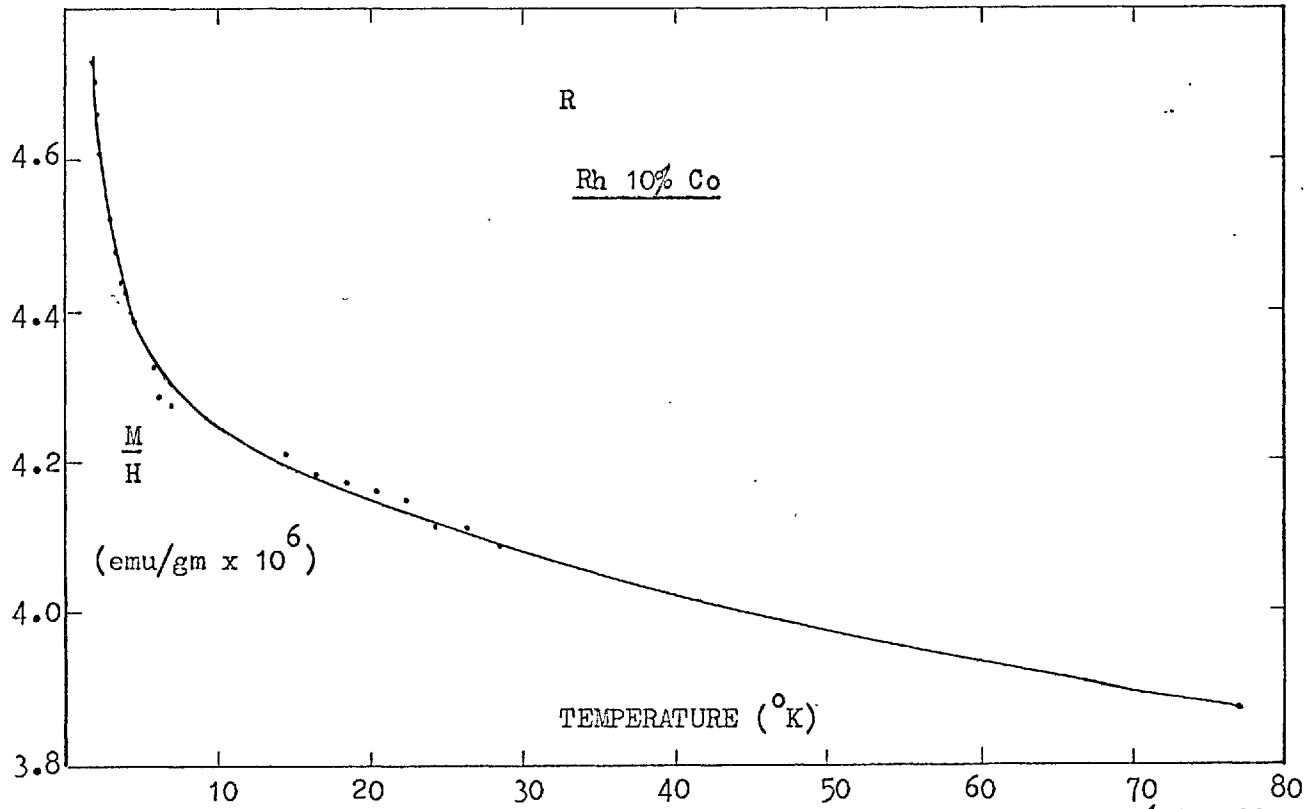

Fig.53 Graphs of Magnetisation vs Field and Temperature for Rh 11% Co Alloys

This is too large a value to be present in the alloy. The increase $\Delta\chi$ at $77^{\circ}K$ due to Co is $\sim 27 \times 10^{-6}$ emu/gm which is in reasonably good agreement with the lower concentration alloy.

The susceptibility of Rh-Co alloys is similar to the Rh-Fe alloys in that there is a large temperature independent increase due to the localised enhancement of the susceptibility on the Co atoms, but the temperature dependent term is much smaller. It seems that Co in Rh is near the threshold for showing a 'well defined' magnetic moment similar to that on the Fe atoms in Rh.

CHAPTER 7

EXPERIMENTAL RESULTS AND DISCUSSION OF SOME GOLD-RARE EARTH ALLOYS

Introduction

The simplest kind of alloy system for the study of interaction effects between solute atoms is one for which the matrix is a simple metal and the solute atoms possess a real, localised, magnetic bound state. Alloys of rare earths dissolved in simple metals such as silver and gold belong to this class of systems. The R.K.K.Y. spin-polarisation set up by the interaction of the local moment with the conduction electrons is expected to be the main mechanism for interaction between the solute atoms.

The electrical resistivity of dilute silver and gold-rare earth alloys has been measured by Bijovet et al (68) and by Lowin (107). Their results disprove the existence of resistance minima and maxima reported by Sugawara (98) for the Ag Gd alloys. It is now believed that the observed resistance minima were due to the contamination of the alloys by transition metal impurities.

Observation of interaction effects between solute atoms

in the magnetic susceptibility of some relatively dilute rare-earth alloys has been reported by Hirst et al (72) and Williams and Hirst (71). A paramagnetic Curie temperature -2°K has been reported for a Ag 0.1 at.% Gd alloy (71). Edwards and Legvold (70) have measured the electrical resistivity of some moderately concentrated gold-rare earth alloys (upto 2 at % rare earth). The authors find a decrease in the resistance below about 6°K for some of the alloys including one with 0.42 at.% Gd. However, the most dramatic result is for the Au 2 at.% Ho alloy for which the authors find a sharp decrease in the resistance below 6°K. This behaviour, the authors suggest, could be due to the onset of magnetic order and the consequent quenching of spin disorder scattering.

The present investigation was attempted with a view to studying in a little more detail the interaction effects reported by the various authors. Only a limited number of alloys have been studied owing to the nonobservation of any significant interaction effects upto the maximum concentration of some rare-earth solutes within their solubility limits in gold. The observed Curie-Weiss intercepts in the susceptibility are explained by taking account of the crystal field splitting of energy levels of the atoms which also explains the temperature dependence of the s-f resistivity.

Sample Preparation

The maximum solubilities of rare earths in gold have been determined by Rider et al (74). They are rather low for the lighter rare earths but increase approximately linearly beyond Gd from $\frac{1}{2}$ at.% Gd to 7 at.% Yb.

The alloys were prepared by arc melting about 2 gm of pure gold with the appropriate mass of rare-earth metal on a water cooled copper hearth in a $\frac{2}{3}$ atmospheric pressure of Argon. The purity of the metals were 99.999% and 99.99% respectively and were obtained from Koch light laboratories Limited. The alloys were melted a total of about 6 times. The two Au-Yb alloys were supplied by Johnson Matthey & Company and were similarly prepared. The buttons were forged using an iron-free copper plate and hammer and then homogenised at 780°K for about 150 hrs. They were then further hammered to obtain pieces 0.7". These were machined in a lathe to obtain small cylinders $\frac{1}{2}$" long and .055" in diameter. The weights of the final specimen were around 0.36 gm. The same specimen was used both for the susceptibility and the electrical resistivity measurements.

Au 0.3 at. % Gd

The field dependence of the magnetisation of the alloy at 4.2°K and 1.57°K is shown in Fig. 54 . Brillouin curvature is clearly visible in the M-H plots which in fact agrees to 1% with the calculated values for $B_{S=7/2}$ (H/T). Measurements of the susceptibility in the range 4.2°K to 1.6°K have been made while the specimen was immersed in a bath of liquid helium. The measurements were made as a function of decreasing temperature, the latter being reduced by pumping on the helium bath through a manostat. The temperature of the specimen is determined accurately from the helium vapour pressure. A plot of $\frac{1}{\chi - \chi_{Au}}$ against T is shown in Fig. 55 from which it is clear that the Curie law is obeyed quite well. A least squares fit of the data to a Curie-Weiss law gave a value of Θ of about -0.05°K. This result is in strong disagreement with the Curie-Weiss intercept of -2°K for the Ag 0.1 at. % Gd alloy reported by Williams and Hirst (71). These authors have also reported the presence of second phase intermetallic compound Ag_3Gd in their more concentrated Ag-Gd alloys. There is a possibility that their observed results for the 0.1 % Gd alloys are due to the presence of undetected traces of the second phase in the alloy. Fig. 56 shows a plot of $\frac{1}{\chi - \chi_{Au}}$ against T measured upto 77°K. The fact that a Curie law dependence

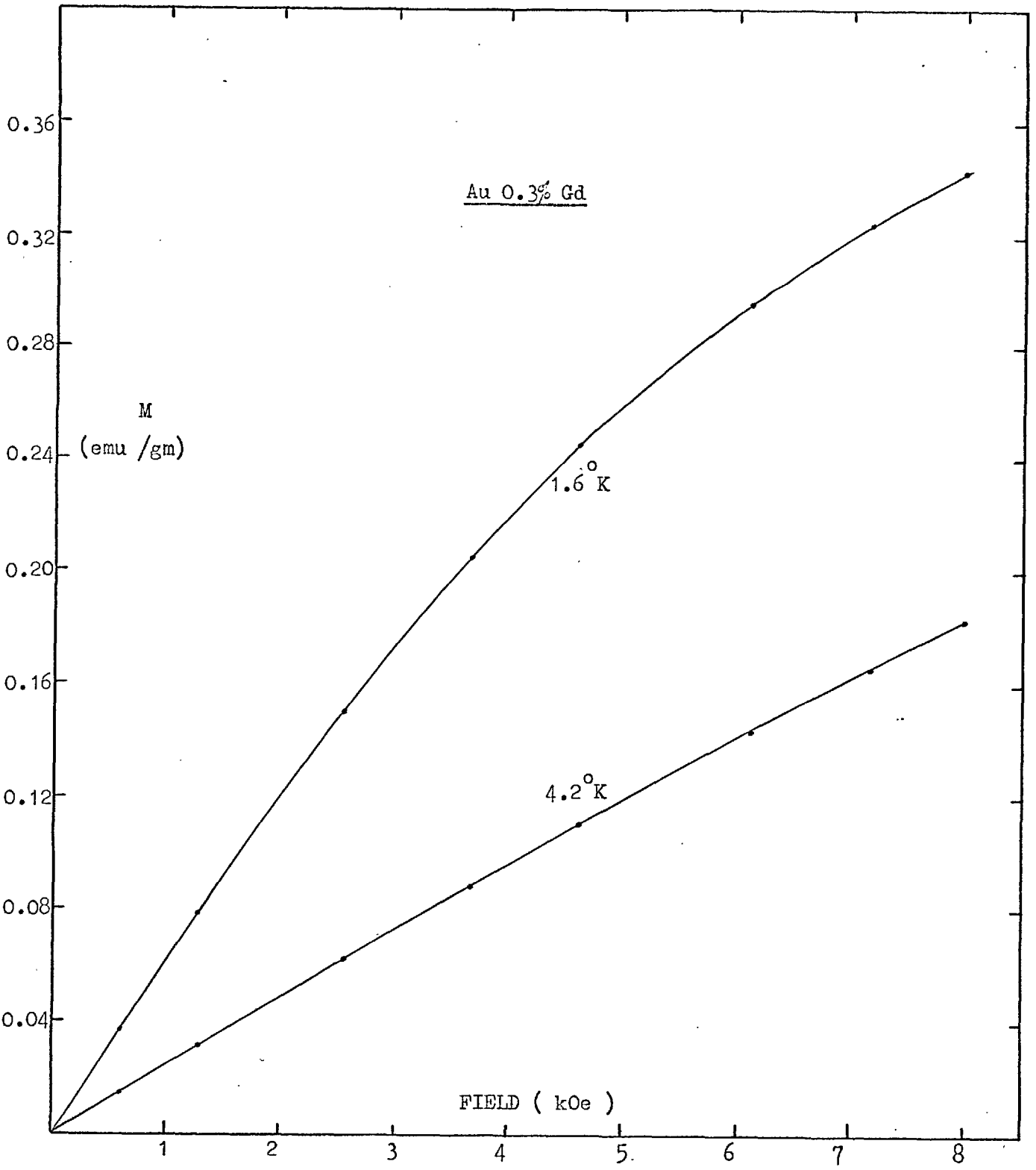

Fig.54 Magnetisation vs Field of Au 0.3% Gd Alloy

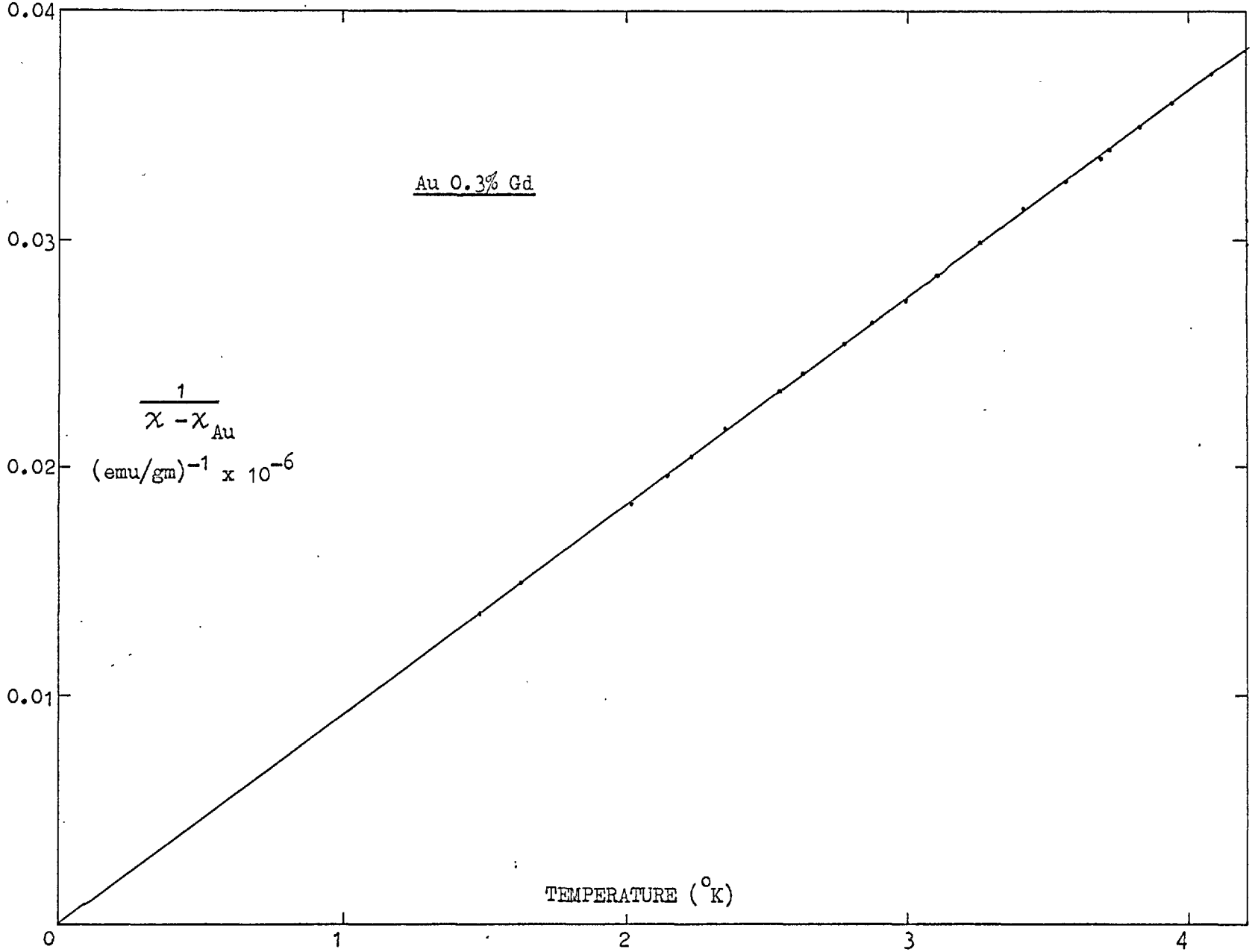

Fig.55 Curie-Weiss Plot for Au 0.3% Gd Alloy

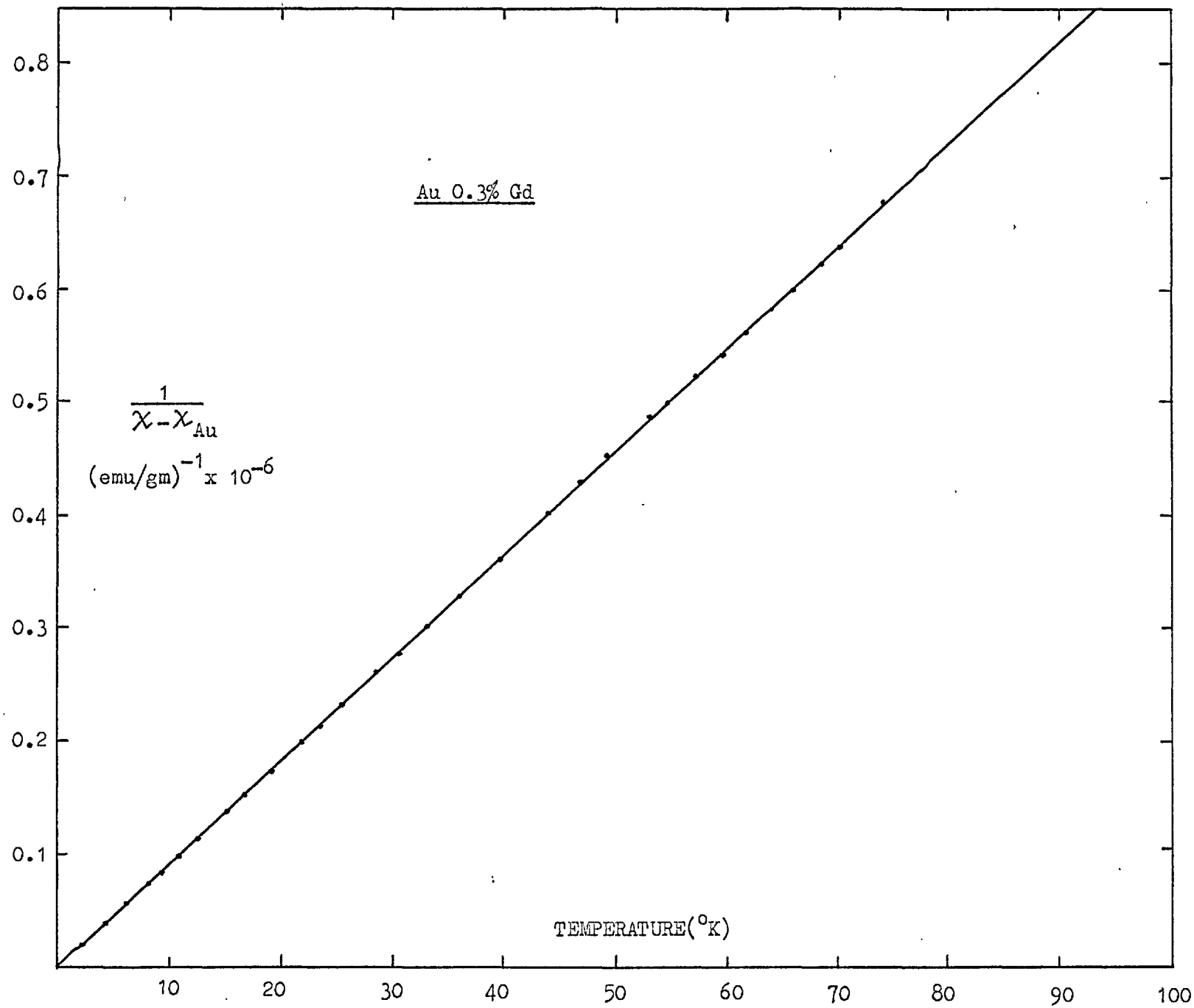

Fig.56 Curie-Weiss Plot for Au 0.3% Gd Alloy

is still observed merely confirms that the thermomentry is accurate.

The concentration of the alloy calculated from the masses of the metals used, and allowing for the weight loss during melting was 0.31 at. % Gd. Using this value, the effective moment per Gd atom is found to be $7.47\,\mu_B$. However, if the theoretical value of the moment of $7.94\,\mu_B$ is assumed, the calculated concentration is found to be 0.274 at. % Gd.

Au 2.3% Yb

The magnetisation of the alloy has been measured at 4.2 and 2.2°K as a function of magnetic field and is shown in Fig.57. Measurements of the susceptibility χ of the alloy as a function of temperature have been made in low fields ($\mu_B H/kT \ll 1$). Fig. 58 shows a graph of $\frac{1}{\chi - \chi_{Au}}$ against T in which the 'bump' characteristic of the crystal field splitting of energy levels can be seen very clearly. The apparent "Curie-Weiss" intercept θ is -7 ± 1°K which is also the result of the crystal field splittings. Calculations of the susceptibility using crystal field theory in terms of the coefficients C_4 and C_6 as variable parameters have been made. Using the measured susceptibilities a graph of $(\chi - \chi_{Au}) \times T$ against temperature was plotted. On the same graph the calculated $\chi \times T$ values using various parameters were also plotted and the best values of C_4, C_6 determined by inspection. Fig.59 shows that a reasonably good fit to the data is obtained with the parameters $C_4 = -30$°K and $C_6 = 6$°K.

The ground state of the crystal field split energy levels is the Γ_7 doublet which is separated from the next level, the Γ_6 doublet, by an energy of about 90 degrees. The next level, the Γ_8 quartet is only 3°K higher. The ground state doublet has a 'g' value of 3.4. This has been confirmed by E.S.R. measurement on the alloy by Griffiths and Coles (134).

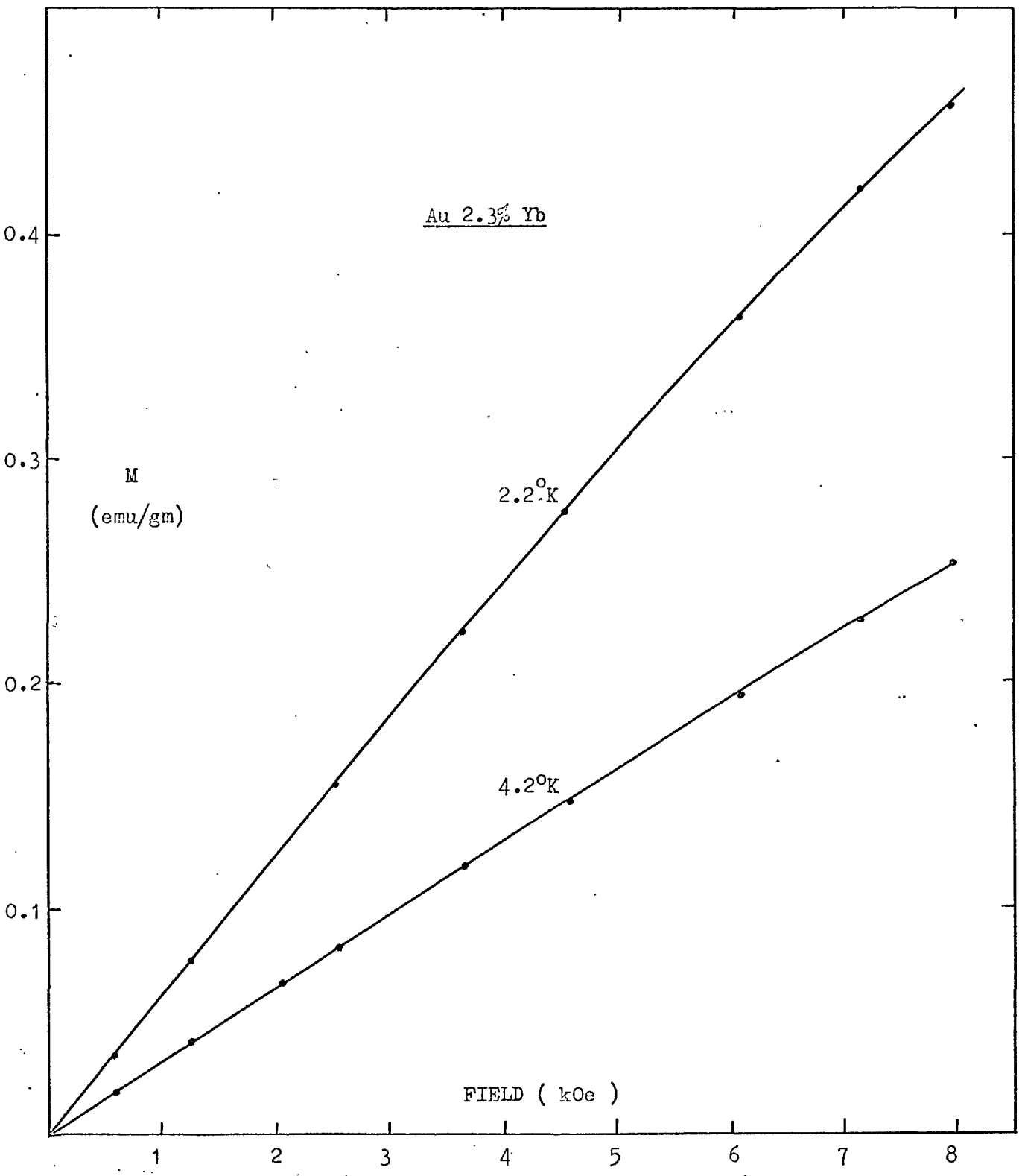

Fig.57 Magnetisation vs Field of Au 2.3% Yb Alloy

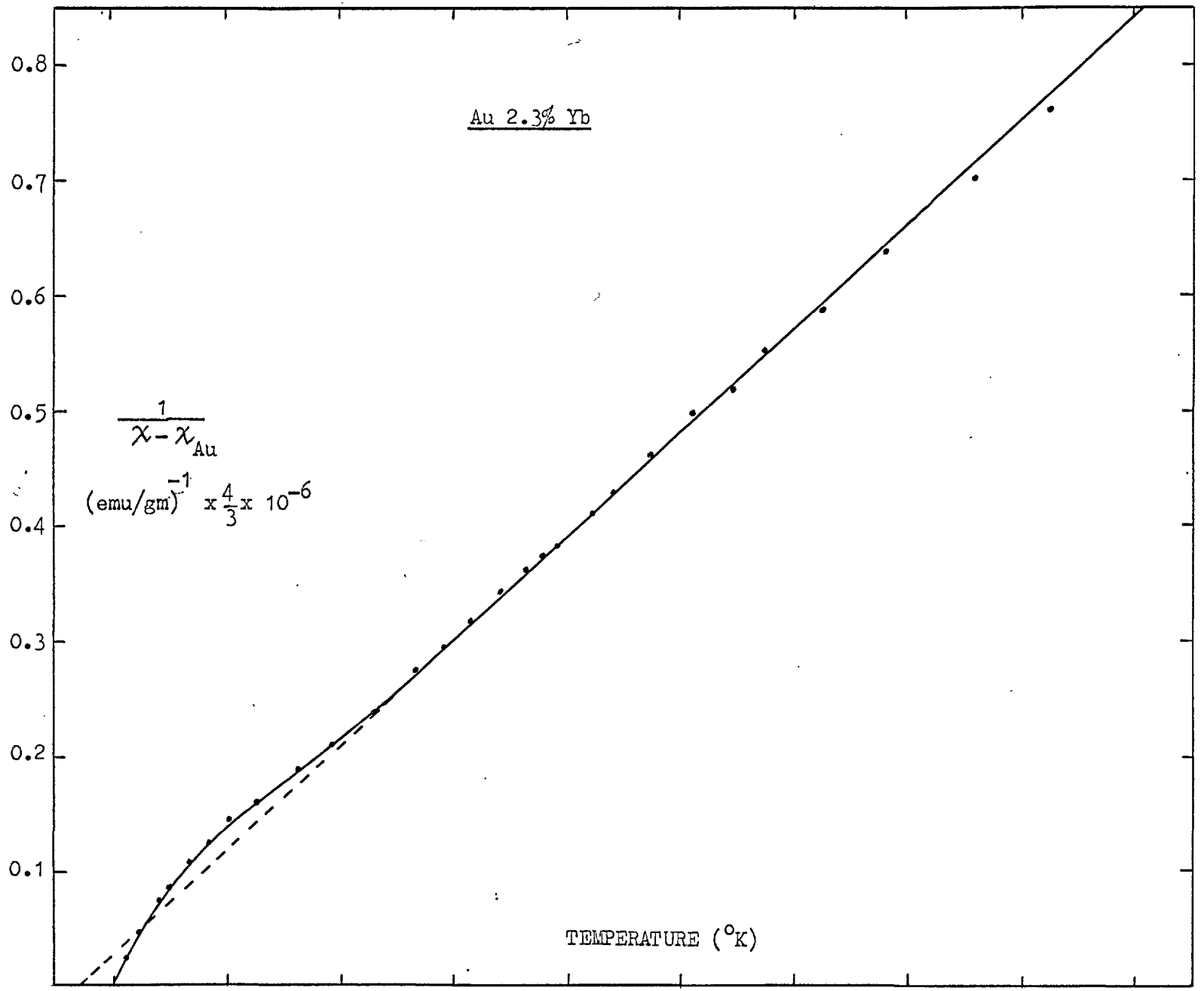

Fig.58 Curie-Weiss Plot for Au 0.3% Yb Alloy

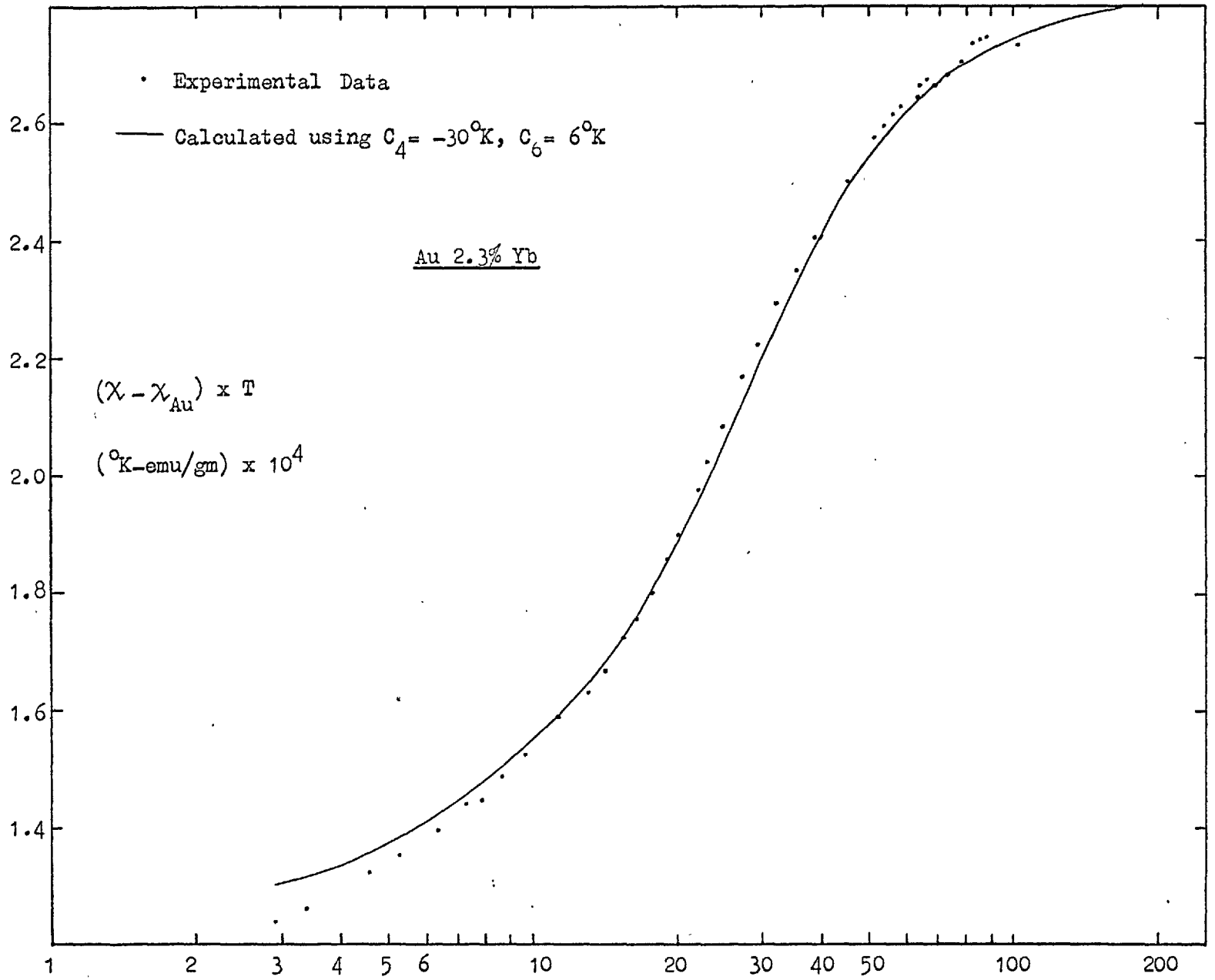

Fig.59 Graph of $(\chi - \chi_{Au}) \times T$ vs Temperature for Au 2.3% Yb Alloy

It is seen that the results of the susceptibility measurements of the alloy can be explained quite well by the crystal field theory. There is very little in the results which can be attributed as being due to interaction effects between Yb atoms.

Au 3.9 % Yb

Fig. 60 shows the magnetisation of the alloy measured as a function of the magnetic field at 4.2 and 1.6°K. The inverse susceptibility $\frac{1}{\chi - \chi_{Au}}$ plotted against T shows a high temperature Curie-Weiss intercept of -7 ± 1°K, Fig. 61. It is found that the susceptibility of this alloy scales quite well ($\pm$ 1%) with that of the 2.3 % Yb alloy and also the same crystal field parameters, $C_4 = -30$°K and $C_6 = 6$°K, give a reasonably good fit to the data, Fig. 62

Measurements of the electrical resistivity of the alloy between 1.6 and 20°K have also been made, Fig. 63 shows the excess resistivity $\rho - \rho_{Au}$ plotted as a function of temperature T. The resistance minimum and the increase in the resistance below 10°K is thought to be due to the presence of iron impurities in the alloy. Somewhat similar results for Ag-Gd alloys reported by Sugawara (98) are now accepted as being due to the presence of transition metal impurities in the alloys. The excess resistivity due to Yb atoms does not obey Mathiessen's rule and the increase in the resistance which becomes apparent above 10°K is the result of this break down, which has been investigated in detail for simple alloys by Dugdale and Basinski (101). Accurate measurements on some gold and silver rare-earth specimens

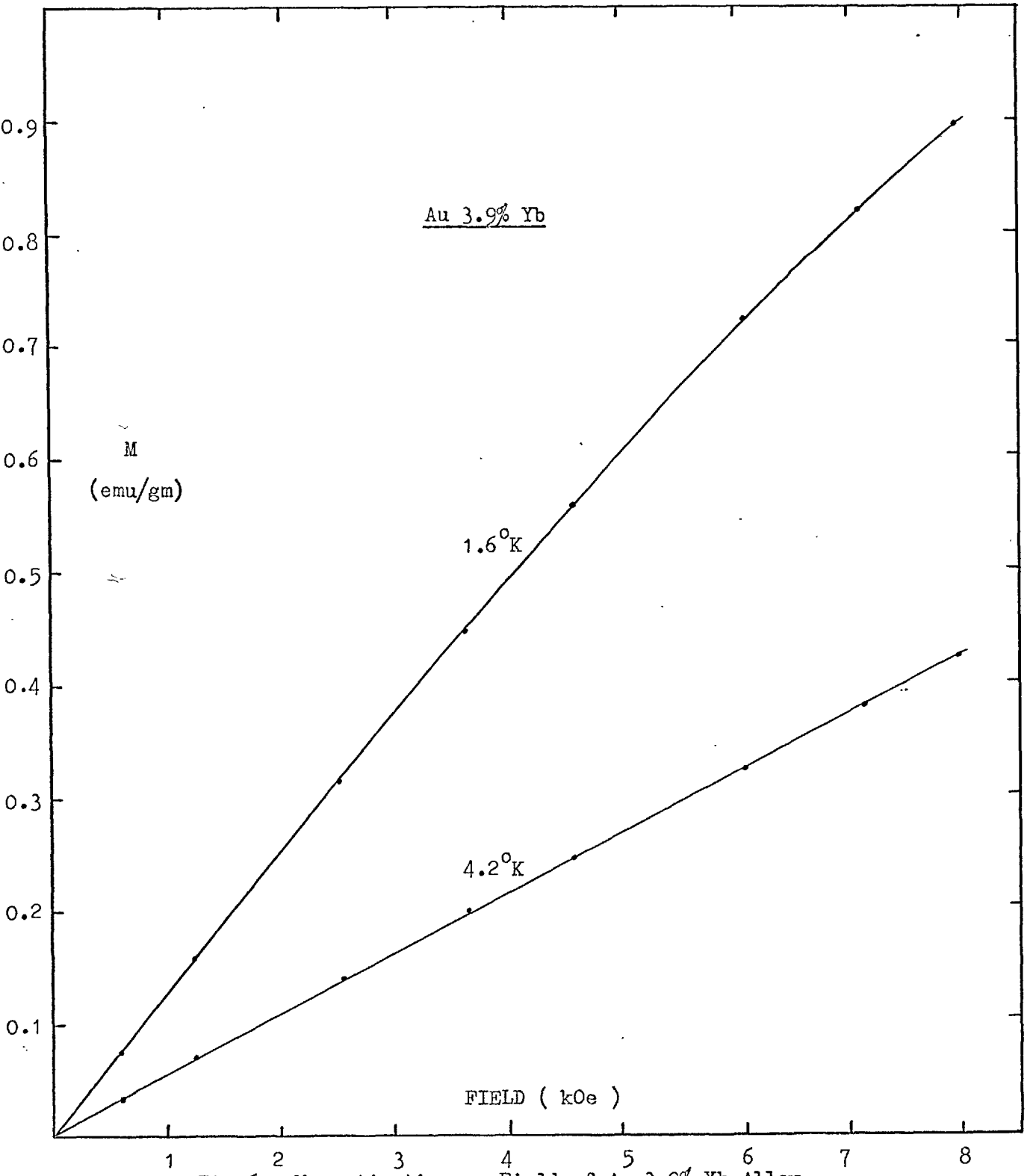

Fig.60 Magnetisation vs Field of Au 3.9% Yb Alloy

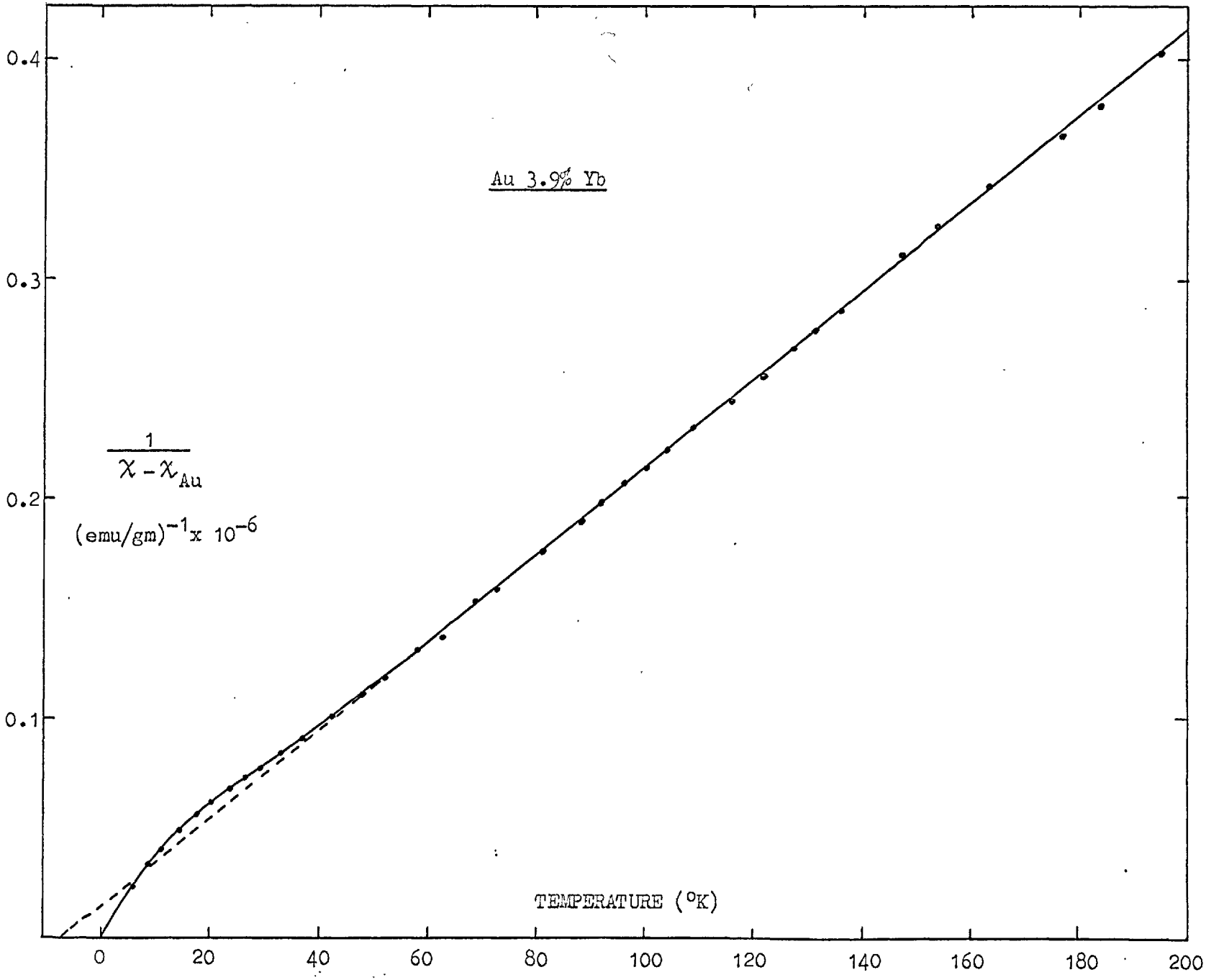

Fig.61 Curie-Weiss Plot for Au 3.9% Yb Alloy

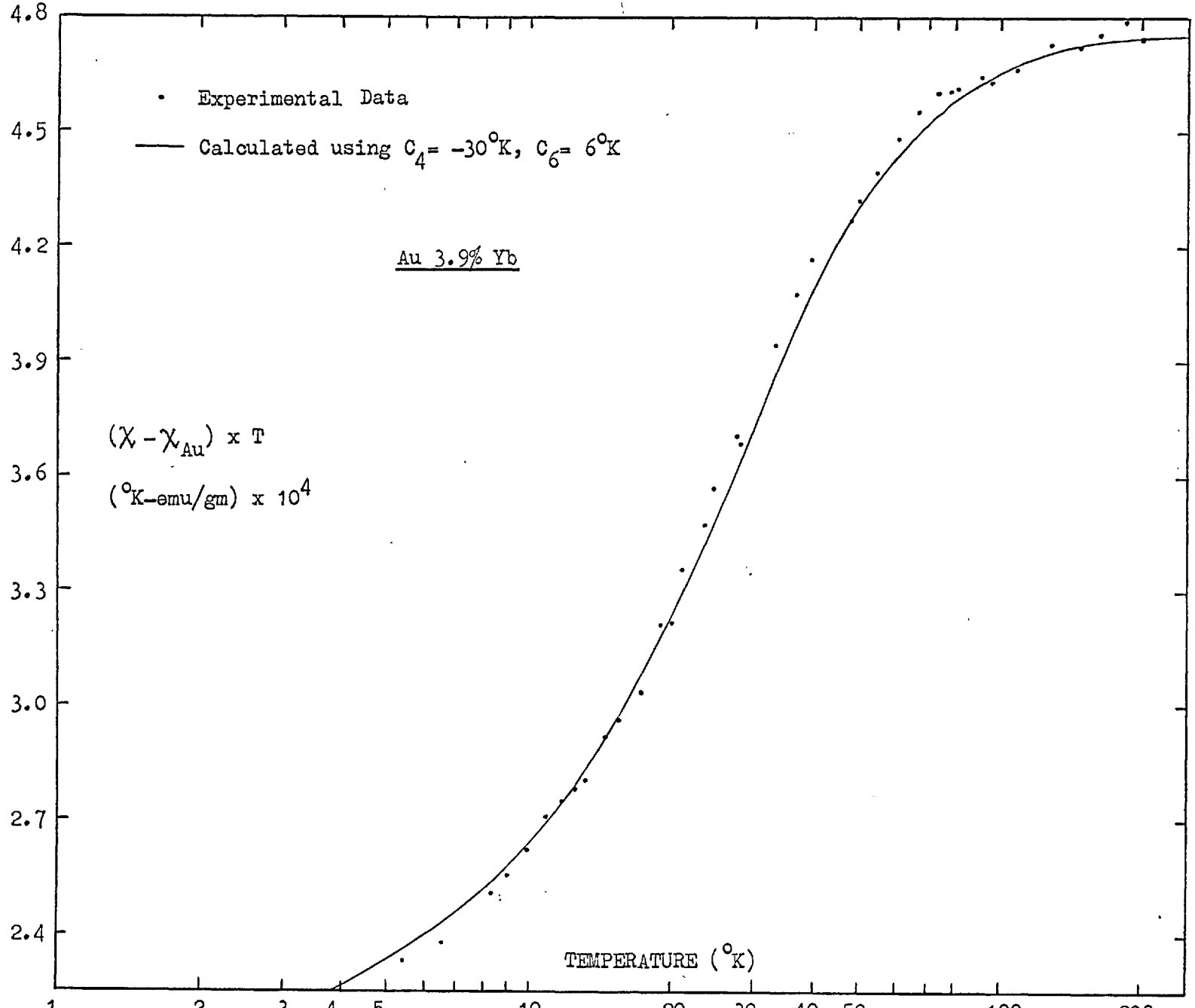

Fig. 62 Graph of $(\chi - \chi_{Au}) \times T$ vs Temperature for Au 3.9% Yb Alloy

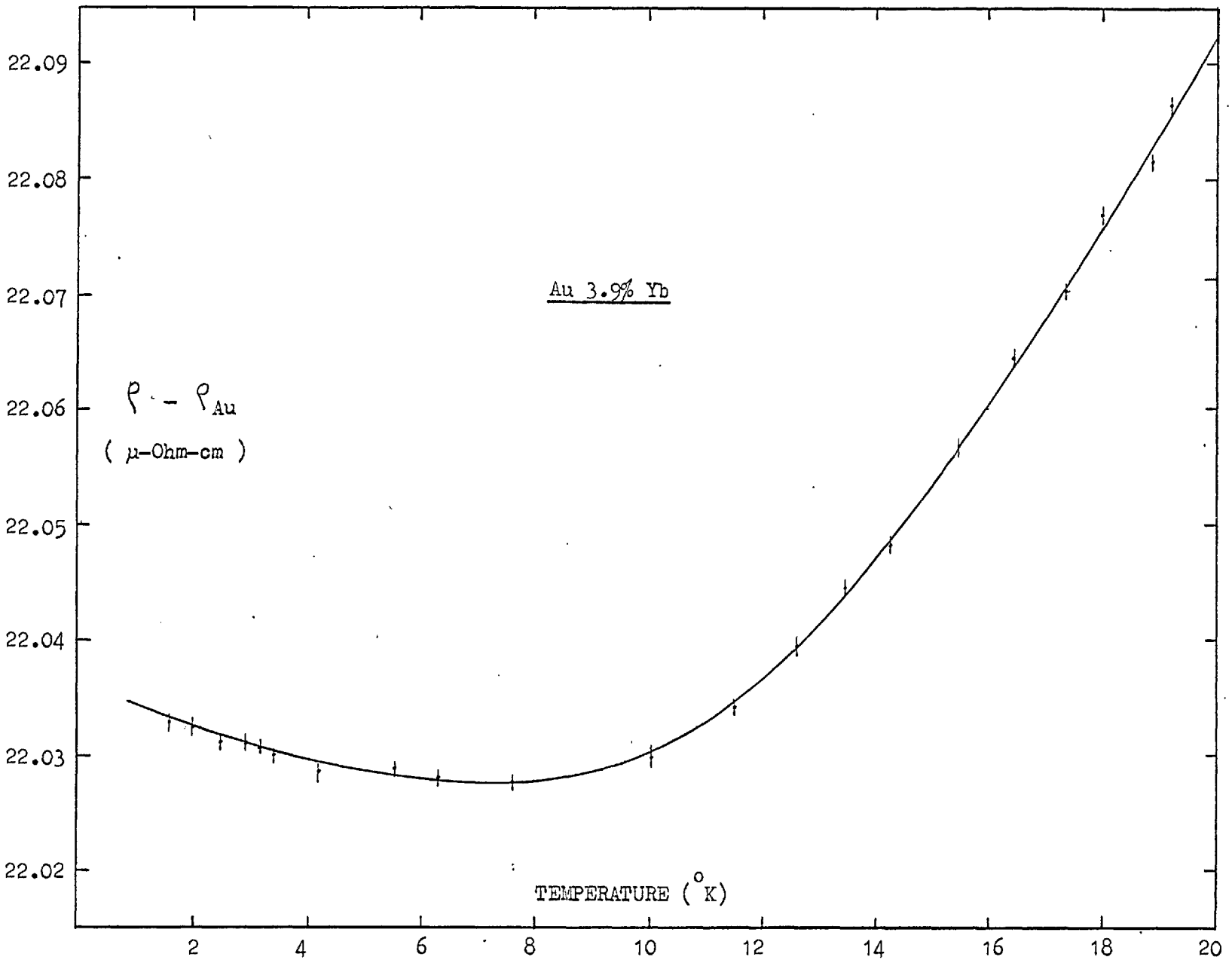

Fig.63 Excess Resistivity vs Temperature of Au 3.9% Yb Alloy

specially prepared for resistivity measurements, have been made by Lowin (107) and are in agreement with the results of Dugdale and Basinski. These also show an increase in the excess resistivity with temperature in agreement with the present results.

Au 2% Ho

Graphs of magnetisation against field measured at 4.2°K and 1.6°K are shown in Fig. 64. The inverse susceptibility $\frac{1}{\chi-\chi_{Au}}$ plotted as a function of temperature, Figs. 65, 66, shows a "Curie-Weiss" intercept of 0.85 ± .1°K, which is the result of the crystalline field splitting of the energy levels. In order to determine the parameters C_4 and C_6 to explain the observed susceptibilities a graph of $(\chi - \chi_{Au}) \times T$ was plotted as a function of T, Fig. 67. The calculated values of χT using various parameters were plotted on the same graph and the best fit determined by inspection. For Au-Ho alloy the best parameters were found to be $C_4 = -20°K$ and $C_6 = -4°K$.

Measurements of the resistance of the alloy between 1.6 and 20°K have been made. Fig. 68 shows the excess resistivity $\rho - \rho_{Au}$ plotted as a function of temperature. A low temperature decrease in the resistance below about 6°K, similar to that found by Edwards and Legvold (70), is also observed, but the magnitude of the total decrease below 6°K is about a $\frac{1}{3}$ of that found by these authors. This may be due to the presence of small amounts of iron impurities in the present specimen which give a small increase in the resistance with decreasing temperature as seen clearly in the Au 4% Yb alloy. Although the

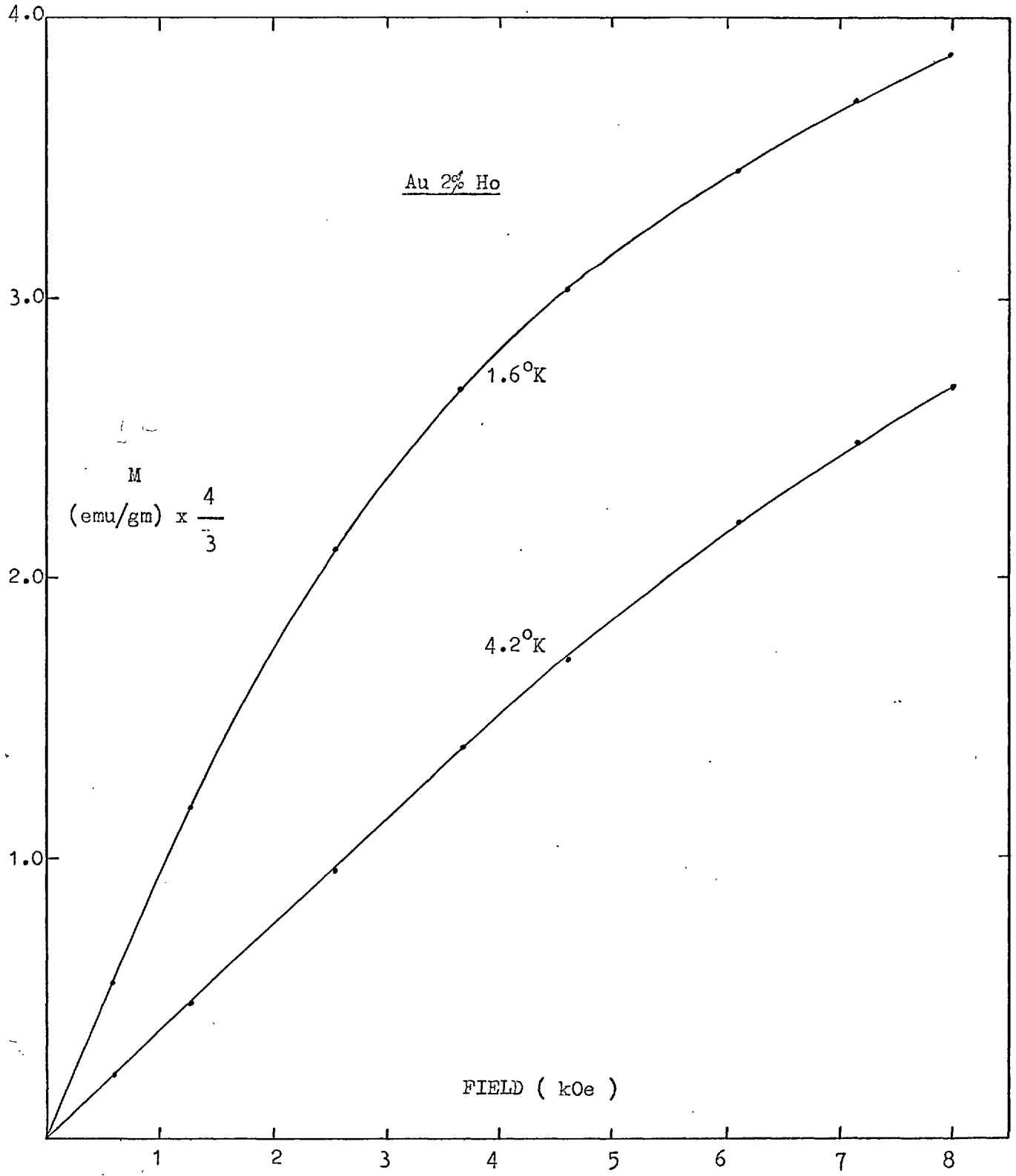

Fig.64 Magnetisation vs Field of Au 2% Ho Alloy

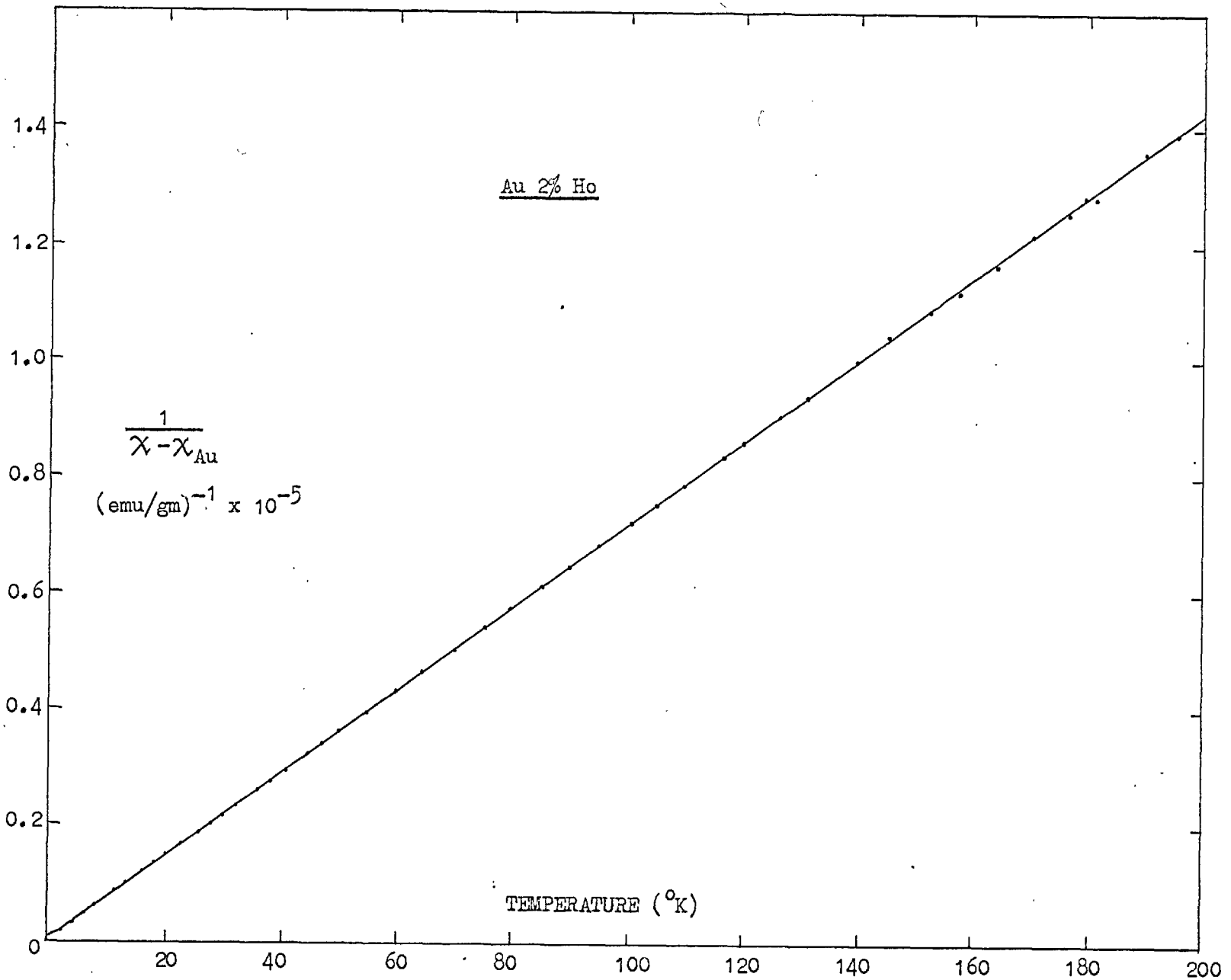

Fig. 65. Curie-Weiss Plot for Au 2% Ho Alloy

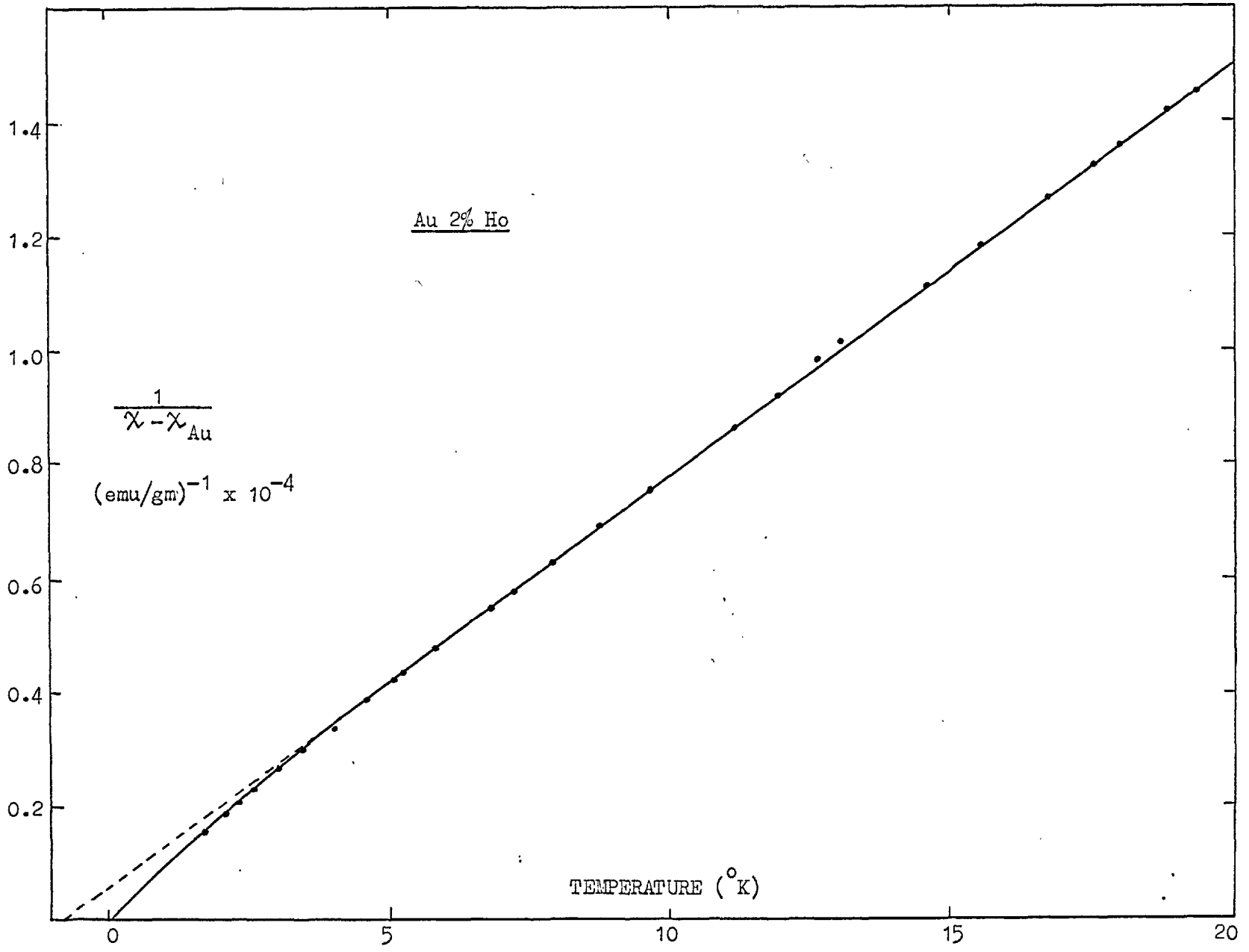

Fig.66 Curie-Weiss Plot for Au 2% Ho Alloy

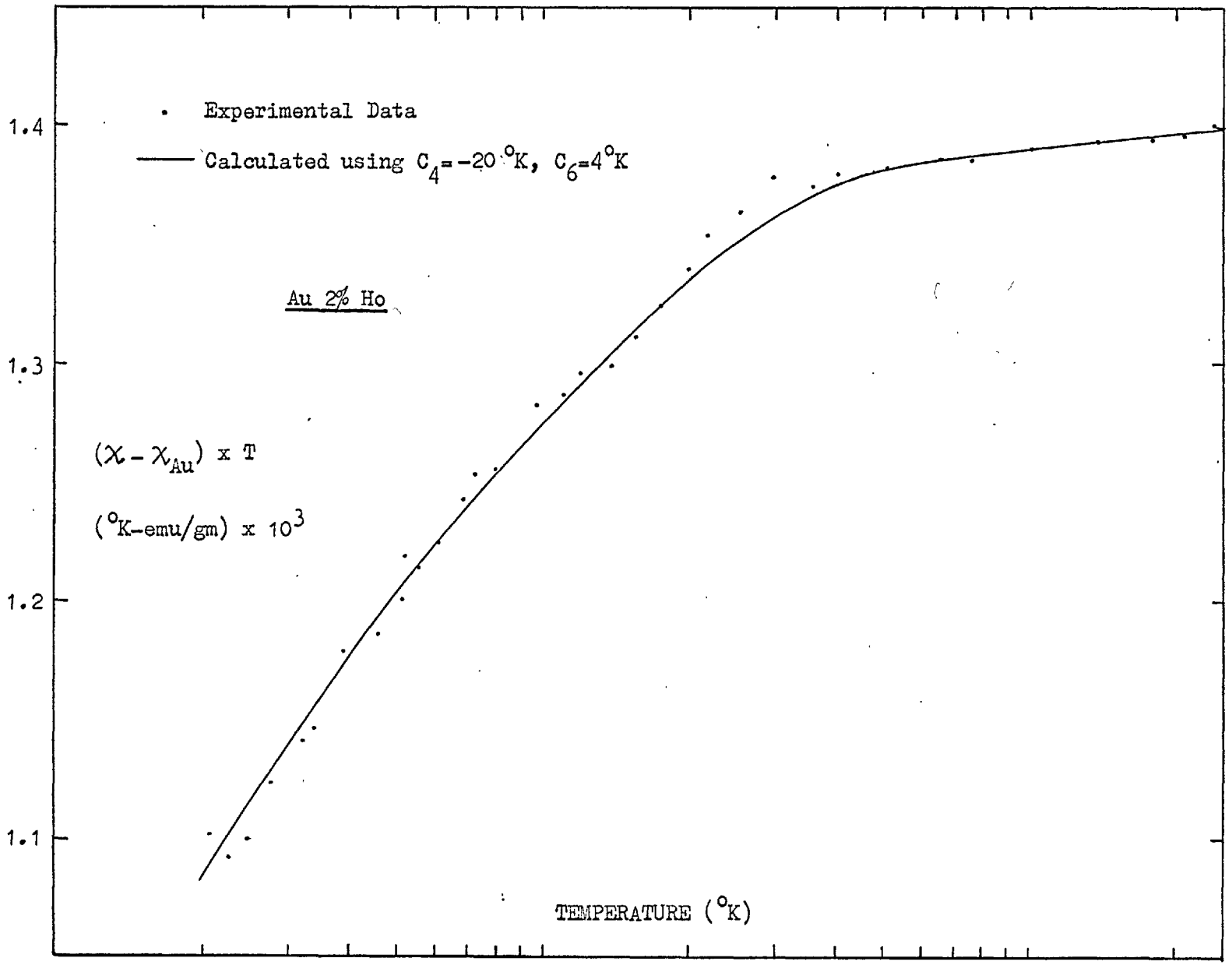

Fig.67 Graph of $(\chi - \chi_{Au})$ x T vs Temperature for Au 2% Ho Alloy

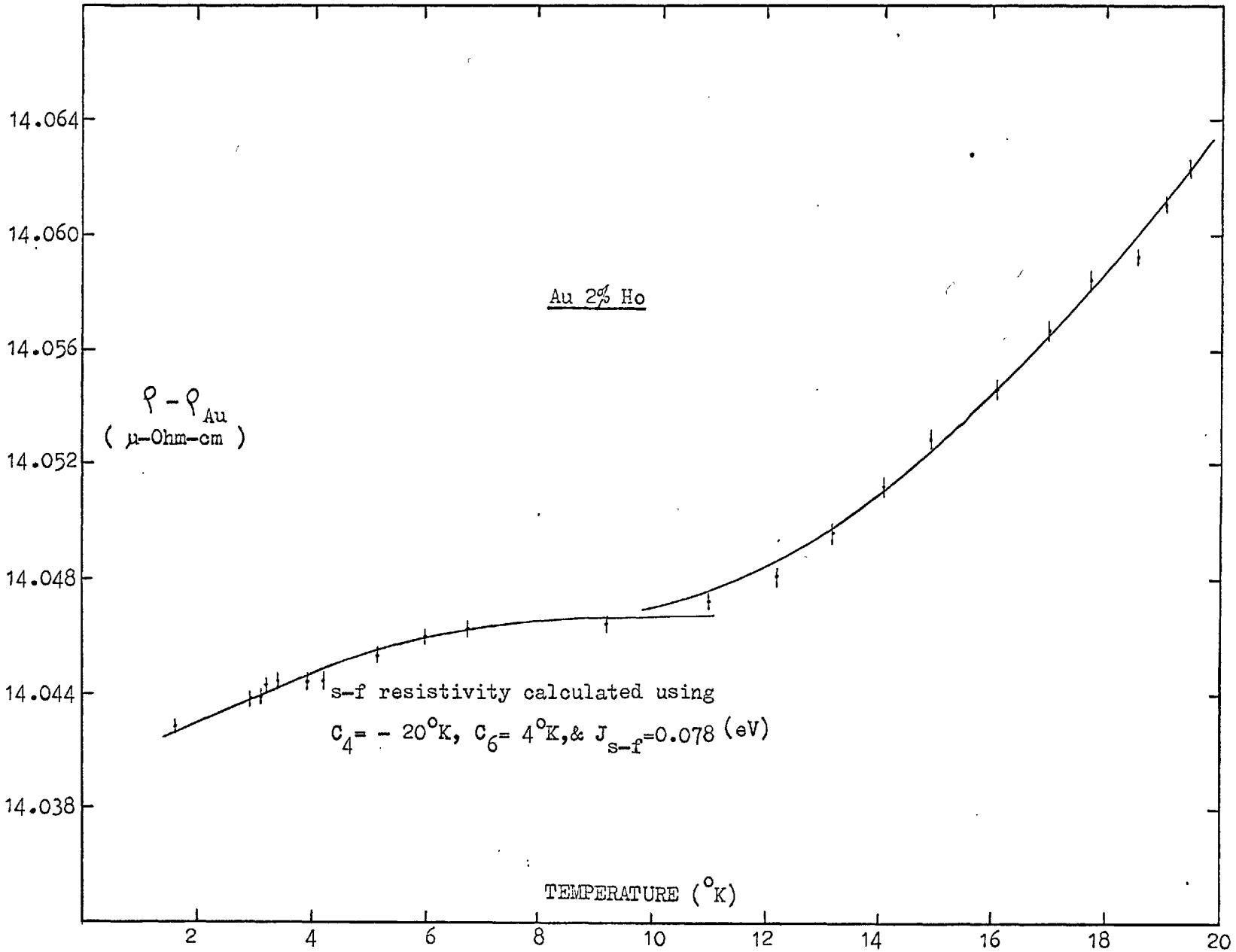

Fig.68 Excess Resistivity vs Temperature of Au 2% Ho Alloy

presence of iron impurities in the alloy will reduce the total fall in the resistance and modify the shape of the curve slightly, an attempt has nevertheless been made to see if the low temperature decrease can be explained by the recent calculation of the s-f resistivity given by Hirst (146). Using the crystal field parameters obtained from the susceptibility fit, the calculated s-f resistivity is found to be in reasonably good agreement with the observed result if a magnitude for the s-f interaction constant J_{s-f} of 0.078 eV is assumed, Fig. 68. It is not suggested, however, that this value of J_{s-f} is the correct one as this depends on the accuracy with which corrections for other contributions to the resistance in this temperature region, such as from iron impurities, are made. It is perhaps worthwhile to remark that by increasing the above J_{s-f} value by less than a factor of 2 the resistance decrease observed by Edwards and Legvold can be accounted for, although the actual shape of the curve is slightly different and the 'kink' observed by the authors (Fig. 69) is replaced by a smooth but definite change of slope. The increase in the excess resistivity is again a result of the break down of Mathiessen's rule.

The energy level scheme for Ho with the parameters -20°K, 4°K is found to have the non-magnetic ground state doublet $\Gamma_3^{(2)}$

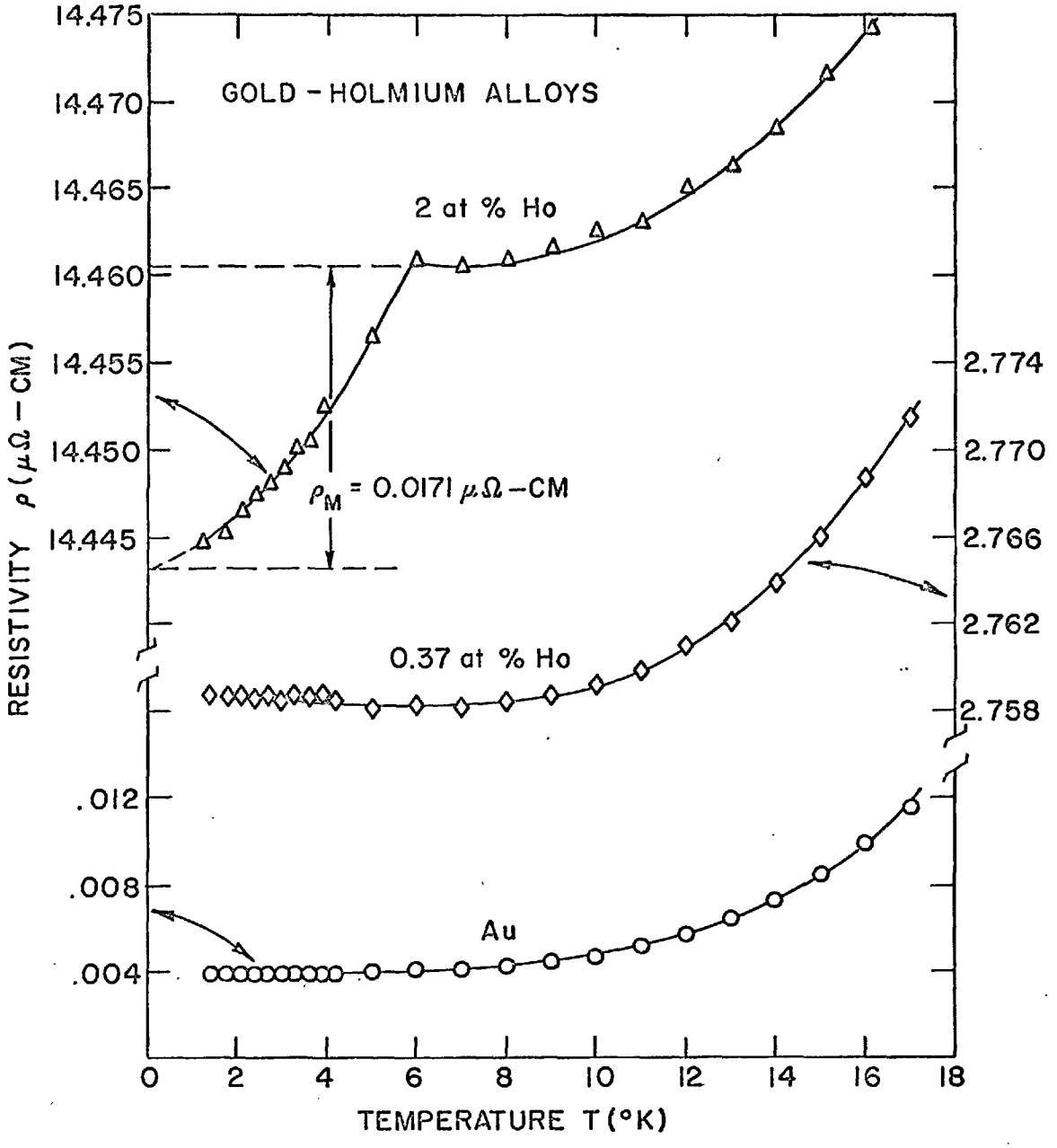

Fig. 69 The electrical resistivity as a function of temperature for the Ho-Au alloys. (After Edwards and Legvold)

separated by the triplet $\Gamma_5^{(2)}$ which is only 0.14°K higher. A third triplet $\Gamma_4^{(2)}$ is 7.6°K above the ground state. The next set of energy levels are more than 40°K higher. The temperature dependence of the s-f resistivity at low temperature is due to the change in the population of these levels each of which represents a different scattering cross section. The inelastic scattering between these energy levels also changes with temperature. Both these effects contribute to the observed temperature dependence.

The magnetoresistance of the alloy in the low field has also been measured at 1.6°K and 4.2°K, Fig. 70. Using the measured values of magnetisation at a given field a plot of the magnetoresistance against M^2 has been obtained. This is also shown in Fig. 70. The small departure from a linear behaviour for the lower temperature set is possibly due to the small difference ($\sim$ .05°K) between the temperatures at which the resistance and the magnetisation of the specimen have been measured.

The properties of the Au-Ho alloy are satisfactorily explained by assuming crystal field splitting of energy levels. The decrease in the low temperature resistance of the alloy is believed not to be the result of the quenching of the spin-disorder resistivity due to an onset of magnetic order, no sign of which can be seen in the magnetisation measurements of the alloy.

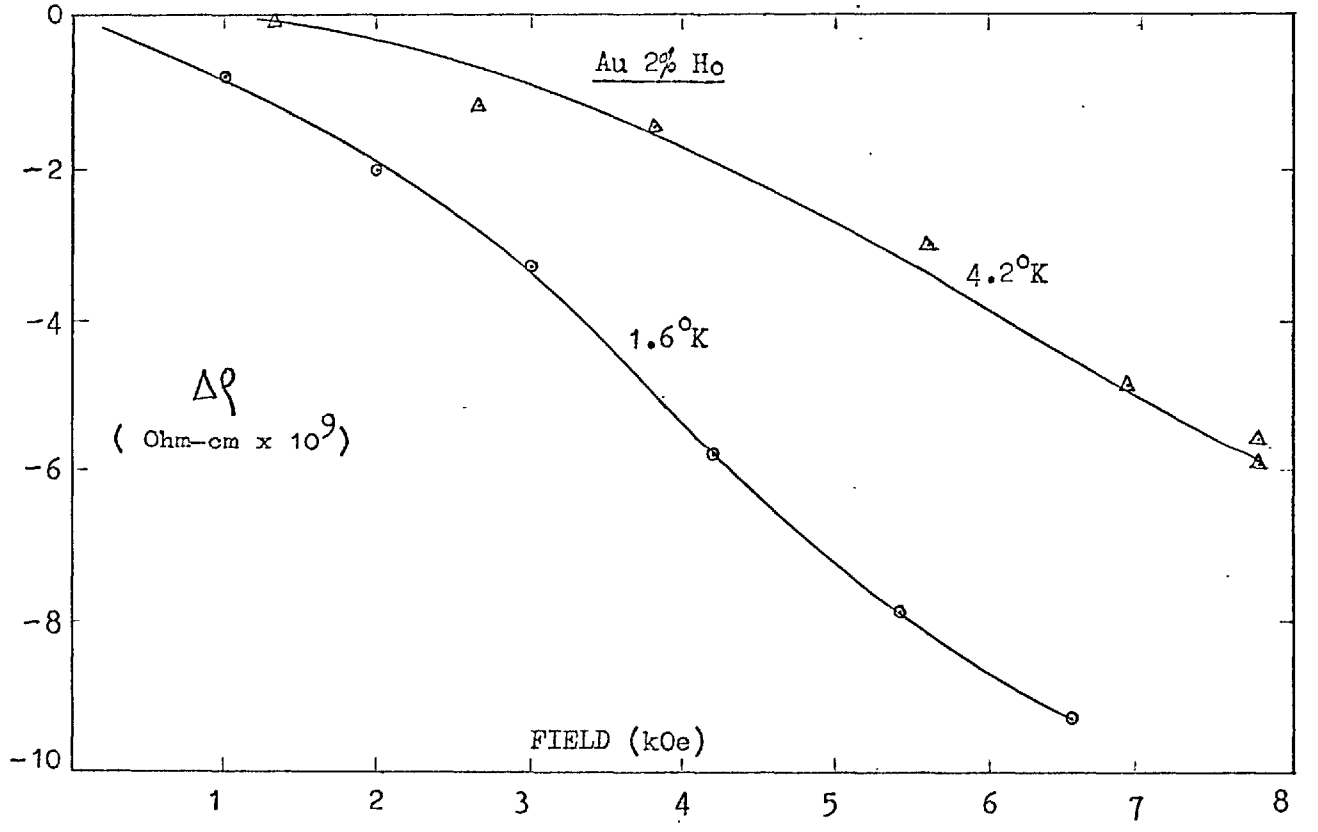

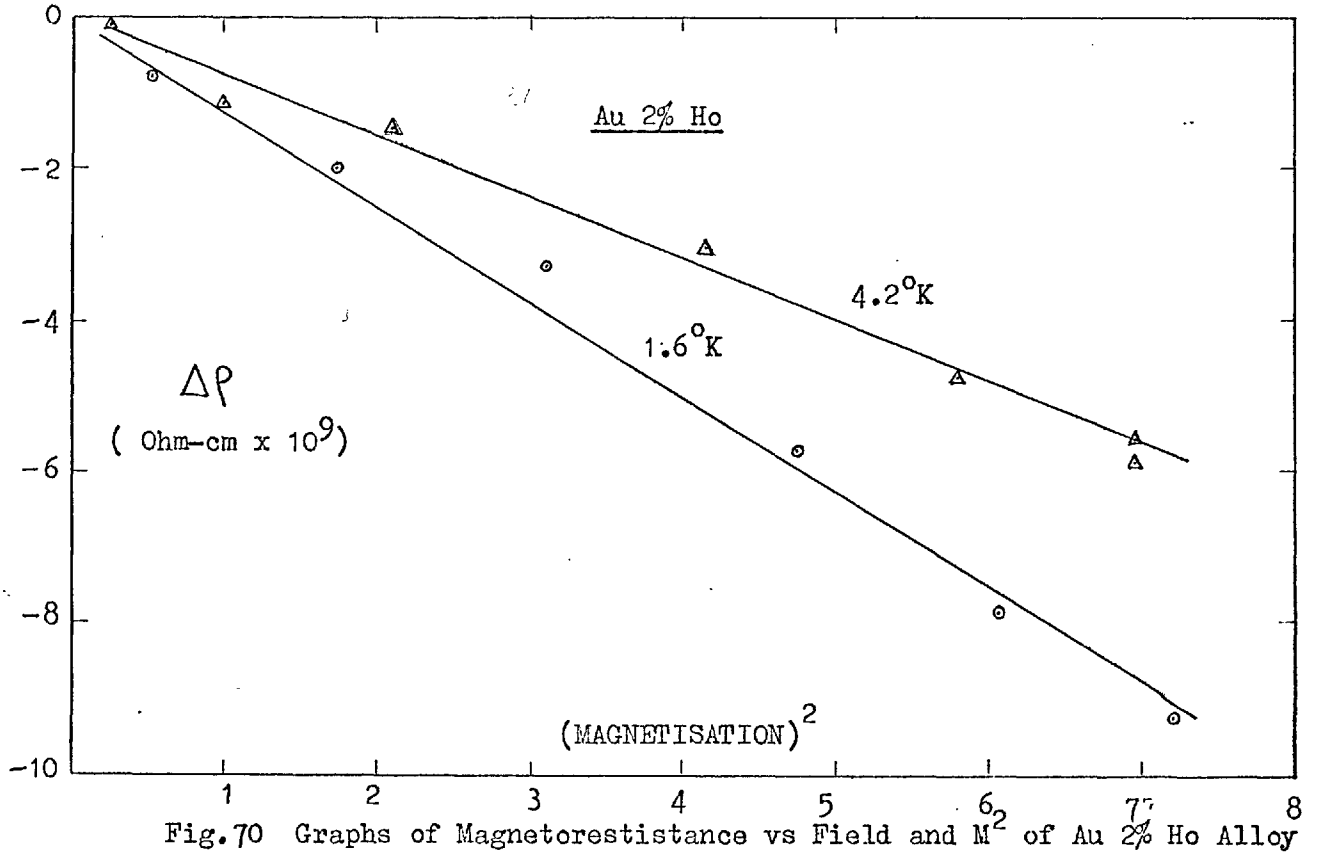

Fig.70 Graphs of Magnetorestistance vs Field and M^2 of Au 2% Ho Alloy

Au 1.5% Dy

The graphs of magnetisation against field measured at 1.6 and 4.2°K are shown in Fig.71 . Measurements of low field susceptibilities χ of the alloy as a function of temperature have also been made. Fig. 72 shows a plot of $\frac{1}{\chi - \chi_{Au}}$ against temperature T. A "Curie-Weiss" intercept of $1.1 \pm .1$°K is obtained which is seen more clearly in Fig. 73 in which the data for the low temperature region upto 20°K are shown. The parameters C_4 and C_6 have again been determined by inspecting the fits of $(\chi - \chi_{Au}) \times T$ vs T with respect to the calculated curves. The continuous line in Fig. 74 shows the calculated results using the parameters $C_4 = -30$°K, $C_6 = 6$°K which are found to give the closest fit to the data.

The crystal field split energy level scheme for these parameters is found to be a ground state doublet Γ_7 with the two quartets $\Gamma_8^{(1)}$ and $\Gamma_8^{(2)}$ at energies of 2.8 and 16°K respectively above it. The next set of levels are the Γ_6 doublet at 57.5°K and the $\Gamma_8^{(3)}$ quartet at 70.9°K.

The presence of the low lying excited states $\Gamma_8^{(1)}$ and $\Gamma_8^{(2)}$ close to the ground state doublet Γ_7 would be expected to give a temperature dependent contribution to the s-f resistivity at low temperatures. This can indeed be seen in the measured

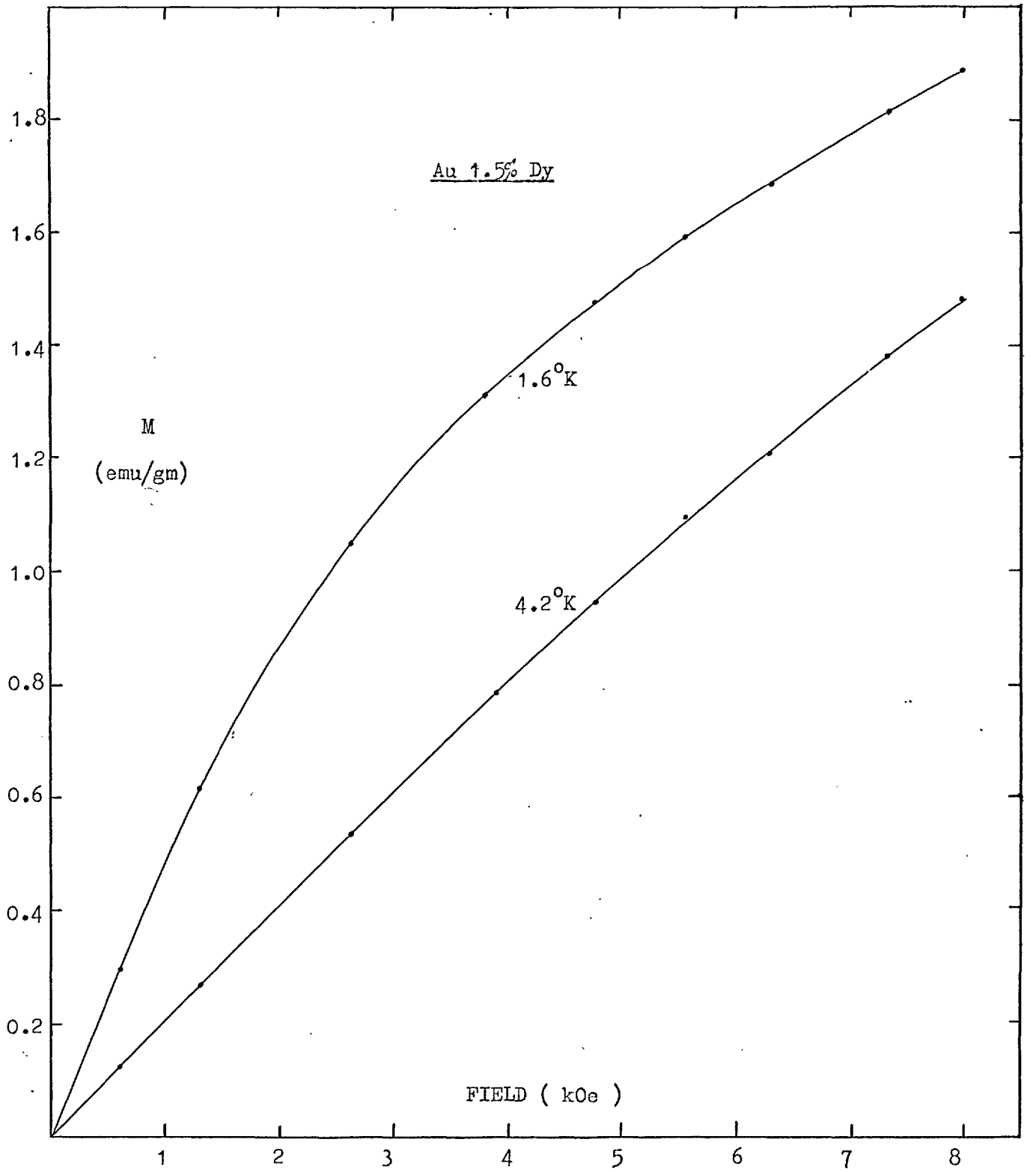

Fig.71 Magnetisation vs Field of Au 1.5% Dy Alloy

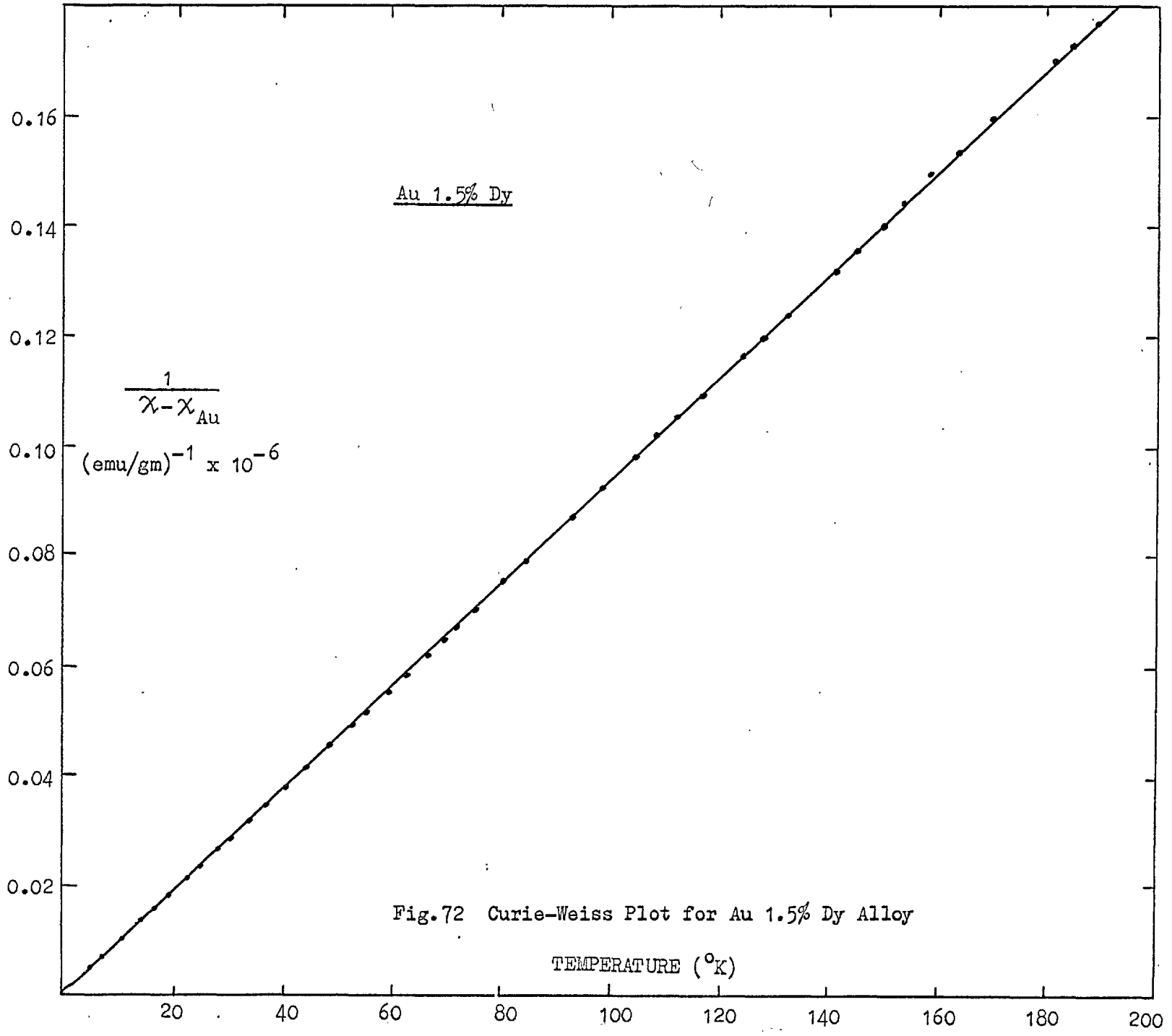

Fig.72 Curie-Weiss Plot for Au 1.5% Dy Alloy

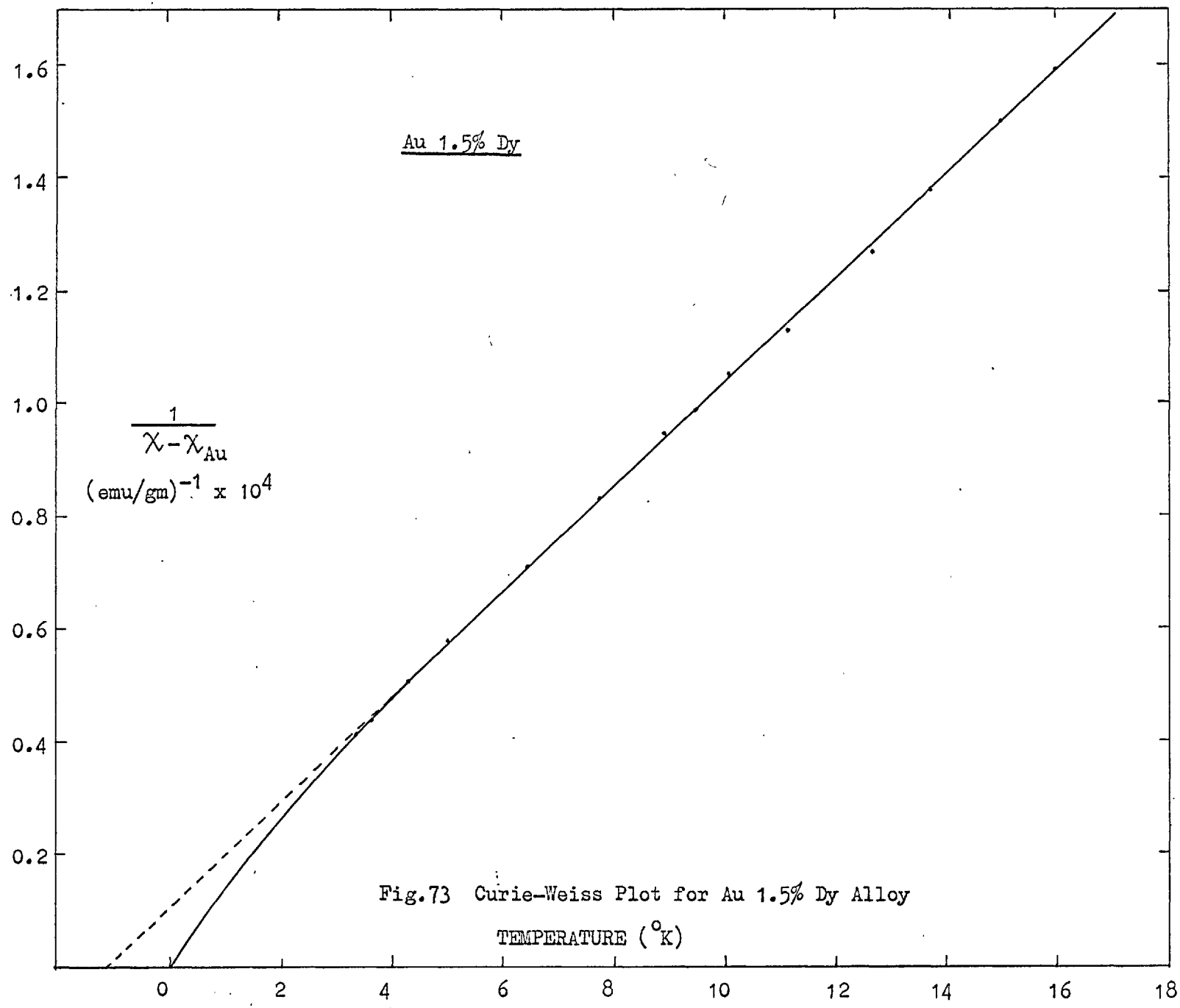

Fig.73 Curie-Weiss Plot for Au 1.5% Dy Alloy

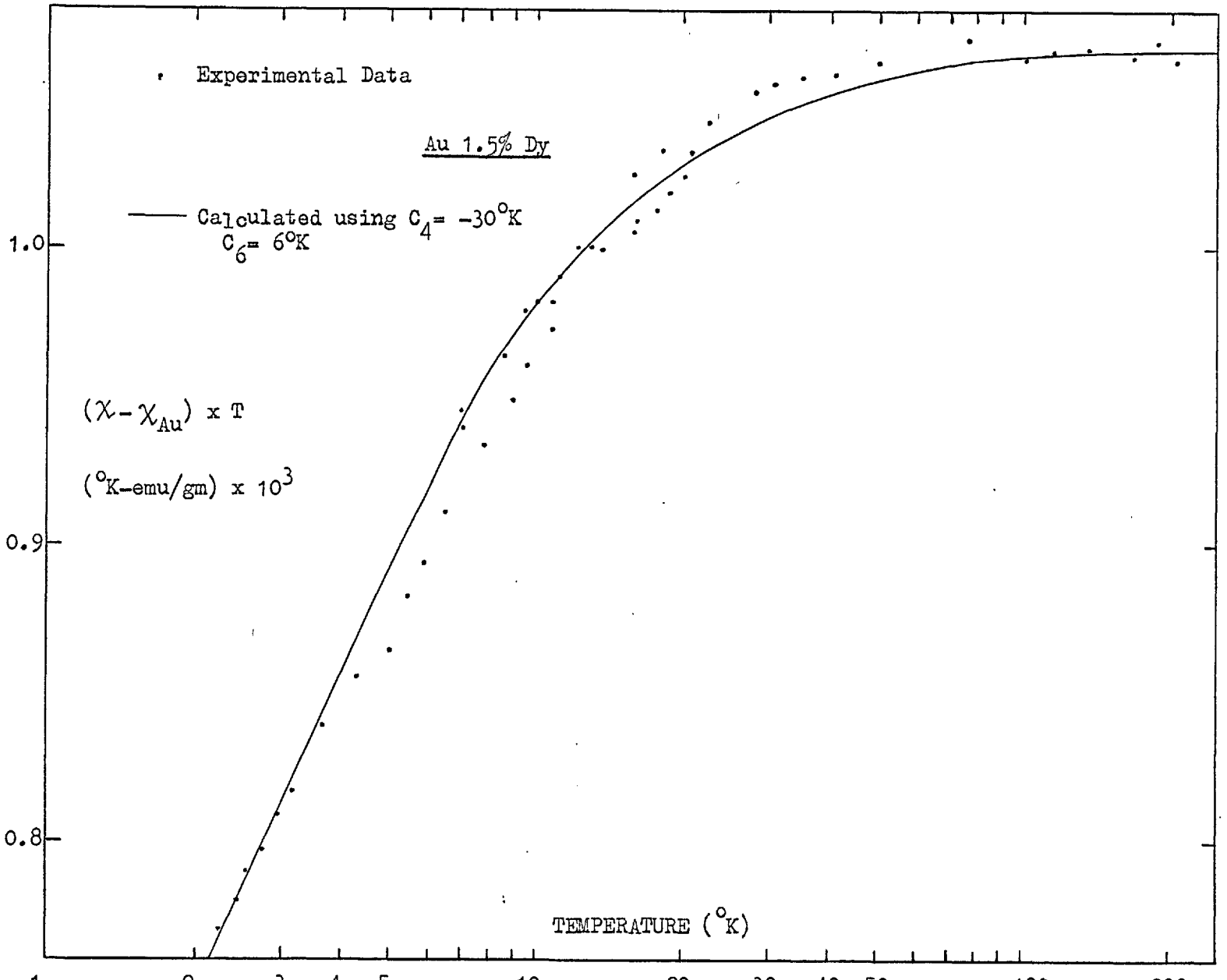

Fig 74 Graph of $(\chi - \chi_{Au}) \times T$ vs Temperature for Au 1.5% Dy Alloy

resistivity which is plotted as $\rho - \rho_{Au}$ against T, Fig.75. The continuous line through the low temperature data point is the calculated resistivity using the crystal field parameter $-30^{\circ}K$, $6^{\circ}K$ and assuming a $J_{s-f} = 0.054$ eV. Here again small amounts of iron impurities are likely to be present so that the actual value of J_{s-f} is uncertain. However it is not expected to be larger by a factor of more than two from the given value.

Fig. 76 shows graphs of magnetoresistance against field and against the square of the magnetisation at 1.6 and $4.2^{\circ}K$. The deviation from the expected linear dependence on M^2 at $1.6^{\circ}K$ is probably due to the difference of $\sim 0.05^{\circ}K$ in the temperatures at which the magnetisation and the magnetoresistance have been measured.

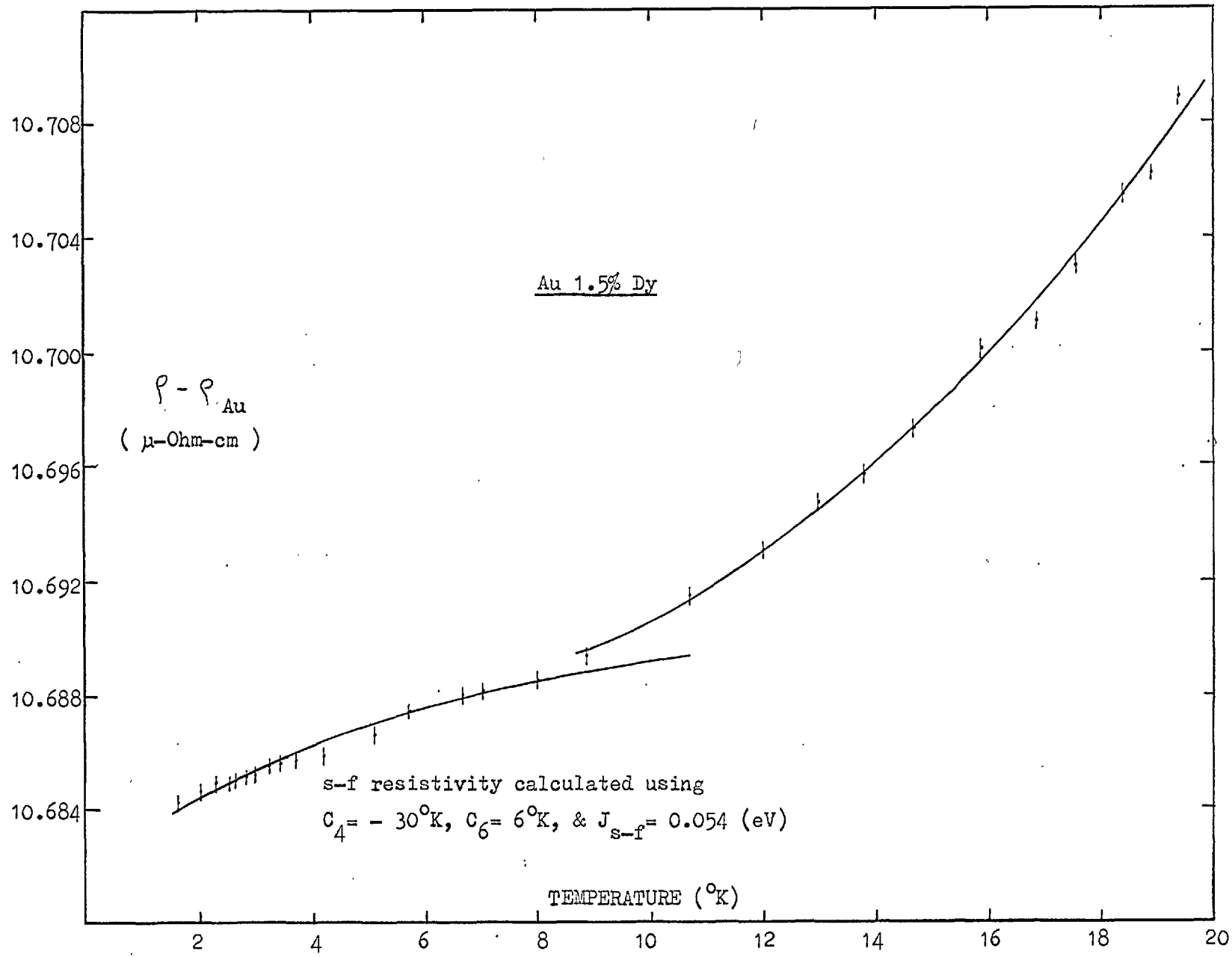

Fig.75 Excess Resistivity vs Temperature for Au 1.5% Dy Alloy

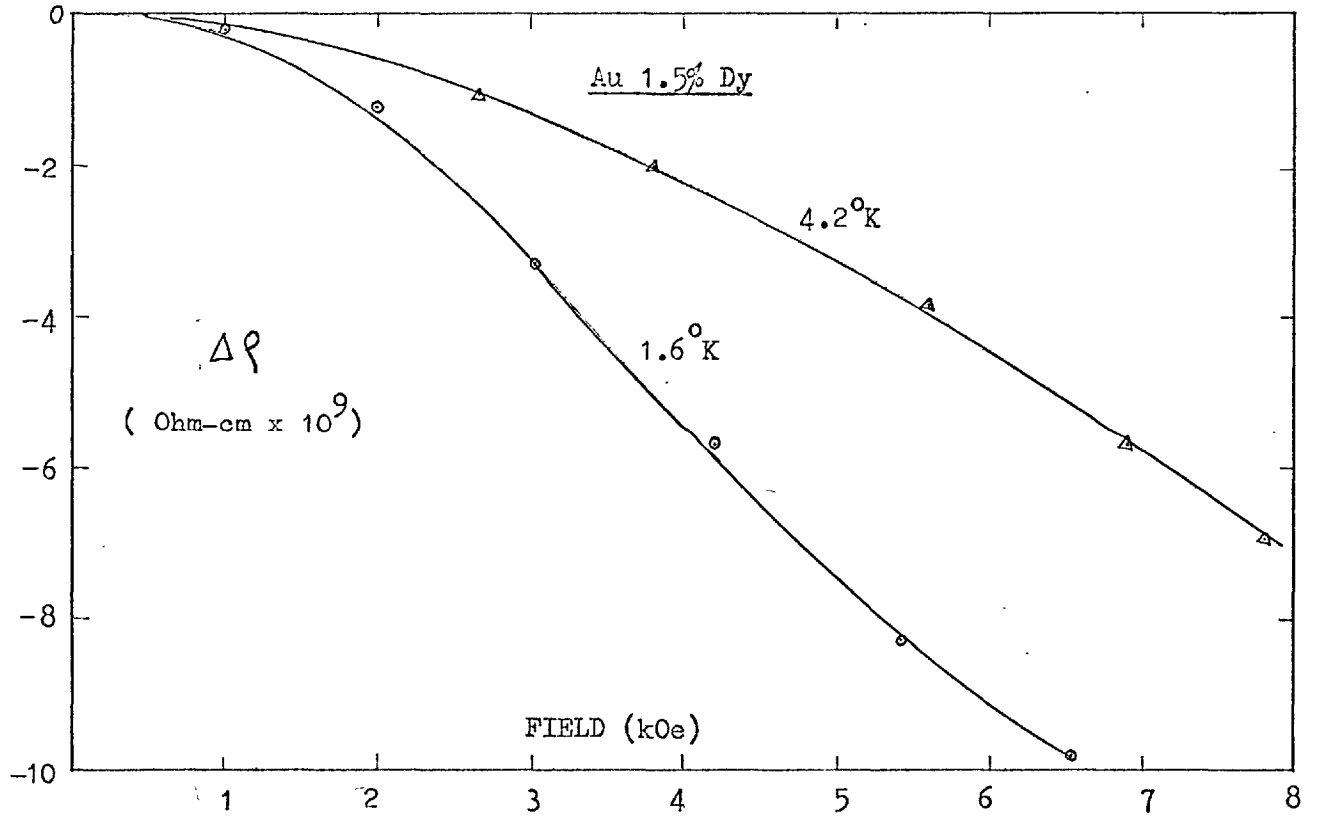

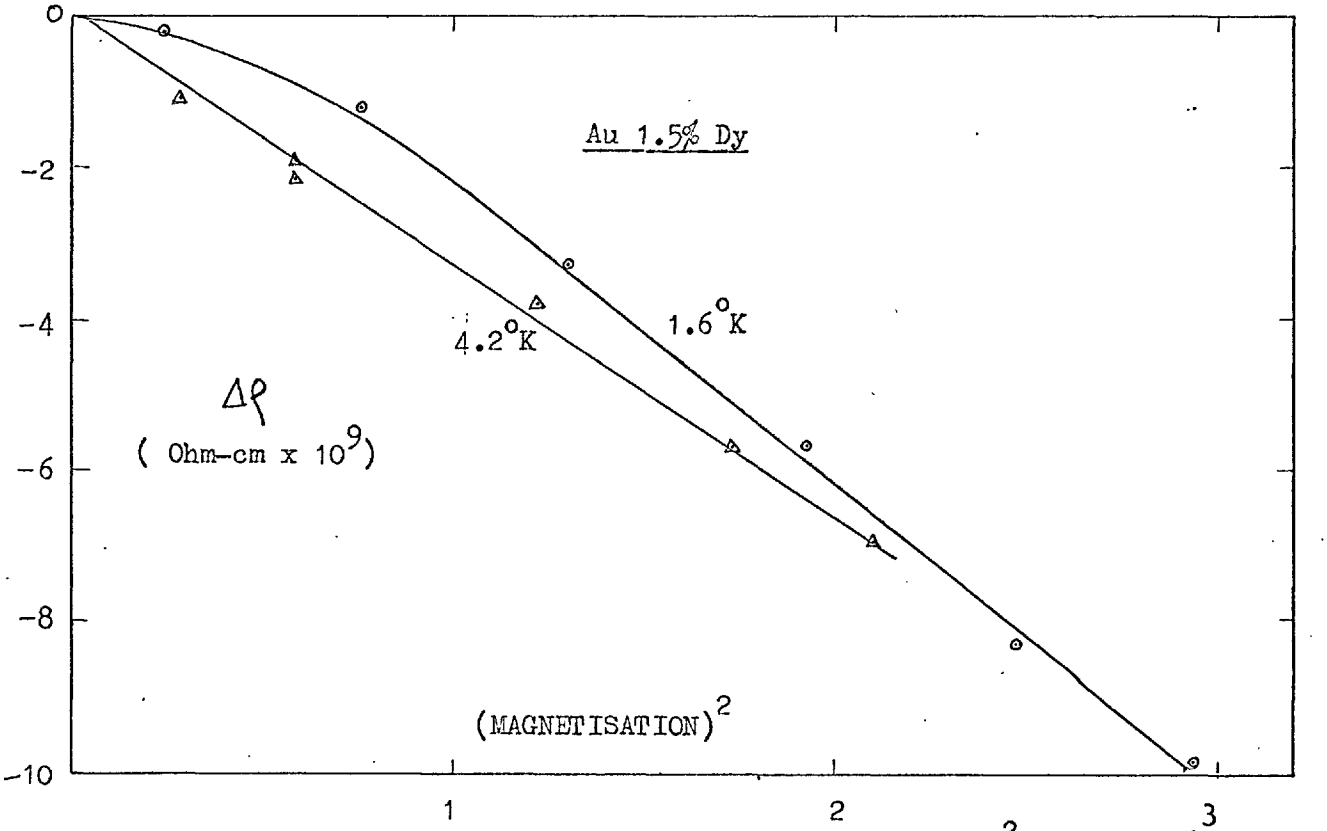

Fig.76 Graphs of Magnetoresistance vs Field and M^2 of Au 1.5% Dy Alloy

Conclusion

The results presented above show that the magnetic properties of the gold-rare earth alloys are dominated by the crystalline field effects. For the Au-Yb alloys the magnetic properties, even at low temperatures, are independent of the concentration upto 4 % Yb. The almost perfect Curie-law behaviour observed for the Au-Gd alloy, and the failure to detect in other systems any of the effects which normally occur as a result of interactions between the solute atoms, suggest that such interactions are rather weak in these systems, and if present are probably masked by the larger crystalline field effects. It has also been shown that the resistance decrease at low temperature can be explained by assuming the crystal field splitting of energy levels if a proper account of both the elastic and the inelastic scattering from these levels is taken.

The values of the crystal field parameters C_4 and C_6 obtained from the susceptibility fits are rather larger in magnitude than obtained from the simple point charge model. The sign of C_4 is also opposite to that given by the point charge model. It is interesting to note that the same crystal field parameters $C_4 = -30^\circ K$, $C_6 = 6^\circ K$ are obtained for both Dy and Yb which are Kramer's ions whereas values for the non-Kramer's ion Ho are smaller ($C_4 = -20^\circ K$, $C_6 = 4^\circ K$). The results of Williams and Hirst (71) for Er,

Tm and Yb dissolved in gold yield significantly smaller parameters also for the non-Kramer's ion Tm. It would seem reasonable to conclude that there is a definite tendency towards smaller crystal field parameters for the non-Kramer's ions. The effect of these smaller parameters is to decrease the overall splitting of the energy levels and also to bring low-lying magnetic multiplets closer to the non-magnetic ground state. If this distinction between the behaviour of Kramer's ions and that of non-Kramer's ions is found in other systems also, a theoretical examination of its possible sources may yield a better insight into the origin of the crystal fields.

REFERENCES

1. B. T. MATTHIAS, M. PETER, H. J. WILLIAMS, A. M. CLOGSTON, E. CORENZWIT and R. C. SHERWOOD, Phys. Rev. Letters 5, 542, 1960.

   A. M. CLOGSTON, B. T. MATTHIAS, M. PETER, H. J. WILLIAMS, E. CORENZWIT and R. C. SHERWOOD, Phys. Rev. 125, 541, 1962.

2. P. W. ANDERSON, Phys. Rev. 124, 41, 1961.

3. P. A. WOLFF, Phys. Rev. 125, 439, 1962.

4. A. M. CLOGSTON et al (see 1)

5. J. FRIEDEL, Ann. Phys. 9, 166, 1954.
   " Phil. Mag. 43, 153, 1952.
   " Can. J. Phys. 34, 1190, 1956.
   " Nuovo Cimento. Suppl. 7, 287, 1958.

6. A. BLANDIN and J. FRIEDEL, J. Phys. Rad. 20, 160, 1956.

7. SLATER and KOSTER, Phys. Rev. 96, 1208, 1954.

8. J. KONDO, Prog. Theor. Phys. 32, 37, 1964.

9. C. ZENER, Phys. Rev. 87, 440, 1951.

10. T. KASUYA, Prog. Theor. Phys. 16, 45, 1956.

11. K. YOSIDA, Phys. Rev. 106, 893, 1957.

12. Y. NAGAOKA, Prog. Theor. Phys. 37, 13, 1967.

13. D. R. HAMMAN, Phys. Rev. 158, 570, 1967.

14. K. YOSIDA, Phys. Rev. 147, 223, 1966.

15. J. R. SCHRIFFER and P. A. WOLFF, Phys. Rev. 149, 491, 1966.

16. A. J. HEEGER and M.A. JENSEN, Phys.Rev. Letters 18,485, 1967

17. A review is given by G. J. VAN der BERG Low Temp. Phys.-LT9 (Part B) 955, 1965

18. J. R. SCHRIEFFER and D. C. MATTIS, Phys. Rev. 140, A1412, 1965.

19. D. J. SCALAPINO, Phys, Rev. Letters 16, 937, 1966.

20. K. YOSIDA and A. OKIJI, Prog. Theor. Phys. 34, 505, 1965.

21. A. J. HEEGER and M. A. JENSEN, Phys. Rev. Letters, 18, 488, 1967.

22. H. ISHII and K. YOSIDA, Prog. Theor. Phys. 34, 505, 1965.

23. M. S. FULLENBAUM and D. S. FALK, Phys. Rev. 157, 452, 1967.

24. H. J. SPENCER and S. DONIACH, Phys. Rev. Letters, 18, 994, 1967.

25. G. S. KNAPP, Thesis; University of California, San Diego, La Jolla, California, 1967.

G. S. KNAPP, J. Appl. Phys. 38, 1267, 1967.

26. M. D. DAYBELL and W. A. STEYERT, Phys. Rev. Letters 18, 398, 1967.

27. H. SUHL, Phys. Rev. Letters, 19, 442, 1967.

28. M. D. DAYBELL and W. A. STEYERT, Rev. Mod. Phys. 40, 380, 1968.

29. M. LEVINE and H. SUHL, Phys. Rev. 171, 567, 1968.

30. M. LEVINE, T. V. RAMAKRISHNAN and R. A. WEINER, Phys. Rev. Letters 20, 1370, 1968.

31. P. G. De GENNES, J. Phys. Rad. 23, 510, 1962.

32. F. FROHLICH and F. R. N. NABARRO, Proc. Roy. Soc. A175, 382, 1940.

33. M. A. RUDERMAN and C. KITTEL, Phys. Rev. 96, 99, 1954.

34. D. R. HAMANN, Preprint

35. A. W. OVERHAUSER, J. Appl. Phys. 34, 1019, 1963.

36. R. E. WATSON and A. J. FREEMAN, Phys. Rev. Letters, 14, 695, 1965.

37. B. GIOVANNINI, M. PETER and J. R. SCHRIEFFER, Phys. Rev. Letters, 12, 736, 1964.

38. D. J. KIM and B. B. SCHWARTZ, Phys, Rev. Letters, 20, 201, 1968.

39. A. J. FEDRO and T. ARAI, Phys. Rev. 170, 583, 1968.

40. B. CAROLI, Thesis: see also A. BLANDIN Int. School Phys. "Enrico Fermi" Course 37. 393, 1967.

41. W. MARSHALL, Phys. Rev. 118, 1519, 1960.

42. M. W. KLEIN and R. BROUT, Phys. Rev. 124, 2412, 1958.

43. M. W. KLEIN, Phys. Rev. 136, A1156, 1964.
" Phys. Rev. Letters, 11, 408, 1963.
" Phys. Rev. 141, 489, 1966.
" Phys. Rev. Letters, 16, 127, 1966.

44. HEEGER, WELSH, JENSEN, and GLADSTONE Phys. Rev. 172, 302, 1968

45. R. BROUT, Phys. Rev. 115, 824, 1959.

46. S. H. LIU, Phys. Rev. 157, 411, 1967.

47. W. MARSHALL, T. E. CRANSHAW, C. E. JOHNSON and M. S. RIDOUT, Rev. Mod. Phys. p.399, 1964.

48. U. GONSER, R. W. GRANT, C. J. MEECHAN, A. H. MUIR Jnr, and H. WIEDERSICH, J. Appl. Phys. 36, 2124, 1965.

49. R. J. HARRISON and M. W. KLEIN, Phys. Rev. 154, 540, 1967.

50. S. D. SILVERSTEIN, Phys. Rev. Letters, 16, 466, 1966.

51. J. OWEN, M. E. BROWNE, V. ARP and A. F. KIP, J. Phys. Chem. Solids, 2, 85, 1957.

J. OWEN, M. E. BROWNE, W. D. KNIGHT and C. KITTEL, Phys. Rev. 102, 1501, 1956.

52. W. OPECHOWSKI, Physica, 4, 181, 1937.

53. S. DONIACH, Proc. Int. School. Phys. "Enrico Fermi", Course 37, p.255, 1967.

54. K. YOSIDA, Phys. Rev. 107, 396, 1957.

55. A. W. OVERHAUSER and M. B. STEARNS, Phys. Rev. Letters, 13, 316, 1964.

56. M. B. STEARNS and S. S. WILSON, Phys. Rev. Letters, 13, 313, 1964.

57. ZIMAN, 'Theory of Solids', Cambridge University Press, 1965.

58. MATTIS, 'The Theory of Magnetism', Harper & Row, 1965.

59. J. E. ZIMMERMAN and F. E. HOARE, J. Phys. Chem Solids, 17, 52, 1960.

60. J. De NOBEL & F. J. Du CHATENIER, Physica 25, 969, 1959.

61. G. T. TRAMMEL, Phys. Rev. 131, 932, 1963.

62. B. R. COOPER, YUNG-LI WANG and B. R. COOPER, Phys. Rev. 172, 539, 1968.

63. P. LEDERER and D. L. MILLS, Phys. Rev. Letters, 20, 1035, 1968.

P. LEDERER and D. L. MILLS, Phys. Rev. 165, 837, 1968.

64. S. ENGLESBERG, W. F. BRINKMAN and S. DONIACH, Phys. Rev. Letters, 20, 1040, 1968.

65. H. COTTET, P. DONZE, J. DUPRAZ, B. GIOVANNINI and M. PETER, Z. Angew. Phys. 249, 1968.

66. STONER MODEL: See for example ZIMAN's 'Theory of Solids' Cambridge University Press, 1965.

67. G. WILLIAM, Thesis, University of London, 1967.

68. J. BIJOVET, B. de HON, J. A. DEKKER and FLORA van BEEK, Solid State Comm. 3, 289, 1965.

69. G. de VRIES and J. BIJOVET, J. Appl. Phys. 39, 797, 1968.

70. L. R. EDWARDS and S. LEGVOLD,

71. G. WILLIAMS and L. L. HIRST (to be published).

72. L. L. HIRST, G. WILLIAMS, D. GRIFFITHS, and B. R. COLES, J. Appl. Phys. 39, 844, 1968.

73. D. GAINON, P. DONZE and J. SIERRO, Solid State Comm. 5, 151, 1967.

74. P. E. RIDER, K. A GSCHNEIDNER, Jnr., and D. O. McMASTERS, Transactions of the Metallurgical Soc. AIME, Vol. 233, Aug. 1965.

75. T. SUGAWARA, J. Phys. Soc. Japan, 20, 199, 1965.

76. H. R. CHILD, W. C. KOEHELER, E. O. WOLLAN and J. W. CABLE, Phys. Rev. 138, A655, 1965.

77. H. NAGASAWA and T. SUGAWARA, J. Phys. Soc. Japan 23, 711, 1967.

78. D. T. NELSON and S. LEGUOLD, Phys. Rev. 123, 80, 1961.

79. T. SUGAWARA and H. EGUCHI, J. Phys. Soc. Japan, 21, 725, 1966.

80. D. SHALTIEL, J. H. WERNICK and H. J. WILLIAMS, Phys. Rev. 135, A1346, 1964.

81. J. CRANGLE, Phys. Rev. Letters 13, 569, 1964.

J. CRANGLE and W. R. SCOTT, J. Appl. Phys. 36, 921, 1965.

82. A. N. GERRITSEN and J. O. LINDE, Physica 17, 573, 1951.

83. A. Van ITTERBEEK, W. PEELAERS, F. STEFFENS, Appl. Sc. Res. B8, 337, 1960.

84. O. S. LUTES and J. L. SCHMIT, Phys. Rev. 134, A676, 1964.

85. J. S. KOUVEL, J. Appl. Phys. 31, 142S, 1960.
" J. Phys. Chem. Solids 21, 57, 1961.

86. D. GRIFFITHS, Proc. Phys. Soc. 90, 707, 1967.

87. B. R. COLES, Phil. Mag. 8, 335, 1963.

88. J. H. WASZINK, Thesis, Univ. of London, 1965.

89. J. CRANGLE, Phil Mag, 5, 335, 1960.

90. G. G. LOW, Proc. Int. Cont. Magnetism, 1964, p.133.

91. B. W. VEAL & J. A. RAYNE Phys. Rev. 135, A442, 1964.

92. B. R. COLES, J. H. WASZINK, J. W. LORAM, Proc. Int, Cont. Magnetism, 1964.

93. G. WILLIAMS and J. W. LORAM, Solid State Conference, Manchester, 1969.

94. P. P. CRAIG, D. E. NAGLE, W. A. STEYERT, and R. D. TAYLOR, Phys. Rev. Letters, 9, 12, 1962.

T. A. KITCHENS, W. A. STEYERT and R. D. TAYLOR, Phys. Rev. 138, A467, 1965.

95. T. TAKAHASHI and M. SHIMIZU, J. Phys. Soc. Japan 20, 26, 1965.

96. S. DONIACH and E. P. WOLFARTH, Proc. Roy. Soc. 266, 422, 1967.

97. S. DONIACH and A. P. MURANI, Solid State Comm. 4, 525, 1966.

98.

99. E. HILDEBRAND, Ann. Physik 30, 593, 1936.

100. R. W. SCHMITT and I. S. JACOBS, J. Phys. Chem. Solids, 3, 324, 1957.

101. J. S. DUGDALE & Z. S. BA SINSKI, Phys. Rev. 157, 552, 1967.

102. C. A. DOMENICALI and F. L. CHRISTENSON, J. Appl. Phys. 32, 2450, 1961.

103. P. J. FORD, T. E. WHALL, and J. W. LORAM, LT-11 Conference, St. Andrews 1968.

104. K. KUME, J. Phys. Soc. Japan, 23, 1226, 1967.

105. A. NARATH, A. C. GOSSARD, and J. H. WERNICK, Phys. Rev. Letters, 20, 795, 1968.

106. J. CREVELLING, Jnr. and H. L. LUO. Phys. Rev. 176, 614, 1968.

107. R. J. LOWIN, (to be published)

108. J. G. BOOTH, K. C. BROG and W. H. JONES, Jnr. Proc. Phys. Soc. 92, 1083, 1967.

109. K. C. BROG, W. H. JONES and J. G. BOOTH, J. Appl. Phys. 38, 1151, 1967.

110. S. MOZUMDER, Thesis, Univ. of London, 1967.

111. T. SUGAWARA, H. NAGASAWA and S. YOSHIDA, LT-11, St. Andresw, 1968, p.1284.

112. B. R. COLES, Physics Letters 8, 243, 1964,

113. M. B. MAPLE and Z. FISK, LT-11, St. Andrews, 1968.

114. R. SCHWALLER, J. WUCHER, C. R. Acad. Sc. Paris, B264, 116, 1967.

115 W. M. STAR, B. M. BOERSTOEL, J. E. Van DAM, C. Van BAARLE, LT-11, St. Andrews, 1968.

116. E. W. PUGH, B. R. COLES, A. AROOT, J. E. GOLDMAN, Phys. Rev. 105, 814, 1057.

117. F. M. RYAN, E. W. PUGH, and R. SMOLUCHOWSKI, Phys. Rev. 116, 1106, 1959.

118. S. A. AHEREN, M. J. C. MARTIN and W. SUCKSMITH, F.R.S. Proc. Roy. Soc. 248, 145, 1958.

119. H. C. Van ELST, B. LUBACH and G. J. Van Den BERG. Phisica, 28, 1297, 1962.

120. T. J. HICKS, B. RAINFORD, J. S. KOUVEL, G. G. LOW, J. B. COMLY,

121. A. R. KAUFMANN, S. T, PAN, and J. R. CLARK, Rev. Mod. Phys, 17, 87,

122. N. D. LANG and H. EHRENREICH, Phys. Rev. 168, 605, 1968.

123. S. KIRKPATRICK and B. VELICKY, N. D. LANG, and H. EHRENREICH. 14th Annual Conference on Magnetism. New York, 1968.

124. B. R. COLES, Proc. Phys. Soc. Vol. LXV, 22, 1951.

125. J. A. APPLEBAUM and J. KONDO, Phys.Rev.Letters 19,906,1967

126. J. A. APPLEBAUM and J. KONDO, Phys.Rev. 170,542, 1968

127. D. J. LAM, D. O. Van OSTENBURG, M.V. NEVITT, H. D. TRAPP and D. W. PRACHT, Phys. Rev. 131, 1428, 1963.

128. E. BUCHER, W. F. BRINKMAN, J. P. MAITA, and H. J. WILLIAMS, Phys. Rev. Letters. 18, 1125, 1967.

W. F. BRINKMAN, E. BUCHER, H. J. WILLIAMS and J. P. MAITA, J. Appl. Phys. 39, 547, 1968.

129. R. E. WALSTEDT, R. C. SHERWOOD and J. H. WERNICK, J. Appl. Phys. 39, 555, 1968.

130. S. DONIACH, (private Communication)

131. A. I. SCHINDLER & C. A. MACKLIET. Phys. Rev. Letters 20, 15, 1968

132. A. I. SCHINDLER & M. J. RICE, Phys. Rev. 164, 759, 1967.

133. S. DONIACH and ENGLESBERG, Phys. Rev. 17, 750, 1966.

134. D. GRIFFITHS and B. R. COLES, Phys. Rev. Letters, 16, 1093, 1966.

135. B. R. COLES, Private Comm.

136. S. DONIACH and K. A. LONG, Solid State Conference, Manchester, 1969.

137. W. LOW, "Paramagnetic Resonance in Solids" Academic Press, 1960.

138. H. BETHE, Ann. Phys. Lpz. 3, 133, 1929.

139. K. W. H. STEVENS, Proc. Phys. Soc. A65, 209, 1952.

140. K. R. LEA, M. J. M. LEASK, and W. P. WOLF, J. Phys. Chem. Solids, 23, 1381, 1962.

141. R. J. ELLIOT and K. W. H. STEVENS, Proc. Roy. Soc. A218, 553, 1953.

142. H. A KRAMERS, Proc. Amsterdam Acad. Sci. 33, 959, 1930.

143. E. WIGNER, Nachr. Akad. Wiss. Gottingen Math.-Physik. Kl.IIa, 546, 1932.

144. H. A. JAHN and E. TELLER, Proc. Roy. Soc. A161, 220, 1937.

145. M. H. L. PRYCE, Nuovo Cimento (Suppl.) Vol. 6, 817, 1957.

146. L. L. HIRST, Solid State Comm. 5, 751, 1967.

147. R. ORBACH, Private Comm.

148. J. H. Van VLECK and W. G. PENNEY, Phil. Mag. 17, 961, 1934.

149. S. FONER, Rev. Sci. Instrum. 30, 548, 1959.

150. D. O. SMITH, Rev. Sci. Instrum. 27, 261, 1956.

151. A. ARROT and J. E. GOLDMAN, Rev. Sci. Instrum. 28, 99, 1957.

152. J. R. CLEMENT and E. H. QUINELL, Phys. Rev. 79, 1028, 1952.

J. R. CLEMENT and E. H. QUINELL, Rev. Sci. Instrum. 23, 213, 1952.

153. E. A. FAULKNER and D. W. HARDING, J. Sci. Instrum. 43, 97, 1966.

154. H. Van DIJK, M. DURIEUX, J. R. CLEMENT and J. K. LOGAN, J. Res. Nat. Bureau of Standards 64A, 4, 1960.

155. J. M. DAUPHINEE and PRESTON-THOMAS, Rev. Sci. Instrum. 25, 884, 1954.

156. G. K. WHITE 'Experimental Techniques in Low-Temperature Physics' Oxford, Clarendon Press, 1959.